CANADIAN THESES ON MICROFICHE

THÈSES CANADIENNES SUR MICROFICHE

NOTICE

The quality of this microfiche is heavily dependent upon the quality of the original thesis submitted for microfilming. Every effort has been made to ensure the highest quality of reproduction possible.

If pages are missing, contact the university which granted the degree.

Some pages may have indistinct print especially if the original pages were typed with a poor typewriter ribbon or if the university sent us an inferior photocopy.

Previously copyrighted materials (journal articles, published tests, etc.) are not filmed.

Reproduction in full or in part of this film is governed by the Canadian Copyright Act, R.S.C. 1970, c. C-30. Please read the authorization forms which accompany this thesis.

AVIS

La qualité de cette microfiche dépend grandement de la qualité de la thèse soumise au microfilmage. Nous avons tout fait pour assurer une qualité supérieure de reproduction.

S'il manque des pages, veuillez communiquer avec l'université qui a conféré le grade.

La qualité d'impression de certaines pages peut laisser à désirer, surtout si les pages originales ont été dactylographiées à l'aide d'un ruban usé ou si l'université nous a fait parvenir une photocopie de qualité inférieure.

Les documents qui font déjà l'objet d'un droit d'auteur (articles de revue, examens publiés, etc.) ne sont pas microfilmés.

La reproduction, même partielle, de ce microfilm est soumise à la Loi canadienne sur le droit d'auteur, SRC 1970, c. C-30. Veuillez prendre connaissance des formules d'autorisation qui accompagnent cette thèse.

THIS DISSERTATION HAS BEEN MICROFILMED EXACTLY AS RECEIVED

LA THÈSE A ÉTÉ MICROFILMÉE TELLE QUE NOUS L'AVONS REÇUE

Canada

67442

PERMISSION TO MICROFILM — AUTORISATION DE MICROFILMER

● Please print or type — Écrire en lettres moulées ou dactylographier

Full Name of Author — Nom complet de l'auteur

SURESH AKELLA

Date of Birth — Date de naissance	Country of Birth — Lieu de naissance
26-6-1956	INDIA

Permanent Address — Résidence fixe

1-8-7/8, SARVODAYA COLONY, Chikkadapally

Hyderabad — 500020
INDIA

Title of Thesis — Titre de la thèse

A Combined Timoshenko Beam/Shaft-Disks
Finite Element: Development and Application
To the Dynamic Analysis of Rotor Systems

University — Université

University of Alberta

Degree for which thesis was presented — Grade pour lequel cette thèse fut présentée

Ph D.

Year this degree conferred — Année d'obtention de ce grade	Name of Supervisor — Nom du directeur de thèse
Spring, 1985	DR. A. Craggs

Permission is hereby granted to the NATIONAL LIBRARY OF CANADA to microfilm this thesis and to lend or sell copies of the film.

The author reserves other publication rights, and neither the thesis nor extensive extracts from it may be printed or otherwise reproduced without the author's written permission.

L'autorisation est, par la présente, accordée à la BIBLIOTHÈQUE NATIONALE DU CANADA de microfilmer cette thèse et de prêter ou de vendre des exemplaires du film.

L'auteur se réserve les autres droits de publication; ni la thèse ni de longs extraits de celle-ci ne doivent être imprimés ou autrement reproduits sans l'autorisation écrite de l'auteur.

Date	Signature
14th Dec, 1984	Suresh.

THE UNIVERSITY OF ALBERTA

A COMBINED TIMOSHENKO BEAM/SHAFT-DISKS FINITE ELEMENT:

DEVELOPMENT AND APPLICATION TO THE DYNAMIC ANALYSIS OF ROTOR

SYSTEMS

by

SURESH AKELLA

A THESIS

SUBMITTED TO THE FACULTY OF GRADUATE STUDIES AND RESEARCH

IN PARTIAL FULFILMENT OF THE REQUIREMENTS FOR THE DEGREE

OF DOCTOR OF PHILOSOPHY

DEPARTMENT OF MECHANICAL ENGINEERING

EDMONTON, ALBERTA

SPRING, 1985

THE UNIVERSITY OF ALBERTA

RELEASE FORM

NAME OF AUTHOR   SURESH AKELLA

TITLE OF THESIS   A COMBINED TIMOSHENKO BEAM/SHAFT-DISKS

FINITE ELEMENT: DEVELOPMENT AND

APPLICATION TO THE DYNAMIC ANALYSIS OF

ROTOR SYSTEMS

DEGREE FOR WHICH THESIS WAS PRESENTED DOCTOR OF PHILOSOPHY

YEAR THIS DEGREE GRANTED   SPRING, 1985

     Permission is hereby granted to THE UNIVERSITY OF

ALBERTA LIBRARY to reproduce single copies of this

thesis and to lend or sell such copies for private,

scholarly or scientific research purposes only.

     The author reserves other publication rights, and

neither the thesis nor extensive extracts from it may

be printed or otherwise reproduced without the author's

written permission.

(SIGNED) _Suresh._

PERMANENT ADDRESS:

1-8-7/8, CHIKKADAPALLY

HYDERABAD - 500020

INDIA

DATED   12th Dec, 1984

THE UNIVERSITY OF ALBERTA

FACULTY OF GRADUATE STUDIES AND RESEARCH

The undersigned certify that they have read, and recommend to the Faculty of Graduate Studies and Research, for acceptance, a thesis entitled A COMBINED TIMOSHENKO BEAM/SHAFT-DISKS FINITE ELEMENT: DEVELOPMENT AND APPLICATION TO THE DYNAMIC ANALYSIS OF ROTOR SYSTEMS submitted by SURESH AKELLA in partial fulfilment of the requirements for the degree of DOCTOR OF PHILOSOPHY.

Supervisor

External Examiner

Date December 12, 1984

ABSTRACT

An accurate, high order beam-shaft finite element is developed for uniform and non-uniform cross-sections. The bending deformation, shear deformation, translatory inertia and rotatory inertia effects of the beam are included. The element is chosen from a set of constrained elements tested in the thesis. The beam finite element is altered to include the gyroscopic effects of shaft and disk, either in a forward or a backward circular whirl.

Different kinds of wheels(disks) are mounted on the turbine span. In a finite element model these intermittent disks are usually placed at the element nodes, forcing the need for a node at every disk location. An equivalent continuous Rayleigh shaft, utilized by Green, is modified to include the shear effects. Yet, difficulties have been noted in using this equivalent model. A more accurate and efficient way to model, without destroying the system geometry and dynamic character, is to include the disks within a single element. Such an element is developed, which successfully compares with simple shaft-disk systems and continuous disk systems. A repeating system can be modelled at a reduced cost using the periodic type shaft-disk element.

The turbine rotor itself is not uniform in cross-section but is, usually, stepped at a number of positions. Representing each of these steps by an element leads to a large system matrix. The shaft discontinuities

iv

are usually approximated using a linear or higher order tapered element. In the present case, the steps are retained as they are by representing them inside a single adaptor or stepped element.

The fluid bearings have anisotropic properties which affect the shaft motion. Holmes' short bearing dynamic coefficients have been considered. Capacity number is used as an independent variable to ease the designer's work. The linear variation of the coefficients, obtained by this method, helps computer modelling. Utilization of the root search method to find the threshold of stability of a flexible rotor supported on fluid film bearings, has been reported as a costly procedure. In this study, a modal reduction method is developed for a shaft with dynamic changes at the bearings, to make the root search method feasible. A dynamic condensation is also formulated to suppress the undesired nodal variables.

A typical turbo-generator unit, with multiple flexible spans and multiple bearings is modelled with a reduced system matrix(19 degrees of freedom). This matrix is used to calculate the dynamic characteristics of the rotor, as defined by the critical speeds, mode shapes and unbalance response. The efficiency of the trim balance planes, located on the turbine shafts, is discussed.

Acknowledgements

Nomenclature

Variables

A	Cross-sectional area
CN	Capacity number
E	Young's modulus
G	Shear modulus
I	Cross-sectional moment of inertia
k	Radius of gyration
K	Shape factor
l	Length of the element
L	Length of the beam
M	Bending moment
N	Mode number; shaft running speed
P	Unit load on a bearing
p	Non-dimensional critical speed
q	Rate of loading; generalized co-ordinate
s	Complex eigenvalue $\lambda + i\omega_d$
SN	Sommerfeld number
V	Shear force
W	Total displacement; load on a bearing
x	Longitudinal co-ordinate
α, β	Taper ratio
δ	Log decrement
ϵ	Eccentricity ratio
λ	Non-dimensional frequency
μ	Oil viscosity

μ_1	Mass effect
μ_2	Disk effect
ν	Poisson's ratio
ξ	Non-dimensional length; damping ratio
ρ	Mass density
ϕ	Bending slope
ψ	Shear slope
ω	Speed of rotor; natural frequency of a beam
ω_0	Threshold critical speed
ω_d	Damped critical speed
Ω	Spin velocity

Subscripts and superscripts

.	Time derivative
'	Spacial derivative
−	Vector
*	Altered variable or matrix
i,1,2	Counters for nodes and axes
x,y,z	Axes
d	Disk; damping
L,R	Left and right
-1	Inverse of a matrix
t,T	Transpose of a matrix

Matrices and vectors

[a]	Non-dimensional bearing stiffness coefficients
[A]	System matrix
[b]	Non-dimensional bearing damping coefficients
[C]	Damping matrix; transformation matrix
[DM]	Disk mass matrix
[DI]	Disk inertia matrix, in rotation
$\{F\}, \{Q\}$	Force vector
[IA]	Rotatory inertia/gyroscopic constants
[K]	Stiffness matrix
[M]	Mass matrix
$\{ q \}$	Generalized co-ordinates
[T]	Transformation matrix
$\{ W \}$	Nodal variable vector
$\{x\}, \{W\}$	Displacement vector
$\{ a \}$	Vector of polynomial constants
[ϕ]	normalized modal matrix

Table of Contents

xi

List of Figures

1. INTRODUCTION

Industrial rotors are usually complex systems, with multiple non-uniform spans and anisotropic fluid bearing supports. A greatly simplified model of the large rotors is necessary before analytical techniques can be applied. Yet, analytical results of the simple models are very useful in testing new numerical methods and comparing different models.

The controlled experiments conducted on a small scale laboratory model may not be directly extended to the large power plant units. Response measurements are easily made on small rotors in the laboratories, whereas a turbo-generator unit will have contributions at each section due to the bearings, pedestal and flexible foundation. To get a reasonable estimate of the contribution of each of these components in the system amplitude and phase, extensive and accurate instrumentation along with reliable measurements are necessary. An easier method for such preliminary analysis is to obtain an accurate computer model of the system.

Another example where experimental methods might be difficult on a real turbo-rotor is the stability analysis. To study the rotor instability due to the bearings it is necessary to operate the rotor system at speeds above the designed speed which could be catastrophic. However, a computer model of the turbo-rotor can easily do this task without causing any damage to the machine.

Thus, numerical methods evolved for rotor dynamic analysis. The transfer matrix method of Prohl[50] was the first to be applied. Because of its limitations it gave way to the finite element method. Gasch[52] and Ruhl[53] used beam finite elements to represent rotors. Immediately, many advantages surfaced: fewer number of elements are necessary to model a rotor; branches and fluid film bearings can be easily prescribed; numerical stability is assured for steady state problems; extra degrees of freedom corresponding to the foundation can easily be added.

Despite the almost unlimited memory and calculation power of large computers, the system matrices of large rotor models were found to exceed the computer capacity, in memory space and cost of calculations. A familiar technique of structural dynamics, Guyan reduction, was used by Rouch[55] to reduce the system size, while retaining most of the accuracy of the original large model. This method uses the static modes to condense the system size and is not as effective in the dynamic condition when the inertia effects of the rotor alter the mode shapes.

In the present study a large rotor, as found at a power generation station, is modelled by a system matrix adaptable, in size, to a micro-computer. The increasing availability of these machines at reduced costs and their portability would encourage the power plants to own them. The operators at these stations would thus be equipped to conduct their own rotor dynamic analysis.

The reduction in the system size is achieved in the following three stages:

1. By having an efficient and accurate beam finite element.

2. During the modelling of the rotor, by developing

    a. a higher order tapered element, to incorporate non-uniform sections,

    b. an element to include disks within itself

    c. and a stepped element or an element which can have sectional discontinuities.

3. In the third stage the excess degrees of freedom are suppressed by a dynamic reduction method, using the undamped system modes. The loss of accuracy at this stage is negligible for the eigenvalue problem.

A brief outline of the layout of the thesis follows.

In the second Chapter and Appendix A, accurate high order Timoshenko beam finite elements are formulated. A generalization is shown for obtaining such elements by choosing the constraint conditions, nodal variables and polynomial functions. An element called TM544 is selected for the present study because of its widespread advantages. Its accuracy, convergence and rate of convergence proves it to be more efficient than the existing elements. The element is used for non-uniform sections, second spectrum analysis and static response of single and multiple span beams. Analytical solutions are obtained for the Timoshenko shaft static response (Appendix B) and simply supported beam critical speeds.

The beam element is applied to a whirling shaft by properly including the gyroscopic effects. The moment acting on the shaft in a circular whirl is derived in Chapter 3 using the Euler equations of motion. The simply supported beam's analytical solution is readily extended to the whirling shaft. Comparison of the present element with Rouch[55] showed impovement in accuracy per degree of freedom. A Ritz method is developed in Appendix C to show the effects of shaft taper and is used to compare with the finite element results.

In Chapter 4, Den Hartog's[58] analytical solution for a shaft-disk system is extended to include the shaft's shear deformation. A method to include the disks within an element is formulated and tested, extensively; comparing with simple analytical cases of Green[59] and also with the lumped results. Lumping at nodes and disks placed inside the element gave very close results. This method of including the disks inside the element is successfully used for a shaft with continuous disks and a shaft with tapering disks as in a turbine stage. A periodic type of shaft-disk element is developed, which can be used for repeating structures, to reduce computational costs.

An adapter type stepped element is formulated in Chapter 5. This element is developed to include shaft discontinuities and performs better than an equivalent tapered element. Comparisons are made with the basic methods of Rayleigh, transfer matrix and equivalent tapered element.

The fluid film bearings have an important role in the dynamics of rotor. The oil film acts like a spring damper system to support the rotor. The dynamic effects are nonlinear in nature, both linear and nonlinear models of these coefficients are available. Linear bearing coefficients are used in the present analysis. Nonlinear effects can be easily added when a particular need arises. Foundation flexibility affects the rotor performance, especially with the modern flexible supports.

In Chapter 6 the stiffness and damping coefficients of Holmes'[64] short bearings are presented. Capacity number is used as the independent parameter instead of the usual eccentricity ratio. Since Capacity number describes any short bearing completely, these charts can be used by a design engineer directly without conversion. The bearing anisotropic effects are also discussed with respect to the shaft motion.

The rotor element is developed in Chapter 7, taking two elements in perpendicular planes. This element represents any asymmetric shaft and can accomodate asymmetric bearings. For the case of an axisymmetric shaft-bearing system a single plane is representative of the total shaft motion. For a bi-symmetric shaft-bearing system motion in two planes has to be considered, but decoupling allows the treatment of the motion in each plane separately.

Ruhl[53] has pointed out the difficulty involved in the root search method for finding the stability zones of the

system. At each running speed the stability is checked by calculating the eigenvalues. For a flexible shaft with many degrees of feedom this method becomes impossible. In this Chapter reduction in the system size is obtained by approximating the system with the lowest modes. Stability and free whirl critical speeds are calculated using the reduced system matrices. A successful comparison is obtained with the Lund[72] model.

The final Chapter deals with the application of the elements and techniques developed. A dynamic reduction method is introduced to retain the desired degrees of freedom. A 3600 rpm, 286 MW capacity turbo-generator unit is analyzed.

An accurate beam element and the inclusion of disks allowed the rotor to be modelled by an 18 element, 76 degrees of freedom system in a representative vertical plane which otherwise would have resulted in a 400 to 500 degrees of freedom model. Usually reduction is achieved by obtaining a geometrically equivalent shaft, reducing the number of elements by suppressing the details such as steps and disks in the system. Whereas, in the present case the rotor is modelled retaining geometric accuracy as much as possible.

The system size was further reduced, from 76 to 19 degrees of freedom, by dynamic condensation. The critical speeds using full system matrix are compared with those obtained by the classical Guyan reduction; dynamic reduction showed no loss of accuracy in the eigenvalue calculation.

The corresponding displacement mode shapes are also shown.

To illustrate the present model's practical value, the effectiveness of the existing turbine trim balance planes is studied. The bearing conditions, running speed and the mode shapes near the running speed directly or indirectly affect the response due to unbalance. The balance planes are efficient when they are at the points of maximum amplitudes for all running speeds for any type, location and distribution of unbalance.

The applications of such a rotor model are many. For instance, bearing nonlinearities and internal damping effects can be studied in detail. Balancing methods can be improved. The number of trials can be reduced in the trim balancing procedure, often performed in-situ.

2. AN ACCURATE TIMOSHENKO BEAM ELEMENT

Abstract

Higher order Timoshenko beam finite elements are formulated using constraint conditions. The element chosen has better accuracy, convergence and rate of convergence than the existing elements. It has total centroidal displacement, bending slope, shear slope and bending moment as nodal variables enabling direct representation of all the boundary conditions. These nodal parameters completely describe the beam when it is in either a static mode or a dynamic mode. Use of trigonometric functions in representing the beam variables is shown. Static response for Timoshenko beams is obtained analytically and used for comparison with the finite element results, which, along with the (standard) eigenvalue tests, confirm the improvements achieved with the present element. The second spectrum associated with Timoshenko beams is also considered; the zero shear mode is discussed. The beam element is extended for higher order non-uniform sections, for which correct boundary conditions are presented. Comparison with the results of other linearly tapered elements again shows improvement in accuracy and convergence.

2.1 Introduction

2.1.1 Beam theory

The flexural deformation of structural members in which one dimension is greater than the other two can be treated theoretically using elementary beam theory provided the basic assumptions are met. The Euler-Bernoulli beam theory provides results to many practical problems. Thus, for longer slender beams, the lower modes of vibration are predicted very accurately. However, when the depth of the section becomes of the same order as the span the results are unreliable.

Lord Rayleigh[1] in 1887 modified the beam theory to include the rotatory inertia effect which adds to the kinetic energy. This effect was tested on beams with end disks whose natural frequencies were considerably lowered.

Yet, no serious effort was made to modify the Euler-Bernoulli beam until the shear effect was considered by Timoshenko[2,3] in 1920. He introduced the concept of shear deformation and shear slope which together with the bending effects gives total deflection and slope. Equations of motion were developed including shear deformation and rotatory inertia; the solution for the simply supported beam was given. Timoshenko concluded that:

1. the correction for shear in the calculation of the natural frequncies, for the case considered, was four times greater than the correction for rotatory inertia;

2.   the corrections are unimportant if the wavelength of the

     transverse vibrations is large when compared with the

     dimensions of the cross-section as in the case of

     slender beams;

3.   the value of the correction increases with

     a.   decrease in wavelength,

     b.   increase in the shape factor,

     c.   increase in the wave number or mode number,

     d.   increase in the slenderness ratio of the beam.

It was a quarter century before further interest was
shown when Anderson[4], Dolph[5] and Trail-Nash and
Collar[6] simultaneously reformulated the equations, gave
solutions and identified the second spectrum due to shear
which had gone unnoticed by Timoshenko.

Trail-Nash and Collar emphasized the effects of shear
flexibility and rotatory inertia for the common rigid
boundary conditions and gave solutions:

1.   for the Timoshenko beam;

2.   neglecting rotatory inertia;

3.   with infinite shear stiffness;

4.   neglecting both shear effect and rotatory inertia

     effect.

Huang was the next to give analytical solutions; using
Ritz and Galerkin methods[7] and later assuming solution of
the type harmonic in time and harmonic and hyperbolic in
space[8].

The shear coefficient is described by Timoshenko as the average shear strain on a cross-section divided by the shear strain at the centroid. The shear coefficient accounts for the fact that the shear stress and shear strain are not uniformly distributed over the cross-section. While accomodating elements with different cross-sections, the appropriate value of shear-coefficient has to be used.

Cowper[9] gave a more exact definition following the three dimensional elasticity approach. This definition of shear coefficient is most satisfactory for static and long wavelength vibrations or low frequency deformations of the beams. Prescott[10] gave values for high frequency modes of vibrations. More recently, Victor and Ellyin[90] solved a Timoshenko beam subjected to an accelerating transient force.

2.1.2 Finite element

The appearance of computers left the analytical solutions as foundation blocks in understanding, developing and testing numerical models. The vast memory storage and the quick calculating power resulted in new techniques to model hitherto insurmountable, problems.

Finite element methods overtook the conventional finite difference and transfer matrix methods. Many good texts on finite element method are available: Zienkiewicz[11], Huebner[12] and Cook[13] among others. Cook has a detailed list of references.

Direct stiffness and flexibility methods gave way to the methods based on the principal of virtual work, energy theorems, Lagrange's equations and weighted residuals. Though all of them lead to the same matrices and equations of motion, the energy methods are the most popular.

The stiffness matrix for the Euler beam was derived by Archer[14] based on the unit displacement method and lately it is derived from the strain energy. The mass matrix was originally considered as a diagonal matrix representing the lumped masses at the nodes. Archer[15] was the first to develop a consistent mass matrix. Now it is commonly derived from the kinetic energy. Internal damping can be achieved as a proportional matrix based on Rayleigh's theory.

Archer's conclusions on the distributed mass matrix were:

1. it is consistent with the true mass distribution and hence improves the results;

2. the required fineness of the structural subdivisions to obtain a given accuracy is greatly reduced;

3. the frequencies obtained by the approximate methods are known to be the upper bounds to the exact solution whereas lumping techniques yield frequencies that can be higher or lower than the exact solution;

4. mass coefficients are computed for individual elements of the structure and combined by simple superposition.

During the last twenty years there have been many finite element models proposed for the Timoshenko beam which

include the effects of shear deformation and rotatory

inertia in addition to the bending displacement and the

lateral inertia terms. Thomas, Wilson and Wilson[22] gave a

review of these elements. Table 2.1 gives a list of the

elements and their important features. The simple elements

have four degrees of freedom per element: shear is included

indirectly as coefficients. McCalley[16], Archer[14], Davis

et al[17] developed simple elements based on the static

solution of a beam subjected to forces and moments applied

at the ends. This means that the shear force within the

element is constrained to be a constant. Complete

compatibility of the end nodal variables is true for

uniform, non-uniform, collinear and non-collinear

structures. Hence it is highly favoured in the analysis of

frames.

Moment and shear force boundary conditions cannot be

applied with these elements. As the depth to length ratio of

the beam increases the application of this element, with the

restricted assumption of constant shear force inside the

element, leads to a poor representation of the shear

deformation and affects the accuracy and convergence of the

higher order frequencies and results of deep beams. The

complex elements, with more than two nodes and/or more than

four degrees of freedom per element are designed to overcome

the difficulties which occur with the simple elements.

Narayanswami and Adelman[18] demonstrated that a

straightforward energy minimization does in fact yield the

Table 2.1. Comparison of Timoshenko beam finite elements

Element	# of nodes	Element d.o.f	Interpolation function	Comments
Mccally,Archer, Davis et al	2	W, ϕ	cubic for W, ϕ	Good for beams with low k/L values
Nickell and Secor	2	W, W'	cubic for W	ϕ should be used instead of W'
Nickell and Secor	3	W', ϕ at ends, ϕ at middle	cubic for w, quadratic ϕ	Same accuracy as Carnegie
Kapur	2	W_b, W_s, W_b', W_s'	cubic for W_b and W_s	Cannot represent all b.cs
Carnegie	4	W, ϕ	Cubic for W and ϕ	Good for non collinear structures
Thomas et al	2	W, ϕ, ψ	Cubic for W and ϕ	Introduced shear as variable, cannot allow all b.cs
Thomas-Abbas	2	W, W', ϕ, ϕ'	Cubic for W and ϕ	Incorporates all b.cs; though not directly
Dawe	3	W, ϕ	Quintic for W, quartic for ϕ	Uses constraint to get 5 constants
To	2	W, W', W'', W'''	Septic for W	Tapered beam; b.cs cannot be accounted
To	2	W, ϕ, ψ	Cubic for W, linear for ψ	Thomas element for tapered beam
Present	2	$W, \phi, A\psi\ I\phi'$	Quartic for W, cubic ϕ	constraint used to get 1 constant

correct finite element behavior when transverse shear effects are included. They also pointed out that the bending slope, ϕ, be retained as a nodal variable and not the total slope, W'. Since,

1. total slope is continuous only in the absence of the transverse shear deformation,

2. built-in-edge has the condition ϕ and not W' as zero.

The earliest complex element was by Kapur[19] who allowed a cubic variation for each of the bending and shear deflections resulting in an eight degrees of freedom element. The four nodal variables used, shear and bending deflections and their spatial derivatives, could not satisfy some of the common boundary conditions. This element performed better than the McCalley's element. Existence of the second spectrum was also noted.

An eight degrees of freedom element was also proposed by Carnegie et al[20] who used two internal nodes and cubic functions for both total displacement, W, and bending slope, ϕ. Nickell and Secor[21] obtained the same order of accuracy as the earlier two using only seven degrees of freedom. This implies that there was a redundant degree of freedom in the Kapur element. Nickell and Secor's TIM7 has a cubic displacement function for W and a quadratic for ϕ. The degrees of freedom at the ends are W, W' and ϕ; the seventh was W at the mid point of the element.

Thomas, Wilson and Wilson[22] introduced, for the first time, shear slope as a nodal variable. Using cubic functions

for displacement and bending slope they developed a six degrees of freedom element. A tapered element with both cross sectional area and second moment varying linearly was obtained. For low k/L ratios the Thomas element was inferior to the Archer and the McCalley elements but gave better results for shorter stubby beams. The disadvantage with this element is that the shear variable is not continuous across stepped sections and bending moment cannot be prescribed as a constraint.

Thomas and Abbas[23] presented an element with total deflection and bending slope and their derivatives as the nodal variables with cubic variation for W and ϕ. They could incorporate all the forced and natural boundary conditions, though not directly. Their claim that their element was the best model for dynamic analysis of Timoshenko beams was contested by Thomas[24] in a very informative letter.

Dawe's element[25] uses a constraint condition to evaluate five extra constants. The three node, six degrees of freedom element has a quintic polynomial for W and a quartic polynomial for ϕ. His element performed better than the existing elements, yet shear force and bending moment cannot be prescribed directly. He concludes that if independent interpolation functions are used for W and ϕ, an increase in efficiency would result.

An accurate finite element was developed by Craggs and Hong[26]. A constraint condition was used to obtain an improvement by Akella and Craggs[27].

2.1.3 Continuously varying elements

These are also called tapered elements where taper can be of any order. It is rare, in practice, to have beams with uniform cross-sections. Idealizing non-uniform sections by uniform elements would require a large number of elements increasing the computational cost and time. To overcome this difficulty tapered elements are used. Though their formulation and evaluation is more tedious, good results can be obtained with a fewer number of elements.

Lindberg[28] presented a general formulation for a tapered element. Using a linearly tapered element he evaluated the non-dimensional frequencies omitting the effect of shear deformation and rotatory inertia. Carnegie[29] studied the vibration characteristics of slender tapered elements such as those of the turbine and compressor blades, using the Euler beam model. His experiments and calculations were in good agreement as the beam cross-sections were small compared to the length.

Thomas[30] developed three elements to represent the tapered Euler beams and obtained the natural frequencies for different boundary conditions. He concludes that having an internal node is advantageous as it improves the convergence. This is because the taper parameters are better represented, yet maintain the external continuity conditions. Increasing the external nodal variables from two to three did not improve the accuracy per degree of freedom which means that the better nodal continuity is outweighed

by the coarser subdivision.

Thomas et. al[22] developed a Timoshenko beam tapered element. Explicit stiffness and mass matrices were obtained for an element with both cross-sectional area and moment of inertia varying linearly. This is a crude approximation for any real variation in the section. Yet he obtained a good comparison for a chimney type structure.

To[31] modified the Thomas[30] element using a fifth order polynomial for displacement and including shear and rotatory inertia terms. Later he improved it to a four degrees of freedom per node tapered element, with a seventh order polynomial for displacement. He evaluated the effect of taper ratios and depth to length ratios of the beams. His results and formulation were for a linearly tapered element as given by Lindberg. The representation of the shear force and bending moment boundary conditions was inaccurate.

To[32] also formulated an element using the Thomas element[22] using a cubic poynomial for displacement and a linear variation for shear variable. However, bending moment could not be prescribed as a boundary condition.

2.1.4 Second spectrum: Shear dominated modes

In their analytical work Anderson[4], Dolph[5] and Trail-Nash and Collar[6] all predicted the existence of a double spectrum of frequencies for the Timoshenko beam, one due to the bending modes and the other for the shear modes. This phenomenon was explicitly obtained for the case of the

hinged-hinged beam, which has the simple trigonometric and hyperbolic solution.

Anderson showed that for a hinged-hinged beam with small $N(k/L)$ corresponding to the lower modes of slender beams, the frequencies approach asymptotically the Euler beam solution. For large $N(k/L)$ corresponding to the higher modes of deep beams, the frequencies approach the frequencies of pure shear vibrations.

Trail-Nash and Collar reasoned that the second spectrum is the resonant interaction between the rotatory inertia forces and the shear stiffness reactions. The relative contributions were checked by looking at the ratio of bending slope and shear slope which are: positive for the first spectrum, the bending and shear slopes being in phase; ve with the slopes out of phase for the second m.

n the first spectrum the proportion of bending eases steadily for the higher modes and the contribution shear increases. Whereas, in the second spectrum the tributions of bending and shear are roughly the same but t of phase.

In the finite element analysis, Kapur[19] noted the econd spectrum but made little comment. Abbas and Thomas[33] devoted a detailed paper on this issue and concluded that except for the case of a hinged-hinged beam there is no separate second spectrum. Different modes were explained as the coupled independent modes of the

Bernoulli-Euler beam, simple shear beam and pure shear beam. Each of these beams could be obtained from a Timoshenko beam either by neglecting certain terms or equating certain displacements to zero.

Bhashyam and Prathap [34] used a simple linear shear flexible beam element with independent linear functions for displacement, W, and bending slope, ϕ. Reduced integration (a one point Gaussian scheme) was used to eliminate shear locking. They reported two separate spectra; one dominated by the Euler-Bernoulli modes and the second by the shear modes.

Downs[35] experimentally found the shear coefficient of a rectangular beam in pure shear to be 1.04. The coefficient varied from 0.85 for a bending mode to about 1.0 in the shear dominated higher modes.

Stephen[36], compared the Timoshenko beam theory with the exact theory of Pochhammer-Chree and failed to find an agreement for the second spectrum. Levinson and Cook[37], also inferred the same from Dolph's[5] results. They point out the difficulty of a beam changing from a first spectrum mode (with bending and shear slopes in phase) to a neighbouring second spectrum mode (with a change in the number of nodes and bending and shear slopes opposing).

Prathap[38], in a letter, pointed out that the division in the frequency spectrum is due to the occurance of two distinct ordered sets of the computed eigenvalues, and not because of a priori assignment.

The controversies in the literature on the second spectrum seem to arise due to the lack of a uniform definition. Each author appears to agree with the results of the others but is objecting to the terminology and classification.

2.2 Theory

Finite element methods are approximations, so one type of element cannot be the best for all circumstances. The choice of the element must depend on the required accuracy, convergence rate, continuity of the nodal variables within and at the element intersections, ability to satisfy the common boundary conditions and the type of structure it is applied to.

The review of the existing elements projects the following requirements for a new element:

1. a higher order element to accelerate convergence and improve accuracy per node and per element yet not over constraining the element to evaluate the extra polynomial coefficients;

2. appropriate choice of the nodal variables so that

    a. the functional can be represented,

    b. all the natural and forced boundary conditions can be met,

    c. they represent some physical parameters,

    d. complete continuity at element intersections for both uniform and stepped sections is achieved;

3. shear deformation is given a higher order representation
   to attain greater accuracy in the natural frequencies of
   deep beams or of higher modes and to analyze the second
   spectrum. As the depth to length ratio of the beam
   increases the shear dominated modes move closer to the
   lower bending mode range. The higher order elements are
   expected to give more accurate results in this range. It
   is suggested here that while a low order element can
   give good results for fairly long beams, the more
   stringent test for a Timoshenko beam is when k/L is
   high(k/L>0.05).

2.2.1 Development of the element

As there is no rigorous way of obtaining the best
element some numerical tests using different polynomials are
done to get to the right model. A brief discussion of the
elements tried is presented followed by the details of the
element chosen.

Appendix A gives the variational procedure for
obtaining the equations of motion and gives the natural
boundary conditions as a consequence. The approximate
functional and the derivation of the stiffness and mass
matrices for the four elements tried are also given.

Simple mathematical relations exist for the number of
nodal variables required for a given constraint condition
and given order of polynomials for the variables.
Let displacement, W, be represented by an Nth order

polynomial and bending slope, ϕ, by an Mth order polynomial. Thus N+1+M+1 polynomial coefficients have to be evaluated. If the shear slope, ψ, is constrained to a (K-1)th order polynomial then the Kth derivative $\psi^k=0$ becomes the constraint condition.

Assume that N>M>K. The geometric equation of deformation, shown in Figure 2.2, is:

$$W' = \phi - \psi.$$

A kth order differentiation of the above equation along with the constraint condition gives:

$$W^{k+1} = \phi^k.$$

This differentiation of the assumed functions gives an algebraic equation which is of the form:

(N-K-1)th order function = (M-K)th order function.

Equating coefficients of equal powers we get (N-K) equations, (N-M-1) of which make the coefficients of higher powers of the polynomial of W zero and the rest (M-K+1) of the equations relate the coefficients of W and ϕ. Therefore, the number of nodal variables to be prescribed are equal to: the total polynomial coefficients - number of relations from the constraint condition.

$$ie., \quad (N+M+2)-(N-K)=M+K+2 \ .$$

Example:

Given $N=8$, $M=6$ and $k=3$. The following equations can be written:

$$W = a_0 + a_1x + a_2x^2 + a_3x^3 + a_4x^4 + a_5x^5 + a_6x^6 + a_7x^7 + a_8$$

$$\phi = b_0 + b_1x + b_2x^2 + b_3x^3 + b_4x^4 + b_5x^5 + b_6x^6$$

$\psi^{111} = 0$. Hence, $w^{IV} = \phi^{111}$

$$\therefore 24a_4 + 120a_5x + 360a_6x^2 + 840a_7x^3 + 1680a_8x^4$$
$$= 6b_3 + 24b_4x + 60b_5x^5 + b_6x^6$$

Equating coefficients of like powers we get ($N-M-1=8-6-1=1$) one coefficient of the highest power of W as zero (ie, $a_8=0$). Four ($M-K+1=6-3+1=4$) relations between the coefficients of W and ϕ exist giving a_4, a_5, a_6, a_7 in terms of b_3, b_4, b_5 and b_6.

Eleven ($M+K+2=6+3+2=11$) nodal variables have to be specified to determine the rest of the constants. As it is not an even number we cannot specify equal number of variables on both end nodes. A solution is to specify one variable, say W, at an internal node and five variables

(say,W, W', W'' ϕ and ϕ') at each end node. Another approach
is to specify the displacement W at three internal nodes and
(W, W', ϕ and ϕ') at each end node.

Thus, a lot of dexterity is involved in choosing the
constraint condition, polynomial orders and nodal variables.
The requirements listed previously do not uniquely narrow
down the best possible elements but would help us select
from a smaller subset.

Mathematical and physical understanding of the
requirements helps us narrow down the subset. A few such
observations are listed below:

1. for the constraint condition used, the displacement
    polynomial need only be one order higher than the
    rotational slope;

2. for a massless beam with forces and moments acting only
    at the nodes, shear force and bending moment vary
    linearly inside the element, bending slope has a
    quadratic variation and displacement has a cubic
    variation;

3. When the mass of a uniform beam is considered the order
    of these variations increases by one. A further increase
    occurs when variation of the mass of the element is
    considered as in a tapered element;

4. When disks or stiffnesses are included in the element
    (discussed in later Chapters) or when mass or elastic
    unbalance occurs at discrete or continuous points, a
    higher order representation is necessary.

Finally, a balance has to be struck between having fewer elements with higher order polynomials and more elements with lower order polynomials. The optimum element gives the required accuracy with minimum elements and minimum global degrees of freedom.

2.2.2 Basis for choosing the nodal variables

The beam in flexure is represented by the end displacement, W, the bending slope, ϕ, the shear force, $A\psi$, and the bending moment, $I\phi'$. Dolph[5], wrote the Timoshenko beam equations using the same variables. It is shown in Appendix A, that all the displacement (forced) and force (natural) boundary conditions can be represented with this choice of nodal variables; also, the energy functional can be completely expressed by them. All the variables are continuous along uniform, non-uniform and discontinuous sections. However, an external force makes the shear force discontinuous and an external moment makes the bending moment discontinuous.

Complete compatibility of the variables at a node allows the use of same set of variables for both the elements at the joint they share. For the present element at each internal joint four degrees of freedom are allowed in the coupled condition compared to the eight degrees of freedom in the uncoupled condition. Thus, a reduction in the global degrees of freedom occurs. Assuming the material parameters G, K and E as constants, the nodal variables

chosen are displacement, W, bending slope, ϕ, shear force, Aψ, and bending moment, Iϕ'.

2.2.3 Element formulation

Th details of formulation of different elements is given in Appendix A. Element matrices in Appendix A are obtained in terms of the selected nodal variables by a transformation. These matrices can also be obtained directly by modifying the functional, as shown below for the element TM544. The energy functional for a Timoshenko beam can be written as:

$$= \int_0^\ell \frac{E}{2I(x)} \left(I(x)\phi'\right)^2 dx + \int_0^\ell \frac{GK}{2A(x)} \left(A(x)\psi\right)^2 dx$$
$$- \frac{\omega^2}{2} \left\{ \int_0^\ell \rho A(x) w^2 dx + \int_0^\ell \rho I(x) \phi^2 dx \right\}$$

As given in Appendix A:

$$W = X0 \{ a \}$$

$$\phi = Y0 \{ a \}$$

$$A\psi = A(x) Z0 \{ a \}$$

$$I\phi' = I(x) Y1 \{ a \}.$$

The variables can be written as:

$$W = \lfloor 1 \quad x \quad x^2 \quad x^3 \quad 0 \quad 0 \quad 0 \quad x^4/4 \rfloor \{\alpha\}$$

$$\phi = \lfloor 0 \quad 0 \quad 0 \quad 0 \quad 1 \quad x \quad x^2 \quad x^3 \rfloor \{\alpha\}$$

$$A\Psi = A(\phi - W') = A\lfloor 0 \quad -1 \quad -2x \quad -3x^2 \quad 1 \quad x \quad x^2 \quad 0 \rfloor \{\alpha\}$$

$$I\phi' = I\lfloor 0 \quad 0 \quad 0 \quad 0 \quad 0 \quad 1 \quad 2x \quad 3x^2 \rfloor \{\alpha\}$$

If the vectors of nodal variables $\{ W_e \}$ and the polynomial coefficients $\{ a \}$ are given as:

$$\{W_e\} = \lfloor w_i \quad \phi_i \quad A_i\Psi_i \quad I_i\phi_i' \quad w_{i+1} \quad \phi_{i+1} \quad \ldots \quad I_{i+1} \quad \phi_{i+1}' \rfloor$$

$$\{\alpha\} = \lfloor a_0 \quad a_1 \quad a_2 \quad a_3 \quad b_0 \quad b_1 \quad b_2 \quad b_3 \rfloor^{\top}$$

then we obtain:

$$\{W_e\} = [C]\{\alpha\}$$

$$\text{and } \{ a \} = [C]^{-1} \{ W_e \}.$$

Where:

$$
[C] = \begin{bmatrix}
1 & 0 & 0 & 0 & 0 & 0 & 0 & 0 \\
0 & 0 & 0 & 0 & 1 & 0 & 0 & 0 \\
0 & -A_i & 0 & 0 & A_i & 0 & 0 & 0 \\
0 & 0 & 0 & 0 & 0 & I_i & 0 & 0 \\
1 & \ell & \ell^2 & \ell^3 & 0 & 0 & 0 & \ell^4/4 \\
0 & 0 & 0 & 0 & 1 & \ell & \ell^2 & \ell^3 \\
0 & -A_{i+1} & -2\ell A_{i+1} & -3\ell^2 A_{i+1} & A_{i+1} & A_{i+1}\ell & A_{i+1}\ell^2 & 0 \\
0 & 0 & 0 & 0 & 0 & I_{i+1} & 2I_{i+1}\ell & 3I_{i+1}\ell^2
\end{bmatrix}
$$

Note that [C], like the transformation matrix [T], remains unaltered for uniform and non-uniform elements. The variation is taken care of while evaluating the variables and the integrals. The approximate functional can be written as:

$$
J = \frac{1}{2}\{w_e\}^T[KB]\{w_e\} + \frac{1}{2}\{w_e\}^T[KS]\{w_e\} - \frac{\omega^2}{2}\{w_e\}^T[MT]\{w_e\}
$$

$$
- \frac{\omega^2}{2}\{w_e\}^T[MR]\{w_e\}
$$

where the component matrices are obtained by four point Gaussian integration:

$$
[KB] = \int_0^\ell EI(x)[C^{-1}]^T \lfloor Y1 \rfloor^T \lfloor Y1 \rfloor [C^{-1}]\, dx
$$

$$[KS] = \int_0^\ell GKA(x)[C^{-1}]^T \lfloor ZO \rfloor^T \lfloor ZO \rfloor [C^{-1}] \, dx$$

$$[MB] = \int_0^\ell \rho A(x) [C^{-1}]^T \lfloor XO \rfloor^T \lfloor XO \rfloor [C^{-1}] \, dx$$

$$[MR] = \int_0^\ell \rho I(x)[C^{-1}]^T \lfloor YO \rfloor^T \lfloor YO \rfloor [C^{-1}] \, dx.$$

The stiffness and mass matrices are now obtained directly in terms of $\{W_e\}$ without any transformation:

$$[K] = [KB] + [KS]$$

$$[M] = [MB] + [MR].$$

2.2.4 Numerical integration

The complex element formulation depends on the accuracy and efficiency of the numerical integration: Gaussian quadrature is found to be the most useful. In this method the integral $1 = \int_a^b f(x) \, dx$ is transformed to:

$$\int_{-1}^1 \frac{b-a}{2} \, f \left\{ \frac{(b-a)t + b + a}{2} \right\} \, dt$$

$$\text{where, } x = \frac{(b-a)t + b + a}{2}$$

$$I_{actual} = \int_{-1}^{1} C_i f(y) \, dy .$$

The integral I can be approximated by using the weighted functional values at n selected points:

$$I_{approx.} = \sum_{i=1}^{n} w_i f(y_i)$$

The error is defined by: $I_{actual} - I_{approx.}$

The sampling points y_i and the weighting factors W_i constitute the vector of unknowns { U }, which are evaluated by minimizing the error, setting $\frac{\partial \varepsilon}{\partial \{u\}} = 0$. The sampling points are located symmetrically with respect to the centre of the interval with the same weightage given for symmetrically paired points.

Gaussian quadrature using N points is exact if the integrand is a polynomial of degree 2N-1 or less, which means that the given function is replaced by a polynomial of degree 2N-1. A non-uniform element with four gaussian points is shown below.
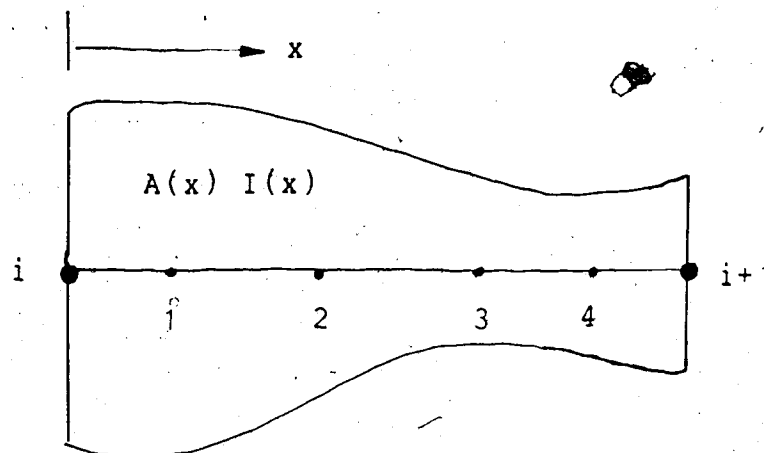
For integration, the area A', cross-sectional moment of inertia I and shape functions are evaluated at the Gaussian points. Four point Gaussian Quadrature is used for all cases of uniform and non-uniform elements thus integrals of functions up to seventh degree polynomial are evaluated exactly.

2.2.5 General non-uniform element

The advantage of using numerical integration over analytical integration is that a higher order cross-sectional variation can be more easily incorporated into the element. For a circular-section with an Nth order variation of the radius, r, in x, the following relations can be written:

..
$$\sum_{i=0}^{N} a_i x^i$$

$$\ldots) = \pi \, r^2(x)$$

$$= \sum_{i=0}^{2N} b_i x^i, \text{a } 2N^{th} \text{ order polynomial}$$

$$\text{moment of inertia; } I(x) = \frac{\pi \, r^4(x)}{4}$$

$$= \sum_{i=0}^{4N} c_i x^i, \text{a } 4N^{th} \text{ order polynomial}$$

Const___s b_i and c_i are evaluated in terms of a_i by equating the ___fficients of like powers of the polynomials.

Similarly for a rectangular cross-section with an Nth order variation of the breadth, b, and an Mth order for the depth, d, the following relations are obtained:

$$b(x) = \sum_{i=0}^{N} a_i x^i$$

$$\text{and } d(x) = \sum_{i=0}^{M} c_i x^i$$

Area, A(x), will have an (N+M)th order polynomial:

$$A(x) = \sum_{i=0}^{N+M} e_i \, x^i$$

and an $(N+3M)$th for the moment of inertia:

$$I(x) = \sum_{i=0}^{N+3M} f_i \, x^i$$

Again e_i and f_i can be evaluated from a_i and c_i.

2.2.6 Linearly tapered element

This particular variation of the element applies to a set of cross-sections. Hence, the same description holds good for all of them. This is advantageous when a program has to be developed for a structure with different cross-sections. It is the most common case in the literature; Lindberg[28] and To[31, 32]. A few of the possible cross-sections are shown below.
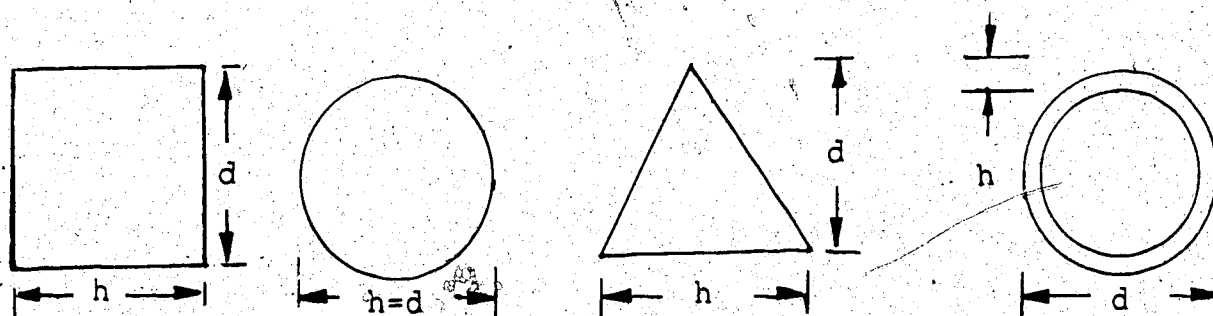
For the hollow circular cross-section, h/d<1 or
h/d=constant is a necessary condition for the analysis to be
correct. For all these elements the area $A=K_1hd$ and
cross-sectional moment of inertia $I=K_2hd^3$; where d and h
have a linear variation. The following relations can be
written:

$$h(x) = h_i \left(1 - (1-H) \frac{x}{\ell}\right)$$

$$\text{with, } H = h_{i+1}/h_i \; ;$$

$$d(x) = d_i \left(1 - (1-D) \frac{x}{\ell}\right)$$

$$\text{with, } D = d_{i+1}/d_i \; ;$$

$$A(x) = A_i \left\{1 + a_1 \frac{x}{\ell} + a_2 \frac{x^2}{\ell^2}\right\}$$

$$I(x) = I_i \left\{1 + b_1 \frac{x}{\ell} + b_2 \left(\frac{x}{\ell}\right)^2 + b_3 \left(\frac{x}{\ell}\right)^3 + b_4 \left(\frac{x}{\ell}\right)^4\right\}$$

For a circular cross-section $K_1 = \pi/4$ and $K_2 = \pi/64$;
for a rectangular cross-section $K_1 = 1$ and $K_2 = 1/12$;
for a triangular cross-section $K_1 = 1/2$; and for a hollow
circular cross-section $K_1 = \pi$ and $K_2 = \pi/8[\ 1 + (h/d)^2\ ]$.

2.2.7 Assembling the elements

The major difference between the Rayleigh- Ritz method
and the finite element method is that the latter makes the
approximate functional of each element stationary instead of
considering the whole structure. The equilibrium equations
are satisfied at the nodal points. The compatibility
conditions give a piecewise approximation. This means that

the element matrices can be added into a global matrix with compatible end nodal variables occupying the same global position. Figure 2.1 shows an assembled unconstrained beam structure.

As discussed before, an external force at a joint makes the shear force discontinuous and an external moment makes the bending moment discontinuous. These discontinuities do not alter the homogeneous solution but they must be properly assembled for forced response studies.

One way to get around this problem is to use a reduction technique, discussed later, to suppress the variables with discontinuities.

1.2.8 Static response

The eigenvalue test is a common method of evaluating the dynamic performance of the element. The static response which uses only the stiffness matrix can also rate the performance of the element; testing the choice of the nodal variables, polynomials, integration and assembly. In Appendix B, following an elementary strength of materials procedure, the Timoshenko beam differential equations are solved together with the boundary conditions and continuity conditions for simple beam structures to obtain the values of displacement, bending slope, shear force and bending moment under static loading. Other types of boundary conditions and loadings can similarly be evaluated for uniform and non-uniform sections. Using the law of
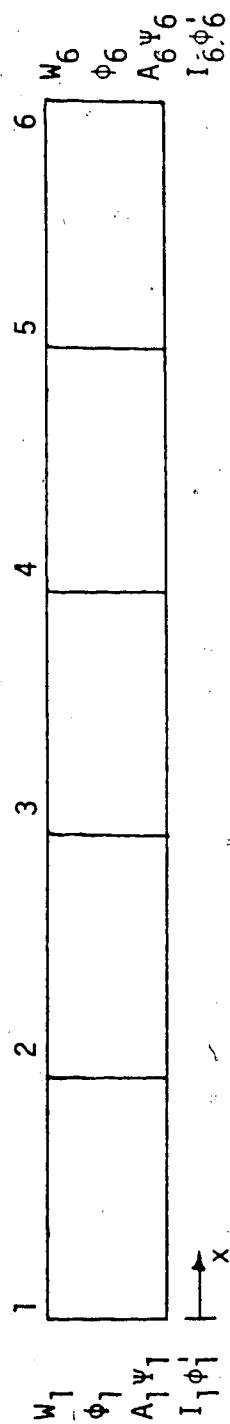
Figure 2.1 A beam assembled with finite elements.

superposition more complicated loadings, continuous beams and indeterminate beams can be solved. In effect, the Euler beam can be replaced, especially for deep beams, to include the shear effects in static response studies.

Static response by finite element analysis is obtained by solving a set of linear equations, $[K]\{ x \} = \{ F \}$. The free free beam stiffness matrix is singular as the rigid body modes corresponding to translation and rotation prevail. These modes are curtailed by prescribing displacement at two points on the beam; or a displacement and a rotation. In elementary analysis static indeterminacy results when the number of unknown reactions are more than the static equations of equilibrium: three for a planar motion.

In a finite element model the beam is subdivided; continuity and equilibrium at the nodes provide extra equations. A statically indeterminate system in a linear equation solver occurs when the number of equations are less than the number of unknowns. Solving continuously supported systems is easier with the finite element method as the problem is represented by a set of linear equations.

There are many ways of specifying displacements and support stiffnesses:

$$\left\{ [K \text{ shaft}] + \begin{bmatrix} K_B & 0 \\ 0 & 0 \end{bmatrix} \right\} \left\{ \begin{matrix} x_B \\ x_u \end{matrix} \right\} = \left\{ \begin{matrix} F_B \\ F_U \end{matrix} \right\}$$

Where $\{ x_B \}$ are the nodal variables with constraint and $\{ x_U \}$ without. $\{ F_B \}$ and $\{ F_U \}$ are the corresponding external forces and $[K_B]$ the support stiffnesses. $[Kshaft]$ is the beam/shaft stiffness matrix. For a rigid support the corresponding stiffness tends to a very large value (infinity), resulting in a small(zero) displacement. The product of the stiffness and the displacement will still be finite giving the corresponding reaction force.

To specify values for the displacements $\{ X_B^* \}$, the stiffness matrix and the force vector are augmented by $[K_B]$.

$$\left\{ \frac{\{F_B\} + [K_B] \{x_B^*\}}{\{F_U\}} \right\}$$

The error, $\{ \epsilon \} = \{ X_B \} - \{ X_B^* \}$, is small as loading $\{ F_B \}$ is far less than $[K_B]\{ X_B \}$ and $[K_B]$ is far greater than $[Kshaft]$, forcing a deflection of $\{ X_B \} = \{ X_B^* \}$.

2.2.9 Analytical solution for a simply supported beam

The exact solution, satisfying the differential equation of motion of a Timoshenko beam with hinged end conditions is obtained. Though such a solution is available from the general results of Huang[8] the simple approach taken is enough to evaluate the bending and shear modes.

The forces acting on a differential Timoshenko element
in harmonic transverse vibrations are shown in Figure 2.2.
The internal forces and the inertial forces deform the
element. The kinematic relationship of deformation is given
as:

$$w' = \phi - \Psi$$

where W' is the total slope, ϕ the bending slope and ψ the
shear slope. The constitutive relationship between the shear
stress and strain gives the force equation:

$$V = G K A \Psi$$

where V is the shear force, G the shear modulus, K the shape
factor and A the cross-sectional area. The relation between
the bending moment, M, and the bending slope, ϕ, is:

$$M = EI \phi'$$

where E is the modulus of elasticity and I is the area
moment of inertia. The force equilibrium gives the equation
of lateral motion:

$$\frac{dw}{dx} = \phi - \psi$$
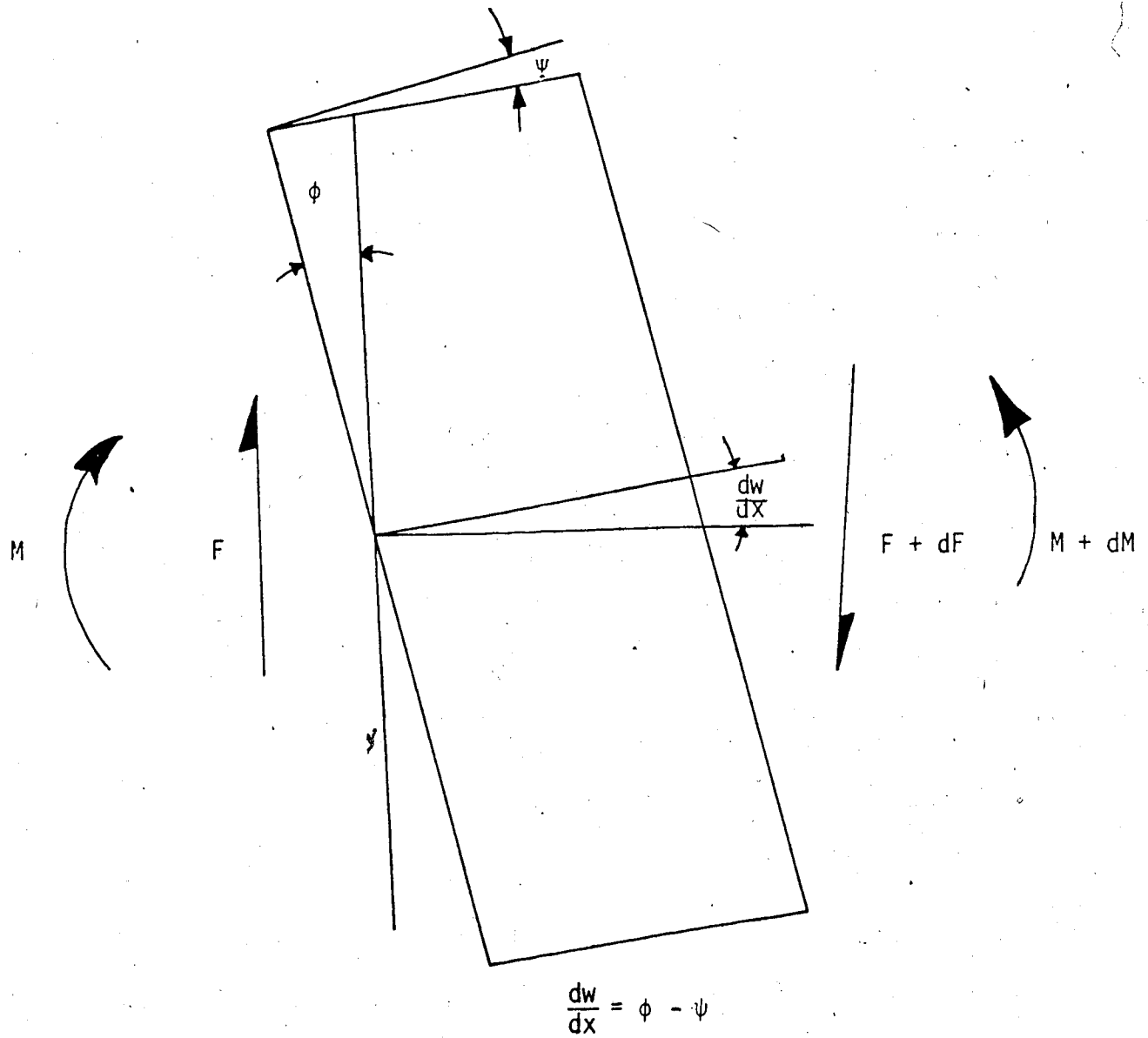
Figure 2.2 Forces and Rotations on a Beam Element

$$GKA (W'' - \phi') + \omega^2 \rho A W = 0$$

where W is the centroidal displacement, ρ is the mass density, ω is the vibrational frequency.

Finally, the equation of motion in rotation is given as

$$EI \phi'' + GKA (W' - \psi) + \omega^2 \rho I \phi = 0.$$

These equations have been derived by other investigators and can also be obtained from the variational principle.

Assume that the variables in the Nth mode are:

$$W = W_0 \sin\left(\frac{N \pi x}{L}\right) e^{J\omega T}$$

$$\phi = \phi \cos\left(\frac{N \pi x}{L}\right) e^{J\omega T}$$

where, the functions in x satisfy the boundary conditions.

Substituting in the equations of motion we get the algebraic equation:

$$\lambda^4 \left(\frac{E}{GK}\left(\frac{k}{L}\right)^4\right) - \lambda^2 \left(1 + \left(\frac{E}{GK} + 1\right)\left(\frac{k}{L}\right)^2 N^2\pi^2\right) + N^4\pi^4 = c$$

where non-dimensional frequency is $\lambda = \sqrt{\dfrac{\rho L^4}{Ek^2}} \cdot \omega$ and N is

the mode number. This is a bi-quadratic equation which can

be reduced to a quadratic with two roots for each value of N

and for given values of k/L and E/GK. The lower root

corresponds to the bending mode and the higher to the shear

mode.

2.3 Results and discussion

2.3.1 Performance of TM544 element

Table 2.2 gives the comparison of the three elements

derived in Appendix A. A thick beam with a k/L value of

0.08, E/G=2.6 and shape factor k=0.85 is used. The three

elements are tested with a beam modelled by eight and four

elements. The degrees of freedom for these two models are:

thirty six and twenty. Thus, the comparison tests the

accuracy of the polynomials chosen and the constraint

conditions used per degree of freedom and per element. It is

seen that TM544 converges to the exact value faster than the

other two; even a four element twenty degree model gives the

first four eigenvalues accurately.

It is interesting to note that the lower shear modes(0

and 1) are accurately obtained in all three elements, even

though the global mode number is high(5 and 7). In the case

of TM654 and TM624 some of the higher shear modes converged

before the lower bending modes.

Table 2.2. Comparison of TM544, TM654 and TM624
for a S.S beam: E/G=2.6, k*L=0.08, K=0.85.

Mode #	Exact	TM544	TM654	TM624
		Using eight elements		
1	8.8398	8.8398	8.8416	8.8398
2	28.461	28.461	28.467	28.464
3	51.497	51.497	51.549	51.546
4	75.364	75.369	75.696	75.693
5*	89.339*	89.339	89.339	89.339
6	99.301	99.341	99.748*	99.748*
7*	99.748*	99.748	100.73	100.73
8	123.09	123.21	123.94*	123.94*
9*	123.92*	123.92	127.55	127.55
		Using four elements		
1	8.8398	8.8398	8.8416	8.8406
2	28.461	28.465	28.535	28.534
3	51.497	51.547	52.891	52.890
4	75.364	75.712	75.712	78.712
5*	89.339*	89.339	89.339	89.339
6	99.301	99.805	99.764*	99.764*
7*	99.748*	99.748	123.98*	123.98*

* shear modes.

If the shear variable is given enough representation, then the lower modes corresponding to bending and shear converge at least equally well irrespective of their global nodal position. This is a definite indication of the independence of the bending and shear modes for a simply supported case.

TM654(with constraint $\psi'' = 0$) implies a linear shear variable and can be expected to perform equally with TM624 for the pure shear modes, if shear mode is independent of the representation of the bending slope. The shear mode frequencies are the same for both four and eight element comparison. The bending modes also, surprisingly, perform equally well: the higher order polynomial representation of TM654 is superfluous.

TM544 with lower order polynomials than TM654 and higher than TM624(with a linear shear variable) has an implied quadratic representation of the shear variable and performs better than the other two elements. The performance gets better at the higher modes where shear has an increasing effect.

Comparison of these three elements is made with different k/L ratios, end conditions and elements. TM544 is found to perform better and is the one selected for the rest of the text.

In Appendix A, an element is presented which uses trigonometric functions instead of the customary algebraic functions.

Table 2.3 gives the exact natural frequencies of a
simply supported beam with E/G=2.6 and K=0.85 for different
k/L ratios and mode numbers(n=0 to 4 for shear and 1 to 5
for bending). An eight element model results are compared
with the exact results to test convergence and accuracy. It
can be seen that for slender beams with low k/L values, the
higher order polynomials are superfluous. For low k/L values
the shear modes occupy very high global position, yet they
are accurately obtained.

The results match closely with the exact solution,
especially for k/L greater than or equal to 0.04. The higher
order Timoshenko beam representation now becomes effective
and the accuracy of the element is maintained even for large
k/L values and mode numbers.

The close prediction of the shear modes, even the
fourth mode, using just eight elements, is very encouraging.
It is a result of allowing a quadratic representation for
the shear variable instead of the usual constant or linear
variation.

Single precision is used in all the calculations of the
finite element analysis and might be responsible for the
discrepancies in the last few digits.

Convergence and rate of convergence are important
aspects of a finite element. Convergence assures that the
expected accuracy can be obtained and rate of convergence
decides how few elements are needed to do so. In Table 2.4
we have the results of a simply supported beam with E/G=2.6,

Table 2.3 Effect of k/L on the natural frequencies

k/L	0.01		0.02		0.04		0.06		0.08		0.12	
Mode	Exact	TM544	Exact	TM544	Exact	TM544	Exact	TM544	Exact	TM544	Exact	TM544
BENDING MODE FREQUENCIES												
1	10.446	10.074	9.8212	9.8174	9.5781	9.5709	9.2406	9.2407	8.8398	8.8398	7.9618	7.9620
2	39.284	39.191	38.292	38.297	35.359	35.357	31.847	31.847	28.461	28.461	22.887	22.887
3	87.309	87.234	83.166	83.171	71.655	71.657	60.542	60.542	51.497	51.498	38.819	38.820
4	153.17	153.17	141.43	141.46	113.84	113.85	91.551	91.562	75.364	75.374	54.710	54.717
5	235.44	235.53	210.11	210.20	159.13	159.19	123.33	123.38	99.301	99.342	70.423	70.451
SHEAR MODE FREQUENCIES												
0	5717.7	5718.7	1429.4	1429.4	357.35	357.35	158.82	158.82	89.339	89.339	39.706	39.705
1	5729.1	5727.9	1440.8	1440.8	368.50	368.50	169.64	169.63	99.748	99.749	49.220	49.220
2	5763.2	5763.1	1474.0	1474.0	398.99	398.99	196.88	196.88	123.92	123.92	68.487	68.487
3	5819.2	5821.1	1526.7	1526.7	442.98	442.99	233.02	233.02	154.09	154.10	90.855	90.857
4	5896.1	5893.1	1595.9	1596.0	495.68	495.69	273.95	273.97	187.19	187.21	114.60	114.61

Effect of k/L on a S-S Beam, E/G = 2.6, K = 0.85, Comparison with Exact Solution

Table 2.4 Eigenvalues for a S-S beam

Mode	Exact	Number of Elements					
		1	2	3	4	5	8
1	8.8393	8.8557	8.8408	8.8398	8.8398	8.8398	8.8398
2	28.461	46.318	28.548	28.477	28.465	28.462	28.461
3	51.497		53.493	51.702	51.547	51.514	51.497
4	75.364			76.671	75.712	75.462	75.369
5*	89.339	89.339	89.339	89.339	89.339	89.339	89.339
6*	99.748			99.748	99.748	99.748	99.748
7	99.301				100.463	99.805	99.341
8*	123.92	89.339			123.92	123.92	123.92
9	123.09						123.21

* Shear Mode Frequencies

Eigenvalues for a S-S Beam, $E/G = 2.6$, $k/L = 0.08$, $K = 0.85$

k/L=0.08 and K=0.85 using 1 to 8 elements. The shear mode frequencies converge fast: the zero order mode is obtained with just one element as it has a constant value. The bending modes also have a healthy convergence.

Rate of convergence of the first few natural frequencies is shown in Figure 2.3; percentage error is given against number of elements used. Efficiency of programming and use of single precision account for part of the error. As the number of elements increases the relative percentage error drops to zero asymptotically, which is a good sign for the element.

Dawe's is the most efficient of the elements present. Comparison of the rate of convergence of the present element with Dawe's and exact values is shown in Table 2.5. For a slender beam, k/L =0.008, Dawe's element converges faster. For thicker beams, k/L =0.04 and 0,08, TM544 is more accurate and converges faster; requiring only eight elements to converge to the exact values. Whereas, Dawe's element doesn't quite converge for higher modes, even with sixteen elements.

This is yet another example of how the constraint condition used can offset the advantages of higher order polynomial representation. Dawe uses a quintic polynomial for the displacement and a quartic for the bending slope. A constraint condition is used to evaluate five constants, which makes the element stiffer than expected from the interpolation functions used. The present element which

Table 2.5 Comparison of convergence for a S-S beam

% Variation

k/L	Mode	Exact	1 Element		2 Elements		3 Elements		4 Elements		6 Elements		8 Elements	
			Dawe's	TM544	Dawe's	TM544	Dawe's	TM544	Dawe's	TM544	Dawe's	TM544	Dawe's	TM544
0.008	1	9.8475	0.03	0.23	0.00	0.09	0.00	0.01	0.00	0.00	0.00	0.00	0.00	0.00
	2	39.278			0.04	0.10	0.00	0.05	0.00	0.01	0.00	0.00	0.00	0.00
	3	87.823			0.37	4.15	0.05	0.10	0.00	0.09	0.00	0.01	0.00	0.00
	4	157.79					0.20	1.95	0.06	0.11	0.00	0.05	0.00	0.00
0.04	1	9.5710	0.08	0.12	0.00	0.01	0.00	0.00	0.00	0.00	0.00	0.00	0.00	0.00
	2	35.359			0.19	0.17	0.02	0.05	0.00	0.01	0.00	0.00	0.00	0.00
	3	71.657			1.40	4.14	0.33	0.24	0.09	0.09	0.04	0.01	0.02	0.01
	4	113.85					1.08	1.05	0.45	0.29	0.13	0.04	0.08	0.04
0.08	1	8.8397	0.19	0.18	0.00	0.01	0.00	0.00	0.00	0.00	0.00	0.00	0.00	0.00
	2	28.461			0.46	0.30	0.13	0.05	0.08	0.01	0.04	0.00	0.03	0.00
	3	51.498			2.46	3.87	0.62	0.39	0.29	0.09	0.14	0.01	0.09	0.01
	4	75.365					1.72	1.12	0.69	0.46	0.27	0.05	0.16	0.05

Comparison of Convergence for S-S Beam, E/G = 2.6, k = 0.85, With Dawe's Element
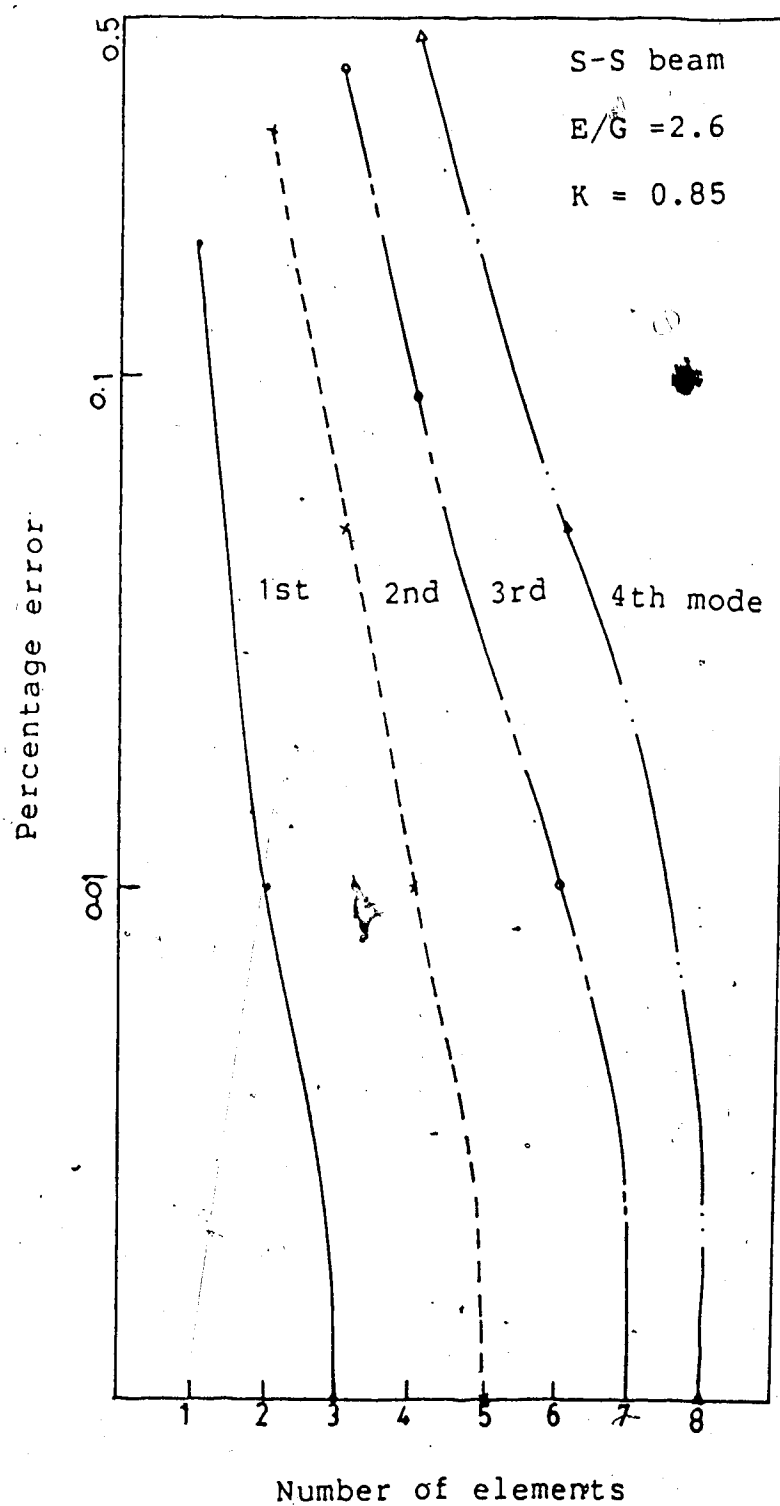
Figure 2.3 Rate of convergence of TM544

obtains only one constant from the constraint condition
appears to be less restrained.

Dawe has not given higher order frequencies, therefore
comparison of the shear frequencies was not possible. Dawe
had a constant shear along the element and may not obtain
the higher order shear frequencies accurately.

Representation of the boundary conditions was a major
problem with the earlier elements. Thomas- Abbas developed
their element to represent all the rigid boundary
conditions. They could do so only for a uniform beam, with a
linear combination of the nodal variables used. The
Timoshenko beam end conditions for non-uniform beam are
developed in Appendix A. In our element all these end
conditions can be directly applied. Thomas Wilson's element
doesn't have ϕ' as a nodal variable and can't represent
bending moment.

Table 2.6 gives a comparison of the present element
with Davis(17), Thomas Abbas[22] and Kapur[19]. Simply
supported and clamped free cases are considered with E/G=2.6
and k/L=0.08. In all the cases TM544 is seen to be more
accurate per degree of freedom. It is also seen that the
error is negligible, though only four elements are
considered.

2.3.2 Second spectrum

Following Trail-Nash and Collar, Thomas-Abbas and
Bhashyam-Pratap classified the Timoshenko beam frequencies

Table 2.6 Comparison with Kapur, Davis, Thomas-Abbas

elements; % variation

a) S.S, E/G = 2.6, K = 0.85, k/L = 0.08, 16 Degrees of Freedom

Mode	1	2	3	4
Exact	8.8397	28.461	51.498	75.364
TM544	0.00	0.01	0.09	0.45
Davis	0.09	0.98	3.19	6.81
Thomas-Abbas	0.00	0.04	0.17	0.86

b) S.S, E/G = 2.6, K = 0.68, k/L = 0.08, 16 Degrees of Freedom

Mode	1	2	3	4
Exact	8.6450	26.960	47.680	68.726
TM544	0.00	0.01	0.09	0.50
Kapur	0.01	0.23	0.74	8.12
Thomas-Abbas	0.00	0.03	0.17	0.82

c) C - F, E/G = 2.6, K = 0.85, k/L = 0.08, 16 Degrees of Freedom

Mode	1	2	3	4
Exact	3.3241	16.289	36.708	58.279
TM544	0.00	0.00	0.03	0.15
Davis	0.01	0.31	1.54	3.69
Thomas-Abbas	0.00	0.00	0.05	0.22

d) C - F, E/G = 2.6, K = 0.65, k/L = 0.08, 16 Degrees of Freedom

Mode	1	2	3	4
Exact	3.3241	16.289	36.708	58.279
TM544	0.00	0.00	0.03	0.14
Kapur	0.00	0.06	0.30	0.66
Thomas-Abbas	0.00	0.01	0.05	0.20

into coupled component modes: Thomas-Abbas denied the existence of two separate spectra while Bhashyam used a reduced one point integration to claim otherwise. The present higher order element is used to obtain the results of Bhashyam. Bhashyam classified the spectrum into two bands: W mode and the θ mode. The first spectrum W mode is bounded by C (natural frequency of the Euler-Bernoulli beam for low k/L and of the simple shear beam for high k/L). The second spectrum θ mode has shear component frequencies C as the lower bound. C_1 and C_2 are the results obtained by Bhashyam for the 1st and 2nd spectrum. Table 2.7 compares the present element results with Bhashyam's for the shear mode. Though his results are confirmed by present analysis, division of the frequencies into two spectra is still a classification to be settled.

The zeroth pure shear mode as obtained in a hinged-hinged beam (from exact and finite element analysis) has interesting physical implications:

1. It is a rigid or zero mode vibration. Unlike the rigid body translation and rotation it occurs at a non-zero frequency. The zero frequency modes are prevented by prescribing a displacement and a rotation at some point on the beam. Similarly the shear rigid mode can be prevented by prescribing bending slope which happens for a fixed end or by prescribing the shear slope which occurs at a free end (In the zero mode, bending and shear slopes are equal prescribing one of them is

Table 2.7 Shear mode comparison with Bhashyam

Mode	Method	0.04				0.08				0.12			
		C-F	H-H	H-C	C-C	C-F	H-H	H-C	C-C	C-F	H-H	H-C	C-C
θ₀	C₂		357.36				89.34				39.71		
	Cps		357.36				89.34				39.71		
	TM544		357.36				89.34				39.71		
θ₁	C₂	370.75	368.51	360.16	369.25	94.86	99.75	92.04	99.59	42.27	49.22	42.51	48.32
	Cps	359.5i	365.89	359.51	365.89	91.47	97.59	91.47	97.59	41.81	47.56	41.81	47.56
	TM544	371.42	368.50	360.30	368.23	94.46	99.75	92.04	99.36	49.28	49.22	42.58	48.26
θ₂	C₂	394.65	399.07	381.40	392.89	107.81	123.92	111.40	123.67	65.56	68.49	58.22	66.70
	Cps	376.28	390.86	376.28	390.26	107.01	118.95	107.01	118.95	55.85	65.71	55.85	65.71
	TM544	388.47	398.99	381.53	399.11	114.76	123.92	110.78	123.25	65.62	68.46	58.70	66.33

sufficient). Thus zeroth shear mode can only occur for the hinged-hinged beam.

2. In the zeroth mode, bending slope and shear slope are equal resulting in zero displacement. Detection of this mode will be difficult though strong rotations occur in the beam.

3. Constant bending slope gives a zero bending moment, hence strain energy in bending is zero. Strain energy is stored in shear alone and kinetic energy is due to rotation. Translation is completely absent. The resulting natural frequency is $\omega = \sqrt{GK/\rho k^2}$.

From the eigenvalue results of a beam with different end conditions, we can get the shear dominant and bending dominant spectra. The effect of the beam thickness on these two spectra is shown for a hinged-hinged (H-H) beam in Figure 2.4 and for a clamped free (C-F) beam in Figure 2.5. The separation of the modes can be quantitatively visualized from the global modal position (global mode numbers are the mode numbers obtained by arranging the eigenvalues in the ascending order). To illustrate, for both H-H and C-F cases, the first ten global modes consist of bending modes only, when $k/L = 0.01$; when $k/L = 0.12$, there are four shear and six bending modes.

For low k/L value, a slender beam, the resistance to bending is low while resistance to shear is high; hence all lower modes are bending dominant. As the thickness of the beam increases the shear stiffness drops, strain energy
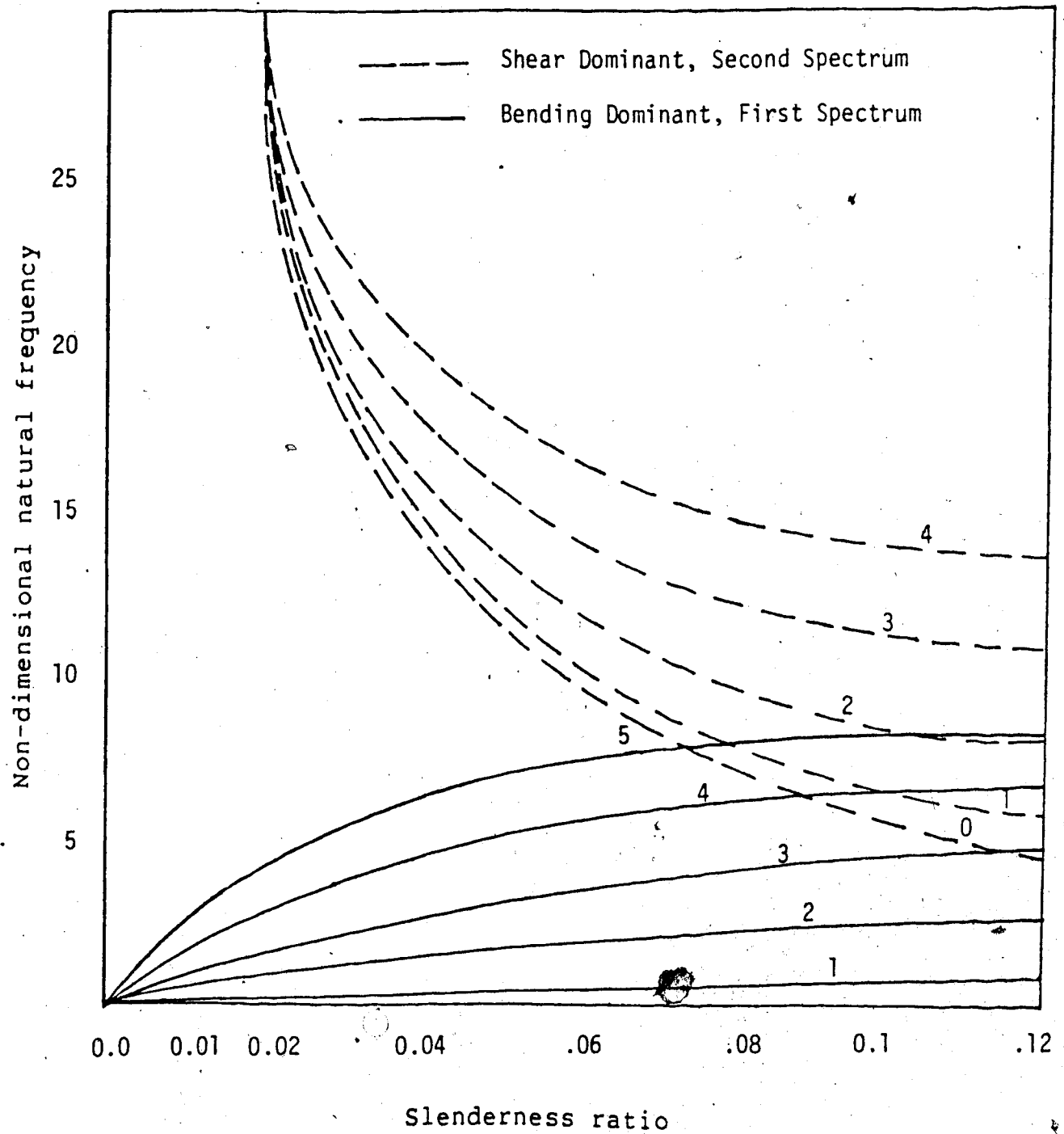
Figure 2.4 First and second spectra of a H-H beam.
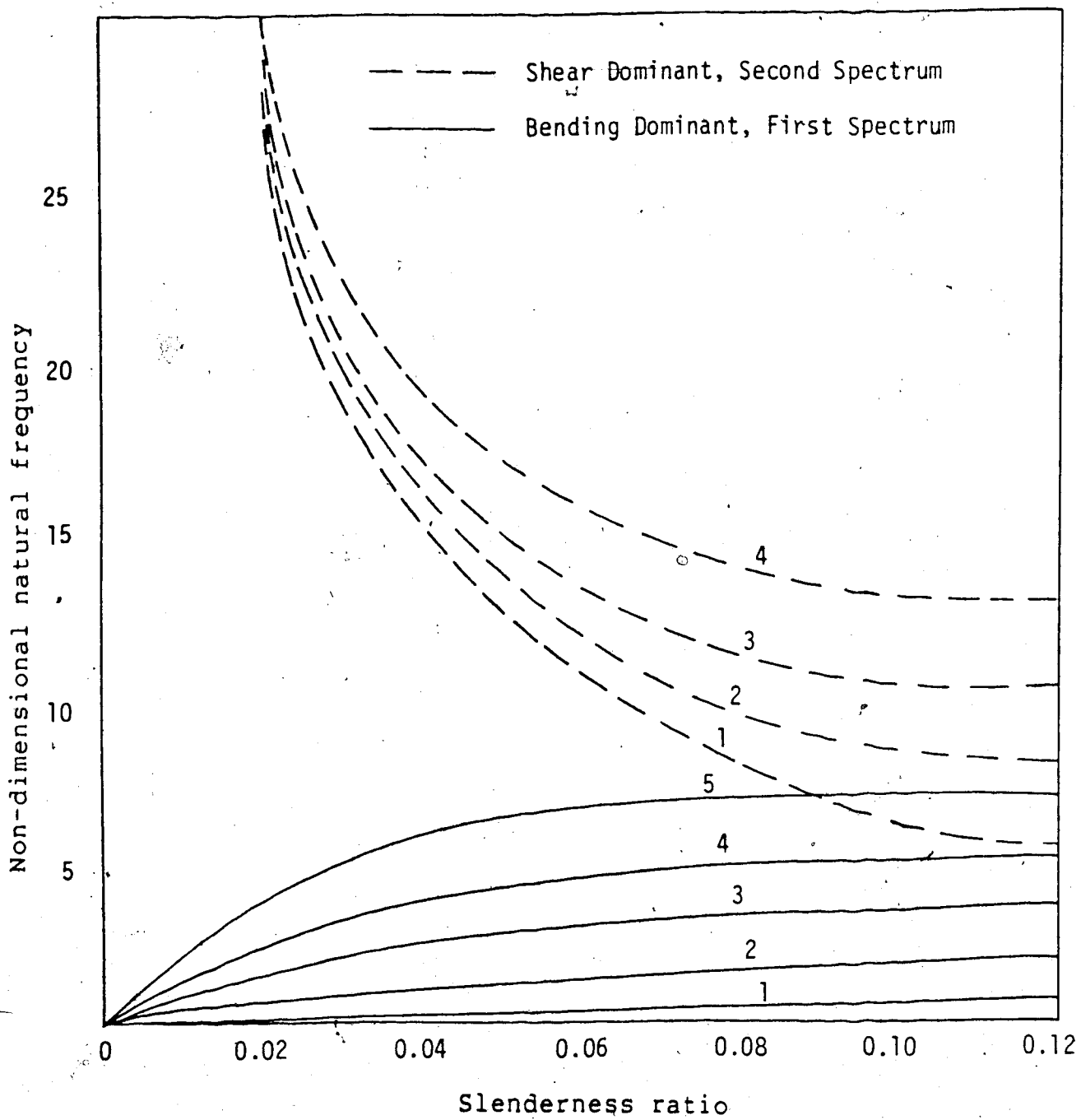
Figure 2.5 First and second spectra of C-F beam

stored in shear increases and the shear dominant frequencies are lowered. For large k/L values shear modes are encountered even for low global modes and a good representation of shear in the finite element becomes necessary.

For large k/L ratios bending and shear modes are interlocked. When k/L = .12 three shear modes interspace the five bending modes of a H-H beam; one shear mode overlaps the lower five bending modes of a C-F beam. The shear frequencies, in the case of a H-H beam, decrease more steeply with increase in k/L, compared to the C-F case, indicating that it has less shear resistance.

Mode shapes for different end conditions and global mode numbers are obtained. For the case of a simply supported beam the division is distinct and can be compared to the analytical solution. The bending dominant and shear dominant modes are shown in Figures 2.6 and 2.7.

In each case the displacement, W, bending slope, ϕ, and shear force, $A\psi$, are drawn. The parameters used are k/L=0.12, K=0.85 and E=2.6. Shear slope is amplified by the area and hence appears to dominate over the bending slope. For a uniform beam, the variable ψ can be used instead of $A\psi$ to obtain the mode shapes to the same scale.

The zeroth shear mode is shown, with equal bending and shear slopes and zero displacement. In the first spectrum, bending and shear slopes are out of phase: ϕ and ψ amplify the displacement amplitude. Whereas in the second spectrum
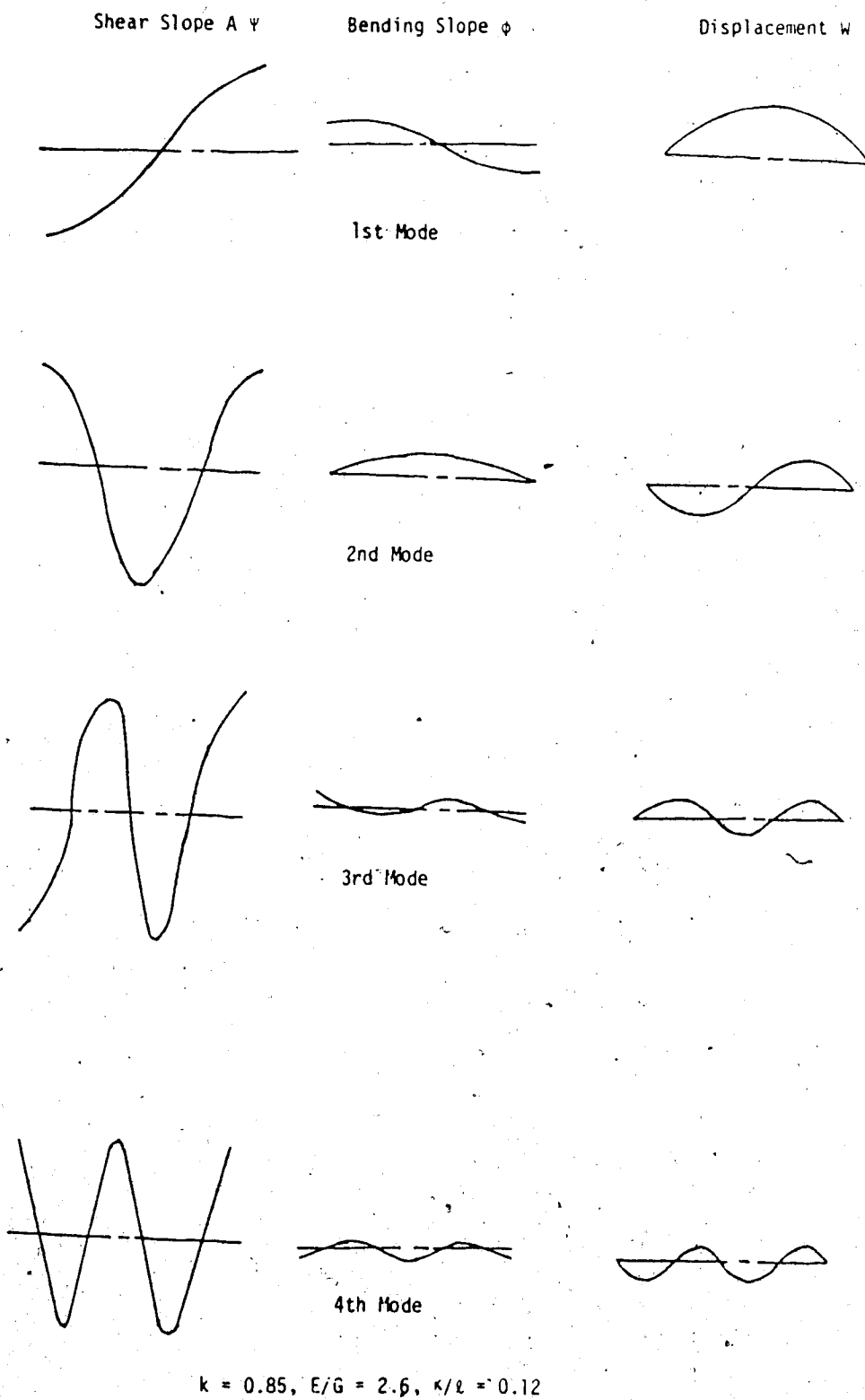
Figure 2.6 Bending dominant, first spectrum, modes

61
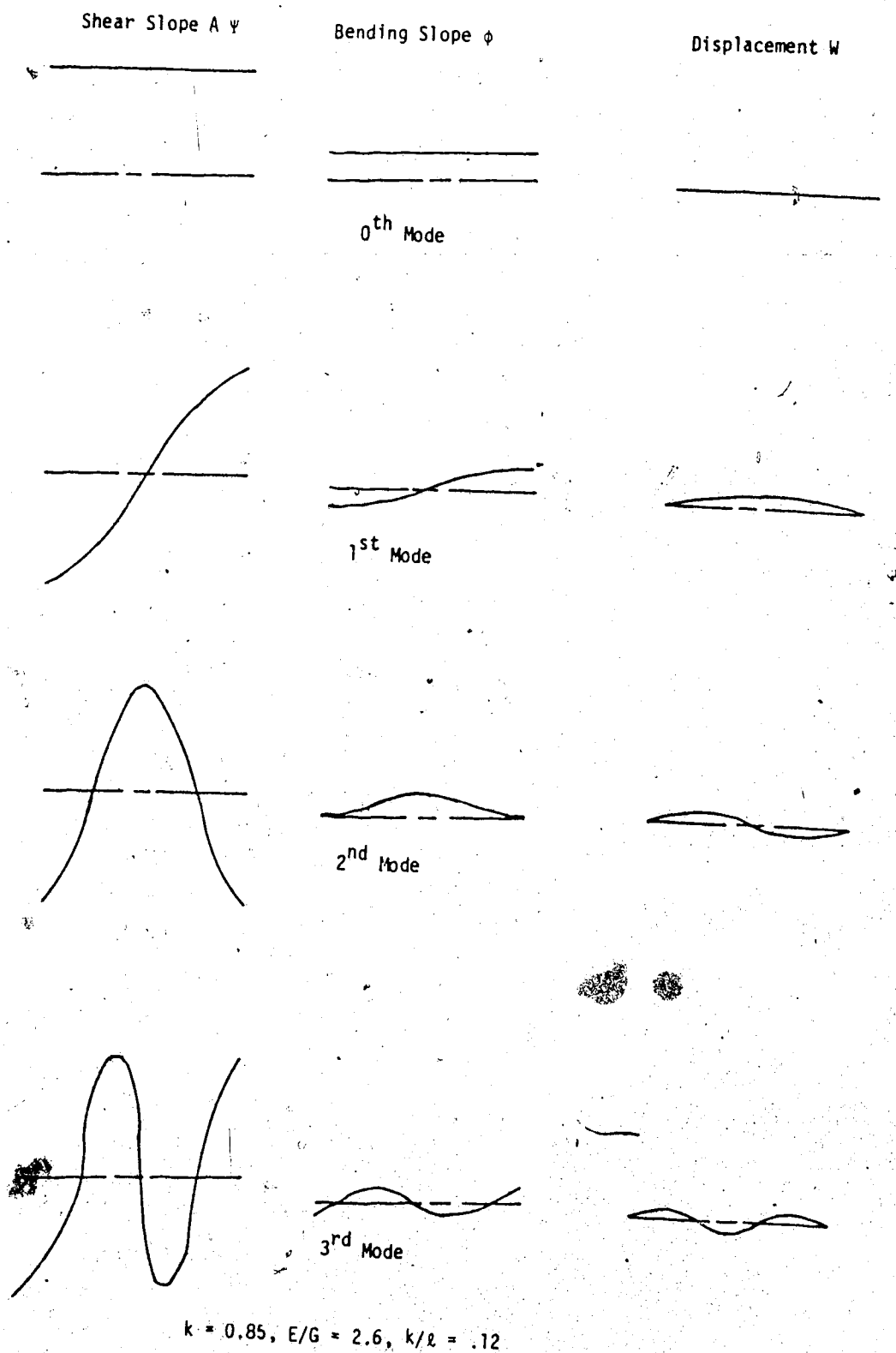
Figure 2.7 Shear dominant, second spectrum, modes

they nullify each other decreasing the displacement
amplitude.

The mode shapes obtained also conform to the exact
trigonometric solution used, giving a sine curve for
displacement and a cosine curve (in and out of phase) for
the bending and shear rotations.

2.3.3 Tapered beam

Table 2.8 shows the comparison of the natural
frequencies for a chimney type structure, with Thomas[22]
and a shell type element given in Thomas. Thomas used a 10
element, 30 degree of freedom model. A 4 element, 16 degree
of freedom model of the present element is used. Good
agreement is shown for the first six modes even with the few
elements used and convergence seems to be faster.

Table 2.9 gives the eigenvalues for double tapered
elements with both dimensions h and b having a linear taper
along the length. Comparison with To[31] is not possible as
he has not given the cross-section type and k/L values,
which are important for a Timoshenko beam. Earlier
authors[28], [29] did not consider these factors as their
model was based on the Euler beam theory.

In Table 2.10 comparison is obtained with To's element.
To[32] modified the Thomas[22] element for a linearly
varying beam and called it TB31. It has 6 degrees of freedom
per element as does his next element TB5 which is also used
for comparison.

Table 2.8. Comparison of the natural frequencies(Hz) of the beam type modes of vibration of a chimney with Thomas.

Mode #	Thomas	TM544	Shell element
# of elements	10	4	20
# of d.o.f	30	16	80
1	0.5096	0.4988	0.5105
2	2.6920	2.6402	2.6955
3	6.5090	6.4046	6.5119
4	11.073	10.927	11.045
5	16.070	16.000	15.910
6	21.338	21.418	20.822

Table 2.9. Natural frequencies $\omega L^2 \sqrt{\rho A_0 / EI}$ of linear double
tapered beams; k/L=0.025, ⊖lar c.s, E/G=2.6, K=0.85,
4 elements, taper is same.

Mode#	Taper $a=\beta=.1$	Taper $a=\beta=.2$	Taper $a=\beta=.4$	Taper $a=\beta=1$
1	3.4264	3.8834	3.8785	3.4739
2	8.6417	10.876	14.203	21.205
3	19.908	24.873	34.101	56.670
4	36.546	47.201	65.170	104.80
5	60.187	71.158	98.330	162.57

Table 2.10. Comparison of eigenvalues, $\omega L^2 \sqrt{\rho A_0 / E I_0}$: a double tapered circular thin walled cantilever beam. $l/d_0 = 10$, with To.

Mode#	Type	# of elmts	$a=1.0, \beta=.6$	$a=1.0, \beta=.8$	$a=1.0, \beta=1.0$
1	TB31	10	3.6818	3.5511	3.9692
	TB5	10	3.7370	3.6082	4.0699
	TM544	4	3.3495	3.3960	3.4584
2	TB31	10	17.717	18.811	22.133
	TB5	10	19.113	20.621	25.443
	TM544	4	16.573	18.307	19.811
3	TB31	10	42.928	46.426	54.062
	TB5	10	50.353	56.192	71.241
	TM544	4	40.612	45.444	49.589
4	TB31	10	75.117	80.776	91.624
	TB5	10	96.995	109.31	139.60
	TM544	4	72.0973	79.530	85.855
5	TB31	10	111.93	119.30	132.30
	TB5	10	159.17	180.16	230.77
	TM544	4	108.42	118.63	126.21

The shape factor used in the present case is K=0.531 for a thin annular cross-section. The eigenvalues obtained by the present element are lower than To's for a lesser number of elements, indicating faster convergence: the higher order element having a better performance. To[31,32] claimed that he could represent all the boundary conditions with his element. Table 2.11 shows how he was wrong in representing bending slope, bending moment and shear force.

2.3.4 Static response

In Appendix B, analytical solutions of a Timoshenko beam are given for different end conditions and loadings. Comparison with a four element model is given in Table 2.12. A beam with length L=50.0", E/G=2.6, K=0.85 and load P=10.0 lbs is used. Only half the beam length is considered for symmetrical structures.

The analytical results given in Appendix B can be used to find the response of a statically indeterminate beam using a superposition technique. Table 2.13 shows the analysis of a 60" long, 2.4" radius beam with hinges at the ends and in the middle. The beam weight is lumped at the node points which is the only static force considered. The shear force is uncoupled at the node points where external load is present since shear discontinuity occurs. The discontinuity is distinguished by $GKA\psi$ and $GKA\psi$ referring to the shear force on the left and right sides of the node i. The six element results compare well with the analytical

Table 2.11 Boundary conditions: Tapered beam

Boundary	Constraint	TM544	TO
Fixed	Bending slope $= 0$	$\phi = 0$	$\dfrac{\partial W}{\partial x} = 0$
Free	Moment $= 0$	$I(x)\,\dfrac{\partial \phi}{\partial x} = 0$	$\dfrac{\partial^2 W}{\partial x^2} = 0$
	Shear force $= 0$	$A(x)\,\Psi = 0$	$I(x)\,\dfrac{\partial^3 W}{\partial x^3} +$
			$\dfrac{\partial I(x)}{\partial x}\,\dfrac{\partial^2 W}{\partial x^2} = 0$

Table 2.12 Static response with Timoshenko beam

Variable	Node	Clamped – Free			Simply Supported			Clamped-Clamped		
		Exact	F.E.	% Error	Exact	F.E.	% Error	Exact	F.E.	% Error
W	1	0.0	-	-	0.0	-	-	0.0	-	-
	2	$.12698 \times 10^{-3}$	$.12732 \times 10^{-3}$	.26	$.63490 \times 10^{-4}$	$.63487 \times 10^{-4}$	0.004	$.11681 \times 10^{-4}$	$.11682 \times 10^{-4}$	0.008
	3	$.46119 \times 10^{-3}$	$.46236 \times 10^{-3}$	.25	$.92441 \times 10^{-4}$	$.92439 \times 10^{-4}$	0.002	$.23364 \times 10^{-4}$	$.23364 \times 10^{-4}$	0.000
	4	$.9335 \times 10^{-3}$	$.93573 \times 10^{-3}$	.23						
	5	1.4750×10^{-3}	1.4782×10^{-3}	.21						
ϕ	1	0.0	-	-	46051×10^{-6}	46049×10^{-6}	0.004	0.0	-	-
	2	$.16118 \times 10^{-5}$	$.16160 \times 10^{-5}$	.26	$.34538 \times 10^{-6}$	$.34548 \times 10^{-6}$	0.000	$.11512 \times 10^{-6}$	$.11513 \times 10^{-6}$	0.008
	3	$.27695 \times 10^{-5}$	$.27695 \times 10^{-5}$	.23	0.0	0.0	-	0.0	0.0	-
	4	$.34538 \times 10^{-5}$	$.34608 \times 10^{-5}$	.20						
	5	$.36841 \times 10^{-5}$	$.36909 \times 10^{-5}$	.18						
AΨ	1	$.10196 \times 10^{-5}$	$.10230 \times 10^{-5}$	.33	$.50980 \times 10^{-6}$	$.50947 \times 10^{-6}$	0.064	$.50980 \times 10^{-6}$	$.50977 \times 10^{-6}$	0.005
	2	$.10196 \times 10^{-5}$	$.10237 \times 10^{-5}$	.40	$.50980 \times 10^{-6}$	$.50985 \times 10^{-6}$	0.009	$.50980 \times 10^{-6}$	$.50987 \times 10^{-6}$	0.013
	3	$.10196 \times 10^{-5}$	$.10230 \times 10^{-5}$	.33	$.50980 \times 10^{-6}$	$.50973 \times 10^{-6}$	0.013	$.50980 \times 10^{-6}$	$.50980 \times 10^{-6}$	0.000
	4	$.10196 \times 10^{-5}$	$.10217 \times 10^{-5}$	.20						
	5	$.10196 \times 10^{-5}$	$.10232 \times 10^{-5}$	.35						
Iϕ'	1	$.19999 \times 10^{-3}$	$.20060 \times 10^{-3}$	.30	0.0	-	-	$.24999 \times 10^{-4}$	$.25003 \times 10^{-4}$	0.016
	2	$.14999 \times 10^{-3}$	$.15038 \times 10^{-3}$	.26	$.24999 \times 10^{-4}$	$.24999 \times 10^{-4}$	0.000	0.0	0.0	-
	3	$.99999 \times 10^{-4}$	$.10017 \times 10^{-3}$	.17	$.49999 \times 10^{-4}$	$.49999 \times 10^{-4}$	0.000	$.04999 \times 10^{-4}$	$.25002 \times 10^{-4}$	0.012
	4	$.49999 \times 10^{-4}$	$.50030 \times 10^{-4}$	.06						
	5	0.0	0.0	-						

Static Test Results of a Beam: Length L = 50.0'; Radius R = 1.0'; E/G = 2.6, k = 0.85; P = 10.0 lbs; 4 Elements

Table 2.13. Continuous steel beam; static analysis due to its own weight. $L=60"$, $r=2.4"$, $K=0.85$, $E/G=2.6$.

Response	Exact results	6 element F.E model
Displacement		
W_1	0.0	.2838E-09
W_2	.2898E-04	.2899E-04
W_3	.2176E-04	.2177E-04
W_4	0.0	.4430E-09
Rotation		
ϕ_1	.3441E-05	.3443E-05
ϕ_2	.1226E-05	.1227E-05
ϕ_3	-.2119E-05	.2119E-05
ϕ_4	0.0	.4876E-20
Bending moment		
$EI\phi_1'$	0.0	-.4963E-04
$EI\phi_2'$	-.3464E+03	-.3464E+03
$EI\phi_3'$	-.1769E+03	-.1769E+03
$EI\phi_4'$	+.5084E+03	+.5084E+03
Shear Force		
$GKA\Psi_1$	-.3464E+02	-.3464E+02
$GKA\Psi_{1L}$	-.3464E+02	-.3464E+02
$GKA\Psi_{1R}$	+.1694E+02	+.1694E+02
$GKA\Psi_{2L}$	+.1694E+02	+.1694E+02
$GKA\Psi_{2R}$	+.6854E+02	+.6854E+02
$GKA\Psi_{3L}$	+.6854E+02	+.6854E+02
$GKA\Psi_{3R}$	-.6854E+02	-.6854E+02
Bearing reactions		
R1	60.4405(lbs)	60.4407(lbs)
R2	188.677(lbs)	188.676(lbs)

solution.

2.4 Conclusions

General development of higher order elements using a constraint condition is shown. Appendix A gives the formulation for four elements, one of which uses trigonometric functions. A particular element, TM544, was chosen. It uses a constraint condition, $\psi''' = 0$, and has eight degrees of freedom, four at each node, to represent the beam parameters: displacement, W, bending slope, ϕ, shear force, $A\psi$, and bending moment, $I\phi'$.

The new element presented converges rapidly to the exact solution. It is found to be more accurate per degree of freedom and per element compared to the existing elements. The nodal variables chosen allow complete compatibility at uniform and non-uniform cross-sections and direct representation of all the rigid boundary conditions.

Appendix A gives the correct boundary conditions for a non-uniform beam. Higher order taper is achieved using numerical integration. Comparisons are made with some standard results.

In the case of a simply supported beam, exact solutions for the two separate spectra are obtained and finite element results match well with these. The zeroth natural frequency corresponding to the pure shear mode is identified. The high order shear representation helps in the accurate and easy convergence of the shear dominated natural frequencies.

Appendix B gives the analytical results for a Timoshenko beam in static equilibrium for some standard cases of loading and boundary conditions. The Euler beam can be replaced by the Timoshenko beam wherever deep beams are present. Superposition can be used to evaluate other loading conditions and indeterminate beams. The stiffness matrix of the finite element is tested for statically determinate and indeterminate structures.

3. APPLICATION OF BEAM ELEMENT TO A WHIRLING SHAFT

Abstract

In continuous shaft whirling with nonparallel whirl and spin axes, an elemental length undergoes a gyroscopic moment. The moment has been calculated for a general asymmetric shaft with an arbitrary spin to whirl ratio by applying the Euler equations of motion. With a proper representation of the gyroscopic moment, the beam element is extended to represent a whirling shaft. The finite element results are compared with the analytical solutions for simple supports with those of Rouch and finally with the Ritz method.

3.1 Introduction

Rankine[40] in 1869 was the first to study rotors, considering the centrifugal forces and the shaft stiffness. Jeffcot's model[41] of a symmetrical rotor with a massive disk in the middle is still used in the experimental studies on bearings and rotor. He was the first to consider viscous damping to explain the phase between the plane of bending and the plane containing unbalance. Kimball[42] studied the effect of internal damping due to hysteresis in the rotor. Bishop[43] reviewed the rotating shaft theory and exposed the mechanical analogy that exists between a simple conical pendulum whose centre of support is given a circular motion,

and a whirling shaft. Bishop, with his associates[44,45,46] developed the receptance method and modal summation method for shafts.

Lowey and Piarulli[47] gave definitions and a detailed list of references concerning different aspects of rotor dynamics. They mentioned that critical speed should be the term used for rotors instead of natural frequency; critical speed is the running speed of the shaft at which the whirling orbit becomes unbounded.

Eshleman and Eubanks[48] gave an analytical solution for the critical speeds of a continuous rotor including the effects of transverse shear, rotatory inertia and gyroscopic moments, and acted upon by an axial torque.

The results show that the change in critical speeds depends on the slenderness ratio k/L. If k/L is below 0.0025, a constant axial torque tends to decrease the effective stiffness of the rotor and lowers its critical speed, other effects having little importance. If the slenderness ratio is above 0.0025, gyroscopic moment, rotatory inertia and transverse shear effects become important and two critical speeds(backward whirl, forward whirl) are obtained. Physically allowable(strength) torques have a negligible effect on the critical speeds for shaft ratios greater than 0.0025.

Myklestad[49] introduced the transfer matrix method for finding the natural frequencies of beam type structures in flexural vibrations. In this method the structure is

subdivided into regions consisting of nodes and fields in between. Every node has a state vector consisting of the displacements and internal forces at that point. A point matrix relates the state vectors across a node and a field matrix relates across a field. The application of proper boundary conditions result in the necessary equations for a homogeneous solution or a response study. The Holzer method is the classical transfer matrix method used in determining the torsional critical speeds of shafts. In this method, incorporation of the boundary conditions needs intuitive manipulations. Calculation of the higher order criticals demand accuracy up to 8 decimal places or more as small differences of large numbers are involved.

Prohl[50] applied the transfer matrix method to rotors. The existing energy methods of Rayleigh-Ritz involved the selection of appropriate functions and tedious calculations. Whereas, with the transfer matrix method higher critical speeds can be calculated for a rotor with varying span lengths, cross-sections and multiple elastic supports. This approximate method is easily adaptable to computers and gained ready popularity. Lund[51], among many others has used this method extensively.

Gasch[52] stated that " Numerical experience even with the improved transfer matrix methods shows that they are not sophisticated enough to guarantee numerical stability". The more popular numerical method of finite elements was introduced for rotor analysis. With a beam element which

neglected the shear effect but included the translatory and rotatory inertia effects; he analyzed a large rotor system including internal and external damping, fluid film bearings and foundation effects.

Ruhl[53] studied the comparative merits of transfer matrix and finite element methods in detail. He used an Euler beam element, based on Archer's consistent mass formulation which possessed the following advantages over Prohl's method:

1. converges quickly even for higher modes with fewer number of elements;

2. mass can be consistently represented;

3. branching and boundary conditions are easily accounted for;

4. the transfer matrix algorithm of Prohl tends to be sensitive to system size; higher modes and rigid supports causing ill-conditioning of matrices;

One advantage in favour of the transfer matrix method is that it requires less computer memory storage than the finite element method; but even this is offset by the present day computer capacities.

Nelson[54] developed a rotating shaft element using a simple Timoshenko beam element in two planes. His element has two nodes and two degrees of freedom at each node, resulting in an eight degrees of freedom rotor element. For a uniform shaft he developed the equations of motion in the rotating and fixed co-ordinate systems.

Rouch and Kao[55], used the Thomas element[22] to obtain a linearly tapered shaft element. Shear deformation, and rotatory inertia terms were included. Shear condensation by static reduction was tried. Gyroscopic effects were found from the Lagrangian equations of motion for the whirling element.

A brief outline of a rotor system will be discussed before proceeding to the theory. A practical industrial rotor is usually a complicated system in physical structure and in its performance. Simplification occurs by identifying the major subsystems which can be individually modelled, studied and then assembled. The rotor system can be classified as:

1. the shaft:

    a.   can be uniform, tapered or stepped;

    b.   can be axisymmetric or asymmetric in cross-section with cross-sectional changes along the length (eg. hollow circular to solid circular);

    c.   contributes to the rotatory inertia/gyroscopic matrices;

    d.   has bending and shear stiffness in flexural motion;

    e.   has internal damping.

2. disks:

    a.   can be thin whose effects are functions of a point on the shaft axis. They contribute to the rotatory inertia and gyroscopic matrices but are rigid in

bending and shear deformation;

b. can be thick whose effects are functions of a portion of the shaft. Apart from the inertia effects they can also contribute to the stiffness and can be considered as steps on the shaft.

3. bearings:

a. rigid or ideal bearings which are incapable of storing energy (eg. bi-symmetric supports with two knife edges in two perpendicular planes or axi-symmetric supports with ball bearings);

b. flexible bearings which can store potential energy(these can be bi-symmetric, axi-symmetric or asymmetric);

c. massive bearings where the inertia of the bearings contributes to the kinetic energy;

d. fluid bearings which contribute asymmetric stiffness and damping matrices. Dissipative and non-conservative forces arise coupling the shaft motion and causing stability problems.

Foundation stiffness acts in series with the bearing stiffness; separate degrees of freedom can be alloted to represent a flexible foundation.

Forcing functions can be identified as:

1. static forces due to the weight of the shaft;

2. local and continuous mass unbalances due to shaft asymmetry and non-homogeneity;

3. concentrated or continuous unbalance due to asymmetric

shaft stiffness;

4. loading due to misalignment of the rigid couplings;

5. external loading due to steam pressure variations, gear meshing etc.

The mass and stiffness matrices developed to represent the beam element can be modified for the rotor element. Structural damping can be added to the rotor element; often called material or hysteresis damping, it is related to energy dissipation in solids due to various forms of internal friction at a macroscopic scale.

For heavy damping, phase difference between force and response occurs and also couples the motion of different modes and planes. If damping is light and uniform, the real modes of the undamped system are appropriate for the damped system, diagonalizing the system matrix. If { x } represents the system degrees of freedom, the homogeneous equations of motion for the damped case are:

$$[M]\{\ddot{x}\} + [C]\{\dot{x}\} + [K]\{x\} = \{0\}$$

$$\{x\} = \{x_0\} e^{st}$$

In general the eigenvalue, s, is complex and so is the eigenvector. The undamped system of equations are given as:

$$[M]\{\ddot{x}\} + [K]\{x\} = \{0\},$$

A solution of the type:

$$\{x\} = \{x_0\}e^{j\omega t}$$

can be assumed. The eigenvalue is ω_i and the eigenvector is $\{ x_0 \}_i$ for the ith mode. The modal matrix $[\phi]$ can be obtained with the eigenvectors forming its columns. The mass and stiffness matrices can be diagonalized with this modal matrix.

The damping matrix can also be diagonalized if it is linear:

$$[\phi]^T[C][\phi] = \lceil Ci \rfloor$$

Rayleigh damping is one such type; given as a linear combination of the mass and stiffness matrices:

$$[C] = c_1[M] + c_2[K]$$

The modes of the undamped system diagonalizes the damping matrix:

$$[C_i] = C_1 [M_i] + C_2 [K_i].$$

From the definition of damping ratio, for the ith mode we get:

$$\xi_i = \frac{C_i}{C_c} = \frac{C_1}{2\omega_i} + \frac{C_2 \omega_i}{2}$$

In each of the i modes we can obtain the damping ratios for selected values of C_1 and C_2. The decoupled equations of motion give the damped critical speeds as:

$$\omega_{Di} = \omega_i \sqrt{1 - \xi_i^2} .$$

In this Chapter we concentrate on the gyroscopic effects of a shaft whirling in a circular orbit. An axi-symmetric shaft with no internal damping but having bending and shear stiffness and a consistent mass is assumed. The higher order element developed in Chapter 2 is used to obtain an accurate shaft element.

3.2 Theory

A beam element vibrates in a plane when the resulting moment due to the rotatory inertia tends to deflect the beam and the natural frequencies are reduced due to the increased effective mass.

A shaft spins about its longitudinal axis and whirls about the undeformed axis resulting in a moment about a perpendicular axis called the gyroscopic couple. In general this moment links the motion in two perpendicular planes, as the moment in one plane depends on the bending slope in a different plane. For small deflections and a circular whirl the motion can be decoupled in each of the planes.

The axi-symmetric whirling shaft element will have similar expressions for the strain energy due to bending and shear deformation and kinetic energy in translatory motion as that of a beam allowing for the different interpretation put on displacement, W. However, the rotational kinetic energy is different.

Consider the force, F, and the moment, M, acting at the centre of an elemental shaft while whirling. The centrifugal force, F, is given as:

$$F = \omega^2 \rho A W dx$$

where ρ is the mass density, ω the whirling speed, A the cross-sectional area and W the displacement in the plane considered from the undeformed central axis. To find the gyroscopic moment of the elemental shaft, Rouch[55] defined the kinetic energy of the element in rotation and obtained the equations of motion from the Lagrange's method.

Here, we will start from the basic definition: the external moment acting on the shaft to sustain the prescribed motion is equal to the time rate of change of the resulting angular momentum. Figure 3.2 shows the undeformed, fixed axes $OX_1Y_1Z_1$ and the body centred rotating axes OXYZ. As the shaft rotates the element's moment of inertia and the product of inertia about the fixed axes change continuously and it will be necessary to find these values as functions of time. Instead, the rotating principal axes are chosen. Hence, the products of inertia vanish and the principal moments of inertia are constant with time. The resulting inertia tensor is diagonal of the form:

$$\rho[I] = \rho \begin{vmatrix} I_{xx} & 0 & 0 \\ 0 & I_{yy} & 0 \\ 0 & 0 & I_{zz} \end{vmatrix}$$

Where I_{xx}, I_{yy} and I_{zz} are the principal moments of inertia of the asymmetric shaft element about the respective axes. Let the spatial vector $\bar{H}$ be the angular momentum vector and $\bar{\omega}$ be the angular velocity vector of the elemental shaft and hence that of the rotating axes fixed to the body as shown in Figure 3.1.

The components of these vectors are:
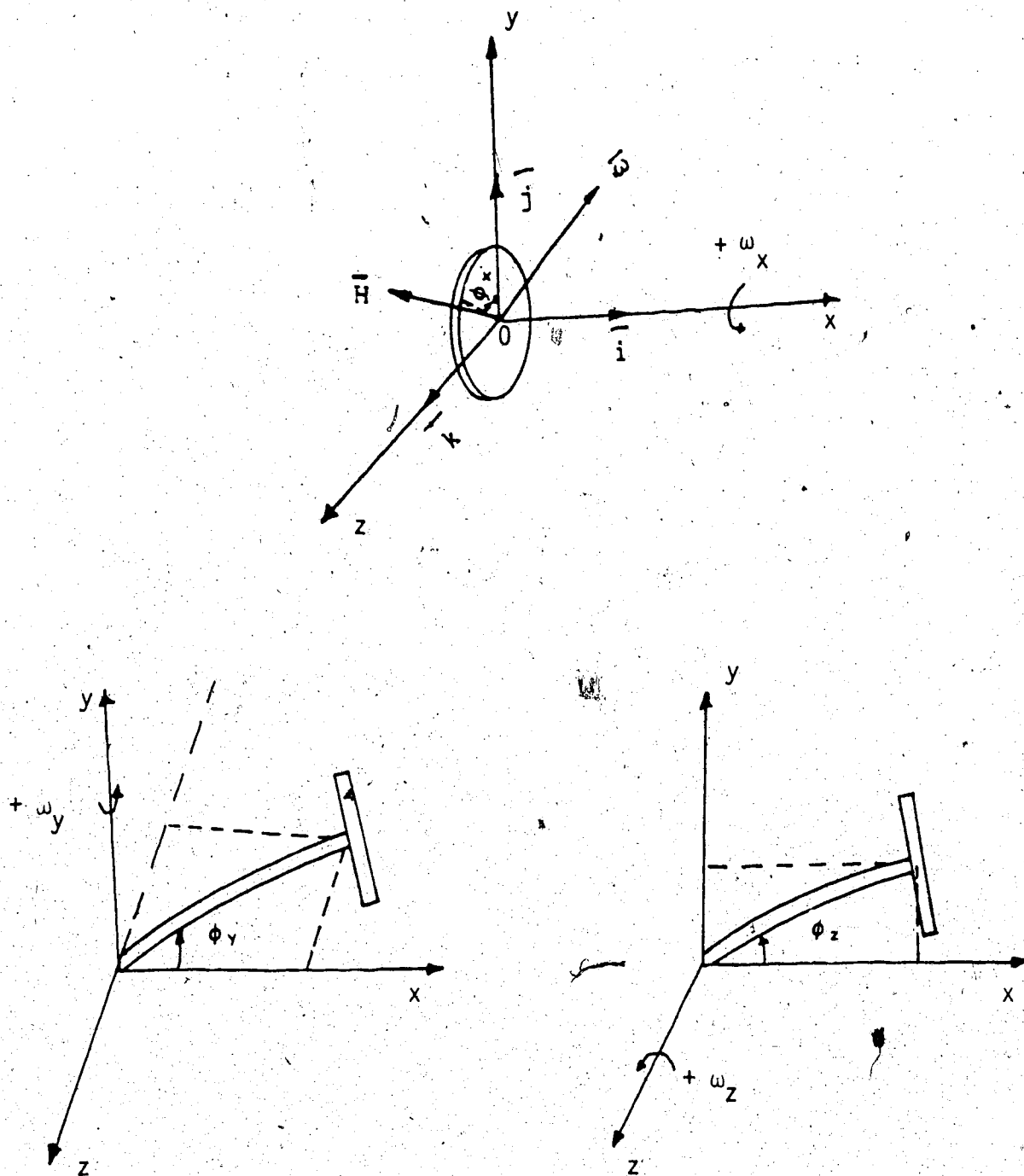
Figure 3.1 Positive rotations of a shaft element

$$\overline{H} = H_x \overline{i} + H_y \overline{j} + H_z \overline{k}$$

$$\overline{\omega} = \omega_x \overline{i} + \omega_y \overline{j} + \omega_z \overline{k}$$

The angular momentum vector components are obtained as

$$\begin{Bmatrix} H_x \\ H_y \\ H_z \end{Bmatrix} = \rho[I] \begin{Bmatrix} \omega_x \\ \omega_y \\ \omega_z \end{Bmatrix}$$

3.2.1 Euler angles: transformation of axes

Any orthogonal transformation of a vector in a three dimensional space needs three independent variables, Goldstein[56]. Euler angles are the common variables used to obtain the transformation matrix.

A rotating system of axes is obtained from the fixed system by three successive rotations. The choice of these rotations is arbitrary giving twelve combinations for the right handed system. The rule that need be observed is that the first angle can be about any one of the three axes but the next two rotations cannot be about the same axis. Figure 3.1 shows the positive directions for angular rotations and velocities. Figure 3.2 shows the rotations and the corresponding Euler angles and the angular velocities.
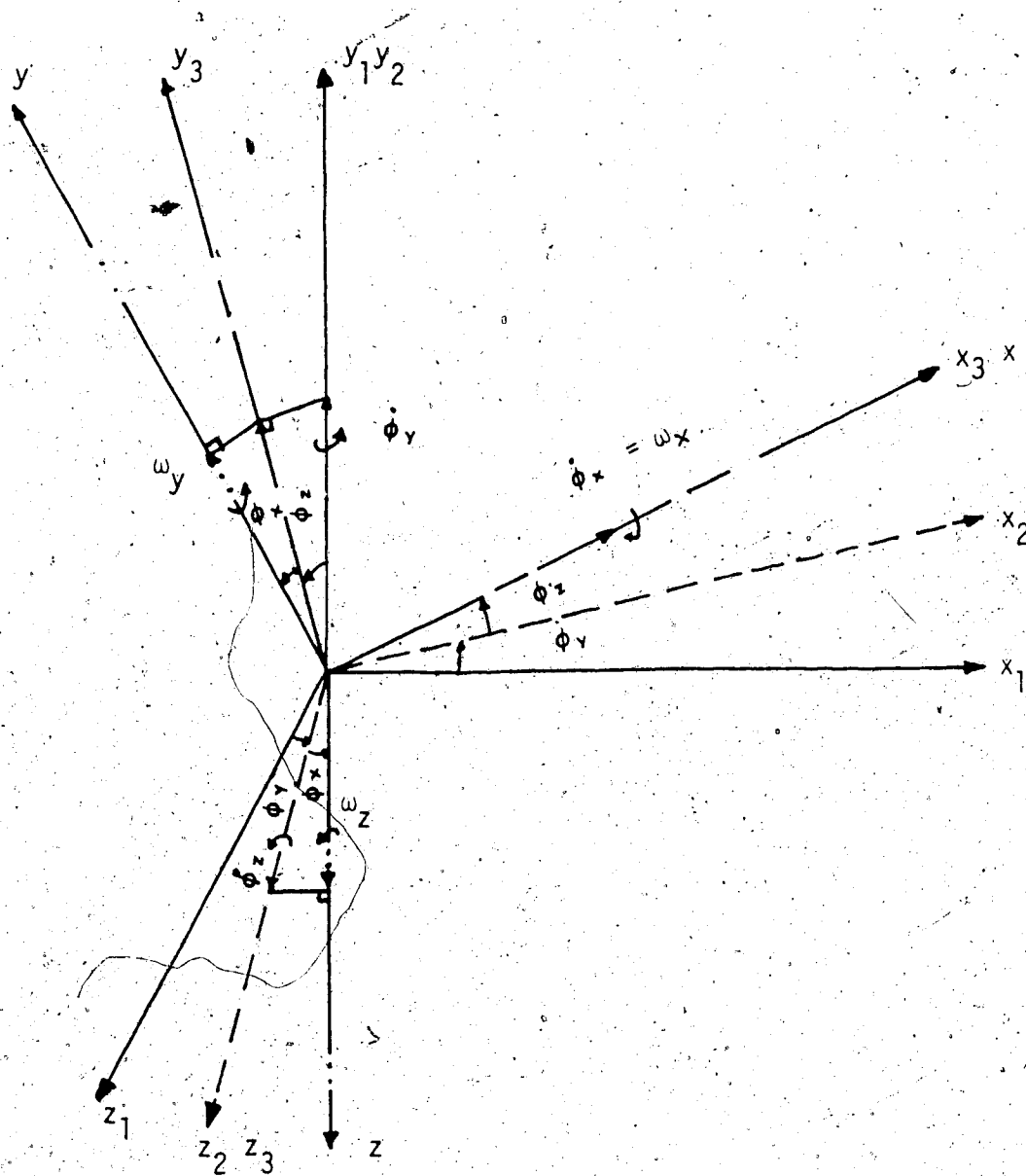
Figure 3.2 Position of principal axes during angular rotation

The order of rotations observed is: 1st by an angle ϕ_y about OY_1 to get $OX_2Y_2Z_2$ axes; then by an angle ϕ_z about OZ_2 to get $OX_3Y_3Z_3$ axes; and finally by an angle ϕ_x about OX_3 to get to the principal axes OXYZ.

The angular velocities about the principal axes are:

$$
\begin{Bmatrix} \omega_y \\ \omega_z \\ \omega_x \end{Bmatrix} = \begin{bmatrix} \cos\phi_x\cos\phi_z & \sin\phi_x & 0 \\ -\sin\phi_x\cos\phi_z & \cos\phi_x & 0 \\ \sin\phi_z & 0 & 1 \end{bmatrix} \cdot \begin{Bmatrix} \dot{\phi}_y \\ \dot{\phi}_z \\ \dot{\phi}_x \end{Bmatrix}
$$

The angular velocities about the intermediate axes and the inertia tensor, $\rho[\ I\ ]$, are known. Hence, we can calculate the angular momentum about the principal axes in the final position.

The moment, $\overline{M}$, acting at the centre of the elemental shaft, shown in Figure 3.3, is equal to the rate of change of angular momentum:

$$
\overline{M} = (\dot{\overline{H}})_{xyz} + \overline{\omega} \times \overline{H}
$$

Where the rate of change of the angular momentum with respect to the rotating axes is given as:
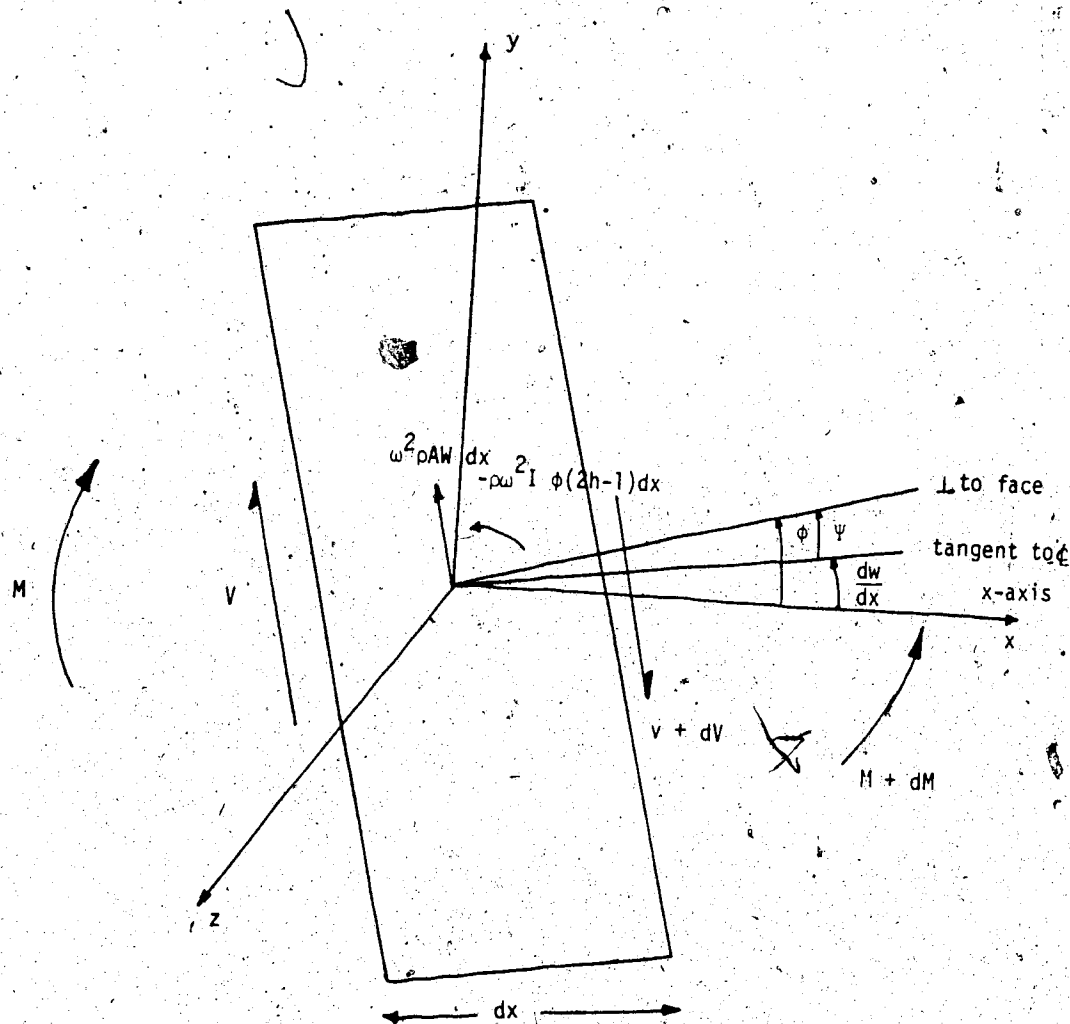
Figure 3.3 Forces on a shaft element

$$(\overline{H})_{xyz} = \rho[I] \cdot \begin{Bmatrix} \dot{\omega}_x \\ \dot{\omega}_y \\ \dot{\omega}_z \end{Bmatrix}$$

Assuming the shaft to be rigid in the deflected position the angular velocity of the shaft and the rotating axes will be the same. The other term $\overline{\omega} \times \overline{H}$ is due to the rotation of the body fixed axes:

$$\begin{bmatrix} \overline{i} & \overline{j} & \overline{k} \\ \omega_x & \omega_y & \omega_z \\ H_x & H_y & H_z \end{bmatrix} = \overline{\omega} \times \overline{H}$$

Substituting for angular momentum components and equating moments along each axis, we get:

$$\begin{Bmatrix} M_x \\ M_y \\ M_z \end{Bmatrix} = \rho \begin{Bmatrix} \omega_y \, \dot{\omega}_z \, (I_{zz} - I_{yy}) \\ \omega_x \, \omega_z \, (I_{xx} - I_{zz}) \\ \omega_x \, \omega_y \, (I_{yy} - I_{xx}) \end{Bmatrix} + \rho \begin{Bmatrix} I_{xx} \, \dot{\omega}_x \\ I_{yy} \, \dot{\omega}_y \\ I_{zz} \, \dot{\omega}_z \end{Bmatrix}$$

The angular accelerations about the final position of the principal axes can be obtained as:

$$\{\omega\} = [T_{ang}]\{\dot{\phi}\}$$

$$\{\dot{\omega}\} = [\dot{T}_{ang}]\{\dot{\phi}\} + [T'_{ang}]\{\ddot{\phi}\}$$

Where [Tang] is the transient transformation matrix for angular velocities.

3.2.2 Circular whirl

Consider the shaft in a circular whirl. Small angles of bending slopes (ϕ_z and ϕ_y) simplify the transformation matrix to:

$$\begin{bmatrix} \cos \phi_x & \sin \phi_x & 0 \\ -\sin \phi_x & \cos \phi_x & 0 \\ \phi_z & 0 & 1 \end{bmatrix}$$

Where $\cos\phi_z = 1$ and $\sin\phi_z = \phi_z$ are used. Note that the transformation matrix is time dependent.

Case 1: Forward whirl, spin velocity = whirl velocity.

Vector representation of small angles, measuring ωt from the OXZ plane, as shown in Figure 3.4. The component slopes, velocities and accelerations are:
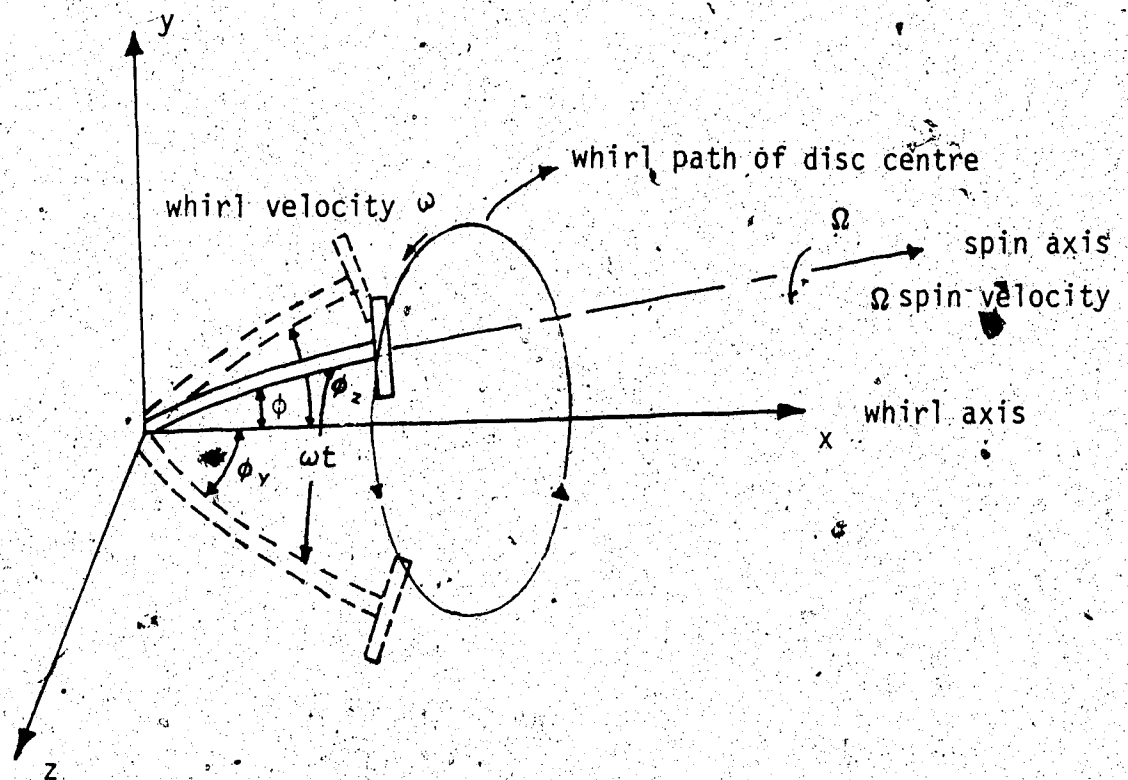
Figure 3.4 Shaft in a circular whirl

$$\phi_y = \phi \cos \omega t$$

$$\phi_z = \phi \sin \omega t$$

$$\dot{\phi}_y = -\phi\Omega \sin \omega t$$

$$\ddot{\phi}_y = -\phi\Omega^2 \cos \omega t$$

$$\dot{\phi}_z = \phi\Omega \cos \omega t$$

$$\ddot{\phi}_z = -\phi\Omega^2 \sin \omega t$$

so $\phi_x = \Omega t$, where Ω is the spin velocity

$$\dot{\phi}_x = \Omega$$

and $\ddot{\phi}_x = 0$

Assume the spin velocity to be a constant, the shaft to be circular in cross-section with $I_{xx} = I$, the polar moment of inertia and $I_{zz} = I_{yy} = I_d$, the transverse moment of inertia. The moment acting on the shaft can be found at any instant: choosing, $\Omega t = \omega t = \pi/2$ the instant when the shaft is in the OXY plane. We obtain the angular velocity components:

$$\begin{Bmatrix} \omega_y \\ \omega_z \\ \omega_x \end{Bmatrix} = \begin{bmatrix} 0 & 1 & 0 \\ -1 & 0 & 0 \\ \phi & 0 & 1 \end{bmatrix} \begin{Bmatrix} -\phi\omega \\ 0 \\ \Omega \end{Bmatrix} = \begin{Bmatrix} 0 \\ \phi\omega \\ \Omega \end{Bmatrix}$$

where the nonlinear terms in ϕ are neglected. The angular acceleration components are:

$$\begin{Bmatrix} \dot{\omega}_y \\ \dot{\omega}_z \\ \dot{\omega}_x \end{Bmatrix} = \begin{bmatrix} -\Omega & 0 & 0 \\ 0 & -\Omega & 0 \\ 0 & 0 & 0 \end{bmatrix} \begin{Bmatrix} -\phi\omega \\ 0 \\ \Omega \end{Bmatrix} + \begin{bmatrix} 0 & 1 & 0 \\ -1 & 0 & 0 \\ \phi & 0 & 1 \end{bmatrix} \begin{Bmatrix} 0 \\ -\phi\omega^2 \\ 0 \end{Bmatrix} = \begin{Bmatrix} 0 \\ 0 \\ 0 \end{Bmatrix}$$

where the relation $\omega = \Omega$ is used. We now obtain the external moment components:

$$\begin{Bmatrix} M_x \\ M_y \\ M_z \end{Bmatrix} \begin{matrix} = \\ = \\ = \end{matrix} \begin{Bmatrix} 0 \\ \rho\,\omega^2\phi\,(I - I_D) \\ 0 \end{Bmatrix}$$

Following the above procedure, substituting the relation between ω and Ω, the moment acting on the shaft for any spin to whirl ratio h can be obtained.

Though, the method used here in deriving the external moment on the shaft, from the Euler equations, is very general its use for other complicated whirl orbits may not be as straight forward. Relation between slopes ϕ_z and ϕ_y will be complicated, resulting in highly non-linear equations even for the case of elliptical orbits, Lund(51).

3.2.3 Equations of motion

Having found the centrifugal force and moment of a rotating shaft element, the equations of motion for an elemental shaft as shown Figure 3.3, can now be written. The

assumption of a circular orbit (relation of angles ϕ_z and ϕ_y) helps in decoupling: vibrations in a plane representing the shaft motion. Let OXY plane be the representative plane. Neglecting gravity forces, the shaft equations of motion are obtained.

From the geometry of deformation we get:

$$\frac{dw}{dx} = \phi - \psi$$

where W' is the total centroidal slope, ϕ the bending slope and ψ the shear slope. The shear force, V, can be expressed in terms of shear strain by the equation:

$$V = G K A \psi$$

Where G is the modulus of rigidity, A is the cross-sectional area and K is the shear coefficient. From the element in equilibrium the equation of motion in translation is:

$$dV = - \omega^2 \rho A W \, dx$$

$$G K A (w'' - \phi') + \omega^2 \rho A W = 0 \qquad (3.1)$$

where W is the centroidal displacement of the element. The

equations of translatory motion for the beam and the shaft are the same, as the whirling action is ineffective. The moment equation, neglecting second order terms is:

$$dM + Vdx = \rho \omega^2 I_D (2h - 1) \phi \, dx$$

From the pure bending theory we get:

$$M = E I \phi'$$

The resulting equation in rotation is:

$$E I \phi'' + G K A (w' - \phi) - \rho \omega^2 I_D (2h - 1) \phi = 0 \qquad (3.2)$$

where h is the ratio of spin to whirl; h=1 for forward whirl, h=0 for a beam and h=-1 for a backward whirl. These equations of motion can be obtained from the variational approach using the functional:

$$J = \frac{1}{2} \int_0^\ell E I (\phi')^2 dx + \frac{1}{2} \int_0^\ell G K A \{(w')^2 - 2w'\phi + \phi^2\} \, dx$$

$$- \frac{\omega^2}{2} \int_0^\ell \rho A W^2 dx + \frac{\omega^2}{2} (2h - 1) \rho \int_0^\ell I_d \phi^2 dx$$

The four terms in the functional are the bending strain, the shear strain, the translational and the rotational kinetic energies. This functional is true for the element with varying cross-section(with the area A and the moment of inertia I as functions of the axial length x).

3.2.4 Approximate equations

The method shown in Appendix A for the beam is directly applicable here. The component stiffness and mass matrices are the same but the inertia matrix in rotation is altered to suit the beam as well as the shaft problem. The whirl affects only the rotational kinetic energy term and is included by the magnitude and sign of h. The approximate functional is:

$$J = \frac{1}{2} \{W_e\}^T [KA] \{W_e\} + \frac{1}{2} \{W_e\}^T [KB] \{W_e\} - \frac{1}{2} \{W_e\}^T [KC] \{W_e\}$$

$$+ \frac{1}{2} \{W_e\}^T [KD] \{W_e\} - \frac{1}{2} \{W_e\}^T [Ke] \{W_e\} - \frac{\omega^2}{2} \{W_e\}^T [MA] \{W_e\}$$

$$+ \frac{\omega^2}{2} (2h - 1) \{W_e\}^T [IA] \{W_e\}$$

Where $\{ W_e \}$ is the nodal variable vector.

The homogeneous equations of motion are given as:

$$\frac{\partial J}{\partial \{W_e\}} = 0 \quad \text{gives} \left\{ \left[[KA] + [KB] - [KC] - [KE] + [KD] \right] \right.$$

$$\left. - \omega^2 \left[[MA] + (2h - 1) [IA] \right] \right\} = 0$$

The standard eigenvalue routine gives the whirling critical speeds, ω. The symmetry of the mass matrix is retained even after the inclusion of the gyroscopic effects. The resulting eigenvalues are all real and positive for a beam or a shaft in backward whirl. However, the shaft in a forward whirl has some negative eigenvalues.

3.2.5 Analytical solution for a simply supported shaft

Equations (3.1) and (3.2) govern the motion of a whirling shaft. For a simply supported shaft the boundary conditions are W=0 and $I\phi'$ = 0 at the two ends. The solution,

$$W = W \sin \frac{n\pi x}{\ell} e^{j\omega t} \quad \text{and} \quad \phi = \phi \cos \frac{n\pi x}{\ell} e^{j\omega t}$$

satisfies both the boundary conditions at x=0 and x=L and also satisfies the differential equations of motion. Substituting the solution in the differential equations and simplifying gives the characteristic equation:

$$\lambda^4 \left\{ \frac{E}{GK} \left(\frac{k}{\ell}\right)^4 (2h - 1) \right\} - \lambda^2 \left\{ -1 + \left(\frac{-E}{GK} + (2h - 1)\right) \left(\frac{k}{\ell}\right)^2 n^2\pi^2 \right\}$$

$$- n^4\pi^4 = 0 .$$

Where $\lambda = \sqrt{\rho L^4/E k^2} \cdot \omega$, k is the radius of gyration of the shaft cross-section, n the mode number and L the length of the shaft.

3.2.6 Non-uniform shafts: Ritz method

The Ritz method allows approximate critical speeds to be calculated if appropriate solutions are assumed. This method is used for a non-uniform Timoshenko shaft in Appendix C. Variables have to be assumed separately for the displacement, W, and the bending slope, ϕ, which satisfy the necessary boundary conditions. This differs from the classical Euler beam where only the displacement variable is assumed. The selection of the trigonometric functions gave the exact first critical for a uniform Timoshenko shaft.

For the case of a linearly tapered shaft, algebraic functions are easier to integrate and at the same time satisfy the necessary boundary conditions. The approximate solutions used are very crude but can be helpful in verifying the finite element results. More terms can be included in the assumed solution for greater accuracy. This method can be extended for other boundary conditions and shafts with higher order cross-sectional variations.

3.3 Results and discussion

Rouch and Kao used Thomas, Wilson and Wilson's element[22] with three degrees of freedom per node W, ϕ, ψ. To reduce the number of degrees of freedom the shear variable was suppressed, assuming that shear cannot be coupled at discontinuous joints. In the present element TM544, the choice of the variables $A\psi$ and $I\phi'$ enables total coupling at discontinuous joints. Table 3.1 compares

FIRST MODE

Table 3.1 Comparison of critical speeds of Rouch and TM544

k/ℓ	Shaft Forward whirl h = 1			Beam h = 0			Shaft Backward whirl h = -1		
	TM544	Rouch	Analytical	TM544	Rouch	Analytical	TM544	Rouch	Analytical
0.02	3.1372	3.1373	3.1371	3.1339	3.1312	3.1317	3.0311	3.1252	3.1270
0.04	3.1244	3.1243	3.1239	3.1013	3.1014	3.1013	3.0794	3.0794	3.0792
0.06	3.1017	3.1021	3.1015	3.0553	3.0556	3.0552	3.0117	3.0120	3.0115
0.08	3.0698	3.0705	3.0696	2.9976	2.9981	2.9974	2.9315	2.9320	2.9313
0.10	3.0284	3.0296	3.0282	2.9323	2.9332	2.9321	2.8457	2.8465	2.8455

SECOND MODE

k/ℓ	Shaft Forward whirl h = 1			Beam h = 0			Shaft Backward whirl h = -1		
	TM544	Rouch	Analytical	TM544	Rouch	Analytical	TM544	Rouch	Analytical
0.02	6.2504	6.2503	6.2477	6.2047	6.2045	6.2027	6.1589	6.1604	6.1584
0.04	6.1449	6.1468	6.1392	5.9996	6.0010	5.9947	5.8670	5.8685	5.8626
0.06	5.9645	5.9715	5.9565	5.7323	5.7368	5.7261	5.5231	5.5278	5.5181
0.08	5.7275	5.7393	5.7172	5.4527	5.4599	5.4454	5.1937	5.2013	5.1884
0.10	5.4633	5.4787	5.4515	5.1850	5.1943	5.1769	4.8983	4.9081	4.8930

$E/GK = 2.4$, k/ℓ = slenderness ratio, $p = \sqrt[4]{\rho A \rho^4 \omega^2 / EI}$

Using 8 degrees of freedom for TM544 and 20 degrees of freedom for Rouch's shear suppressed element model.

critical speeds pf a two element and eight degrees of freedom TM544 model and Rouch's ten element model (shear suppressed) possessing 20 degrees of freedom. Percentage errors are calculated by using the exact results obtained. The percentage errors for different k/L values for the shaft using TM544 elements vary from 0.003% to 0.06% compared to a variation of 0.006% to 0.046% using Rouch's elements for the first forward whirl. For the second mode the variation is 0.042% to 0.216% using the present elements and .042% to 0.498% using Rouch's elements.

The performance of the present element is an improvement over Rouch's element. The behavior is better for larger values of k/L and higher modes. This is not surprising as the basic beam element used is superior as shown in the previous Chapter. Figure 3.5 and Figure 3.6 show the variation in the 1st and 2nd mode critical speeds for different k/L ratios; k/L ratio is not only the slenderness ratio for a shaft but also represents the disk effect (the relative importance of moment of inertia to the mass of the shaft). The present finite element results agree well with the analytical results for the first as well as the second critical speeds.

Table 3.2 compares the two elements for k/L=0.1; with the shaft in forward (h=+1) and backward whirls (h=-1). The rate of convergence is better for TM544 in all the cases. Rouch's 10 elements regular (unsuppressed) model and the 3 elements model using the present element converge to the 1st

Table 3.2 Convergence of shaft critical speeds: comparison with Rouch

No. of Elements	Mode 1				Mode 2			
	Forward whirl h = +1		Backward whirl h = -1		Forward whirl h = +1		Backward whirl h = -1	
	Rouch	TM544	Rouch	TM544	Rouch	TM544	Rouch	TM544
1	3.1546	3.0316	2.9752	2.8479	8.1188	5.6810	5.7786	6.1047
2		3.0284		2.8457		5.4633		4.8983
3	3.0295	3.0282	2.8457	2.8455	5.5131	5.4529	4.9325	4.8942
4		3.0282		2.8455		5.4516		4.8932
5	3.0284		2.8457		5.4572		4.8974	
7	3.0283		2.8456		5.4528		4.8941	
10	3.0282		2.8455		5.4515		4.8932	
Analytical	3.0282		2.8455		5.4515		4.8930	

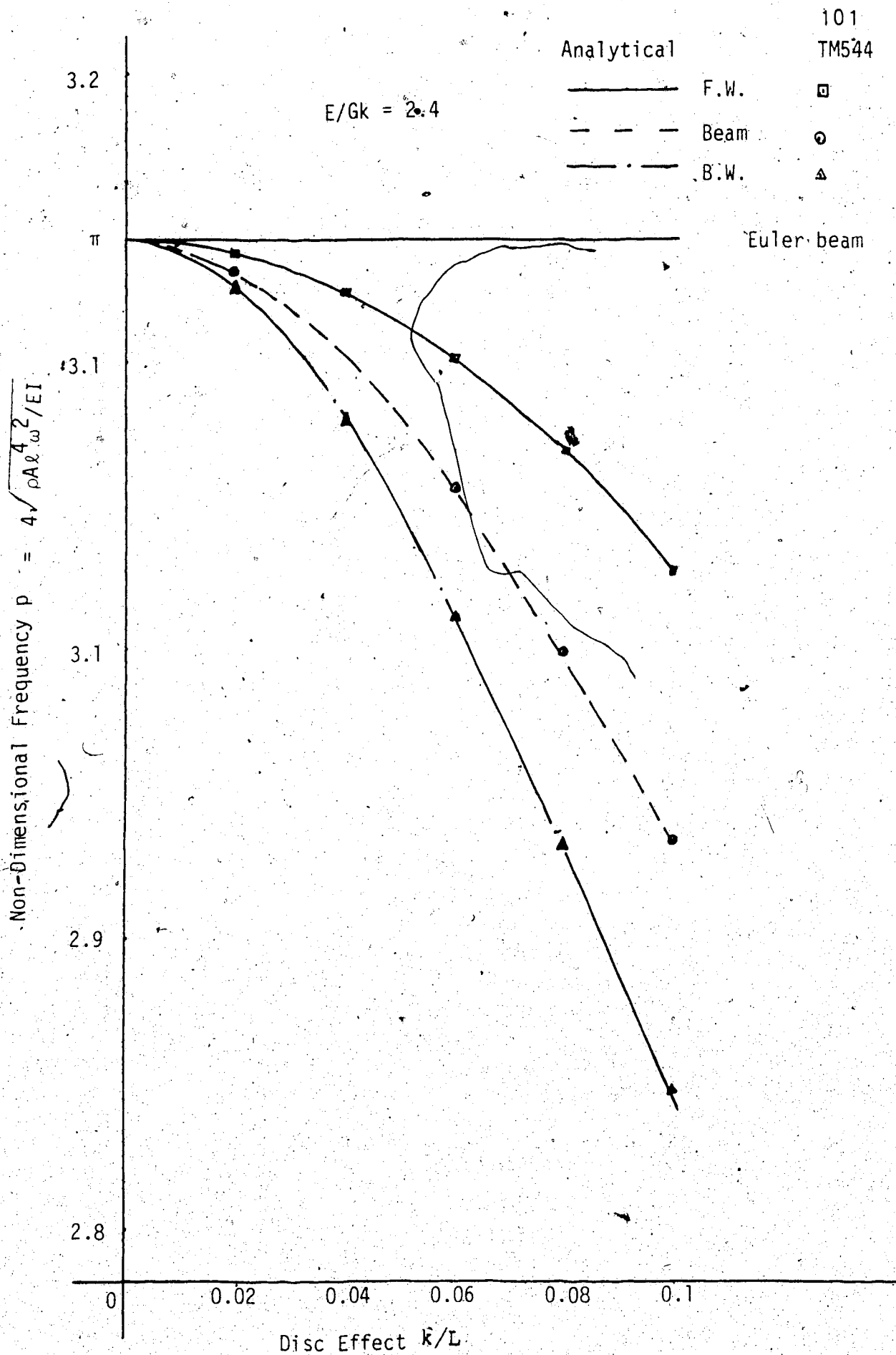$E/GK' = 2.4$, $p = 4\sqrt{\rho A \ell^4 \omega^2 / EI}$, $k/\ell = 0.1$

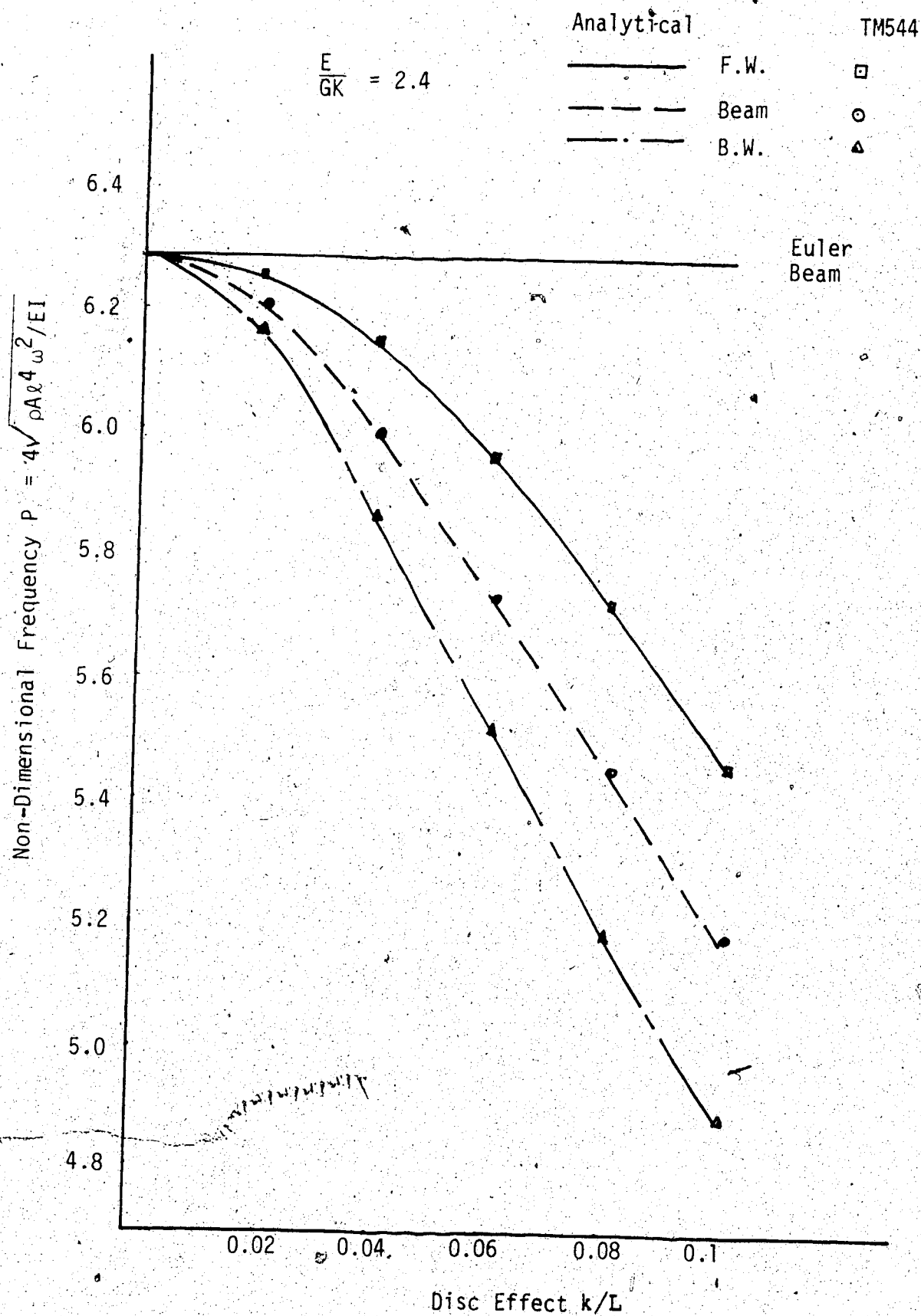Figure 3.5 Comparison of 1st critical speeds for H-H shaft

Figure 3.6 Comparison of 2nd critical speeds for H-H shaft

critical speed given by the analytical method.

Table 3.3 compares the results of the exact solution and the results obtained using Ritz's method for a simply supported uniform beam. Trigonometric functions give the exact solution; whereas, the one term algebraic functions yield crude results. The effect of k/L can be obtained since a Timoshenko shaft is used for the Ritz's method; the Euler beam cannot see this effect.

The single term approximation used has the disadvantage of having a lower order displacement (quadratic) compared to the bending slope(cubic). An extra term in W, $C_2 x(\ell - x)^2$ or $C_2 x^2 (\ell - x)$, can be included but the characteristic equation will no longer be quadratic and root search methods have to be used to find the critical speed.

The effect of the slenderness ratio, k/L, and the taper ratio, a, on the shaft critical speeds is shown in Figure 3.7 for a shaft in forward whirl. As the bearing conditions are symmetric the direction of the taper is immaterial as far as the critical speeds are concerned, but parameters are non-dimensionalized with respect to the root values which will be altered if taper is reversed. Thus, the slenderness ratio is k_i/L and the non-dimensional critical speed is defined as:

$$p = \sqrt[4]{\frac{\omega^2 \rho A_i L^4}{EI_i}}.$$

Table 3.3. Comparison of 1st critical speed of a simply supported shaft using Ritz and finite element methods; Effect of taper and slenderness ratio

Beam

k_i/L	1.0 F.E	1.0 Ritz Trig	1.0 Ritz Alg	0.8 F.E	0.8 Ritz Alg	0.4 F.E	0.4 Ritz Alg	0.2 F.E	0.2 Ritz Alg
0.02	3.1307	3.1313	3.7221	2.6975	3.4961	.9969	3.2708	1.7244	3.2295
0.04	3.0955	3.0950	3.2784	2.6802	2.9488	.9925	2.5197	1.7220	2.4087
0.06	3.0420	3.0409	3.1299	2.6530	2.7845	.9852	2.2675	1.7181	2.1086
0.08	2.9758	2.9742	3.0280	2.6176	2.6963	.9754	2.1563	1.7127	1.9623
0.10	2.9021	2.9000	2.9371	2.5761	2.6292	.9633	2.0826	1.7060	1.8790

Backward whirl

k_i/L	1.0 F.E	1.0 Ritz Trig	1.0 Ritz Alg	0.8 F.E	0.8 Ritz Alg	0.4 F.E	0.4 Ritz Alg	0.2 F.E	0.2 Ritz Alg
0.02	3.1247	3.1251	3.7288	2.6946	3.4932	1.9960	3.2664	1.7238	3.2248
0.04	3.0739	3.0732	3.2555	2.6691	2.9363	1.9890	2.5153	1.7198	2.4054
0.06	3.0001	2.9991	3.0868	2.6302	2.7605	1.9777	2.2590	1.7133	2.1022
0.08	2.9138	2.9124	2.9650	2.5815	2.6589	1.9627	2.1361	1.7044	1.9526
0.10	2.8227	2.8211	2.8569	2.5269	2.5786	1.9446	2.0622	1.6935	1.8649

Forward whirl

| k_i/L	1.0 F.E	1.0 Ritz Trig	1.0 Ritz Alg	0.8 F.E	0.8 Ritz Alg	0.4 F.E	0.4 Ritz Alg	0.2 F.E	0.2 Ritz Alg
0.02	3.1367	3.1359	3.7148	2.7005	3.4961	1.9978	3.2708	1.7250	3.2295
0.04	3.1179	3.1171	3.3021	2.6916	2.9606	1.9960	2.5239	1.7242	2.4109
0.06	3.0864	3.0851	3.1755	2.6767	2.8095	1.9929	2.2763	1.7230	2.1142
0.08	3.0428	3.0409	3.0960	2.6558	2.7359	1.9886	2.1649	1.7212	1.9721
0.10	2.9883	2.9821	3.0239	2.6290	2.6838	1.9829	2.1041	1.7189	1.8935
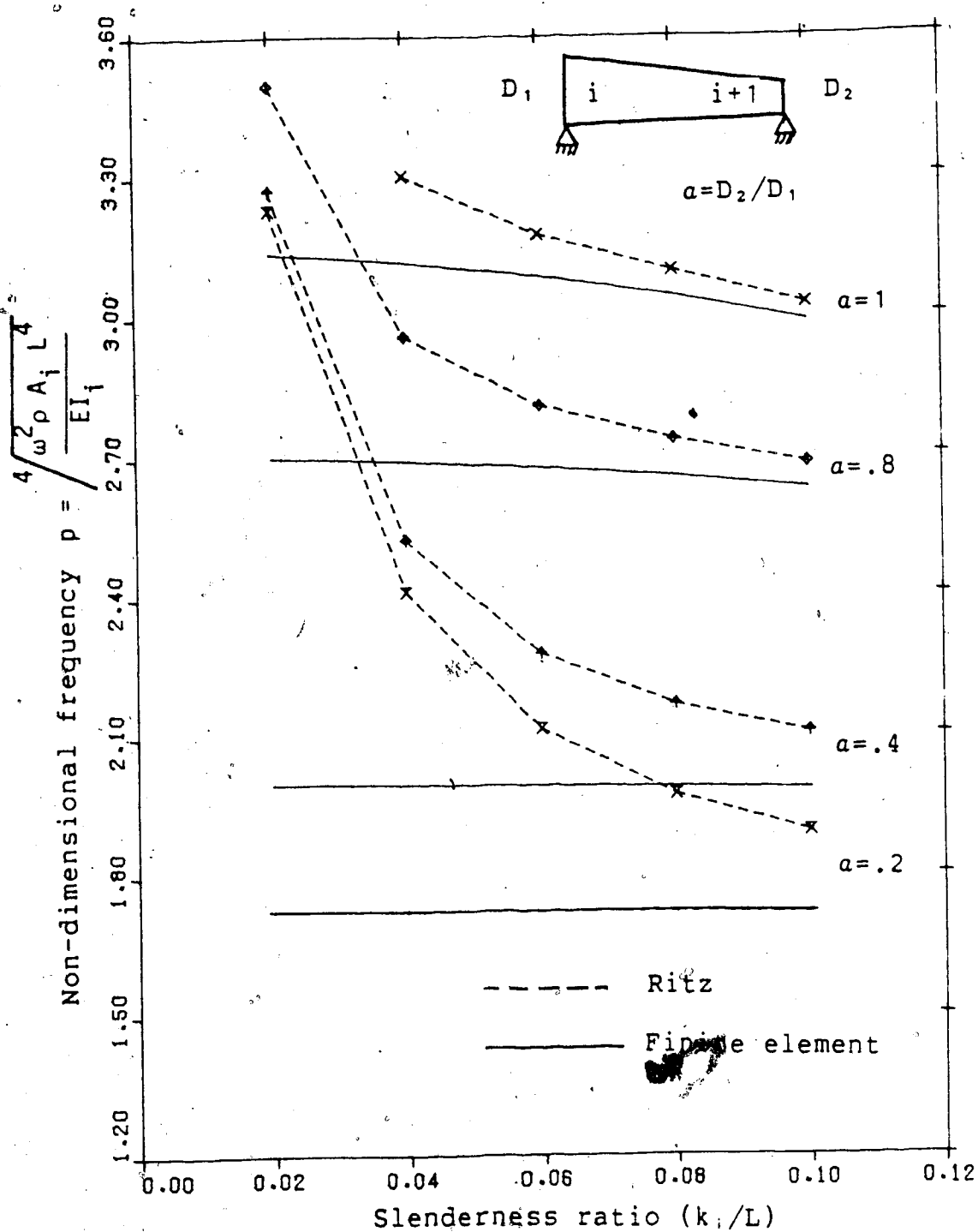
Figure 3.7 Effect of taper and k/L on a H-H shaft in a forward whirl.

The effect of k_i/L is greater for a uniform shaft than for the tapered. Effect of lowering the taper ratio (from 1.0 to 0.2) is to decrease the critical speeds. The Ritz method tends towards the uniform Euler beam for low k_i/L values. Euler beam values are expected for small k_i/L and uniform shafts($a=1$). For higher values of k_i/L and taper ratios (a =1.0 and 0.8), the comparison gets better.

3.4 Conclusions

The moment acting on an elemental shaft in a circular whirl is derived from the Euler equations of motion using a rotating co-ordinate system. For the circular orbit it is shown that the equations of motion can be uncoupled.

The beam element developed in Chapter 2 is modified to represent the axisymmetric shaft in a circular whirl. The present shaft element proves to be better than Rouch's. Retaining the shear variable allows more accurate results per degree of freedom and faster convergence. The present element is superior for higher modes and for thick shafts implying its usefulness in representing large rotors. Exact solutions are obtained for the simply supported shaft and the critical speeds thus obtained are used to evaluate the finite elements.

In Appendix C, Ritz's method is developed for a tapered shaft with shear, rotatory inertia and gyroscopic effects included. Results are given for uniform and non-uniform shafts. These results are used to analyze the effect of

taper ratios and slenderness ratios of simply supported shafts. The Ritz method shown can be used for other boundary conditions using appropriate solutions.

4. SHAFT-DISK SYSTEMS

Abstract

    A finite element is developed with the disks included
within the element at any given points along its length.
This element is tested extensively for shafts with single,
double and multiple disks. Comparison is made with
analytical solutions and with the finite element results
obtained by lumping the disks at nodal points. This method
helps in reducing the size of the system matrix, retaining
the accuracy of the results.

4.1 Introduction

    Den Hartog[58] analyzed the whirling shaft's critical
speeds with a rigid thin disk located on an elastic massless
shaft. The flexibility approach used gave the equations of
deflection and slope from which the characteristic equation
was obtained. The shaft mass and shear stiffness were
neglected. An axially symmetric shaft-disk system was
assumed and the disk effect in translation and rotation was
lumped. For a cantilever shaft with an end disk he obtained
the critical speeds for the cases of forward and backward
whirl.

    Green[59] extended the analysis to a shaft on simple
supports with one, two and multiple disks. The mass and
shear effects of the shaft were neglected as before.

Eshelman and Eubanks[60] investigated the shaft disk system including the mass of the shaft, lumping the disk effects and neglecting the shear deformation of the shaft.

Craggs and Akella[61] used shaft finite elements which included continuous mass, bending and shear deformations and rotatory inertia and gyroscopic effects. Simple shaft-disks systems were evaluated by lumping the disk effects at the element nodes. Craggs and Akella[62] also reported the finite element results of a shaft with continuous disks; the model lumped the disks at the nodal points.

In the present Chapter Den Hartog's analytical approach is extended to include the shear deformation of the shaft which was neglected by Den Hartog, Green and Eshelman.

The shaft element is allowed to include one or more disks inside itself. Thus, a shaft-disk system can be represented by just one element. A great reduction in the number of elements and degrees of freedom occurs while modelling large rotors. This is of immediate use considering the size of modern turbo-generator sets with each of its turbine stages mounted with blade carrying disks.

The alternate shaft disk system of each stage can be modelled with an element for each section which requires 20 to 40 elements.

Alternately, the inertia effects of the thin and rigid disks can be lumped at the appropriate nodal points. A node is inevitable at every disk location with this method and gives a 10 to 20 elements representation of each stage and a

40 to 100 elements model for the whole rotor system.

A large model requires more memory space, extensive calculations and increased cost. For an N degrees of freedom system, a linear equation solver performs N^2 calculations and N^3 calculations are made for obtaining the eigenvalues and the eigenvectors. By including the disks inside the element a 3 to 5 elements model for each stage and a 12 to 20 elements model for the whole system is obtained, which will be compatible even with a micro computer.

This method is evaluated by comparing it with the lumped finite element model and the analytical results of Green. A few simple shaft-disk systems are tested. A repeated system with four disks is modelled using a periodic type element. The model is also used for a continuous shaft-disks system.

4.2 Theory

Consider an axi-symmetric cantilever type shaft-disk system. For a beam, the end can be fixed as the beam does not spin. For a shaft, the fixed end condition is obtained by a long sleeve bearing which restricts the displacement and bending slope to be zero but enables rotation about the shaft axis.

If the disk is a concentrated mass or the disk is perpendicular to the shaft axis and is placed at a point where the bending slope is zero (eg. centre point of a simply supported shaft); then such a non-rotating system

will vibrate in a plane at its natural frequency and a rotating shaft-disk system will have no rotatory inertia/gyroscopic effects due to the disk. Figure 4.1 shows the type of motion occurring when the end of the beam is subjected to a force, $m_d\omega^2W$, and to a moment due to rotatory inertia, $I_d\omega^2\phi$. Where m_d and I_d are the mass and the transverse moment of inertia of the disk, W and ϕ are the end deflection and the bending slope amplitudes.

When the disk is not a concentrated mass and/or placed where bending slope is non-zero or is tilted though located at a zero slope point; the shaft will then whirl around, with the disk not remaining in a single plane, causing gyroscopic moment (as the whirl and spin axes will no longer be parallel).

When the spin and whirl rotations are in the same direction a forward whirl is obtained and a backward whirl occurs when they are in opposite directions. In both the cases centrifugal force and moment due to rotatory inertia occur due to the disk; the same as in the case of a beam-disk system. In addition, the whirling of the disk causes a gyroscopic moment of $-2I_d\omega\Omega\phi$ in the first forward whirl and $I_d\omega\Omega\phi$ in the first backward whirl.

At the critical speed, for a rotating overhung cantilever shaft, Den Hartog gives the equations of displacement and rotation, considering the static equilibrium at any instant:

Beam vibration

Forward whirl

Backward whirl
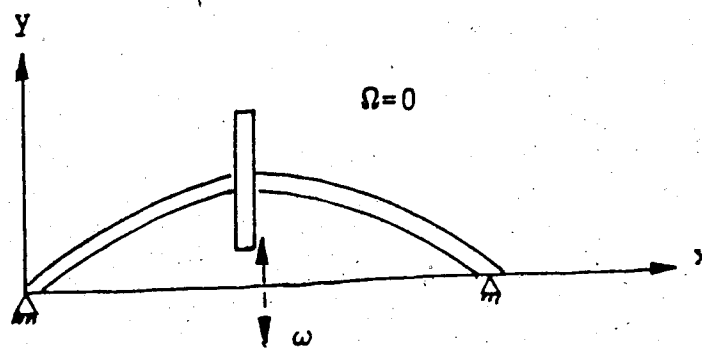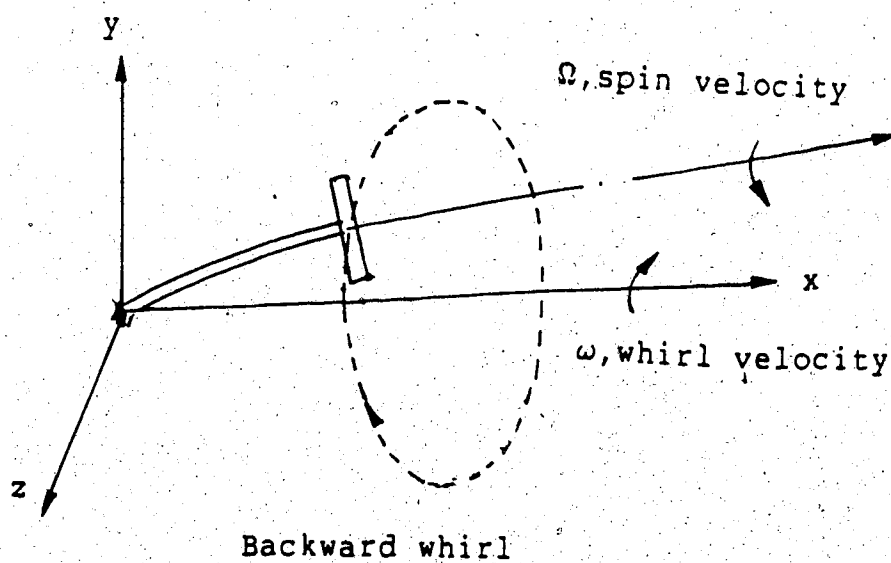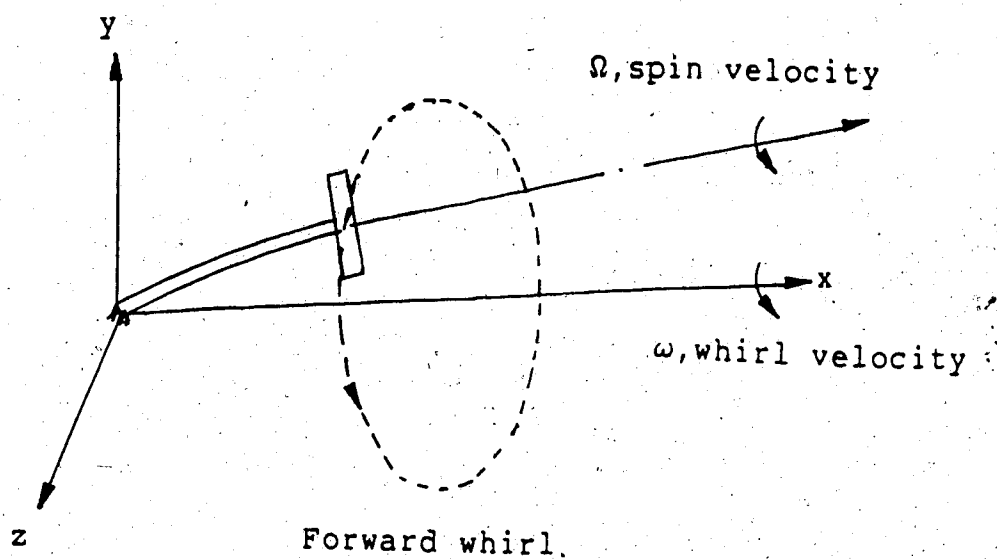
Figure 4.1 Whirling of shaft disk system

$$w = \alpha_{11} \, m_d \, \omega^2 \, w - \alpha_{12} \, I_d \, \omega(2\Omega - \omega)\phi$$

$$\phi = \alpha_{21} \, m_d \, \omega^2 w - \alpha_{22} \, I_d \, \omega(2\Omega - \omega)\phi$$

where a_{11}, a_{12}, a_{21} and a_{22} are the flexibility coefficients. Den Hartog used the flexibility coefficients of the Euler beam. Taking the flexibility coefficients of a Timoshenko beam given in Appendix B, we can account for the shear stiffness of the shaft. Substituting:

$$\alpha_{11} = \frac{L}{GKA} + \frac{L}{3EI}$$

$$\alpha_{12} = \alpha_{21} = \frac{L^2}{2EI}$$

$$\alpha_{22} = \frac{L}{EI}$$

$$I_d' = I_d(2h-1),$$

where h= spin velocity/ whirl velocity. The equilibrium equations are:

$$w \left\{ m_d \, \omega^2 \left(\frac{L}{GKA} + \frac{L^3}{3EI} \right) - 1 \right\} + \left(- I'_d \, \omega^2 \, \frac{L^2}{2EI} \right) \phi = 0$$

$$- m_d \, \omega^2 \, \frac{L^2}{2EI} \, w + \left(\omega^2 \, I'_d \, \frac{L}{EI} + 1 \right) \phi = 0$$

For non-zero values of ω, the determinant of the coefficient matrix corresponding to the variables W and ϕ should be zero. The resulting characteristic equation is:

$$\omega^4 \left(1 + \frac{12EI}{GKAL^2} \right) + \omega^2 \left\{ \frac{12EI}{m_d I'_d \, L^3} \left(\frac{m_d \, L^2}{3} - I'_d \right) + \frac{12E^2 \, I^2}{GKA \, I_d \, L^3} \right\}$$
$$- \frac{12E^2 \, I^2}{m_d I_d \, L^4} = 0$$

The critical speeds for the cases of forward whirl, backward whirl and beam are obtained by substituting h=1, h=-1 and h=0 in describing I_d'. Results of Appendix B can be used to include the effects of shear in the other cases considered by Green.

4.2.1 Inclusion of disks within an element

The disks are assumed to be thin (can be related to a single point on the shaft) and rigid (no deformation possible) and that they contribute only to the inertia terms.

The disk effects are usually lumped at the nodal points by adding disk inertia terms to the appropriate diagonal terms of the shaft translatory and rotatory inertia matrices. Here, we obtain the disk effects as consistent disk matrices and add to the shaft mass matrix.

Addition of the centrifugal force and the moment due to the disks introduces discontinuities in the distribution of the shear force, $A\psi$ and bending moment, $I\phi'$, though displacement, W, and slope, ϕ, remain continuous. The order of the interpolation functions used in the basic shaft element determines the accuracy to which these discontinuities are represented.

Thus a higher order element becomes effective; and the representation of the shear force and the bending moment by quadratic functions (Appendix A), instead of the normally given linear or constant variation, is justified.

Using the notation of Appendix A and Figure 4.2, the translatory inertia matrix for the disks is:

$$[DM] = \sum_{i=1}^{N} M_{di} [C^{-1}]^T \lfloor xo(x_i) \rfloor^T \lfloor xo(x_i) \rfloor [C^{-1}]$$

and the rotatory inertia matrix for the disks is:

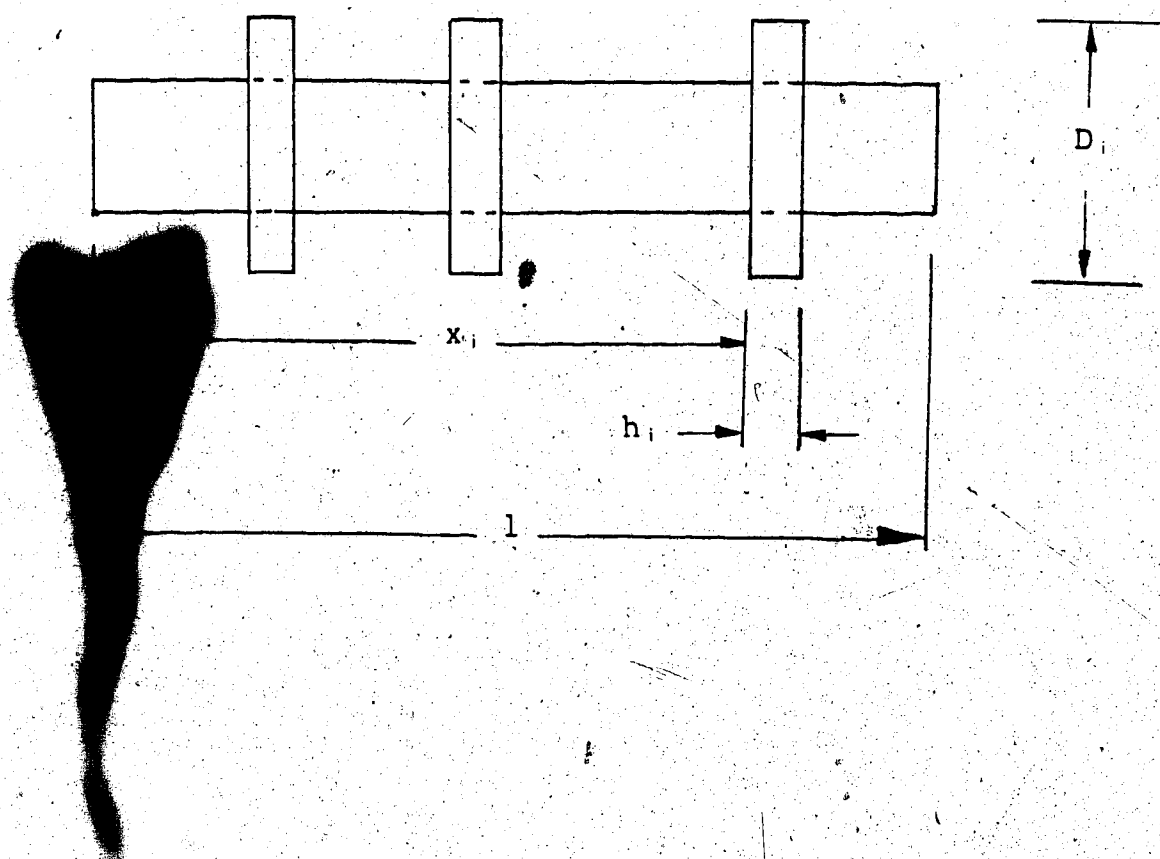$$[DI] = (1 - 2h) \sum_{i=1}^{N} I_{di} [C^{-1}]^T \lfloor YO(x_i) \rfloor^T \lfloor YO(x_i) \rfloor [C^{-1}]$$

Figure 4.2 Disks within an element

Where M_{di} is the mass and I_{di} is the diametric moment of inertia of the ith disk, N is the number of disks in the element and [C] is the transformation matrix to change the generalized co-ordinates from the polynomial coefficients to the nodal variables. $\lfloor X0(x_i) \rfloor [C^{-1}]\{W_e\}$ and $\lfloor Y0(x_i) \rfloor [C^{-1}]\{W_e\}$ are the displacement, W, and bending slope, ϕ, at distance, x_i, from the element root. The resulting matrices [DM] and [DI], obtained by discrete integration, are in terms of the element nodal variables and can be added directly to the element inertia matrices.

The disk inertia matrices are in general non-diagonal except when the disks are included only at the element nodes in which case the effect is the same as the lumped disk system.

4.2.2 Continuous disks on shaft

In the case of axial turbines and compressors a number of blade carrying disks are mounted on a shaft. The discrete shaft-disk system was approximated by an equivalent continuous shaft by Green; using a Rayleigh shaft. A more accurate representation is obtained by considering a Timoshenko shaft which includes the shear effect.

In the previous Chapter the characteristic equation for a simply supported shaft was given as:

$$\lambda^4 - \{\frac{E}{GK} (\frac{k}{\ell})^4 (2h - 1)\} - \lambda^2 \{ -1 + (\frac{-E}{GK} + (2h - 1)\} (\frac{k}{\ell})^2 n^2\pi^2\}$$

$$- n^4\pi^4 = 0$$

If we take $\lambda = p^2$ and $k/L=r$ we will get the same equation for the critical speeds as obtained by Eshelman[60]:

$$p = \sqrt[4]{\frac{N^4\pi^4}{1 + r^2 N^2 \pi^2 (\frac{E}{GK} - (2h-1))}}$$

where h is the spin to whirl ratio and N the mode number. From a Timoshenko shaft, shear can be eliminated by specifying a large shear stiffness (GKA = infinity) which gives E/GK=0. Neglecting the shear term we get the critical speeds of a Rayleigh shaft:

$$p = \sqrt[4]{\frac{N^2\pi^2}{1 - N^2 r^2 \pi^2 (2h-1)}}$$

Green gave the critical speeds for the first mode, when N=1.

For a very slender shaft k/L=r=0, so that the rotatory inertia term and the shear deformation effects are zero, and the Euler beam representation can be used, with the critical speeds given as:

$$p = N\pi$$

In this case, a vibrating beam and a rotating shaft have the same critical speeds.

For describing a shaft with continuous disks by an equivalent shaft, Green introduced the following parameters: m = mass per unit length=mass of shaft + mass of disks/shaft length; i_d = diametric moment of inertia per unit length = diametric moment of inertia of shaft and all disks/shaft length. The radius of the equivalent shaft is found by equating the disk effect of the two systems.

The critical speeds of the discrete shaft-disks system can be obtained by the finite element method: either by lumping the disks or placing them internally. The equivalent shaft's critical speeds can be obtained from the formulae given or from the finite element method. It is to be noted that though the disk effect is the same for the actual and the equivalent systems, the cross-sectional moment of inertia is not.

4.3 Results and discussion

A few parameters are introduced which appear in the discussion:

1. Disk effect is $\mu_2 = k_d/L^2$, where k_d is the disk radius of gyration. This term compares the effect of the disk

in rotation to its effect in translation. For a
concentrated mass, disk effect is zero and for a ring
type disk with all the mass located at a large radius
from the centre, the ratio is very large (infinity). It
is shown in the graphs that the disk effect has a
monotonic* influence on the critical speeds both in the
forward as well as in the backward whirl.

2. Mass effect, μ_1, is the ratio of the mass of the disk to
   the mass of the shaft. This term gives an idea of the
   importance of the mass of the shaft in comparison to
   that of the disk.

3. Slenderness ratio is k/L, where k is the shaft radius of
   gyration. This term shows the importance of shear
   deformation and rotatory inertia effects of the shaft,
   applicable for thick shafts and higher modes.

   In Table 4.1, comparison is made between Den Hartog's
first critical speeds with the present results which
includes the shaft's shear effect for a cantilever-disk
system. For the cantilever chosen, k/L=0.04. The effect of
the shear is not much hence the second mode critical speeds
are shown. Though the effect is more than in the 1st mode it
is still negligible, the disk effect being dominant. For
different values of disk effect, $\mu_2 = (k_d/L)^2$, the
non-dimensional critical speed is given as:

$$p = \sqrt[4]{\frac{\omega^2 \rho A L^4}{EI}}$$

Table 4.1. Cantilever-Disk system; k/L=.04, L=6", t=.5"
Comparison of Den Hartog's and present analytical solutions.

Disk Effect	Beam (h=0)		Backward whirl(h=-1)	
	Den Hartog	Present	Den Hartog	Present
.01	5.4030	5.3403	4.1511	4.1016
.02	3.8418	3.7966	2.9832	2.9464
.04	2.7465	2.7134	2.1755	2.1472
.06	2.2667	2.2388	1.8278	1.8031
.08	1.9839	1.9588	1.6254	1.6028
.10	1.7927	1.7697	1.4897	1.4686
.20	1.3295	1.3114	1.1623	1.1451
.40	1.0170	1.0022	0.9346	0.9204
.60	0.8832	0.8701	0.8310	0.8183
.80	0.8042	0.7921	0.7670	0.7552
1.0	0.7503	0.7389	0.7217	0.7107
2.0	0.6130	0.6036	0.6008	0.5915
3.0	0.5484	0.5400	0.5410	0.5327
4.0	0.5078	0.5000	0.5026	0.4948

The finite element results with the disks included within the element and lumping at the nodes gave very close values; identical to the third decimal place. Thus, internally placed disk results are shown in the graphs. The abscissa for Figures 4.3 to 4.8 is the disk effect given by $(k_d/L)^2$ and the ordinate by the non-dimensional frequency, p. For Figures 4.11 and 4.12 the abscissa is the disk effect i_d/mL^2, where i_d is the diametric mass moment of inertia per unit shaft length and m is the mass per unit shaft length. The ordinate is the non-dimensional frequency,

$$\omega^2 \ mL^4/\pi^4 \ EI \ .$$

Figure 4.3 shows the critical speeds of a cantilever-disk system, using a 4 elements shaft model to study the disk effect. The gyroscopic effect raises the frequency in the forward whirl and lowers it in the backward whirl as compared to that of a beam. The internal representation and lumping of the disk at the node are identical as expected. As the disk effect increases the rotatory inertia/gyroscopic effect dominates the mass effect and the shear effect; thus, the results coincide with Green's.

Figure 4.4 gives the comparison for the second critical speed. Results of forward whirl are not shown as they are complex for Green's case.

In Figure 4.5, the first critical of a simply supported double disk system is shown. Two elements are used for the internal disks model and four for the lumped model. The disk

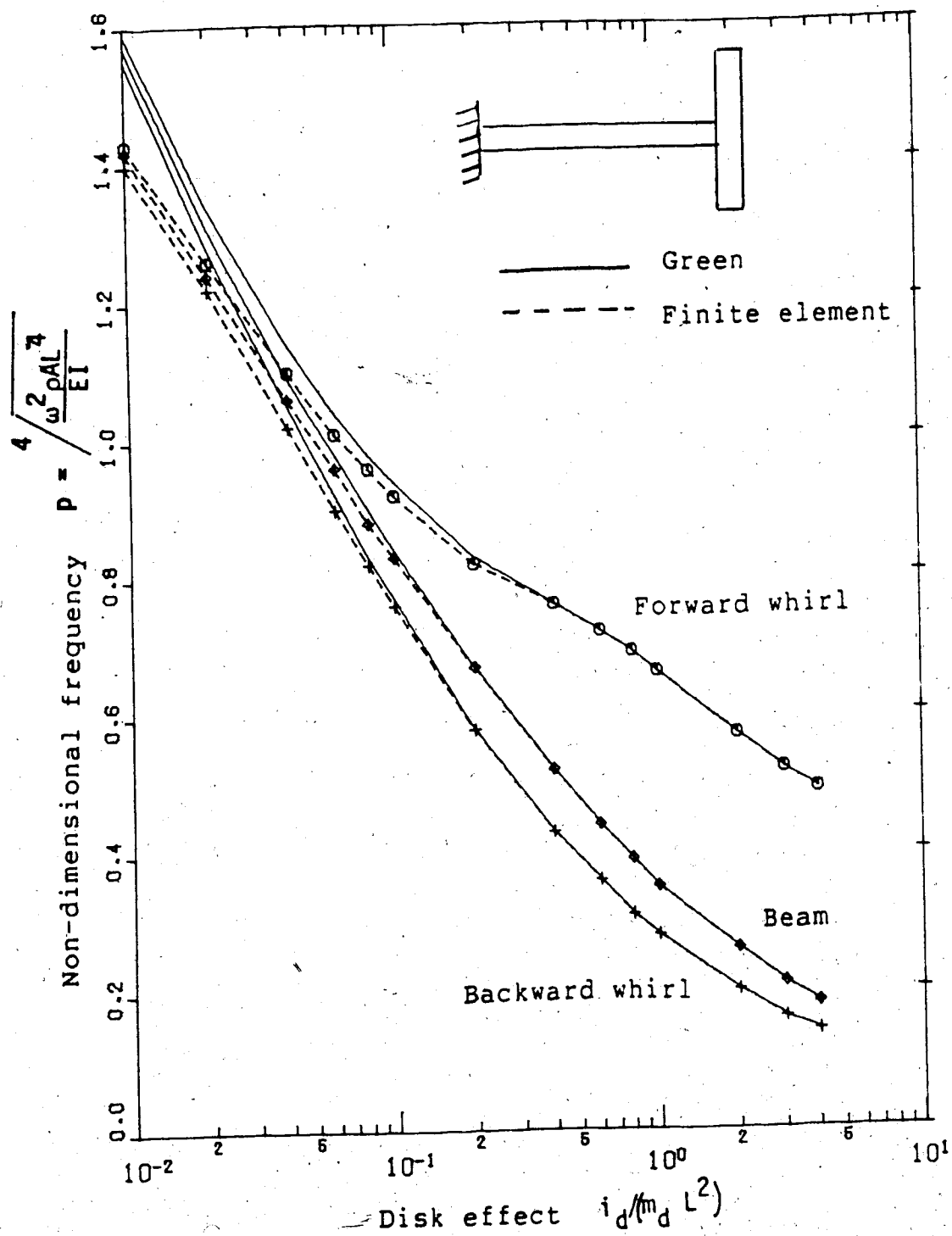$$P = \sqrt[4]{\dfrac{\omega^2 \rho A L^4}{EI}}$$

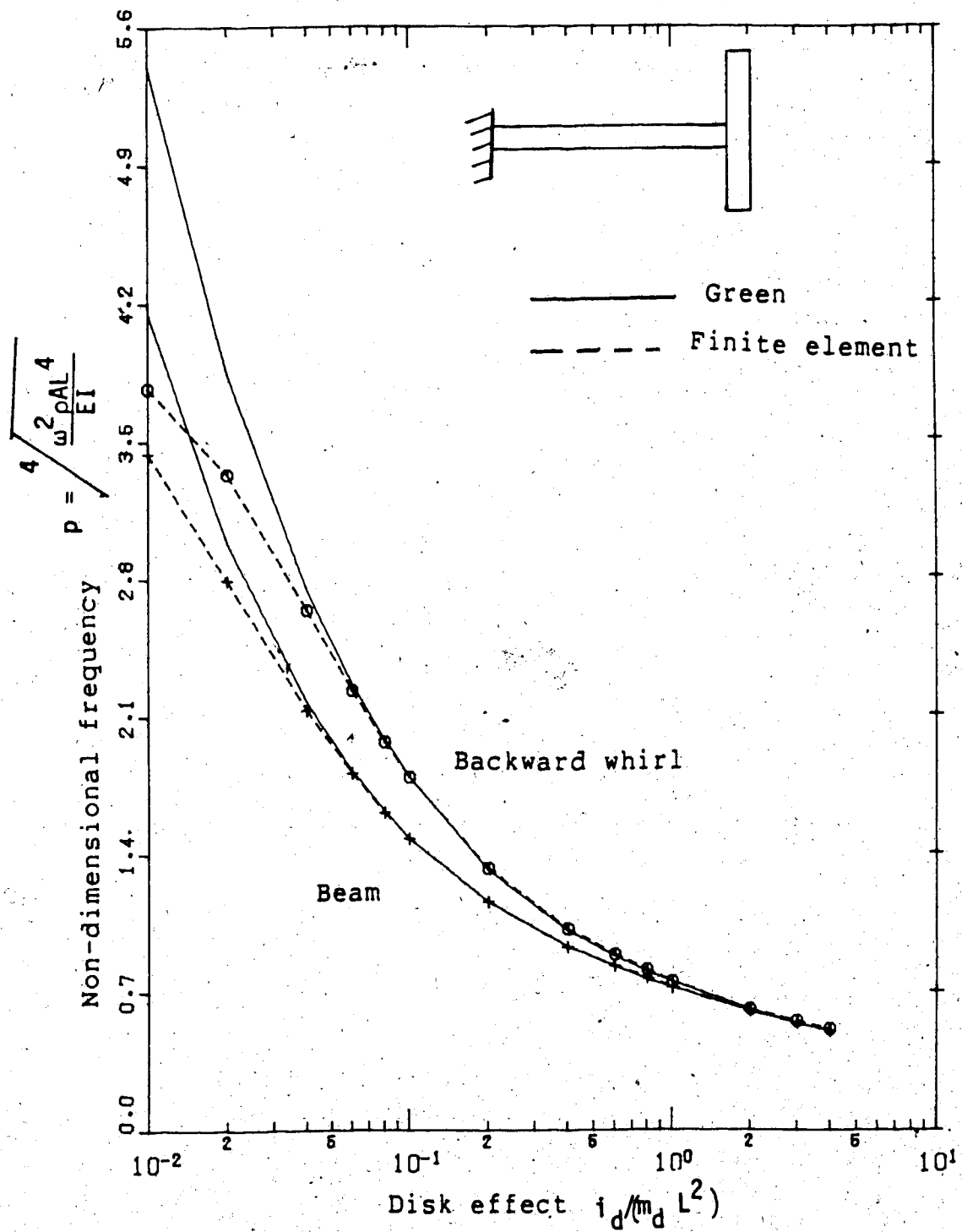Figure 4.3 1st critical speed of a cantilever disk system

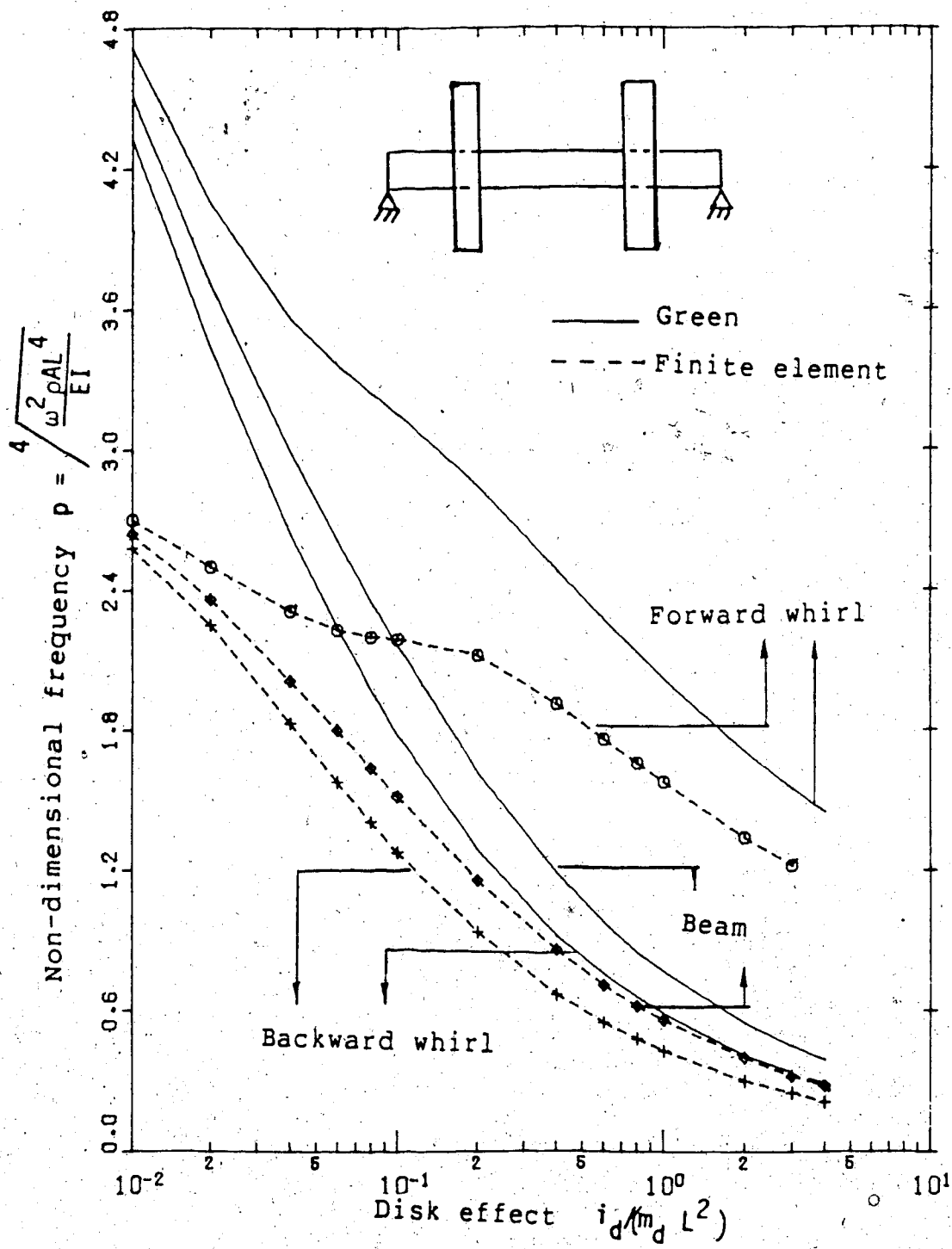Figure 4.4 2nd critical speed of a cantilever disk system

Figure 4.5 1st critical of a H-H double disk system

effect is not as dominant here as in a cantilever type system due to the double supports and the symmetry in the disk location.

Figure 4.6 shows the second critical speeds. With the disks placed a quarter of the way from the ends they will be at antinodes in the second mode and hence the gyroscopic effect is absent and the three types of motion; beam, forward and backward whirl have the same criticals as seen at low disk effects. As the disk effect increases, the mode shapes along with the antinode points change and the critical speeds of the three cases separate.

Figure 4.7 compares Green's, Eubank's and the finite element models. The disk is placed at a point one quarter of the length from the bearing, $\xi=0.25$ and mass effect, μ_1, is 22.2 times the disk effect, μ_2. Green's values are generally higher as he neglects the shaft's mass and shear effects. As the disk effect becomes zero, Green's theory gives infinity since the shaft is assumed to be massless. Whereas, with the finite element and the Eubank models, the critical speeds approach that of a uniform shaft for zero disk effect. For increasing disk effect, all three methods give decreasing critical speeds compared to that of a uniform shaft. For large disk effect, all three values converge as the disk effect is dominant and other effects become secondary.

Table 4.2 gives the results for a four disk shaft system. The critical speeds are given in rpm, periodic type elements are used to reduce computation. Four elements of

Table 4.2. Comparison of 1st critical speed(R.P.M) using
lumped and internally placed disk methods for
uniform disks and tapering disks.

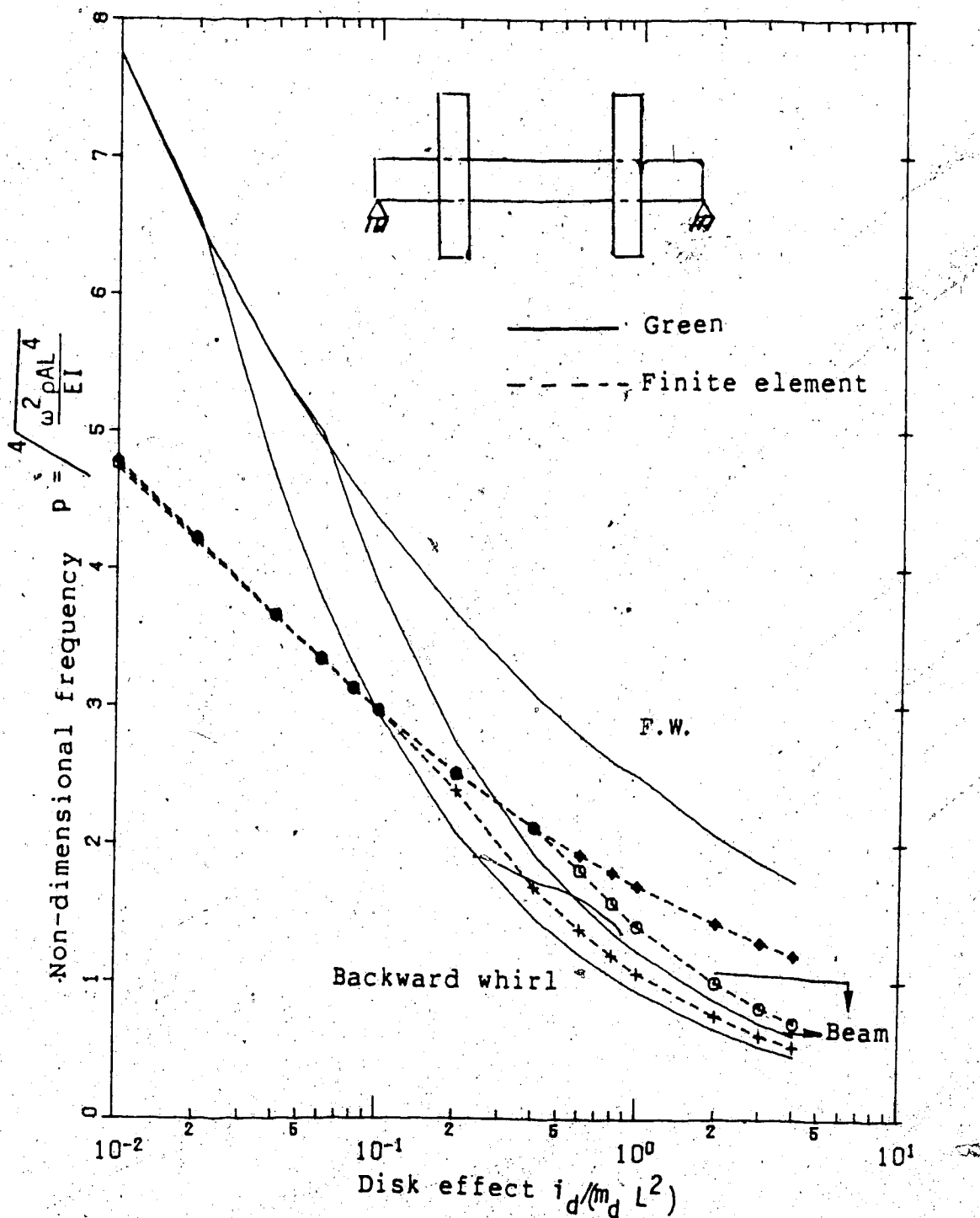| Method	# of disks per element	# of Elements	Beam	Forward whirl	Backward whirl
No Disks					
Analytical	0		7828.06	7874.73	7781.78
4 Uniform Disks					
Internal	1	4	6327.69	6654.75	6033.16
Internal	2	2	6321.70	6652.36	6028.03
Internal	4	1	6315.73	6652.29	6028.03
Lumped		8	6317.63	6650.19	6028.06
4 Tapering Disks					
Internal	1	4	6935.20	7159.0	6728.91
Lumped		8	6934.87	7158.84	6727.52

Figure 4.6 2nd critical speed of a H-H double disk system
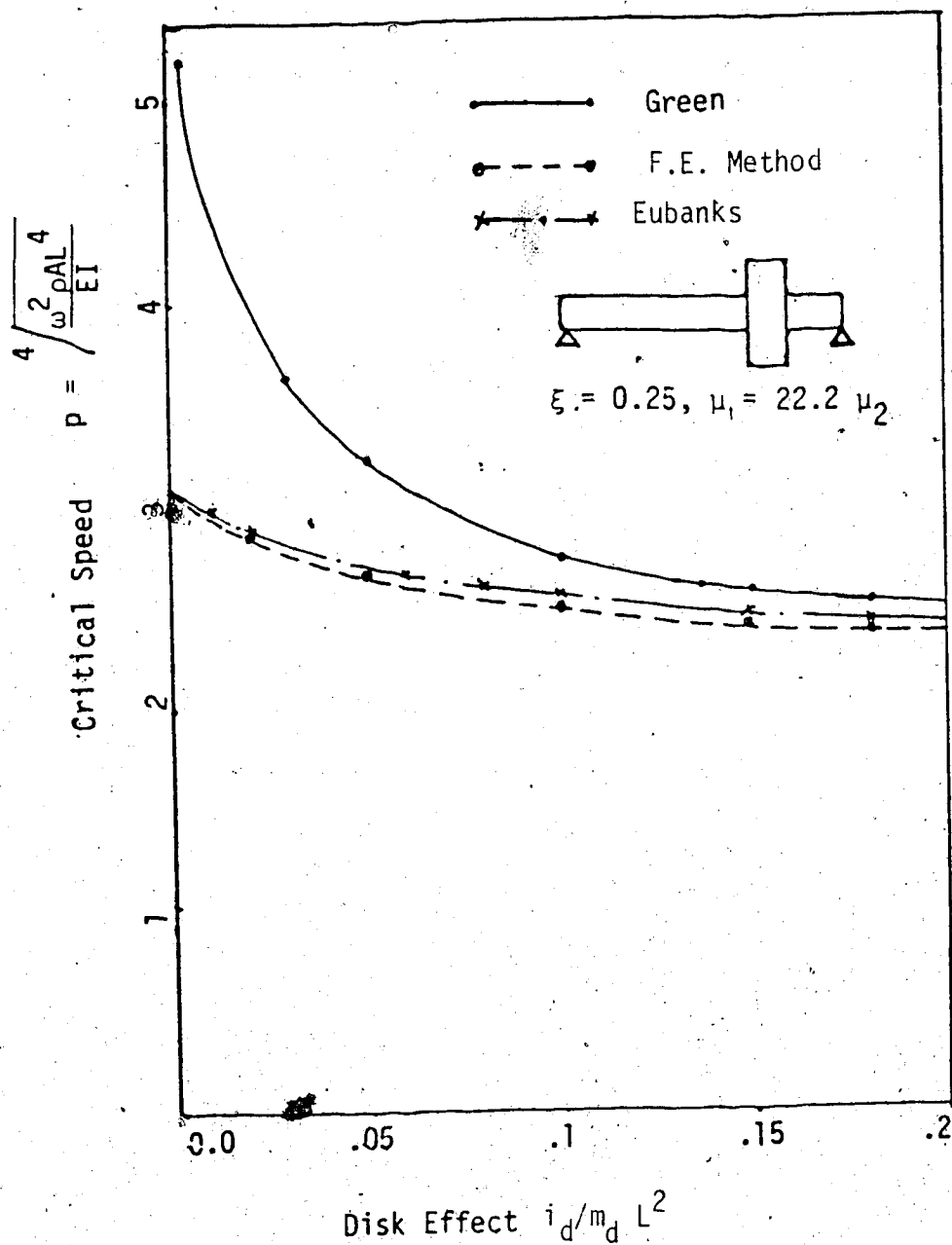
Figure 4.7 1st forward whirl of a H-H shaft-disk system

the type shown in Figure 4.9 are assembled to form the
shaft-d▮▮▮tem. Even one element with all the four disks
include▮ ▮▮qually accurate results compared to the 8
element▮ ▮▮del. Results are also given for a uniform
s▮ wi▮ ▮ring disks, shown in Figure 4.10. The disks
ar▮ ▮duc▮ in size (compared to uniform disks), hence the
dis▮ ▮ff▮▮ is less and critical speeds are higher compared
to t▮ ▮f the shaft with uniform disks.

4.3.1 ▮resentation of continuous disks on shaft

F▮▮re 4.11 pictures the three methods of inclusion of
continu▮s disks on a shaft: lumping at nodes, placing
inside a shaft element and an equivalent continuous shaft.

Figure 4.8 compares analytical solution of Euler,
Green(Ra▮▮▮gh) and the Timoshenko shafts. For the Rayleigh
shaft, ▮▮tory inertia effect is included and the critical
speeds are lowered compared to the Euler beam for the the
backward whirl and raised for the forward whirl. The
Timoshenko shaft includes the shear effect, in addition to
the rotatory inertia effect which further lowers the
critical speed. The finite element results of Chapter 3
coincide with those of a Timoshenko shaft; when shear
rigidity GKA is taken as infinite the results coincided with
Rayleigh's, as expected.

A 15 disk, 16 element, 64 degrees of freedom model for
the lumped case and a 5 element, 3 disks per element and 20
degrees of freedom internal disk model are used for
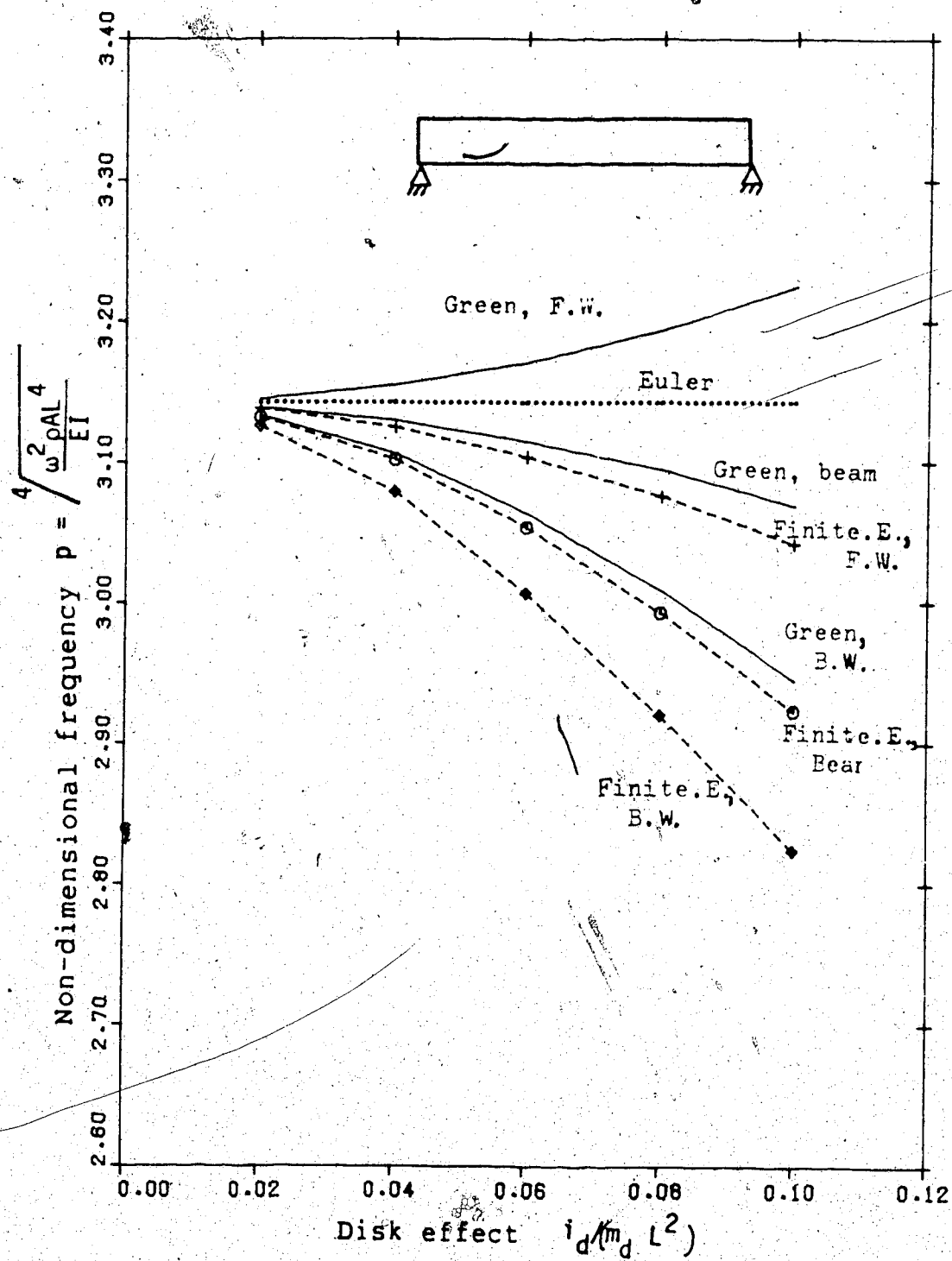
Figure 4.8 1st critical speed of a H-H continuous shaft
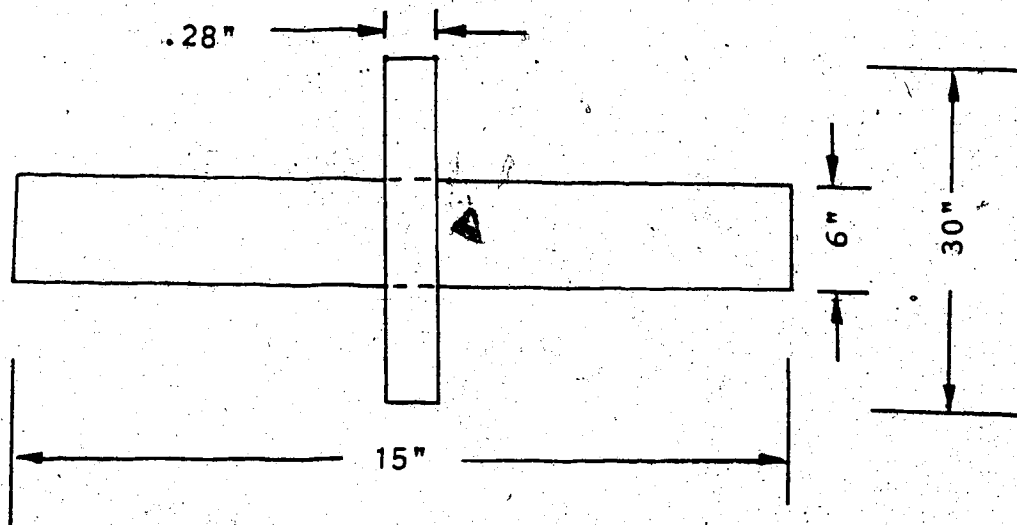
Figure 4.9 Periodic type shaft-disk element
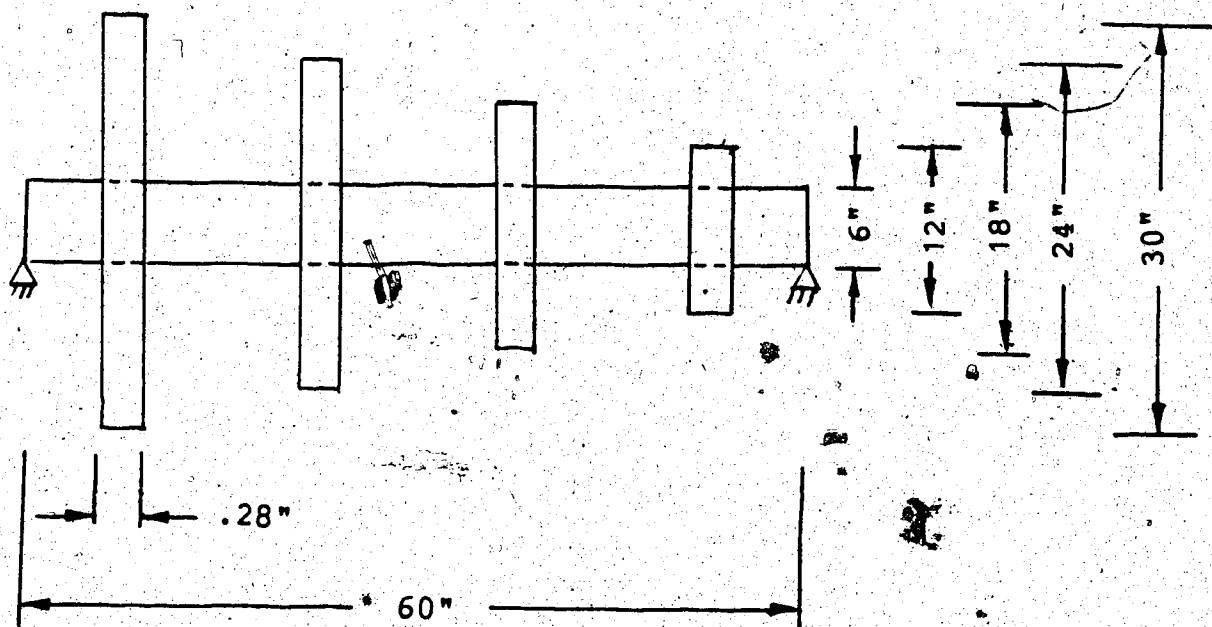
Figure 4.10 Shaft with tapering disks

1) Representation with disks at element nodes:
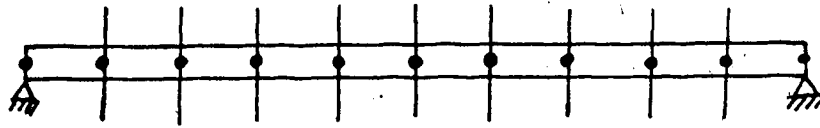
2) Representation with disks within an element:

M_{di}, I_{di}

1   i^{th} Disc   2

x_i
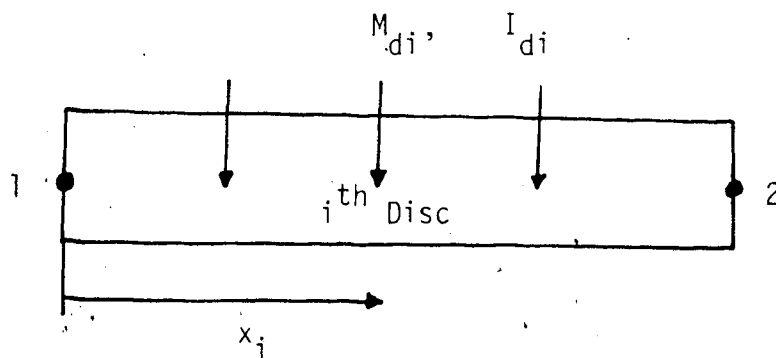
3) Representation as a continuous element:

$\omega^2 \rho \, A \, W \, dx$

$\rho \, \omega^2 I_D \, \phi \, (2h - 1)dx$

M   M + dM

V   V + dV

dx
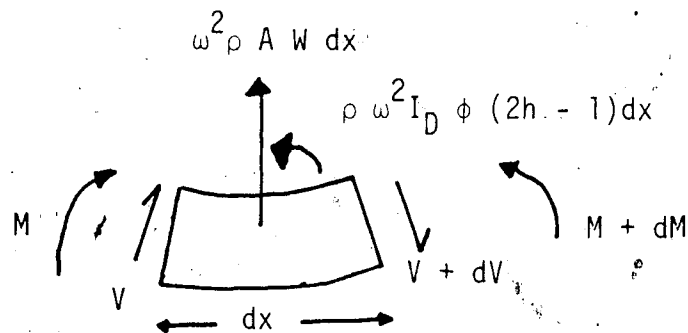
Figure 4.11 Representation of a shaft with continuous disks

comparison. Results of the two models matched closely.
Figure 4.12 compares the first critical speed of the finite
element method with Green's and the second critical is
compared in Figure 4.13. Discrepancy in the forward whirl is
because Green neglects the shear effect. Inclusion of the
shear effect will reduce the critical speeds of the
equivalent shaft.

Forward whirl in the second mode for Green's model is
not considered as it gives a negative root even for small
disk effect(.003).

4.4 Conclusions

Inclusion of disks inside a shaft element is useful in
modelling shaft-disk systems. No loss of accuracy is found
compared to the lumped method which uses more elements. The
reduction in degrees of freedom exponentially decreases the
computational cost. A system with tapering disks on a
uniform shaft, found in turbine stages of the turbo-rotor
system, is modelled.

For repeated structures the use of a periodic type
element, with one or more disks, reduces the computation
time.

The concept of inclusion of the disk effects within an
element can be extended to other local effects such as
bearings, to avoid nodes at those points. In the next
Chapter this method is extended to represent steps inside an
element.
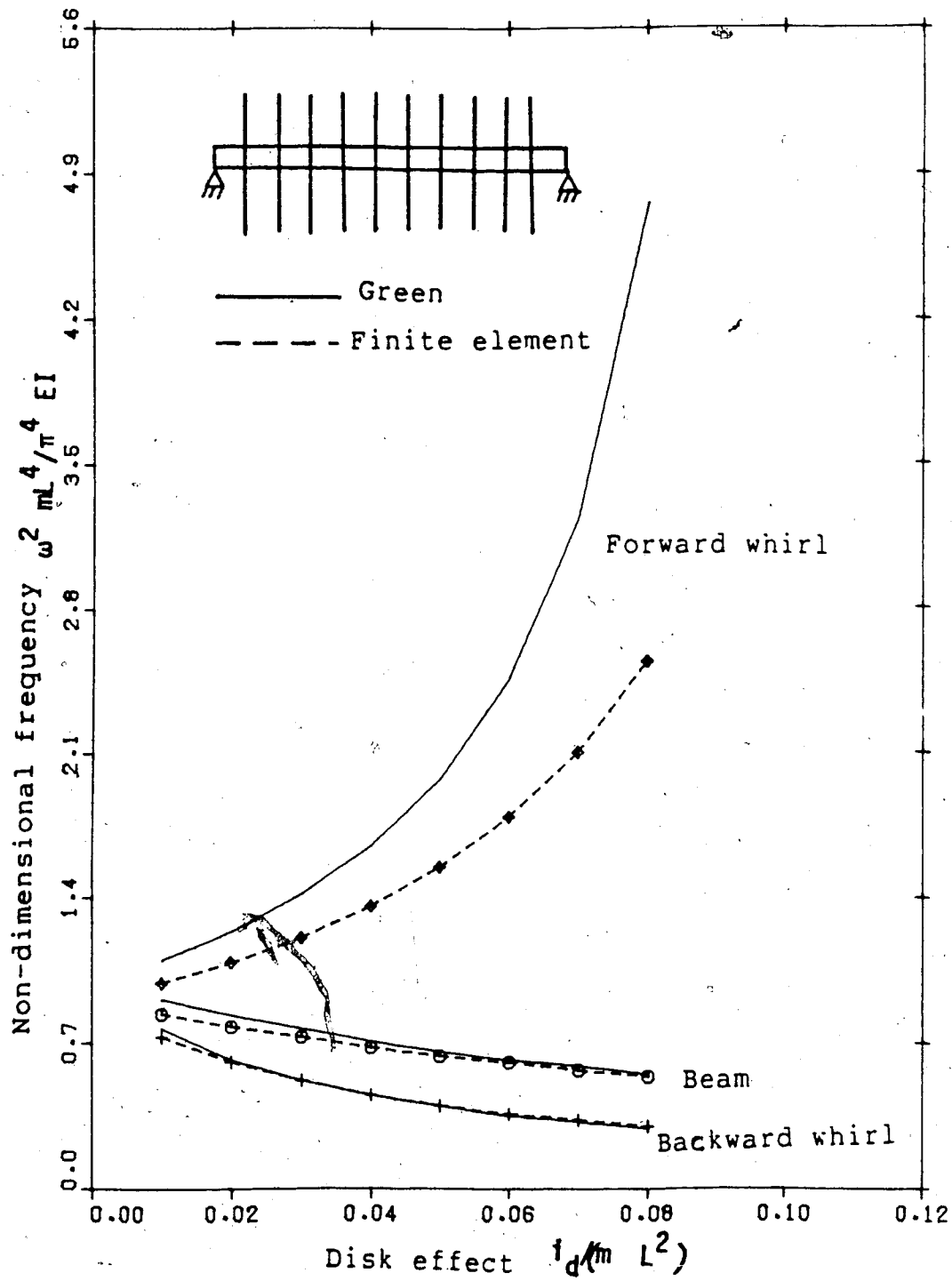
Figure 4.12 1st critical speed; shaft with continuous disks
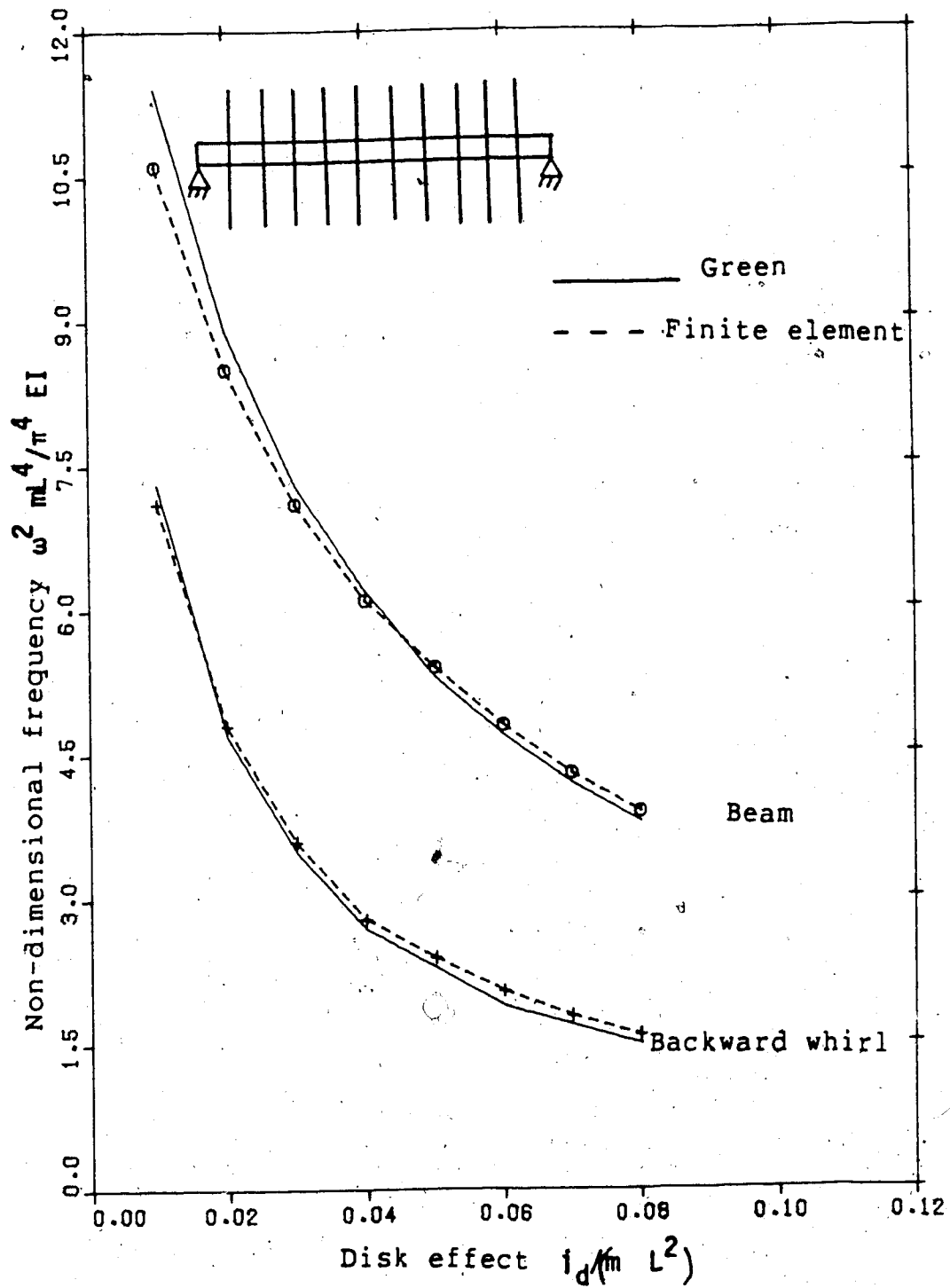
Figure 4.13 2nd critical speed; shaft with continuous disks

The Den Hartog's basic shaft-disk model is extended to include the shaft shear deformation and is illustrated for a cantilever-disk system. For other cases of Green, a similar analysis can be made using the Timoshenko beam flexibility coefficients from Appendix B.

For a shaft with continuous disks, the lumped disk model and the disks included model gave the same results. Not many elements are required if the disks are included inside the element. Thus, design and usage of equivalent continuous shaft can be avoided. If a designer insists otherwise (doesn't want to use the finite element method), then it is suggested that he should use the more accurate Timoshenko shaft to represent the shaft-disks system, instead of Green's.

5. MODELLING DISCONTINUITIES IN A ROTOR

Abstract

Optimization of the weight and strength of an actual rotor often results in a shaft with many steps. In a finite element model, representing each of these steps by individual elements leads to an unmanageable system size. The designer normally overcomes this problem by obtaining an averaged cross-sectional variation.

In this Chapter, a stepped element is formulated which performs better than the linearly tapered element in representing shaft discontinuities.

5.1 Introduction

Rotors of industrial machinery have discontinuities or stepped sections. Some of the disks are not thin and can store strain energy. They cannot be lumped at a point, their effects being functions of a portion of the length of the shaft and not just of a point.

While modelling such rotors for finite element analysis these intersections have to be represented accurately, yet the number of elements and the nodal degrees of freedom have to be minimized. The most accurate model considers each intermittent portion as a section, each section divided into one or more elements as shown in Figure 5.1. Typically, the rotor of each stage of a turbo-generator has ten to twenty

138
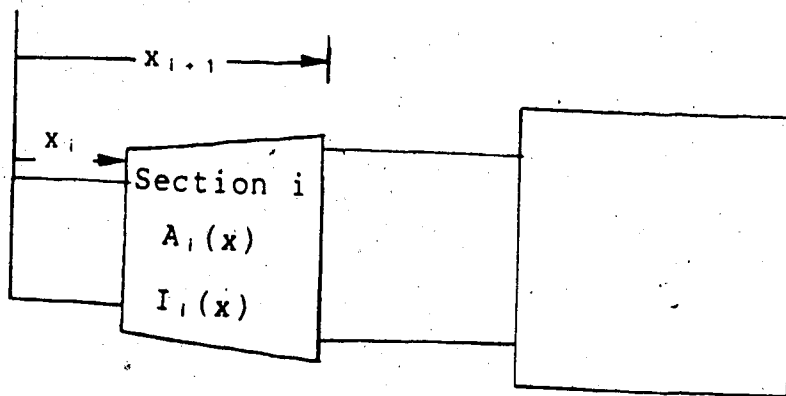
Figure 5.1 Rotor with discontinuous sections
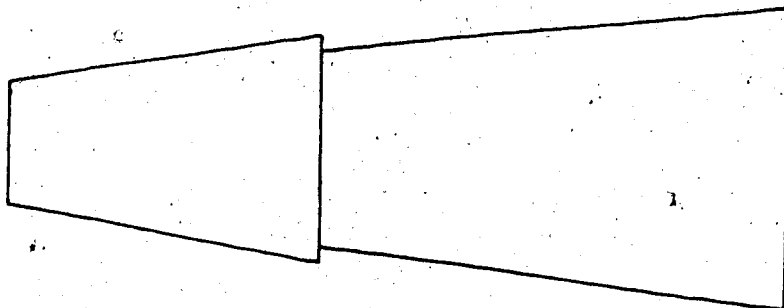
Figure 5.2 Approximate model using tapered sections

sectional changes. An accurate representation is again limited by the computing costs and storage capacity.

An economical model can be achieved by combining two or more sections into a linear or higher order tapered section as shown in Figure 5.2. The easiest model will be to join the end cross-sections with a linear taper inbetween. For sections with unequal lengths some weighting factors may be introduced to obtain a tapered model with equivalent kinetic and potential energies. However, a more useful element will be a coupling element which can include one or more discontinuities inside. The rotor of Figure 5.1 can be modelled, as it is, with just one such element.

5.2 Modelling

A stepped element can be obtained as follows:

1. using a Gaussian integration scheme to have integration points on each side of the step as shown in Figure 5.3;
2. using piecewise integration as shown in Figure 5.4;
3. adding the effect of the extra material to a uniform base element, Figure 5.5.

In the first method, a single Gaussian four point integration gives the mass and stiffness matrices. For a single step with equal lengths on either side of the step there will be two Gaussian points on each side. The disadvantage with this model is that the maximum number of steps that it can accomodate is limited by the number of Gaussian integration points used. Also, one has to be
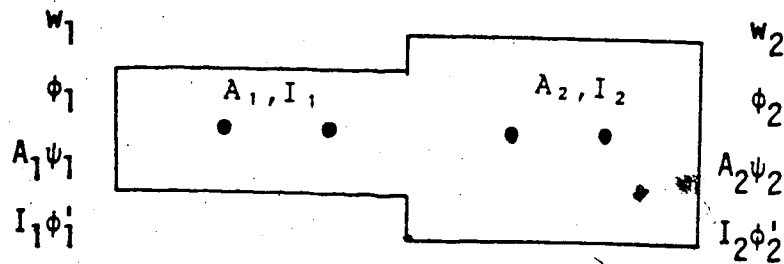
Figure 5.3 Step element: four point Gaussian integration
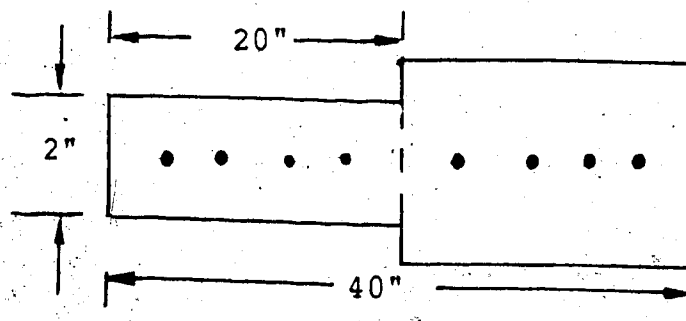
Figure 5.4 Step element: piecewise integration
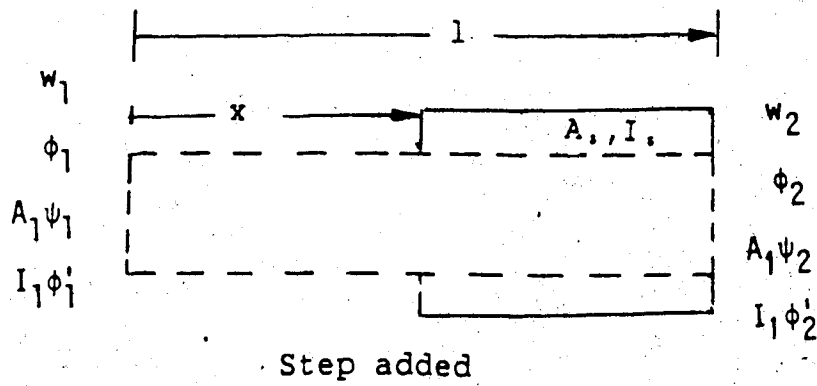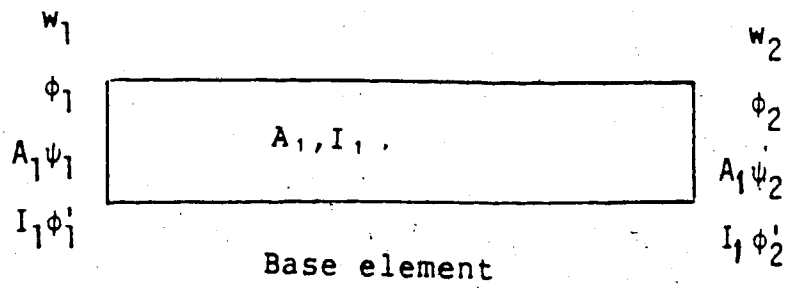
Figure 5.5 Step element: added to a base element

careful to have at least a Gaussian point in each section as these points occur at specified distances in the element and some sections might get neglected.

A second scheme can be used to overcome these drawbacks by introducing piecewise integration as shown in Figure 5.4. Each section is individually integrated and its mass and stiffness matrices are obtained in terms of the intermediate variable values. All the sectional matrices are then transformed to the stepped shaft end nodal variables and summed to give the element matrices. The computational effort involved in getting the mass and stiffness matrices is the same as the case with individual elements for each side of the step. But, the number of degrees of freedom is greatly reduced which eases further calculations (as in eigenvalue evaluation). This method can theoretically accomodate unlimited steps in a single element as does the next method.

The third method has a base element, Figure 5.5, which can be either uniform or tapered. To the mass and stiffness matrices of the base element are added the mass and stiffness matrices of each step, Figure 5.5, to form the element matrices. These matrices are in terms of the base element nodal variables and have to be transformed to conform to the actual end nodal variables.

The three methods performed equally well when tested with uniform shafts, and for a shaft with a single step.

5.3 Theory

The direct formulation of the element shown in Chapter 2 is used. For the first method of inclusion of the step inside an element a single integration will give the mass and stiffness matrices. For the second method, integration of the ith section between the limits x_i and x_{i+1}, Figure 5.1, gives the mass and stiffness matrices of the section in terms of the intermediate variables. Let [M_i] and [K_i] be the mass and stiffness matrices of the ith section transformed to the step element nodal variables. Summation of all the N sectional matrices gives the element matrix:

$$[K] = \sum_{i=1}^{N} [K_i]$$

$$[M] = \sum_{i=1}^{N} [M_i]$$

For the third method the element matrices are obtained as:

$$[K^*] = [K_b] + \sum_{i=1}^{N} [K_i]$$

$$[M^*] = [M_b] + \sum_{i=1}^{N} [M_i]$$

Where [K_b] and [M_b] are the base element matrices and [K_i] and [M_i] are matrices for the ith step. Correponding cross-sectional areas and second moments (A_1, I_1) and (A_i, I_i) are used as shown in Figure 5.5, in each ▆▆▆▆ calculating the step matrices integration is

done for the step length, say x to L. Interpolation functions of the base elements are used. Hence, the stepped element matrices are obtained in terms of the base element nodal variables. The transformation to the end nodal variables of the stepped shaft is given as:

$$\{w_B\} = [T]\{w_e\}$$

where $\{W_B\}$ is the base element nodal variable vector, $\{W_e\}$ the stepped shaft nodal variable vector and $[T]$ the transformation matrix. In the expanded form:

$$
\begin{Bmatrix} w_1 \\ \phi_1 \\ A_1\psi_1 \\ I_1\phi_1' \\ w_2 \\ \phi_2 \\ A_1\psi_2 \\ I_1\phi_2' \end{Bmatrix}
=
\begin{bmatrix}
1 & 0 & 0 & 0 & 0 & 0 & 0 & 0 \\
0 & 1 & 0 & 0 & 0 & 0 & 0 & 0 \\
0 & 0 & 1 & 0 & 0 & 0 & 0 & 0 \\
0 & 0 & 0 & 1 & 0 & 0 & 0 & 0 \\
0 & 0 & 0 & 0 & 1 & 0 & 0 & 0 \\
0 & 0 & 0 & 0 & 0 & 1 & 0 & 0 \\
0 & 0 & 0 & 0 & 0 & 0 & A_1/A_2 & 0 \\
0 & 0 & 0 & 0 & 0 & 0 & 0 & I_1/I_2
\end{bmatrix}
\begin{Bmatrix} w_1 \\ \phi_1 \\ A_1\psi_1 \\ I_1\phi_1' \\ w_2 \\ \phi_2 \\ A_2\psi_2 \\ I_2\phi_2' \end{Bmatrix}
$$

The transformation of the mass and stiffness matrices is as follows:

$$[K] = [T^T][K*][T]$$

$$[M] = [T^T][M^*][T].$$

5.3.1 Transfer matrix method

The mass of each section is divided equally between the nodes, a three node, lumped mass system is obtained. An Euler beam model is shown below:
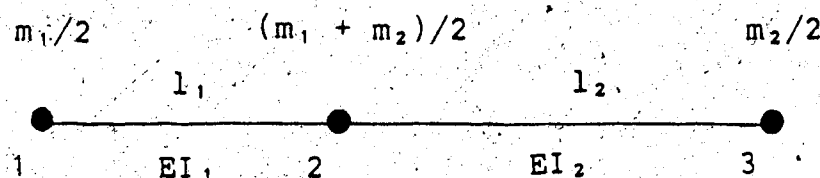
$$[P_i] = \begin{bmatrix} 1 & 0 & 0 & 0 \\ 0 & 1 & 0 & 0 \\ 0 & 0 & 1 & 0 \\ m\omega^2 & 0 & 0 & 1 \end{bmatrix}$$

the state vector is:

$$\{w_e\} = \begin{Bmatrix} -w \\ \phi \\ M \\ V \end{Bmatrix}$$

the field matrix for the ith span is:

$$[F_i] = \begin{bmatrix} 1 & \ell_i & \dfrac{\ell_i^2}{2EI_i} & \dfrac{\ell_i^3}{6EI_i} \\ 0 & 1 & \dfrac{\ell_i}{EI_i} & \dfrac{\ell_i^2}{2EI_i} \\ 0 & 0 & 1 & \ell_i \\ 0 & 0 & 0 & 1 \end{bmatrix}$$

where, $\{W_e\}$ is the nodal variable vector, $[P_i]$ the point matrix and $[F_i]$ the field matrix. This method is discussed in detail by Pestel and Leckie[63]. The system equation relating the extreme state vectors is:

$$\{W_e\}^{3L} = [P_3][F_2][P_2][F_1][P_1]\ \{W_e\}^{1L}$$

which can be written as:

$$= [U]\ \{W_e\}^{1L}$$

where $[U]$ is the system transfer matrix relating variables at one end to the other. Application of the simply supported boundary conditions $W = M = 0$ at both ends gives the characteristic equation:

$$\begin{bmatrix} U_{12} & U_{14} \\ U_{32} & U_{34} \end{bmatrix} = 0$$

each element of this matrix is a function of the rotational speed, ω. Hence, a root search method is used to obtain the actual critical speeds of the system.

5.3.2 Rayleigh quotient

In this method, for an Euler beam, the ratio of maximum potential and kinetic energies gives:

$$\omega^2 = \frac{\int_0^{\ell_1} EI_1 (w'')^2 dx + \int_{\ell_1}^{L} EI_2 (w'')^2 dx}{\int_0^{\ell_1} \rho A_1 w^2 dx + \int_{\ell_1}^{L} \rho A_2 w^2 dx}$$

Assuming a solution $w = w_0 \sin \frac{\pi x}{L}$, which satisfies the simply supported boundary conditions at both ends, we get:

$$\omega^2 = \frac{E\pi^4}{\rho L^4} \left[\frac{I_1 + I_2}{A_1 + A_2} \right] , \text{ when } \ell_1 = L/2 .$$

5.4 Results and discussion

A complex Timoshenko beam finite element can have more than two variables per node. Continuity of all the variables to be coupled is established, for the element TM544, especially at the points of discontinuities. In Table 5.1

Table 5.1. Coupling a stepped beam using 2 elements.
Critical speeds(in rpm) of first three modes.

Using Nodal Variables (W, W', ϕ, ϕ')		Using Nodal Variables (W, W', $A\psi$, $I\phi'$)	
Coupling W, 14 d.o.f	Total Coupling 12 d.o.f	Coupling W, 14 d.o.f	Total Coupling 12 d.o.f
5595.70	6376.44	5595.7	5595.76
34667.4	41650.2	34667.4	34669.7
71045.3	95063.8	71045.3	71301.27
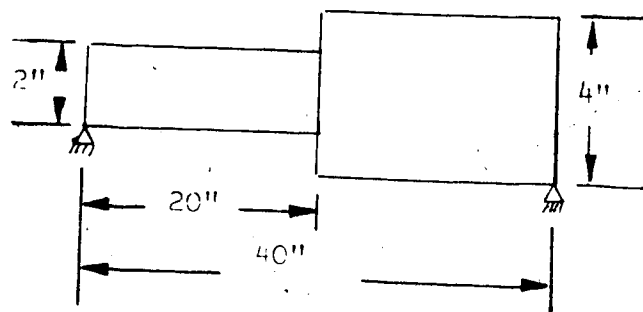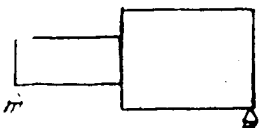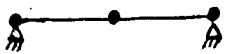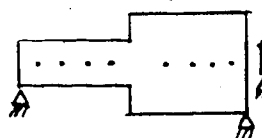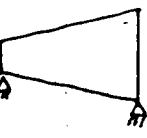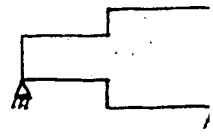
Table 5.2. Comparison of 1st critical speed(in rpm) of a
stepped beam. K=0.85, E/G=2.6.

$\frac{D1}{D2}$	Finite Element	Transfer Mat -rix	Step inc- luded	Tapered	Rayleigh Quotient
	2 Elements	3 Nodes	1 Element	1 Element	1 Elem
1.0	5919.82	5896.69	5923.4	5924.77	5942.
.95	6057.21	6030.38	6088.1	6407.47	6108.
0.9	6171.63	6125.87	6292.8	6987.70	6315.
.85	6257.43	6192.71	6545.6	7695.25	6571.
0.8	6308.77	6202.26	6856.2	8572.36	6886.
0.7	6285.15	6068.57	7699.4	11110.2	7744.
0.6	6058.44	5705.70	8948.5	15540.1	9025.
0.5	5595.76	5113.64	10799.1	22089.7	10957

% errors with 2 element finite element model as the standard.

1.0	0.0	.39	.06	.08	.37
.95	0.0	.44	.51	5.78	.85
.9	0.0	.74	1.96	13.22	2.33
.85	0.0	1.03	4.60	22.97	5.01
.8	0.0	1.68	8.67	35.88	9.15
.7	0.0	3.44	22.5	76.76	23.2
.6	0.0	5.82	47.70	156.5	48.98
.5	0.0	8.61	92.98	294.75	95.80

two sets of nodal variables are compared. The first set has centroidal displacement, W, its derivative, W', bending slope, ϕ and its derivative ϕ' as the nodal variables and the second set has W, ϕ, Aψ and Iϕ' as the nodal variables.

For a uniform beam both these sets of variables give the same results as total coupling can be used at the element interphases. However, for a stepped beam only the second set can have total coupling , Table 5.1, as bending moment and shear forces are continuous even at points where sectional change occurs. If external forces or moments are applied, then even the second set becomes discontinuous as discussed in Chapter 2. Thus, one has to check the compatibility of the nodal variables when a step is included in an element to avoid discontinuity of the variables inside the element. The second set is used in the present analysis.

Table 5.2 has a comparison of the 1st critical speed, for a stepped beam. The two element model; one on each side of the step, can be considered as a standard for comparison of other methods(transfer matrix, Rayleigh, tapered and stepped element).

Only one method of inclusion of step (piecewise integration) is presented as the other two methods performed equally well.

For increasing step ratio the standard two element models(finite element and transfer matrix) have decreasing critical speeds; whereas, the one element models(Rayleigh, tapered and stepped element) have increasing critical

speeds.

The transfer matrix method, using the Euler beam, is closest to the standard model, as it also represents the step with an element on each side. Among the one element models; the Rayleigh's method using the Euler beam and the finite step element perform equally well. The linearly tapered element has an error double that of a stepped element for all step ratios. The error in critical speed becomes prohibitive; greater than 5% for a step ratio of .8 using a stepped element and 9.5% using a linearly tapered element.

Comparison shows that with small steps (step ratio between .8 and 1) accurate results are obtained using a stepped element and it performs better than the tapered element.

For large steps (step ratio less than .8) use of one element, either tapered or stepped, is inadvisable. A two element model, one on each side of the step, is required to represent shafts with large steps.

5.5 Conclusions

An adaptor element is developed, useful to connect shaft sections of different diameters. Three methods of including sectional discontinuities within an element are presented. A stepped element performs better than a tapered element in representing a shaft with steps.

Caution is required while reducing the degrees of freedom during the modelling of a shaft with a large stepped joint. The effect of incorrect modelling may not surface during the study of a large turbo-generator, as this effect is lost in the size of the rotor involved; but, it will for a smaller size shaft system.

A curve of revolution fitted through the small steps of an axi-symmetric shaft gives a higher order tapered shaft element which might be comparable to the element with the discontinuities included within.

6. SHORT BEARINGS

Abstract

Heavy rotors, operating at medium speeds are usually supported by fluid film bearings. Short journal bearings are the most commonly found rotor supports in turbo-generator systems. The bearing fluid film provides spring and damping effects which greatly influence the dynamic character and performance of the rotor. Capacity number completely describes a short bearing and can be readily calculated for a given bearing, running speed, oil viscosity and load. The bearing non-dimensional stiffness and damping coefficients have been plotted with this parameter as the independent co-ordinate, using Holmes' equations. The asymmetric bearing coefficients are discussed and have been included in the equations of the shaft motion.

6.1 Introduction

Rotor supports of the rigid or ideal type increase the critical speeds as shown in Figure 6.1. Their use is restricted to analytical calculations and interpretations. Rarely do such end conditions appear in practice as the dynamic forces transmitted will be large and the relative motion will wear off the supports quickly.

The simplest alteration that can be suggested is the use of isotropic flexible supports. A representative beam in

flexure on such mountings has support stiffness dependent

dynamic characteristics: effect on the shaft critical speeds

is shown in Figure 6.1. Very low support stiffness

corresponds to a free-free beam with rigid body motion in

the first two modes. The third and higher modes are always

flexible, with the shaft bending due to its elastic

properties.

The support stiffness of a practical rotor occupies the

middle region, representative of fluid/rolling element

bearings. The dotted line separates this as the elastic

shaft region calling for a flexible balancing procedure. The

lower left end has the shaft in rigid body motion where

dynamic balancing of the first two modes will suffice.

The fluid film region of Figure 6.1 accounts for the

reactions due to the supports that are displacement

proportional. The bearing stiffness can be obtained by

differentiating the static load-displacement curve for a

given eccentricity ratio. However, the load, in general, is

dynamic in nature. The fluid endures a squeeze film action

giving rise to velocity dependent forces or the damping

reactions. Also, the forces need not be due to the inplane

displacements and velocities alone: the quadrature

components provide the cross-coupling dynamic coefficients.

The fluid film dynamic coefficients are frequency dependent.

The turbine-generator rotors are mounted on fluid film

bearings. Recently, with the knowledge from the extensive

study on stability of rotors many types of bearings are
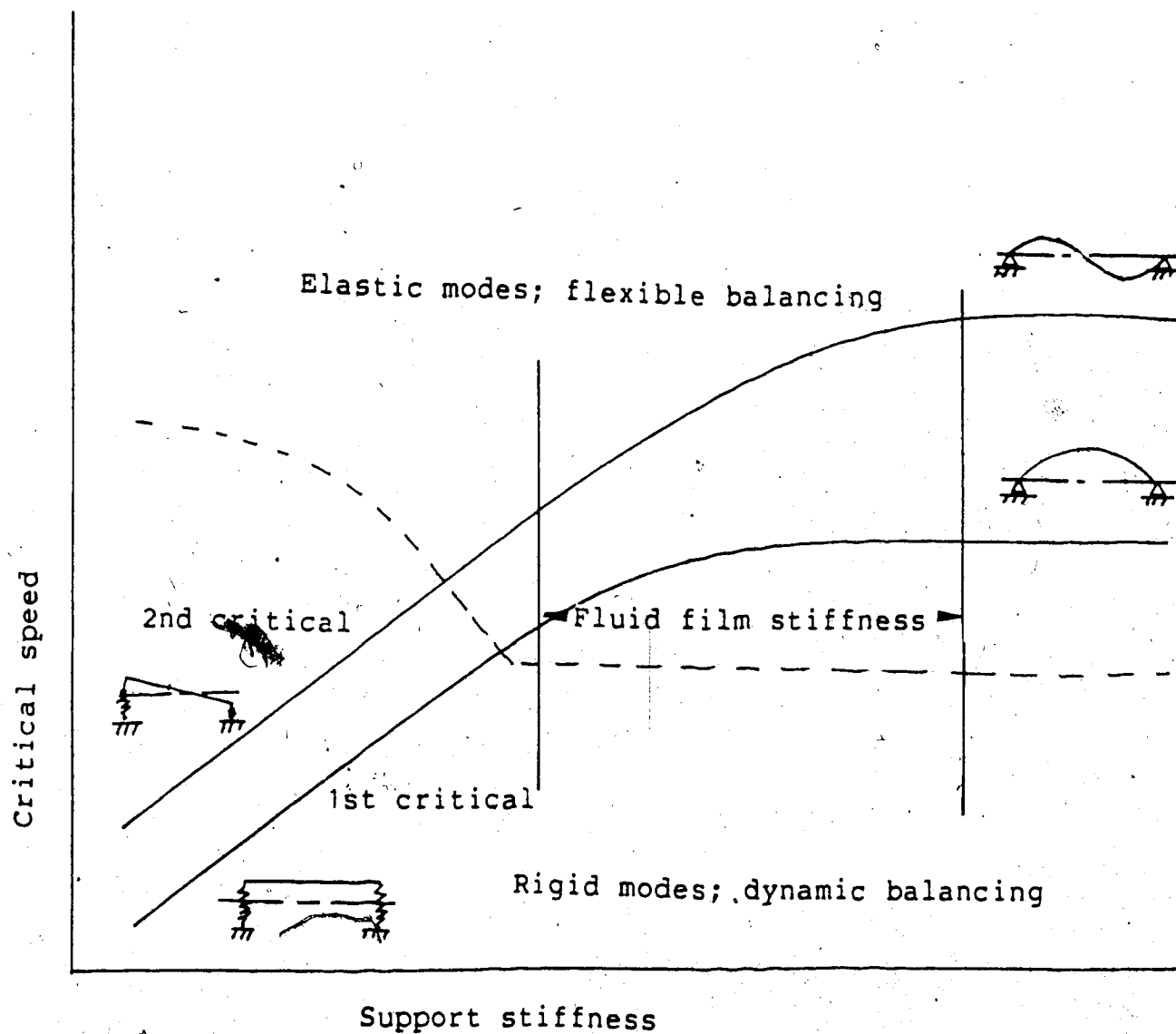
Figure 6.1 Effect of support stiffness on the shaft critical speed

suggested and used: elliptical, tilted pad and partial
journal bearings to mention a few. Yet, the most common type
of bearing used in power plants is the short bearing with
the length to diameter ratio less than one.

Dubois.G.B and Ocvirk[63] have given the equations
governing the pressure distribution of a short sleeve
bearing and the parameters involved. Their theory was
supplemented by experimental evidence, leading to further
research on the subject.

Holmes[64], obtained the stiffness and damping
coefficients of short bearings; and used them to obtain the
response and stability of a rigid rotor supported at the
ends in short bearings. Recently in an N.R.C. report, Kim
and Lowe[65], the bearing damping and stiffness coefficients
have been plotted against the Sommerfeld number instead of
the usual independent parameter of eccentricity ratio; full
and partial bearings were considered for finite bearings.

Padovan and Adams[66] have given a very good account of
the treatment of rotor dynamics. Among other factors,
inclusion of the bearing effects was discussed enhancing the
understanding and computer modelling of the rotor systems.

In the present Chapter, a short bearing is used to
review the dynamic coefficients of Holmes'. These
coefficients are plotted with respect to the capacity
number.

Sommerfeld number is a useful parameter which includes
all the other parameters affecting a finite bearing, except

L/D ratio. Capacity number is a more appropriate independent variable for short bearings as it includes variations in load, viscosity, speed, L/D and C/R values of the bearing.

6.2 Theory

The basic assumption of a short bearing, apart from those used for finite bearings, is that the pressure gradient in the axial direction is much more than in the circumferential, which leads to the assumption of total flow of the lubricant from the ends. This assumption is true for bearings with short axial lengths (L/D less than 1.)

Figure 6.2 shows the bearing-journal configuration. Under static load the journal rests on the bearing, acted upon by the vertical gravitational load. As the journal rotational speed and/or the load varies the shaft centre follows the locus shown by the dotted lines. C_{j_s} is the shaft steady state position. Due to disturbances such as mass unbalance, the journal assumes a whirl path about the steady state position. The dynamic journal centre C_{j_d} causes a change in the attitude angle by a. The linear treatment by Holmes implies that the angle a is small and the distance $C_{j_s}C_{j_d}$ is small compared to the steady state eccentricity, e_0. Thus the dynamic eccentricity, e, and the attitude angle, ϕ, can be expanded about the steady state values e_0 and ϕ_0 by using the Taylor series; retaining the linear terms.

Figure 6.2 Journal-bearing configuration

Holmes obtained the fluid pressure forces, linear in terms of the distances and the velocities r, s, $\dot{r}$ and $\dot{s}$, which give the dynamic coefficients about the steady state axes, $C_j.rs$. The coefficients are given explicitly by Holmes as functions of the steady state eccentricity ratio, ϵ: a_{rr}, a_{rs}, a_{sr} and a_{ss} are the stiffness coefficients and b_{rr}, b_{rs}, b_{sr} and b_{ss} are the damping coefficients. These coefficients are implicit functions of the rotational speed and load as the eccentricity ratio is dependent on these values. This dependence has to be borne in mind as the dynamic coefficients have to be evaluated afresh at each running speed.

As the dynamic axes, $C_j.rs$, change with the steady state condition, it will be convenient to obtain these coefficients about a fixed system of axes say the $C_j.yz$ axes.

Smith.D.M[67], Hahn[68] and others have given explicit functions for the coefficients. Table 6.1 gives the explicit values of Smith, transformed to Holmes' axes. These values are also for the short bearings with the linear assumptions. Two misprints in Smith's equations have been corrected, here.

In our study the coefficients are obtained numerically using a linear transformation:

Table 6.1 Dynamic Coefficients: explicit values

$$a_{yy} = \frac{4\{\pi^2(2-\epsilon^2) + 16\epsilon^2\}}{[\pi^2(1-\epsilon^2) + 16\epsilon^2]^{3/2}}$$

$$a_{yz} = \frac{\pi\{\pi^2(1-\epsilon^2)^2 - 16\epsilon^4\}}{\epsilon(1-\epsilon^2)^{1/2}[\pi^2(1-\epsilon^2) + 16\epsilon^2]^{3/2}}$$

$$a_{zy} = \frac{-\pi\{\pi^2(1-\epsilon^2)^2(1+2\epsilon^2) + 32\epsilon^2(1+\epsilon^2)\}}{\epsilon(1-\epsilon^2)^{1/2}[\pi^2(1-\epsilon^2) + 16\epsilon^2]^{3/2}}$$

$$a_{zz} = \frac{4\{\pi^2(1-\epsilon^2)(1+2\epsilon^2) + 32\epsilon^2(1+\epsilon^2)\}}{(1-\epsilon^2)[\pi^2(1-\epsilon^2) + 16\epsilon^2]^{3/2}}$$

Smith, has a misprint; $32\epsilon^2(1-\epsilon^2)$ in the numerator

$$b_{yy} = \frac{2\pi(1-\epsilon^2)^{1/2}\{\pi^2(1+2\epsilon^2) - 16\epsilon^2\}}{\epsilon[\pi^2(1-\epsilon^2) + 16\epsilon^2]^{3/2}}$$

$$b_{zz} = \frac{2\pi\{\pi^2(1-\epsilon^2)^2 + 48\epsilon^2\}}{\epsilon(1-\epsilon^2)^{1/2}[\pi^2(1-\epsilon^2) + 16\epsilon^2]^{3/2}}$$

$$b_{zy} = b_{yz} = \frac{8\{\pi^2(1+2\epsilon^2) - 16\epsilon^2\}}{[\pi^2(1-\epsilon^2) + 16\epsilon^2]^{3/2}}$$

$$[T] = \begin{bmatrix} \cos \phi_0 & -\sin \phi_0 \\ \sin \phi_0 & \cos \phi_0 \end{bmatrix}$$

where ϕ_0 is the steady state attitude angle related to the steady state eccentricity ratio, ϵ, as:

$$\tan \phi_0 = \frac{\pi(1 - \epsilon^2)^{1/2}}{4\epsilon}$$

The resulting fluid film forces on the journal due to the weight of the shaft, F, and the steady state running speed, Ω, are:

$$\begin{Bmatrix} B_y(\Omega) \\ B_z(\Omega) \end{Bmatrix} = \frac{F}{C} [T]^T \begin{bmatrix} -a_{rr} & -a_{rs} \\ a_{sr} & -a_{ss} \end{bmatrix} [T] \begin{Bmatrix} y \\ z \end{Bmatrix}$$

$$+ \frac{F}{C\Omega} [T]^T \begin{bmatrix} -b_{rr} & -b_{rs} \\ -b_{sr} & -b_{ss} \end{bmatrix} [T] \begin{Bmatrix} \dot{y} \\ \dot{z} \end{Bmatrix} \qquad (6.1)$$

Where B_y the vertical and B_z is the horizontal bearing film force component and C is the radial clearance. The component journal displacements, y and z, are harmonic in time; with a frequency Ω for the synchronous whirl and ω during the

asynchronous whirl (eg. gyroscopic or bearing effects). We can rewrite the bearng forces as:

$$
\begin{Bmatrix} B_y(\Omega) \\ B_z(\Omega) \end{Bmatrix} = \frac{F}{C} \begin{bmatrix} -a_{yy} & -a_{yz} \\ a_{zy} & -a_{zy} \end{bmatrix} \begin{Bmatrix} y \\ z \end{Bmatrix} + \frac{F}{C\Omega} \begin{bmatrix} -b_{yy} & -b_{yz} \\ -b_{zy} & -b_{zz} \end{bmatrix} \begin{Bmatrix} \dot{y} \\ \dot{z} \end{Bmatrix} \tag{6.2}
$$

For given rotor mass, [M], stiffness, [K] and damping, [C], matrices the equations of motion under dynamic force conditions are:

$$
[K] \begin{Bmatrix} y \\ z \end{Bmatrix} + [M] \begin{Bmatrix} \ddot{y} \\ \ddot{z} \end{Bmatrix} + [C] \begin{Bmatrix} \dot{y} \\ \dot{z} \end{Bmatrix} = \begin{Bmatrix} B_y(\Omega) \\ B_z(\Omega) \end{Bmatrix} + \begin{Bmatrix} F_y(t) \\ F_z(t) \end{Bmatrix} + \begin{Bmatrix} F \\ 0 \end{Bmatrix} \tag{6.3}
$$

where F is the static weight of the rotor, $F_y(t)$ and $F_z(t)$ are the components of external forces which can be synchronous with running speed (rotating unbalance) or asynchronous (misalignment forces, gear mesh forces). The homogeneous equations of motion with the bearing supports included as end conditions are:

$$
\left\{ [K] + \frac{F}{C} \begin{bmatrix} a_{yy} & a_{yz} \\ -a_{zy} & a_{zz} \end{bmatrix} \right\} \begin{Bmatrix} y \\ z \end{Bmatrix} + \left\{ [C] + \frac{F}{C\Omega} \begin{bmatrix} b_{yy} & b_{yz} \\ b_{zy} & b_{zz} \end{bmatrix} \right\} \begin{Bmatrix} \dot{y} \\ \dot{z} \end{Bmatrix}
$$

$$
+ [M] \begin{Bmatrix} \ddot{y} \\ \ddot{z} \end{Bmatrix} = \{0\} \tag{6.4}
$$

Figure 6.3 shows the variation of the non-dimensional stiffness coefficients and Figure 6.4 the non-dimensional damping coefficients with variation in the capacity number CN. Capacity number, introduced by Ocvirk, is given as:

$$CN = SN \left(\frac{L}{D} \right)^2$$

$$CN = \frac{\mu N L D}{F} \left(\frac{R}{C} \right)^2 \left(\frac{L}{D} \right)^2 = \frac{(1 - \epsilon^2)^2}{\pi \epsilon [\pi^2 (1-\epsilon^2) + 16\epsilon^2]^{1/2}}$$

where SN is the Sommerfeld number. L, D and C are the bearing length, diameter and radial clearance respectively and R is the journal radius. A single curve of eccentricity versus capacity number exists, valid for any L/D ratio of a short bearing. The reciprocal of the capacity number is called the load number. The usual range of the capacity number is below 1. For each value of the capacity number, in this range, the dynamic coefficients are calculated and plotted in Figures 6.3 and 6.4.

6.3 Discussion

The bearing dynamic coefficients are obtained about the fixed set of axes. The stiffness, damping and inertia of the pillarbox, foundation, soil and other supporting systems obtained about these axes will act in series with the
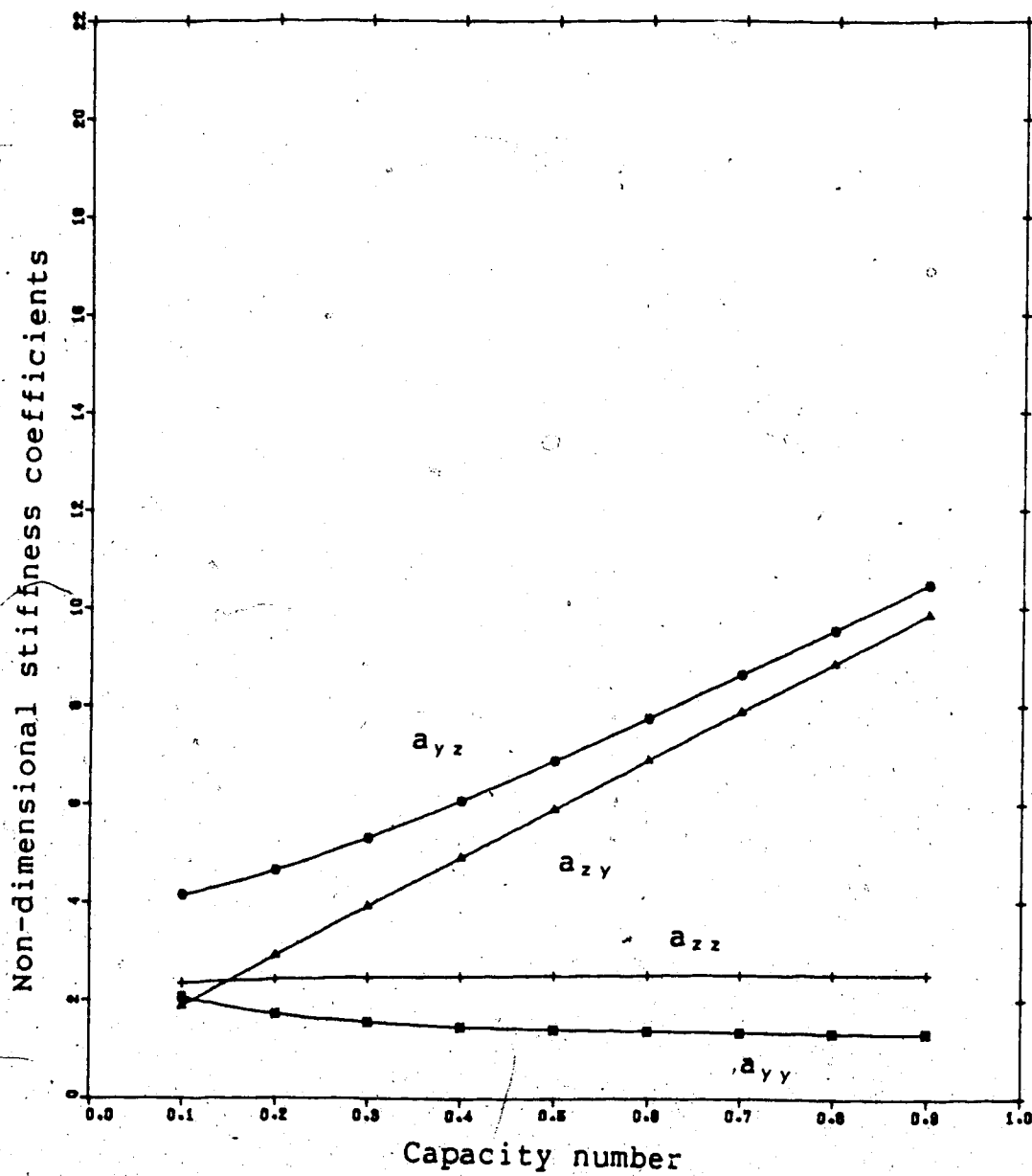
Figure 6.3 Stiffness coefficients of short bearings
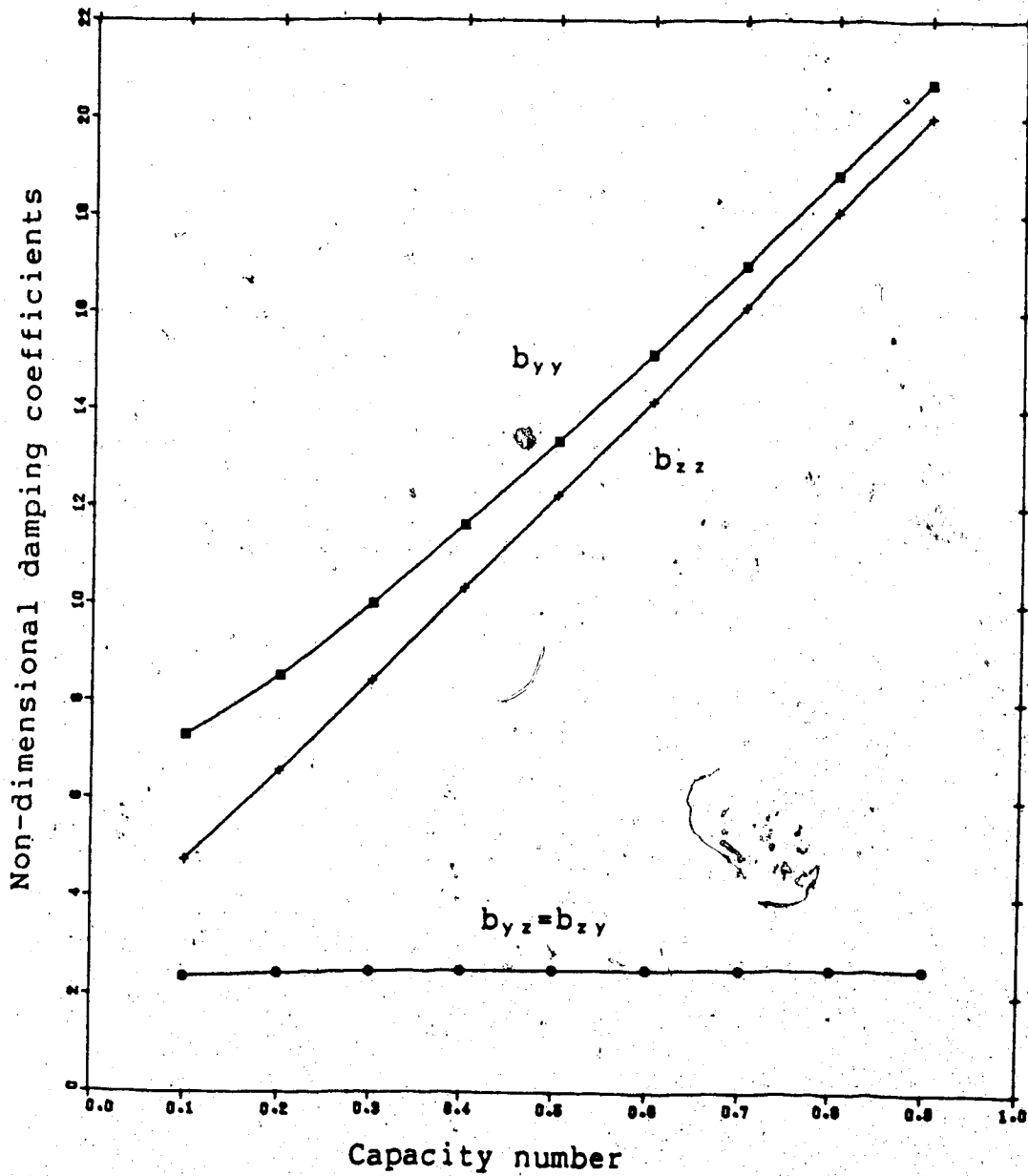
Figure 6.4 Damping coefficients of short bearings

bearing effects.

The bearing load in this analysis is the static load due to the shaft and time dependent unbalance forces are neglected. Holmes[69] considered the nonlinear bearings including the unbalance forces and the nonlinear ϕ and e terms. He found that for turbo-rotors with typical eccentricity ratios of .7 and .4 linearity may be assumed for peak to peak vibration values of about one third of the radial clearance and full radial clearance respectively.

For a turbo-generator mounted on multiple bearings, the static load on each bearing can be calculated assuming rigid supports. The steady state load depends on the eccentricity at a given speed and oil viscosity. An iterative scheme has to be used to find these dynamic reactions. Assuming that the steady state load is equal to the static load, we can calculate the capacity number for a given speed and oil viscosity. The corresponding stiffness and damping coefficients can be read from Figures 6.3 and 6.4.

From the graphs, we observe that the variation of all the dynamic coefficients is either linear or constant with the variation in the capacity number. Simple equations can be obtained by curve fitting. These relations can be used to build computer models of the bearing coefficients, reducing the calculations occuring with the change in capacity number due to a change in speed, viscosity, load or bearing.

6.3.1 Asymmetry of bearing dynamic coefficients

Pure flexible support in the vertical and the horizontal directions makes the damping terms and the cross-stiffness terms zero. Using a Koenig model for the support in the two directions makes the cross-coupling terms of stiffness and damping matrices zero. For these two cases the decoupling allows the oxz and oyx planes to be considered separately using beam elements; analysis in one plane being sufficient for the isotropic case with $a_{yy} = a_z$ and $b_{yy} = b_{zz}$.

For the short bearing, the stiffness matrix is asymmetric and the damping matrix is symmetric, with nonzero coupling terms. This asymmetry leads to rotor dynamic instability and a split in the critical speeds (separating the horizontal and the vertical critical speeds). Use of one representative plane is no longer valid, two orthogonal planes are considered for a complete description of the rotor motion.

Asymmetry of the system matrices can also occur due to other factors. In Chapter 3 the gyroscopic moment is given as:

$$\begin{Bmatrix} My(t) \\ Mz(t) \end{Bmatrix} = [C_{gyr}] \begin{Bmatrix} \phi_y \\ \phi_z \end{Bmatrix}$$

where:

$$[C_{gyr}] = \begin{bmatrix} 0 & -1 \\ 1 & 0 \end{bmatrix} \Omega I_p$$

The generator rotor, with slots for the coils, might introduce asymmetry in the shaft stiffness matrix. Thus, the overall rotor stiffness and damping matrices can be asymmetric. Adams and Padovan[66] explain the decomposed symmetric and skew symmetric parts as:

$$C = C' + C''$$

$$K = K' + K''$$

where C'' and K' are the conservative terms and C' and K'' are non-conservative. The C'' matrix, due to gyroscopic effect, is called the GYROSCOPIC MATRIX. The K'' matrix is called the CIRCULATORY MATRIX, as it produces a circulatory force instead of a restoring force.

6.4 Conclusions

The fluid film bearings introduce asymmetric stiffness and damping coefficients. The results obtained by Holmes have been reviewed . The dynamic coefficients are plotted with capacity number as the independent parameter, which eases the designer's work. Effect of the bearing asymmetry is also emphasized, as it plays a major role in the dynamic

analysis of the rotor system.

7. STABILITY OF ROTORS IN SHORT BEARINGS

Abstract

Short bearings have asymmetric stiffness coefficients which can cause instability to the rotor operation. The complex eigenvalues of the rotor-bearing system can be used to describe the rotor stability. Use of the eigenvalues to find the threshold of instability by a root search method, has been accepted as a costly endeavor by the earlier authors. In this Chapter a modal reduction method is presented which includes the influence of the dynamic bearings. The reduced system matrix, approximated by the first few modes, has been successfully used to find the threshold of instability of a flexible rotor. This method can be applied to find the system stability of large rotors.

7.1 Introduction

Newkirk[69] was the first to find an upper bound for the safe operational speed of a turbo rotor since the capability of sustained operation above the rotor's lowest critical speed was achieved by Gustave De Lavel in 1895. The running speed at which instability is imminent is called the threshold speed. The bearing damping capacity is lost at this point and a further increase in the rotor speed induces a positive damping. It cannot, thus, be "passed through" by going to higher speeds in contrast to critical speeds. This

lead to the development of the tilted pad bearing which gives a stable rotor operation under all dynamic conditions and bearings with greater stable regions such as the partial, grooved, elliptical, multilobed bearings etc.

More recently Holmes[70], among others, found that the nonlinear bearing representation will in fact stabilize the rotor operation beyond the threshold speed. Adams and Padovan[66] have shown theoretically that destabilizing occurs only in the co-rotational (forward) journal orbits. Energy is imparted to the rotor by the non-conservative bearing forces, arising due to the symmetric damping terms C' and the skew symmetric stiffness terms K'', during the rotor harmonic motion. If the net energy transmitted to the rotor is negative then damping has a dissipative action, otherwise it causes rotor instability.

At increasing rotor speed, the K'' terms become progressively stronger in comparison to the C' terms, due to the inherent influence of the journal speed on the bearing dynamic coefficients. At the threshold speed, ω_0, the two effects exactly cancel.

At the threshold of instability, damping becomes ineffective causing a free whirl. Adams and Padovan have shown that the asymmetric part of the bearing stiffness contributes to damping. So, at the threshold of instability the critical speed should be the same as that of a support consisting of the symmetric stiffness terms of the bearing, calculated at the threshold speed. Furthermore, the

stability analysis of the rotor is affected by the skew symmetric stiffness matrix and the symmetric damping matrix only.

Holmes[64] used his short bearing theory to evaluate the stability of a rigid rotor with half of its weight lumped at each bearing. Stability condition was obtained using Routh's criteria.

It can be mentioned here that knowledge of the unbalance of the rotor is not necessary to find regions of instability, as the homogeneous solution is sought. Thus, the external forcing functions are omitted, bearing dynamic coefficients alone being responsible for the rotor instability. During operation, unbalance acts as a driver or initiator, promoting vibrations at the threshold speed.

Routh's criteria gives the lowest speed(threshold) of the unstable region and can be calculated for various loads to obtain the stability regions. Yet, the amount of damping and the damped critical speeds above and below the threshold speed cannot be obtained by this method. This information is important since the region of instability extends beyond the onset speed, the growth rate depending on the amount of damping present. The whirl to spin ratio remains fractional and the exact ratio can be important in vibration monitoring and detection.

Ruhl[53] used an Euler beam finite element model to study the stability of a rotor, mounted on Holmes' bearings. He found that for a shaft with a ratio of the central

deflection to the radial clearance less than 0.1, the shaft flexibility does not change the threshold speed; a rigid rotor model is applicable. For the case of a flexible rotor Ruhl pointed out that the eigenvalue search method to find the threshold speed is exorbitant in cost.

Lund[72] used the transfer matrix method of Prohl-Myklestad to represent a uniform shaft, disregarding shear deformations, rotatory inertia and gyroscopic effects to calculate the threshold speed of instability and the damped critical speeds using Lund's[73] linear cylindrical bearing coefficients.

He showed, with his model, that at the threshold of instability, the rotor whirls in its first mode (with forward precession) but not at the first critical speed, as is generally accepted. For his example rotor, the first two criticals are always subsynchronous and will not get excited by a synchronous (forcing speed same as shaft's) force such as due to a rotating unbalance. The critical speeds remain below the synchronous excitation for all running speeds (due to the dynamic bearing effects). But, the rotor becomes critical for subsynchronous bearing excitation. Hence, a response study alone is not sufficient for a complete dynamic behaviour evaluation, eigenvalues should also be calculated.

In the present study, a rotor finite element is described using the higher order Timoshenko element developed in Chapter 2. The nodal degrees of freedom have

been rearranged to allow chain assembly, which will not be required if a general assembly procedure is used. The eigenvalue problem for the rotor bearing system is viewed in depth to get a better understanding of the stability criteria involved. A modal reduction method is introduced to reduce the system size. As the lower modes are the first to be subjected to instability, it is sufficient to retain the first three or four lower modes for modal approximation. The bearing asymmetric coefficients have to be properly treated during this reduction.

7.2 Theory and discussion

7.2.1 Rotor Element

In Chapter 3, a shaft in a circular whirl, under the gyroscopic action, is analyzed by a beam element in a representative plane. However, the bearing dynamic coefficients do not permit decoupling of the motion. We are forced to use two beam elements, to study the shaft motion in two representative perpendicular planes, to completely describe the rotor motion. A beam element in the XZ plane is shown in Figure 7.1, together with a similar beam element in the XY plane it forms a rotor element. The double beam rotor element is shown in Figure 7.2. It has 16 degrees of freedom per element, 5 at each node. All the nodal variables are compatible at the joints as explained earlier for the case of a beam.
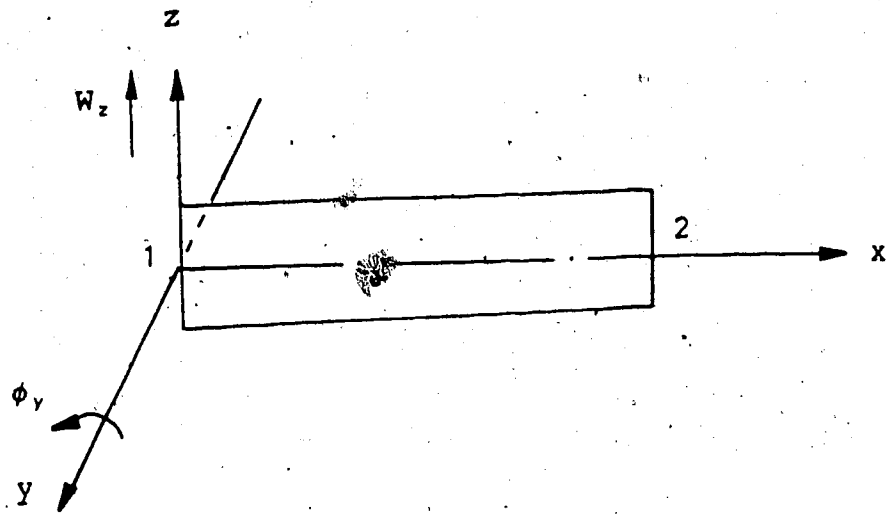
Figure 7.1 Beam element in XZ plane
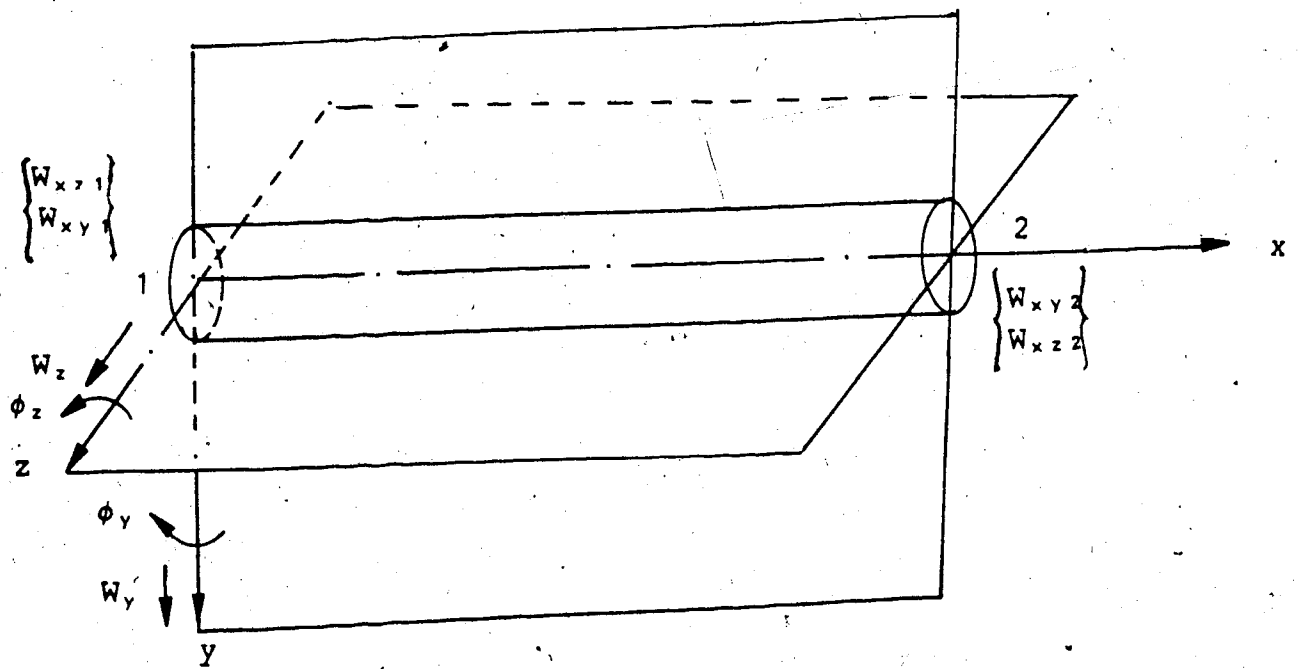
Figure 7.2 Rotor element

The beam element gives the stiffness matrix, [K], the mass matrix, [M], and a proportional damping matrix, [C]. The beam dynamic system matrix, [A], is given as:

$$[A(\Omega)] = [K] + j \Omega [C] - \Omega^2 [M]$$

(7.1)

where Ω is the running speed. The system matrix of a rotor element is obtained by combining two beam elements and is given as:

$$\begin{bmatrix} A & 0 \\ 0 & A \end{bmatrix} \begin{Bmatrix} w_{xz1} \\ w_{xz2} \\ w_{xy1} \\ w_{xy2} \end{Bmatrix}$$

For chain assembly it is more convenient to have the nodal variables transformed as follows:

$$\begin{Bmatrix} w_{xz1} \\ w_{xy1} \\ w_{xz2} \\ w_{xy2} \end{Bmatrix} = \begin{bmatrix} I & 0 & 0 & 0 \\ 0 & 0 & I & 0 \\ 0 & I & 0 & 0 \\ 0 & 0 & 0 & I \end{bmatrix} \begin{Bmatrix} w_{xz1} \\ w_{xz2} \\ w_{xy1} \\ w_{xy2} \end{Bmatrix}$$

The transformed matrix is still uncoupled. However, the gyroscopic moment in a non-circular whirl, asymmetric shaft stiffness and the bearing dynamic coefficients induce coupling into the system matrices. The system matrix is also time/speed independent, it is again the bearing and gyroscopic terms that make it speed dependent.

7.2.2 Eigenvalues for rotor stability study

The rotor equation of motion is of the type:

$$[K(\Omega)]\{w\} + [C(\Omega)]\{\dot{w}\} + [M]\{\ddot{w}\} = \{F(t)\} \qquad (7.2)$$

Where { w } is the global nodal variable vector of the rotor. Matrices [K] and [C] include the bearing and gyroscopic effects, and are asymmetric and speed dependent.

For the homogeneous solution, when the forcing function vector is zero, we can assume a solution of the type:

$$\{w\} = \{W\} e^{st}$$

Where s is a complex eigenvalue of the type:

$$s = \lambda + i\omega_d$$

The real part λ indicates the amount of damping present and affects the motion for any slight disturbance from the steady running state:

1. when λ is negative the vibration dies out exponentially with time, ensuring stable motion;

2. when λ is positive the vibration amplitude builds up exponentially with time. Energy is added to the rotor instead of being dissipated. This is an unfavourable state denoting instability;

3. when λ is zero, system damping is ineffective, no net

energy is imparted to the system and the vibration

amplitude is neither amplified nor attenuated.

At the threshold of instability, the motion is purely

harmonic and undamped as the real part of the eigenvalue is

zero.

The imaginary part denotes the damped critical speed of

the system in a harmonic motion; which is possible for

lightly damped or under damped systems only:

1. when ω_d is positive the shaft is in forward precession,

   with the whirl direction coinciding with the spin;

2. when ω_d is negative the shaft is in backward precession

   with the whirl opposing the spin direction;

3. when ω_d is zero the shaft centre is stationary or the

   whirl path is a point. This condition can occur for

   highly damped or over damped modes.

The complex conjugate eigenvalues mean that in every

mode a forward and a backward whirl is possible. For a

multi-degree of freedom system each mode can have a

different degree of damping resulting in a stable, unstable

or neutral operation when a particular mode is excited.

A rotor in the fluid bearings is known to be unstable

in the forward whirl when the imaginary part of the

eigenvalue, ω_{dn}, is greater than zero. The stability

conditions can be specified as:

for neutral stability of the nth mode s_n is such that

λ_n is equal to zero, and ω_{dn} is greater than zero; and for

strict stability of the nth mode s_n is such that λ_n is less

than zero and ω_{dn} is greater than zero. The system is unstable in the nth mode when λ_n is greater than zero and ω_{dn} is greater than zero.

The second degree characteristic equation in s can be transformed to the first degree in s by adding and subtracting [M] { W } to the homogeneous equation, which is now written as:

$$\begin{bmatrix} M & C(\Omega) \\ 0 & M \end{bmatrix} \begin{Bmatrix} \ddot{w} \\ \dot{w} \end{Bmatrix} + \begin{bmatrix} 0 & K(\Omega) \\ -M & 0 \end{bmatrix} \begin{Bmatrix} \dot{w} \\ w \end{Bmatrix} = \begin{Bmatrix} 0 \\ 0 \end{Bmatrix}$$

say $\begin{Bmatrix} \ddot{w} \\ \dot{w} \end{Bmatrix} = S \begin{Bmatrix} \dot{w} \\ w \end{Bmatrix} = S\{q\}$

we get:

$$\left\{ \begin{bmatrix} 0 & K(\Omega) \\ -M & 0 \end{bmatrix} - S \begin{bmatrix} -M & -C(\Omega) \\ 0 & -M \end{bmatrix} \right\} \{q\} = \{0\} \qquad (7.3)$$

This is a standard eigenvalue problem and gives complex eigenvalues, s, and modes, { q }. It is to be noted here that each of the rotor matrices are double the size of the corresponding beam element matrix and the reduction of the damped problem to a standard eigenvalue problem redoubles the beam matrix size. Moreover, the stiffness and damping matrices are running speed, Ω, dependent and have to be evaluated at each speed and added to the constant rotor

matrix.

The threshold speed of the rotor is obtained by starting at a low running speed, calculating the bearing matrices and solving the resulting eigenvalue problem. The root search is made by increasing the running speed and calculating the eigenvalues, manually controlling the step size. Common schemes to reduce the iterations, such as the bi-section method, are not recommended as the bearing characteristics are highly nonlinear with respect to the changes in the running speed.

Holmes' rigid rotor, detailed in Table 7.1, is analyzed for stability. The threshold speeds calculated from the eigenvalues match with those from Routh's conditions given by Holmes. The system matrix for the eigenvalue solution is of order four. The huge calculations involved, even for the small system, especially with the costly eigenvalue solver, prompted a reduction in the global degrees of freedom to find the flexible rotor's stability.

From Table 7.1 we see that for low eccentricity ratios and capacity numbers(1.0 to 0.1) the whirl to spin ratio is about 0.5. That is, the shaft whirling speed will be about half the rotational speed at the threshold. For smaller values of capacity number the ratio gets smaller. For a capacity number of .048, the whirl to running speed ratio is about .343. For values of capacity number smaller than 0.04 (or eccentricity ratio greater than .75) the shaft remains stable under any loading. The loading on the shaft is given

Table 7.1. Comparison of Routh's criterion with eigenvalues
for a rigid shaft.

Rotor details:

length = 10"
diameter = 3.2"

Bearing details:

width = 2.0"
diameter = 3.2"
radial clearance = 0.004"
viscosity = 10 centipoise

Eccentricity ϵ_0	Capacity# CN	static force / dynamic force $F/mC\omega^2$	Eigenvalue method ω_0/Ω	Routh criterion (from graph) ω_0/Ω
0.1	1.0	.132	.502	.5
0.3	.33	.146	.518	.52
0.5	.10	.150	.508	.51
0.6	.06	.135	.471	.47
0.7	.048	.075	.343	.34

as the non-dimensional ratio of static to dynamic forces.

From the definition of the capacity number we can deduce that stability of the rigid rotor improves with an increase in the unit load or a decrease in speed, oil viscosity, L/D ratio or R/C ratio: all of which reduce the value of the capacity number, leading to a more stable region of operation..

7.2.3 Modal reduction

Dynamic behavior of the rotor in its lower modes can be approximated by a reduced set of degrees of freedom. Such reduction techniques are commonly applied in structural dynamics to reduce eigenvalue extraction time, condense internal element degrees of freedom or as a part of the substructuring approach.

The Guyan method(discussed in Chapter 8) uses the static modes to suppress the degrees of freedom which are not externally loaded. This reduction works well for low running speeds, below the first critical speed.

A more costly but accurate method uses the undamped normalized modes to reduce the system matrix size. The global degrees of freedom are expressed in terms of a few generalized or normal co-ordinates. The undamped equations of motion are given as:

$$[M]\{\ddot{w}\} + [K]\{w\} = \{0\}$$

Assuming a harmonic motion, of frequency ω, we obtain N eigenvalues, ω_n, and N eigenvectors, $\{ W \}_n$. The first M modes, enough to obtain the required accuracy, form the columns of the modal transformation matrix, $[\phi]$. The reduced damped equations of motion are:

$$\{[\phi]^T[K(\omega)][\phi] + S[\phi]^T[C(\omega)][\phi] + S^2[\phi]^T[M][\phi]\} \{q\} = \{0\}$$

which can be written as:

$$[K^*(\omega)] + S[C^*(\omega)] + S^2[M^*]\} \{q\} = \{0\}$$

where

$$[K^*(\omega)] = [\phi]'[K(\omega)][\phi]$$

$$[C^*(\omega)] = [\phi]'[C(\omega)][\phi]$$

$$[M^*] = [\phi]'[M][\phi]$$

The reduced matrices are of size M instead of N. The usual rule is to consider up to at least one mode higher than the operating speed. From the orthogonality principle we expect that the transformation diagonalizes the M and K matrices and also the C matrix if it is a proportional type damping.

With the fluid bearings used, the existence of the cross-coupling terms make the modes non-orthogonal. Further approximation, apart from that due to the reduction, occurs due to the use of the undamped modes for reducing the damped matrices.

If all the matrices are diagonalized, the damped eigenvalues can be found from the individual decoupled equations. For the Nth mode the decoupled equation is:

$$(K_n^* + S_n C_n^* + S_n^2 M^*) \, q_n = 0$$

the corresponding damped complex eigenvalue for a non-trivial solution is:

$$S_n = \frac{-C_n^* \pm \sqrt{C_n^{*2} - 4K_n^* M_n^*}}{2M_n^*}.$$

7.2.4 Boundary Conditions

While solving the undamped homogeneous equations, to obtain the modal matrix, introduction of the full bearing stiffness matrix causes complex eigenvalues and eigenvectors which are tedious to deal with. The fluid bearing stiffness matrix is decomposed as:

$$[K]brg = [K']avg + [K(\Omega)]remainder$$

The bearing stiffness, [K]brg and the damping, [C]brg, matrices change with the running speed. A representative symmetric average stiffness matrix, [K']avg is used in the undamped rotor equation to obtain modes close to those of the actual system, in the range of speeds tested.

Thus, the rotor mass and stiffness matrices and the modal matrix need be calculated only once. The bearing stiffness and damping matrices are calculated at each running speed using Holmes' bearings. The [K(\Omega)]remainder and the [C]brg matrices are applied to the damped equations of motion before reduction. The reduced matrices are solved for the first M, approximated, eigenvalues of the system to study its stability.

The reduced matrices can also be used for response analysis, by using the generalized forces, [ϕ]' { F(t) }. The generalized response, { q }, can be calculated and thereby the actual response, using the relation:

$$\{ W \} = [\phi] \{ q \}.$$

7.2.5 Case Study

Lund's rotor[72] is used to study the stability and damped critical speeds. Instead of using Lund's

bearings[73], short bearings of Holmes' are used. Lund
disregarded the shear deformations, rotatory inertia and the
gyroscopic effects. A uniform shaft mounted on identical
bearings was considered. In the present case, shear
deformation of the rotor is included. The rotor and bearing
details along with the capacity number for each speed are
given in Table 7.2. Comparison is obtained between Lund's
results and the eigenvalues from the finite element method
with modal reduction; Table 7.3 and Figure 7.4 show these
results.

The real part of the eigenvalue called the damped
exponent is non-dimensionalized to give the log decrement,
δ:

$$\delta = -2\pi\lambda/\omega_d.$$

The rotor is first put on pinned supports, in each
plane and at each end. This results in a bi-symmetric system
with double frequencies, one for each plane. These rigid
modes and frequencies are the same as of a beam element in
one of these planes. Decoupling and symmetry of the system
allows motion of a beam to represent the rotor's circular
whirl.

The rotor critical speed on rigid bearings is found to
be 125 cps instead of 127 cps, as calculated by Lund. The
difference is due to the inclusion of the shear effect in
the finite element model.

Table 7.2. Details of Lund's rotor.

Rotor:

length = 50"
diameter= 4"
material is steel

Bearing:

length=1"
diameter=4"
radial clearance=0.002"
viscosity=6.9 centipoise
static load = 89.9 lb

Critical speed on rigid support:

Lund: 127 cps
finite element: 125 cps

rotational speed R.P.M.	eccentricity e/c	capacity # Cn
2000	.5259	.093
4000	.3808	.1861
6000	.2945	.2793
8000	.2379	.3723
9000	.2165	.4189
9160	.2134	.4263

Table 7.3. Comparison of eigenvalues, using modal reduction, with Lunds
for instability of a flexible shaft.

| Running speed R.P.M. | 1 F.W | | | | 2 F.W | | | |
	δ Lund	ω_d	Modal δ	ω_d	Lund δ	ω_d	Modal δ	ω_d
2000	5.88	22	6.64	20.79	5.45	24	5.08	48.90
4000	4.10	38	4.53	39.00	3.23	44	2.47	60.57
6000	2.97	56	3.24	56.98	1.58	64	1.23	68.44
8000	2.27	75	2.35	74.51	0.41	75	0.40	74.94
9000	1.91	82	2.00	83.08	0.05	78	0.04	77.88
9160*	-	83	1.95	78.25	-	78	0.01	78.25

* Threshold speed, ω_o

Whirl to spin ratio at threshold is 78×60/9160=0.51 = ω_o/Ω

ω_d is in c.p.s

δ is non-dimensional

Value of ω_d for Lund is from graph.
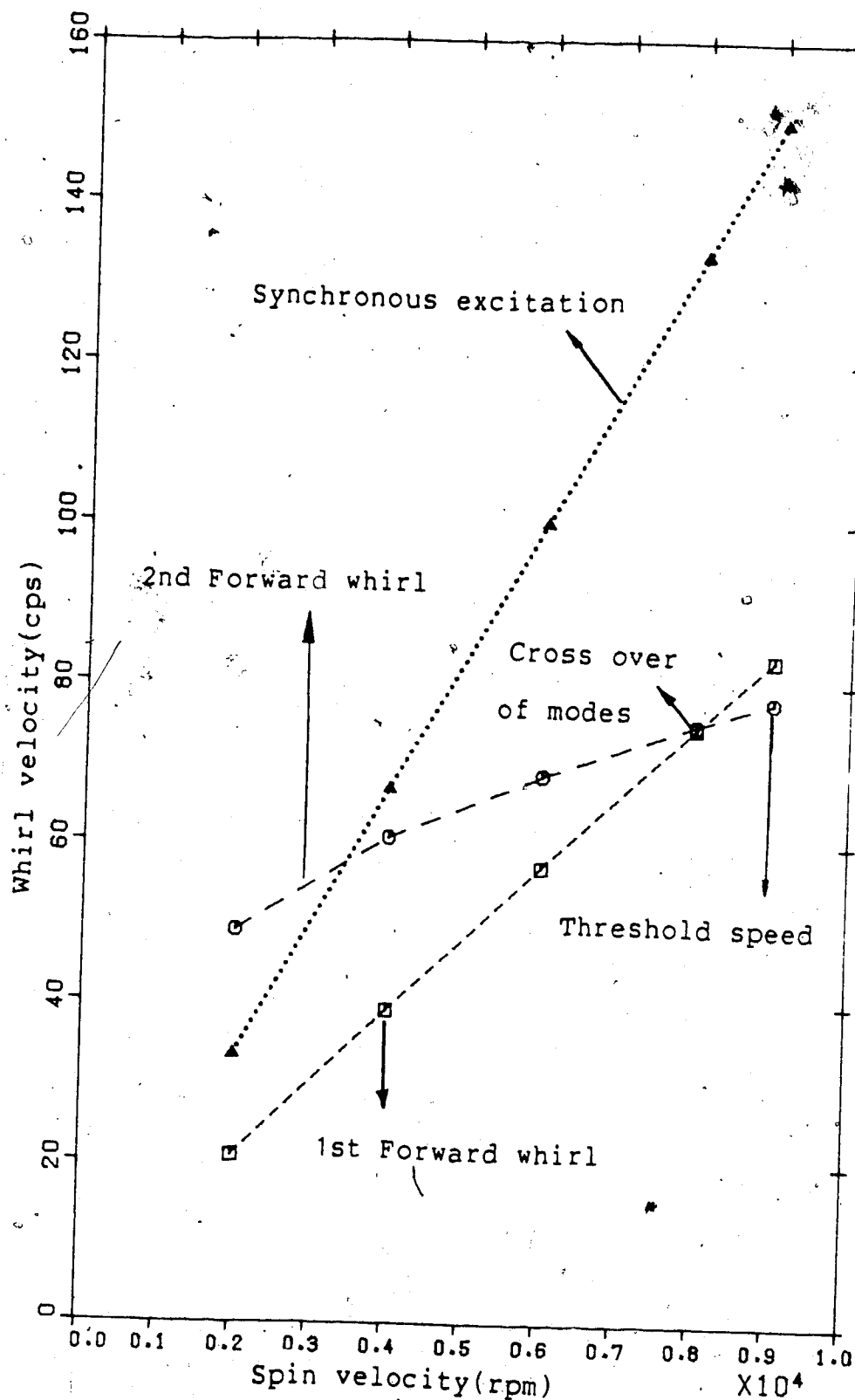
Figure 7.3 Damped critical speeds and threshold speed

Holmes' short bearings are now prescribed at both rotor ends, including all stiffness and damping terms. The average modal matrix is used to reduce the system matrix and then the eigenvalues are calculated at different running speeds. Calculations are continued till the threshold speed is reached.

The whirl frequency at the onset of instability, ω_0, is obtained as 78.25 in close agreement with Lund's 78 cps. It is to be noted that the second forward whirl critical speed attains instability before the first forward whirl, though it whirls in the first mode.

The damped critical speeds are more appropriate to identify the vulnerable points in the rotor operation. The log decrement gives an estimate of the damping thereby the response amplification factor in each of the modes at each running speed.

The lowest log decrement in the operating range also determines the closeness to the threshold speed, suggesting system or bearing changes, when necessary.

The model chosen is supported on two identical bearings, extension to multi-bearing systems is direct. However, for the multi-bearing system identification of the bearing which is responsible for the instability is not possible from the eigenvalue study. A response study at each of the bearings, at the threshold speed, is necessary.

7.2.6 Possible application

The cross-coupling terms of the bearings are responsible for the double beam element rotor model, instead of a single beam model. This doubles the matrix size, increases the calculating time and limits the use of the microcomputer.

When the cross-coupling is feeble, rotor motion in the two planes can be treated separately. From the graphs of the dynamic coefficients in Chapter 6, we observe that both stiffness and damping cross-coupling terms are dominant for all values of the capacity number, with respect to the direct terms. This fact should discourage any attempts of decoupling. However, we observe that the direct terms remain fairly constant while the cross terms decay linearly with a reduction in the capacity number. Also, the turbo-generators operate at low capacity numbers (about 0.1 to 0.3). Cross-coupling effect may be tested in this range and neglected if found to be weak.

Ramsden[87] proposed a method of describing the dynamic character of the rotor by calculating the damped eigenvalues and eigenvectors in the range of run up and run down speeds. The damping limits have to be set first, based on practical experience, experiments and theory. For a fixed percentage of the critical speed(+ and-5%), the amount of damping available in that mode is calculated and checked with the prescribed limits to ensure stability of the rotor operation.

With our present method of modal reduction, the reduced system matrix can be used to obtain the critical speeds at different running speeds at a reasonable cost. Thus, stability of large turbo-generators can be checked.

7.3 Conclusions

Holmes' bearing is used to obtain the threshold of instability of a rigid and a flexible rotor. A modal reduction method for rotors supported on fluid bearings is introduced, with success, to obtain the damped critical values of flexible rotors. The system matrix size is reduced to facilitate the study of large rotor systems. The modal reduction method used is also a popular tool for response studies.

Application of the stability analysis to determine large rotor performance is suggested. If weak cross-coupling bearing coefficients are recognized the rotor motion can be decoupled.

8. APPLICATION: A TURBO-GENERATOR UNIT

Abstract

A large rotor of a power plant is selected for dynamic
analysis. A dynamic condensation method is presented which
reduces the system size, retaining only the necessary
degrees of freedom. The system is modelled using uniform and
linearly tapered Timoshenko shaft elements and including the
disks within the elements. Support conditions are
represented by the dynamic coefficients of the short
bearings. Motion in a representative vertical plane is
considered for the axi-symmetric rotor-disk system. Critical
speeds, mode shapes and unbalance response are obtained.
Effectiveness of the available trim balance planes, located
on the turbine rotors, is discussed.

8.1 Introduction

Turbo-machinery are a regular sight in industry:
turbo-generators for power production, turbo-pumps and
compressors as fluid drivers in industrial plants. The
common feature of all these machines is the presence of the
rotating shaft, with various bearings and supports. The size
and speed of the rotating machines has been continuously
increasing, to meet the mounting demand for power. However,
centrifugal stresses put limits on the diameter of the
shafts, resulting in a rotor of increased length with more

194

stages and wheels. An increase in length makes the system more flexible and hence leads to dynamic problems.

The practical importance of the subject prompted many researchers from industries and acadamic institutions to develop, apply and evaluate experimental, theoretical and numerical methods of analyzing large rotor systems.

Bishop, Gladwell and Parkinson[44,75,76] developed the modal method where the first few modes are superposed to obtain the response at running or any off critical speed. Balancing is done mode by mode. The condition to be observed is that the correction weight balances the present mode without disturbing the balance of any of the previous modes. Federn[77] and Kellenberger[78] also used the modal balancing method, with the two rigid modes balanced initially. Hence, their method is known as the N+2 method as against the N method (at least N modes are to be balanced, for operation between N and N-1 modes) of Bishop.

Goodman[79] developed the influence coefficient method which balances the rotor at specified speeds (running or soaking speeds of rotor) by a least squares method, minimizing the response at specified points on the rotor by placing correction weights in a given number of balance planes.

These two basic methods (modal and influence coefficients) have been modified and advanced for better balancing: Lund[74], Parkinson[80], Tessarzic et al[81], Shiraki and Kanki[82], Gnielka[83]. All these methods depend

on the turbo-rotor in-situ measurements to obtain the mode shapes, influence coefficients and polar plots of the response.

The experimental procedure is tedious, often the measurements have to be taken very quickly, especially when the rotor is at the critical speeds, leading to inaccuracies. It is costly and cumbersome, if not unthinkable, to repeat the measurements. The modal matrices and the influence coefficient matrices, thus obtained, are limited by the accuracy of the instruments used.

A design engineer is often uncertain of the rotor dynamics, until tests are conducted on the actual system. Modifications become necessary to accommodate the system dynamics: changing the dimensions to allow dynamic stresses and altering the system to shift the criticals off the running speed.

Balancing planes are usually located by designers at points which ease the design and the production processes. However, a knowledge of the rotor dynamics allows the selection of optimal points for the balance planes. A good location for a balance plane is near an antinode where the correction weights can be minimal. The bearings might be wrongly positioned, closer to the antinodes, due to lack of mode shape information, resulting in increased transmitted forces.

The foundation hitherto has been the rigid type, made of concrete walls, with its critical speed above the running

speed (high tuned). A smoother operation is expected if a flexible foundation (low tuned), such as a steel structure, is provided; Ellyin[80].

The dynamic unbalance forces, transmitted through the bearing oil film have to be evaluated beforehand to provide safe operation. An unstable rotor(in oil whirl) can have a dynamic magnification factor of more than one, Gunter[85], increasing the foundation loads by two to three times.

Morton[86] has nicely combined the theoretical and practical aspects of large turbo-generators. Many recommendations are available here, to those conducting either laboratory or in-situ experiments.

Ramsden[87], has proposed a way to describe the dynamic character of rotating machinery, to indicate the system stability due to disturbances in the balance by considering the effectiveness of damping in each mode. He also formulated the mixed rotating(rotor) and non-rotating (flexible foundation) system.

Misalignment of the shafts at the coupling points causes shear forces and moments which tend to dislocate the rotor axis from its continuity. Bearings are mounted on a curve (catenary) to avoid this unwanted loading. Sometimes the catenary is set by a trial and error procedure using shims under the bearings, or it may be specified by the designer.

It is not uncommon for the design conditions to change under continuous operation: Lindley-Bishop[88] and Last[89].

1. Inspite of thermal soaking at low speeds, the rotors distort due to uneven heating or cooling during runup, rundown or operation.

2. Ventilation gases used in cooling the rotor (the generator is cooled by hydrogen gas) might not have been accounted for, while balancing, and can change the running operation.

3. Bearing dimensions, loads and operating temperatures vary.

4. Movement of components, generator coils, give rise to internal friction due to the relative motion of the parts.

5. Chipped blades and loose components affect the normal operation.

The bearing parameters: oil viscosity, load and bearing dimensions change with the running speed; and with prolonged steady state operation. The designed capacity number and dynamic coefficients are altered and stability of operation has to be ensured for any such variations.

The maintainance crew are equipped with a continuous monitoring system and are usually warned immediately, at the occurance of any rough operation, above 4mils (.001" = 1mil) of peak to peak vibration level of absolute amplitude (relative to the ground). A fine rebalancing, called the trim balancing, becomes necessary for further rotor operation. The rotor need not be stripped of its casing but is stopped to shift the correction weights in the accessible

balancing planes. The practicing engineer finds it a frustrating ordeal with nothing more than intuition to guide him. In each such trial, the rotor is run up to the operating speed and the vibration level is checked for smoothness in running. In all large rotor systems operational changes can be made at a low cost if the dynamic analysis is constantly updated.

The efficient and accurate finite rotor element developed, with its ability to incorporate shear deformation, rotatory inertia and gyroscopic effects, the disk effects, non-uniform cross-sections and fluid bearings is useful in modelling large rotors. We note here that the use of the present finite element, because of the choice of the nodal variables, $A\psi$ and $I\phi'$, directly gives the dynamic shear force and bending moment at every section of the rotor at any speed and load conditions. This is not possible with the other elements.

Though any type of rotor and fluid bearings can be incorporated with this model the structural damping and foundation stiffness have to be guessed. Whereas in the experimental methods in-situ measurements eliminate the need to guess.

For the present analysis data from an Associated Electrical Industries' turbo-generator rotor was made available. It is presently located at the Lake Wabamun power plant. Installed in 1968 it operates at 3600 rpm with a capacity of 286 MW.

A dynamic reduction method is developed in this Chapter to reduce the system matrix size using the normalized modal vectors. With this reduction a set of desired nodal variables can be retained with a greater accuracy than with the commonly used, Rouch[55], Guyan reduction.

The reduced system matrices are solved for the critical speeds, displacement mode shapes, and unbalance response. Any of the balancing methods can now be used with this model, without any trial runs, to balance the rotor; for a given unbalance response as proposed by Craggs[61].

8.2 Problems with the generator rotor

Two sister units of the selected turbo-generator, located at the Sundance power plant, of the Trans Alta Company have recorded histories of generator unbalance, transmitting vibrations to other parts of the rotor and forces to the foundation and surroundings. These units have been forced to shut down (one in 1975 and another in 1976). The generator-collector rotors were shipped to experts for balancing and repair. The first unit encountered overheating, burning the generator coils. Rewinding of the copper coils destroyed the existing balance. The coils and the insulation consolidate at overspeed, thus a low speed balancing will not be effective at higher operational speed, necessitating an overspeed balancing. For the second unit the axial movement of the end coil retaining rings were the source of the vibration problem. These rings were replaced

along with an overall generator balancing.

The generator rotor is provided with 10 to 20 balancing planes along its length. Each of these planes is provided with four slots for plugging in the correction weights. The slots are located in the cicumferential portions corresponding to the poles of the rotor. These planes are accessible only when the rotor is taken out of the stator, which is done when a total balancing is required. Balancing planes are also provided at either ends of the rotor, corresponding to the planes of, small fans, turbine wheel for speed measurement, slip rings of collector and sometimes the main Lp1-Generator coupling. The following information on generator balancing is from the reports made by the generator balancing company. The generator-collector rotor shown in Figure 8.1 was mounted on three bearings during balancing; two of them support the generator and the third (called the steady bearing) is at the collector end. The first four criticals were found to be 880, 2300, 2700 and 3400 rpm all of them occuring below the operational speed of 3600 rpm.

A flexible modal balancing scheme was adopted to eliminate vibrations at the first four critical speeds. Theoretically speaking, four balancing planes should suffice this process. Yet, about 25 planes were used in the first rotor and about 15 in the second. For a very flexible rotor the correction weight has to be in the plane of unbalance, to be effective. The generator being fairly flexible, the
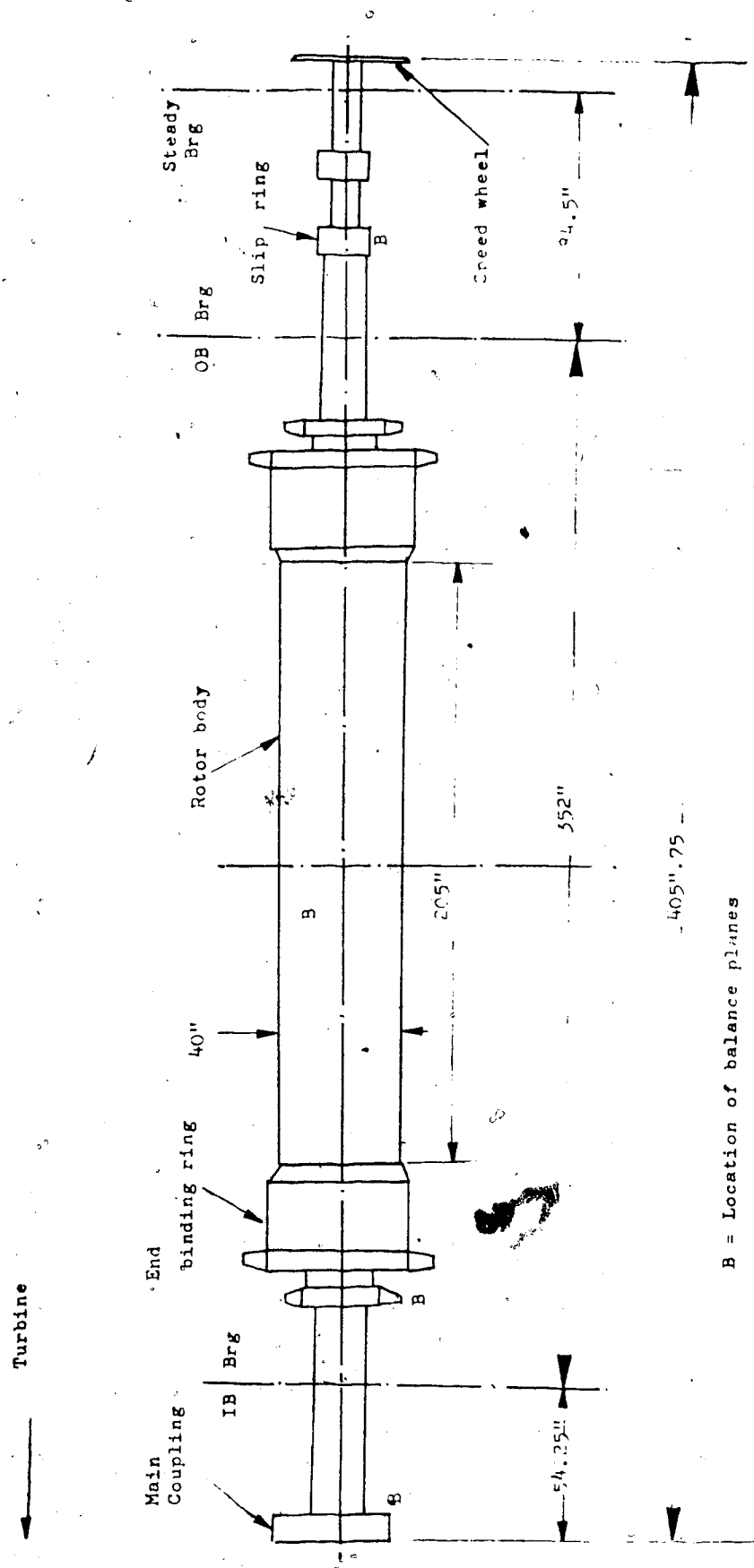
Figure 8.1 Generator rotor

use of the extra planes is probably necessary to ease the balancing process.

Severe vibration standards were imposed. The fundamental, synchronous component of the bearing peak to peak amplitudes were limited to below .003"(3 mils) for the generator bearings and below .004" (4 mils) for the steady bearing. These amplitudes were checked at the critical speeds, at the operating speed and in the range of 3300-3900 rpm.

Trim balancing of the generator is often essential during the rotor operation. This is done mainly using the outer balancing planes of the generator rotor..Frequently . these planes are overloaded, with the correction weights occupying most of the available slot space.

The rotor considered in this Chapter has also been showing inconvenient levels of vibrations causing execessive noise and vibration pollution in the shop.

As the generator is the most probable cause of trouble, the effect of an unbalance in the generator on the total turbo-generator rotor length, at different speeds, is studied.

This study helps in obtaining the effective coupling between the spans as indicated by the response at a span due to an imbalance in another. This will also help us decide the possibility of using the available trim balance planes on the turbine rotors to correct unbalance in the generator.

Imbalances are also placed in the other rotor spans, one at a time, to obtain the response at the running speed. This test will help us judge the effectiveness of the available trim balancing planes to correct imbalances in their own and other spans.

8.3 Details and modelling of the Turbo-generator unit

The turbo-generator unit is made up of six shafts. One each for the high pressure(Hp), intermediate pressure(Ip) and two for the low pressure (Lp1 and Lp2) turbine stages and one each for the generator and the collector. These rotors form a tandem connected flexible rotor, shown in Figure 8.2. The Hp and Ip rotors are hollow in cross-section. The turbine rotors are provided with blade carrying diaphragms called wheels or disks. The blades are twisted in space and occur intermittently around the circumference. The blade effects are included in the model by appropriately increasing the blade carrying disk dimensions. The disks of each stage are assumed to be of uniform size to ease data input, though the finite element program allows disks of different sizes to be included inside an element. The couplings and gears are also included inside the corresponding elements. Balancing planes are provided along the rotor, consisting of 3/4 inch grooves at a radius of 6.25 inch radius in which the correction weights are positioned and welded. The Hp and Ip have a balance plane each and the low pressure turbines have two balancing

planes each. The Hp-Ip, Ip-Lp1, Lp1-Lp2 couplings are rigid
while the Lp2-generator coupling is flexible.

Figure 8.2 shows the half sectional view of the
turbo-generator model used in the finite element analysis.
The actual shafts have many steps and intricate grooves. For
the present analysis either a linear taper or uniform
cross-section approximates each element of the shaft.

The turbo-generator is modelled using 18 elements. For
an axisymmetric system, as in the present analysis,
consideration of motion in one plane by beam elements is
enough. A 76 degrees of freedom system is obtained. It is to
be noted that this is quite small in size for a large rotor
unit. The accurate finite element and inclusion of disks
within are responsible for this achievement. To illustrate
this point element 9 which includes 10 blade carrying disks
within itself, belonging to the Lp stage, is shown in
Figure 8.3. If they are lumped at nodal points, as is
usually done, an 11 element model is obtained, instead of
the 1 element model of the present analysis. Lumping of all
such disks will require at least 100 elements to represent
the whole rotor system with 400 to 500 degrees of freedom in
each plane.

The positions of the disks (wheels) are shown by dots
in Figure 8.2. The balance planes are located at sections BB
and couplings at sections CC. The generator is hollow with
longitudinal slots to carry the conductor coils, made of
material different from the generator rotor. These aspects
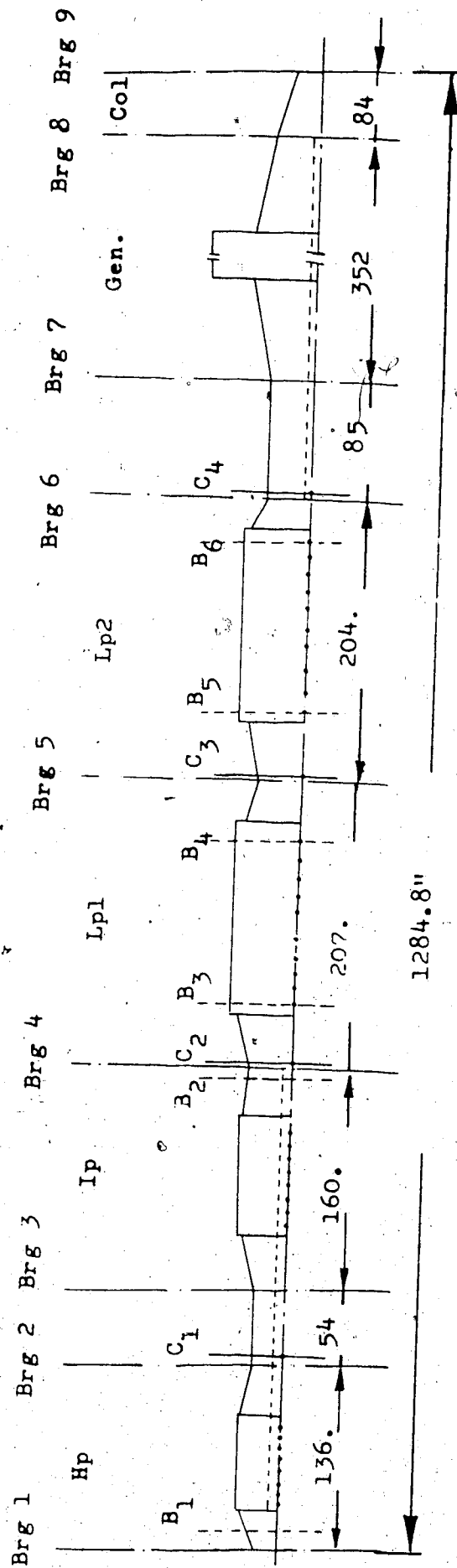
Figure 8.2 Turbo-generator model for F.E
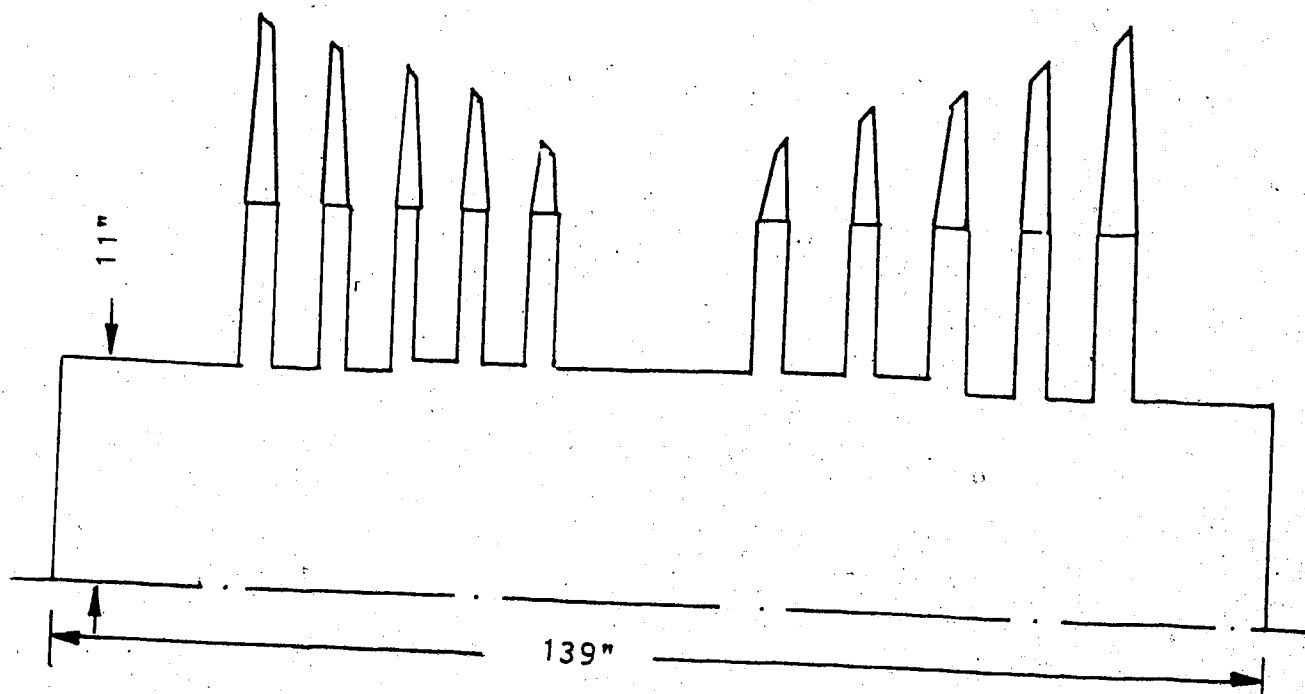
Figure 8.3 Lp1 rotor
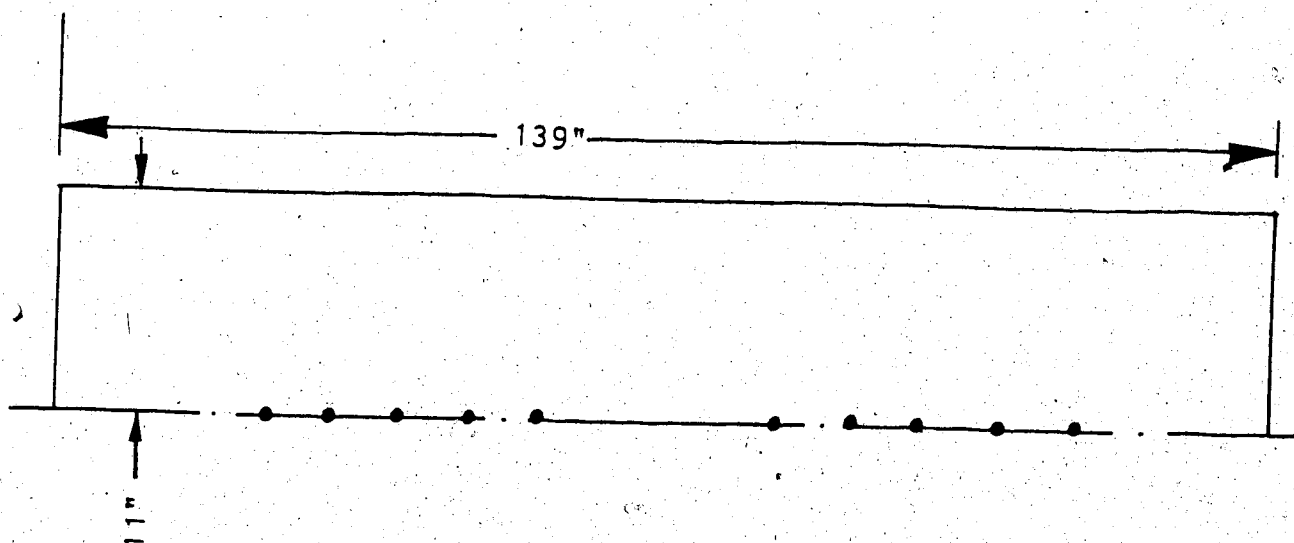
Figure 8.4 F.E model, element 9

have been neglected, approximating the generator as a
uniform solid rotor of homogeneous material.

Slight modification of the program used will
incorporate these factors, if deemed necessary. The shape
factor K and the constants used in the linear taper finite
element, K_1 for area and K_2 for the second moment of
inertia, have to be changed from solid circular to hollow
circular to adopt the sectional changes. For a
non-homogeneous material equivalent modulus of elasticity
and density have to be evaluated and used. Tables 8.1 to 8.3
give the element details, coupling locations, balance plane
locations and information of the disks of each element.

There are nine bearings supporting the turbo-generator.
All of them belong to the short bearing group with L/D
ratios less than 1. The bearing details are given in
Table 8.4. The dynamic coefficients of damping and stiffness
are calculated according to Holmes' theory of Chapter 6.
Though the bearings have different L/D ratios, capacity
number being the independent parameter, the graphs of
damping and stiffness are applicable to all of them.

8.3.1 Instrumentation

The turbo-generator unit is equipped with Bently Nevada
instrumentation. The vibration sensors are mounted on the
bearing caps. Steady state data is continuously obtained.
Run up and run down data, through the critical speeds is
recorded whenever possible, such as during overhaul and fine

Table8.1. Details of rotor elements

Element#	Element length	Root Dia.	Taper ratio	#Disks
1	29.840	9.00	1.6667	0
2	69.600	16.50	1.0000	8
3	37.375	15.75	0.7619	0
4	53.750	12.00	1.0000	1
5	39.875	12.00	1.4583	0
6	87.000	19.00	1.0000	8
7	34.000	18.00	0.8889	0
8	38.250	16.00	1.3437	1
9	139.000	25.00	1.0000	10
10	30.250	21.50	0.7907	0
11	43.250	17.00	1.2647	1
12	139.000	25.00	1.0000	10
13	21.750	22.00	0.7727	0
14	85.375	17.00	1.0000	1
15	73.500	17.00	1.4117	0
16	205.000	40.125	1.0000	0
17	73.500	24.000	0.7083	0
18	84.500	17.000	0.5294	0

Taper ratio = Tip dia/ Root dia

solid circular section is assumed for all elements

Shape factor = 0.85, E=30000000psi, E/G=2.6,

Table8.2.   Details of couplings and bearings.

Coupling type	Distance	Balance plane on	Distance
Hp-Ip	145.94	Hp	26.812
Ip-Lp1	365.69	Ip	342.315
Lp1-Lp2	576.19	Lp1	395.428
		Lp1	522.890
Lp2-Gen	792.12	Lp2	607.928
		Lp2	735.390

All dimensions in inches

Table 8.3.   Details of disks included in the elements

| Element# | Shaft-dia | Disk-dia | Disk-thick | Distance of disks from the element root | | | | | | | | | |
				#1	#2	#3	#4	#5	#6	#7	#8	#9	#10
1													
2	16.50	35.00	2.50	9.250	15.00	20.60	26.30	32.10	37.90	43.90	51.35		
3													
4	12.00	27.75	4.75	9.125									
5													
6	19.0	43.00	4.50	13.625	24.625	33.125	41.625	51.125	61.125	71.125	83.125		
7													
8	18.00	34.875	12.00	14.25									
9	25.00	55.00	4.50	9.188	27.688	42.438	52.438	60.438	78.438	86.438	96.438	111.188	129.688
10													
11	18.50	34.875	13.50	17.25									
12	25.00	55.00	4.50	9.188	27.688	42.438	52.438	60.438	78.438	86.438	96.438	111.188	129.688
13													
14	17.00	32.75	3.125	29.1875									
15													
16													
17													
18													

Table 8.4.   Details of bearings

Brg#	Location	Nominal size DxL'	White metal Length L	Radial clearance	Catenary
1	Hp exhaust	9x7	5.0	.007	.275
2	Hp inlet	12x9	7.0	.009	.194
3	Ip inlet	12x9	7.0	.00875	.166
4	Lp front	16x14	10.0	.01075	.095
5	Lp centre	17x16	11.0	.0115	.029
6	Lp rear	17x12	8.0	.0115	.003
7	Gen inboard	17x13.5	11.5	.01125	
8	Gen outboard	17x13.5	10.5	.01125	
9	Collector	9x6	6.0	.007	

Calculated values

Brg#	Viscosity mu(Reyans)	Load F'	Load with Catenary,F	Unit load,P	L/D	Sommer- feld#SN	Capacity# CN
1	.3886E-5	5094.2	5770.0	128.2	.5556	.7515	.2319
2	.5833E-5	7158.3	7595.0	90.42	.5833	.7356	.2503
3	.3262E-5	10174.0	10754.0	128.0	.5833	.7189	.2446
4	.2566E-5	39262.0	34384.0	214.9	.6250	.3968	.1550
5	.2595E-5	54764.0	44111.0	235.9	.6471	.3607	.1510
6	.2624E-5	17515.0	27974.0	205.7	.4706	.4182	.9262
7	.2755E-5	56519.0	53000.0	271.1	.6765	.3481	.1593
8	.2871E-5	57472.0	50000.0	280.1	.6176	.3511	.1339
9	.3378E-5	-50148.	2000.0	37.4	.6667	.2262	1.005

Calculations at a running speed of 3600 rpm.

balancing. The instrumentation consists of vibration sensors and a remotely placed, a few yards from the unit, display system.

Bearing 9 is not monitored. Bearings 1 to 8 are provided with proximity probes (displacement transducers) which measure the shaft motion relative to the bearing. These are placed in a plane located 45 degrees to the horizontal plane (The horizontal plane is avoided for measurement of the response since it contains the bearing split). 90 degrees to this plane, the dual probes are placed (velocity transducers, integrated for displacement) on bearings 1 to 6. These probes measure the bearing absolute displacement (relative to the ground). The display system is provided with amplifiers and digital vector filters (DVF 2), which vectorially add the bearing absolute displacement to the relative displacement to give the shaft absolute displacement.

A key phasor is provided to give a time reference to all the measurements made. A speed wheel is located at the outboard end of the collector which helps measure the rotor speed using a proximity (inductive) pickup. Eight channel tape recorders are used for data collection.

8. Theory

For a multi-support system, the bearing reactions are indeterminate from the basic strength of materials approach. The continuity conditions provide extra equations in the

finite element method, providing enough equations to solve the reactions considering the static equilibrium alone.

8.4.1 Initially straight shaft on horizontal bearings

The static equilibrium equations are:

$$\begin{bmatrix} K_{WW} & K_{WB} \\ K_{BW} & K_{BB} \end{bmatrix} \begin{Bmatrix} W \\ B \end{Bmatrix} = \begin{Bmatrix} F_W \\ F_B \end{Bmatrix} + \begin{Bmatrix} 0 \\ R_B \end{Bmatrix}$$

where F is the static loading on the shaft and F the static loading at the bearing points, W is the set of unconstrained nodal variables, B is the set of constrained nodal variables and R_B is the set of constraint forces.

For the shaft on rigid supports, the nodal variables B are equal to zero. R_B can be found from:

$$\{W\} = [K_{WW}]^{-1} \{F_W\},$$

$$\{R_B\} = [K_{BW}]\{W\} - \{F_B\}.$$

8.4.2 Initially bent shaft on horizontal supports

Bishop[43] and Morton[86] have considered the effects of an initially bent shaft for the whirling problem.

Consider an initially bent shaft mounted on horizontal rigid bearings. Let the initial bend of the shaft be { W_0 }; and { W } be the static displacement when mounted on rigid supports. The actual displacement under the static weight is { $W-W_0$ }. We obtain the static equilibrium equations as:

$$\begin{bmatrix} K_{WW} & K_{WB} \\ K_{BW} & K_{BB} \end{bmatrix} \begin{Bmatrix} W - W_0 \\ B \end{Bmatrix} = \begin{Bmatrix} F_W \\ F_B \end{Bmatrix} + \begin{Bmatrix} 0 \\ R_B \end{Bmatrix}.$$

For rigid bearings on a straight line, B=0. Which gives:

$$[K_{WW}]^{-1} \{F_W\} + \{W_0\} = \{W\}$$

and

$$[K_{BW}]\{W - W_0\} - \{F_B\} = \{R_B\}$$

note that this equation is the same as the equation in the first case if { W_0 } is made zero.

8.4.3 Catenary

The turbo-generator is not a single rotor system. The high pressure, intermediate pressure, low pressure and generator units are articulated by couplings. The couplings are designed such that shear force and bending moment are not transmitted across; and continuity of displacement and bending slope is maintained. These conditions in an ideal

situation allow only axial torque and axial force to be
transmitted across the rotor. Zero shear force and bending
moment at the coupling points also means easy disassembly of
the rotors during maintenance and overhauls. The shaft
alignment at the couplings is achieved by changing the
bearing axis from horizontal to a curve called the catenary.

For the present turbo-generator unit, not all couplings
can be enforced with zero shear and bending moment. The Lp1
rotor will then be supported on one edge, this reaction
along with the internal elastic reactions of the statically
deformed shaft has to balance the rotor weight and the
bending moment.

Design of catenary

The support reactions $\{R\}$ are obtained with an
initially straight shaft and bearings. Let the nodal
variables be divided into U and C, where C is the set of
constrained variables at the couplings consisting of moment
$I\phi'$ and shear force $A\psi$, which are required to be zero. For
static equilibrium, internal elastic forces of the deformed
shaft balance the external forces due to the shaft weight
and the bearing reactions. The static equilibrium equations
are given as:

$$[K] \left\{ \begin{array}{c} U \\ B \\ C \end{array} \right\} = \left\{ \begin{array}{c} F_U \\ F_B \\ F_C \end{array} \right\} + \left\{ \begin{array}{c} 0 \\ R_B \\ 0 \end{array} \right\}$$

cancelling rows and columns corresponding to the variables C, we get:

$$\begin{bmatrix} K_{UU} & K_{UB} \\ K_{BU} & K_{BB} \end{bmatrix} \left\{ \begin{array}{c} U \\ B \end{array} \right\} = \left\{ \begin{array}{c} F_U \\ F_B \end{array} \right\} + \left\{ \begin{array}{c} 0 \\ R_B \end{array} \right\}$$

The catenary for setting the bearings { B } can be solved for. It can be noted here that the finite element developed is the only element which has shear force and bending moment as nodal variables allowing this direct method of calculation of the catenary.

To find the reactions for a given catenary:

The bearing reactions {R_B} can be calculated for a given static loading { F_U} and { F_B} and catenary { B }. The displacement at non-bearing nodes { U } is given by:

$$\{U\} = [K_{UU}]^{-1} \left\{ \{F_U\} - [K_{UB}] \{B\} \right\}$$

Hence bearing reactions are:

$$\{R_B\} = [K_{BU}] \{U\} + [K_{BB}]\{B\}.$$

Thus the static loads acting on the turbo-generator rotor can be found.

8.4.4 Fluid film bearings

In the static case the rotor rests on the bearing surface and the reactions are obtained from the rigid supports. In the dynamic condition the rotor is lifted inside the bearing and is supported by the fluid film. It is the fluid film dynamic characteristics which provide the necessary reactions to counter the static and dynamic forces.

When unbalance and other dynamic forces are absent the shaft is in a steady state motion, the only forces that act on the shaft are the static forces. Equation (6.2) of Chapter 6 gives the bearing reactions. The steady state response can be obtained from equation (6.3), after deleting the dynamic force terms.

Dynamic response at any running speed, Ω, for given dynamic forces, $\{F_y(t)\}$ and $\{F_z(t)\}$, can be found from equation (6.3). Dynamic response about the steady state equilibrium position is obtained by neglecting the static forces, $\{F\}$, in the equations of motion.

For obtaining the eigenvalues and eigenvectors of a
shaft supported on fluid film bearings the homogeneous
equations of motion, given in equation (6.4), are solved.

As discussed in Chapter 6, the damping and stiffness
matrices are dynamic in nature. For a given viscosity, unit
load, speed and bearing these coefficients are given.

Since linear bearings are considered, the dynamic
forces are neglected compared to the static (steady state)
forces. This assumption of linearity is valid for well
balanced rotors, with small unbalances, and small amplitudes
about the steady state equilibrium point. Thus, for a given
static bearing load { F }, running speed Ω, viscosity μ and
bearing dimensions the capacity number CN is found. From
Chapter 6, the corresponding dynamic coefficients are read
from the graphs. Note that the intermediate calculation of
eccentricity ratio is avoided.

8.4.5 System equations

Let [A(Ω)] be the dynamic system matrix, including
shaft stiffness, damping, inertia and bearing stiffness and
damping terms. This is a complex matrix due to the
damping/gyroscopic terms. The forcing function, say, due to
unbalance distributed along the rotor need not be in an
axial plane. The general forcing function can be represented
by a complex vector { Q(Ω) + iQ'(Ω) }. The response also
need not belong to a single axial plane(can be spacially
twisted along the rotor), again it can be represented as a

complex vector { q + iq }.

Craggs[61] suggested a method of calculating the correction weights using this complex system matrix. Difficulties might arise while handling complex equation solvers when working with micro computers, because of the limited software support. Matrix algebra allows the conversion of this equation to a system of real equations, also given by Morton[86]:

$$[A(\Omega)]\{q + iq'\} = \{Q(\Omega) + iQ'(\Omega)\}$$

expanding the system matrix, we get:

$$[K(\Omega) + i\,\Omega\,C(\Omega) - \Omega^2 M]\{q + iq'\} = \{Q(\Omega) + iQ'(\Omega)\}$$

Equating the real and imaginary parts of the equation we obtain the system of real equations:

$$\begin{bmatrix} K(\Omega) - \Omega^2 M & -\Omega\,C(\Omega) \\ \Omega\,C(\Omega) & K(\Omega) - \Omega^2 M \end{bmatrix} \begin{Bmatrix} q \\ q' \end{Bmatrix} = \begin{Bmatrix} Q(\Omega) \\ Q'(\Omega) \end{Bmatrix}$$

The system matrix can be directly multiplied to give the correction weights for a measured unbalance response.

Also the inversion of this matrix can be used for the response for a given force (unbalance).

8.4.6 Condensation of system size: dynamic reduction

The accurate high order finite element with non-uniform cross-section and disks included inside the elements, allowed the whole turbo-generator unit to be modelled by just 18 elements. The global degrees of freedom are 76 in each plane or 152 for the whole rotor. For a response study, a linear equation of order 152 has to be solved for each running speed. For the damped eigenvalue problem the system size doubles resulting in a 304 degrees of freedom real asymmetric system matrix with complex eigenvalues and eigenvectors.

Even for a large computer the system matrix size is prohibitive. The calculations, if at all feasible, are costly. The eigenvalues obtained from the total system lie much above the operating speed, except for the first few. It will be of great advantage if the accuracy obtained by considering all the global degrees of freedom is retained when only a few master degrees of freedom are used. The modal reduction used in the analysis of stability had the generalized or the orthonormal co-ordinates as the retained degrees of freedom. As no physical meaning can be attached to these variables, retained degrees of freedom are chosen to meet the following considerations:

1. The accuracy of the reduced system depends on how well

the retained modes(lower modes) approximate the motion, upon superposition. Good accuracy is obtained by selecting the nodal variables corresponding to large mass to stiffness ratio and distributed over the structure instead of picking them from a single region of the shaft.

2. The loading acting on the shaft has to be completely represented by the forces corresponding to the retained variables. The loading causing flexure is either a force or a moment; both of these can be represented by forces corresponding to the displacement, W, variable . Thus ϕ, $A\psi$ and $I\phi'$ variables can be suppressed.

3. Compatibility of the retained variables is important. Displacement variable, W, is continuous all along the shaft including joints and points with loading.

4. The bearing conditions of stiffness and damping can be accommodated using displacement variables as the retained degrees of freedom.

5. The input data (usually the bearing displacement) and the output (usually the correction weights in the balance planes) can be represented with displacement variables retained.

Thus all or some of the displacement variables can be retained according to the accuracy needed, apart from other considerations.

If the aim is to find the dynamic shear force and moments acting on the shaft, to find the dynamic stresses,

then the retained variables should include $A\psi$ and $I\phi'$.

The classical reduction by Guyan is obtained from the static equilibrium equation. The retained nodal variables $\{X\}$ corresponding to the applied forces dictate the motion of the suppressed variables $\{X_S\}$. Accordingly, $\{X_R\}$ are designated as the master and $\{X_S\}$ as the slave variables. The reduced set $\{X_R\}$ approximates any shape of the shaft deformation by superposition of the static modes that result from unit loads applied one at a time to the master degrees of freedom. Let the static equilibrium equation be:

$$\begin{bmatrix} K_{RR} & K_{RS} \\ \hline K_{SR} & K_{SS} \end{bmatrix} \left\{ \begin{array}{c} X_R \\ X_S \end{array} \right\} = \left\{ \begin{array}{c} F \\ \hline 0 \end{array} \right\}$$

Expressing the suppressed degrees of freedom in terms of the retained, we get:

$$\left\{ \begin{array}{c} X_R \\ \hline X_S \end{array} \right\} = \left[\begin{array}{c} I \\ \hline -[K_{SS}]^{-1}[K_{SR}] \end{array} \right] \left\{ X_R \right\} = \left[T_{static} \right] \left\{ X_R \right\}$$

The $[\ T\ static\ ]$ matrix is used to transform the mass, stiffness and damping matrices, to reduce the system size. This method is widely used in structural dynamics.

Rouch[55] used the Guyan reduction to suppress the shear variable ψ which is not continuous at sectional joints. The static condensation is limited in its application because of the following reasons:

1. Useful only for low speed dynamics (around first critical) as in structures. The critical speeds obtained are higher because of the imposed constraints and due to the use of inaccurate modes.

2. Cannot suppress the nodes where the forces are nonzero.

3. Inertia effects are neglected.

The accuracy and the speed range of application greatly improves by using modal reduction. A method is derived to obtain a modal transformation matrix in terms of the desired variables $\{X_R\}$. Let the undamped equations of free motion be:

$$\left\{ [K] - \omega^2 \ [M] \right\} \left\{ \begin{array}{c} X_R \\ X_S \end{array} \right\} = \left\{ 0 \right\}$$

The solution of which gives the eigenvalues and the eigenvectors. The normalized modal matrix formed with the eigenvectors of ascending modes occupying columns from left to right relate the nodal degrees of freedom to the generalized co-ordinates:

$$\left\{ \begin{array}{c} x_R \\ x_S \end{array} \right\} = \left[\begin{array}{cc} \phi_{RR} & \phi_{RS} \\ \phi_{SR} & \phi_{SS} \end{array} \right] \left\{ \begin{array}{c} q_R \\ q_S \end{array} \right\}$$

Using the first R modes for an approximation, we obtain:

$$\left\{ \begin{array}{c} x_R \\ x_S \end{array} \right\} = \left[\begin{array}{c} \phi_{RR} \\ \phi_{SR} \end{array} \right] \left\{ q_R \right\}$$

The retained generalized co-ordinates can be expressed in terms of the retained nodal variables as:

$$\{q_R\} = [Q_{RR}]^{-1} \{x_R\}$$

Hence we obtain the relation:

$$\left\{ \begin{array}{c} x_R \\ x_S \end{array} \right\} = \left[\begin{array}{c} \phi_{RR} \\ \phi_{SR} \end{array} \right] \left[\phi_{RR} \right]^{-1} \{x_R\}$$

$$= [T_{dynamic}]\{x_R\}$$

This dynamic transformation matrix can be used for reducing the system size. This method is preferred to the

static method for high speed machines such as

turbo-generator shafts:

1. The suppressed variables need not be the ones with

   forces absent.

2. The dynamic modes represent the higher frequency

   response better than the static modes.

The method though has some disadvantages:

1. Costly eigenvalue problem has to be solved to get the

   modal matrix from which the transformation matrix is

   obtained.

2. The undamped system is considered to obtain a real

   transformation matrix. The actual damped system has a

   complex transformation matrix.

3. The accuracy of the higher modes, which are included in

   the transformation matrix, depends on the number of

   elements or global degrees of freedom used to represent

   the system. Thus, all the modal vectors are not of the

   same accuracy, limiting the number of modes that can be

   considered and hence the number of degrees of freedom

   that can be retained. The lower limit on the number of

   retained degrees of freedom is the running speed; at

   least one mode above the running speed has to be used to

   obtain a reasonable accuracy.

8.5 Results and discussion

The rotor system matrix in a plane is of the order 76. Dynamic reduction has been used to bring down the size to 19. Displacement variable, W, at each node has been retained. Shaft motion in the vertical plane is considered. The corresponding direct stiffness due to the fluid film is accounted for. The cross-coupling stiffness and all the damping terms are omitted to avoid complex eigenvalues and eigenvectors as discussed in the Chapter on stability.

Static loads on each of the nine bearings is calculated, with the catenary effect included. Capacity number is calculated at the running speed for all the bearings, and hence the dynamic coefficients. The vertical stiffness of the fluid film alone is considered, reducing the problem to a symmetric shaft supported on flexible bearings vibrating in the vertical plane. Further analysis is referred to this undamped system. The foundation and pedestal are assumed to be rigid. Internal and other sources of damping have been neglected.

The bearing dynamic characteristics have been shown to vary with the running speed and hence the system matrices, eigenvalues and eigenvectors. As discussed in the Chapter on stability, the eigenvalues and vectors have to be determined at each operational speed. For the present analysis the eigenvalues and vectors are obtained at the running speed of 3600 rpm.

Table 8.5 gives the first 10 critical speeds of the turbo-generator unit. The corresponding mode shapes are shown in Figures 8.5 to 8.14. The dots in the mode shape diagrams indicate the node points of the elements. The nearest critical to the operating speed (3600) is 3312.17 rpm.

Table 8.5 compares the methods of Guyan and the dynamic reduction for the eigenvalue calculation. The system size is reduced from 76 to 19 in both the cases. The critical speeds for the dynamically reduced system and the full system match exactly which is not very surprising as the modes corresponding to the actual dynamic system have been used. The Guyan reduction doesn't seem to match in its performance. This is because the dynamic (stiffness+inertia controlled) modes have been approximated by the static modes (stiffness controlled), which additionally constrain the system. The error in using the static modes for condensation is estimated, in each of the modes, by calculating the difference between the critical speeds using full and statically reduced matrices. The 6th mode (collector mode) has the greatest error (5.02%). The error for the lower modes ranges from 1.35% to 5.02%, for the first 6 modes and for the higher modes(7th to 10th) between 0.8% to 1.95%. The error reduces if more retained variables participate in the mode under consideration.

The question might now arise, why one should evaluate the eigenvalues by the reduced system when the more accurate

Table 8.5. First 10 critical speeds of the rotor system (Rpm)

Mode #	Mode type	Full matrix (76 d.o.f)	Dynamic red. (19 d.o.f)	Guyan red. (19 d.o.f)	% error
1	Generator	1138.48	1138.48	1160.75	1.96
2	Ip- Lp	1716.78	1716.78	1789.66	4.24
3	Ip- Lp	1836.24	1836.24	1917.88	4.44
4	Hp- Ip	2078.30	2078.30	2114.43	1.74
5	Hp- Ip	2177.60	2177.60	2207.13	1.35
6	Collector	2651.69	2651.69	2784.90	5.02
7	Generator	3312.17	3312.17	3338.83	0.80
8	Combined (Hp- Lp)	4539.04	4539.05	4585.39	1.02
9	Combined (Hp- Lp)	5185.54	5185.54	5253.99	1.32
10	Combined	5504.59	5504.59	5612.34	1.95
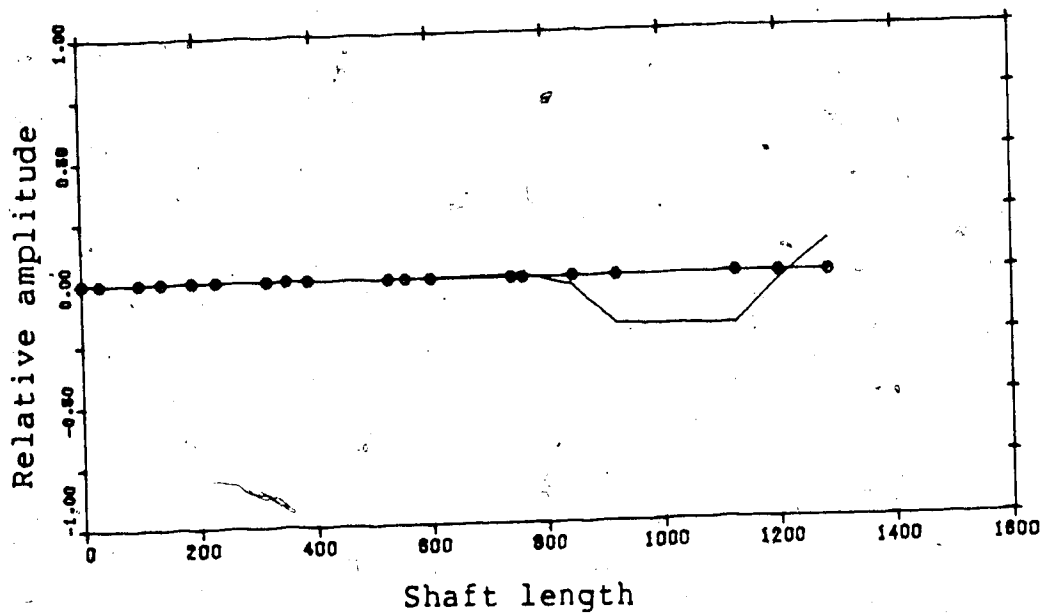
Figure 8.5 1st Cr. 1138rpm: Generator mode
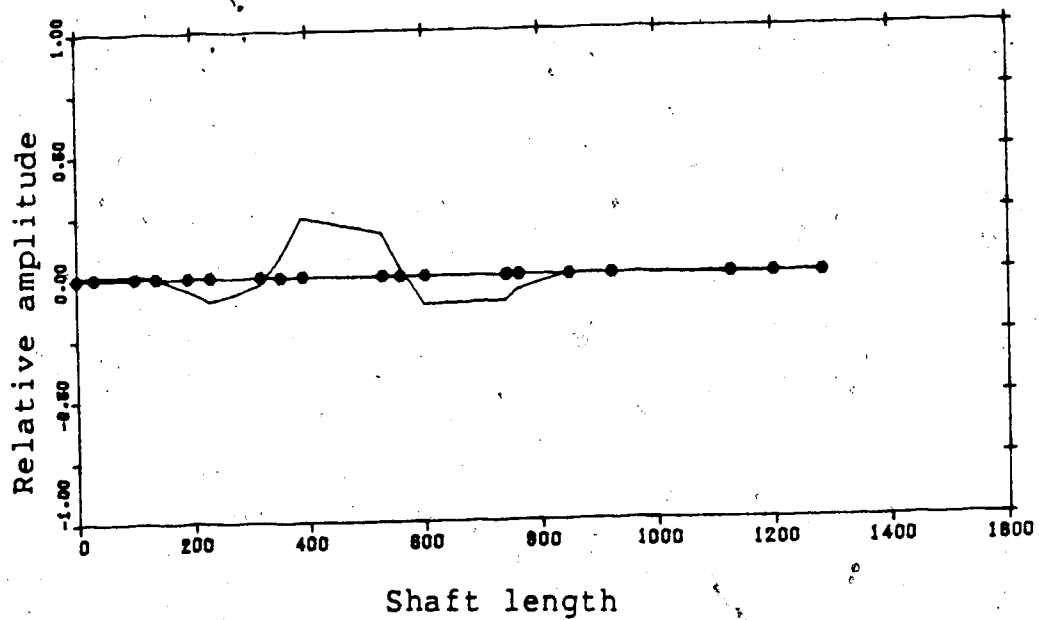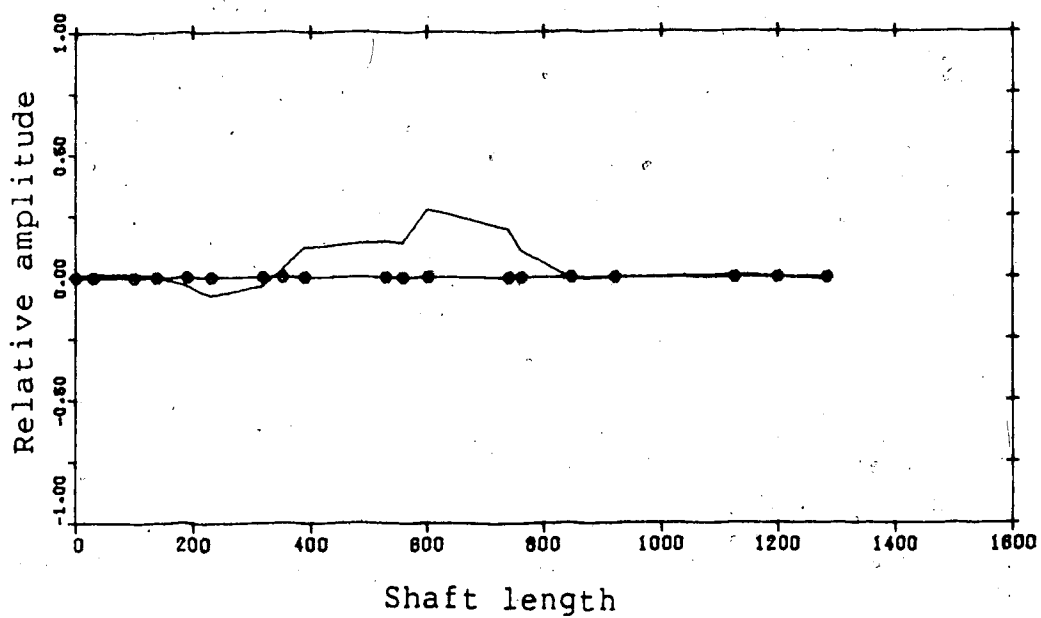

Figure 8.6 2nd Cr. 1716rpm: Ip-Lp mode

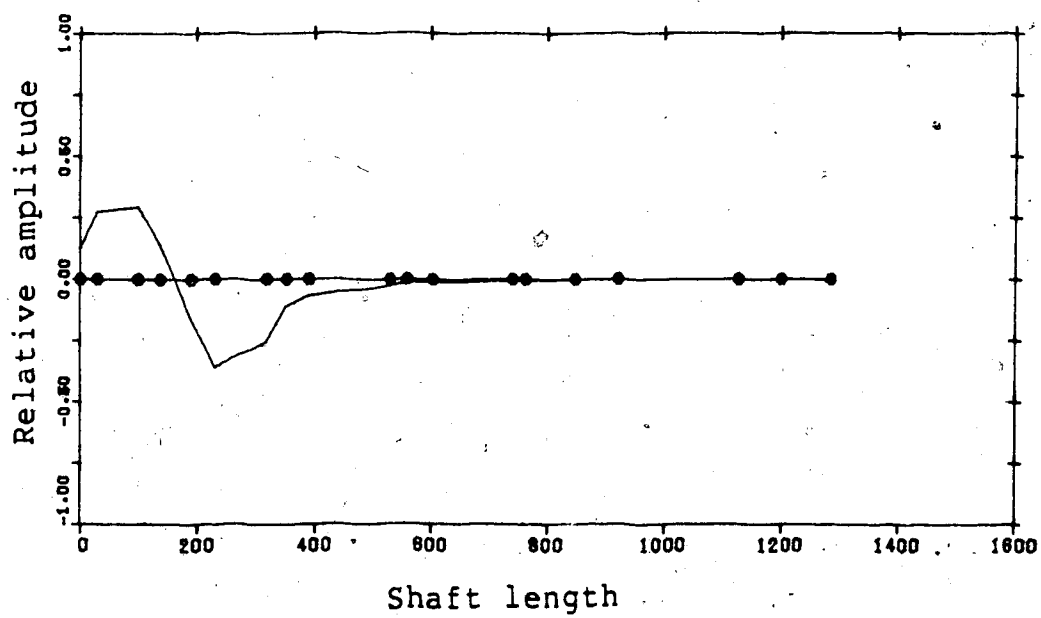Figure 8.7 3rd Cr. 1836rpm: Ip-Lp mode

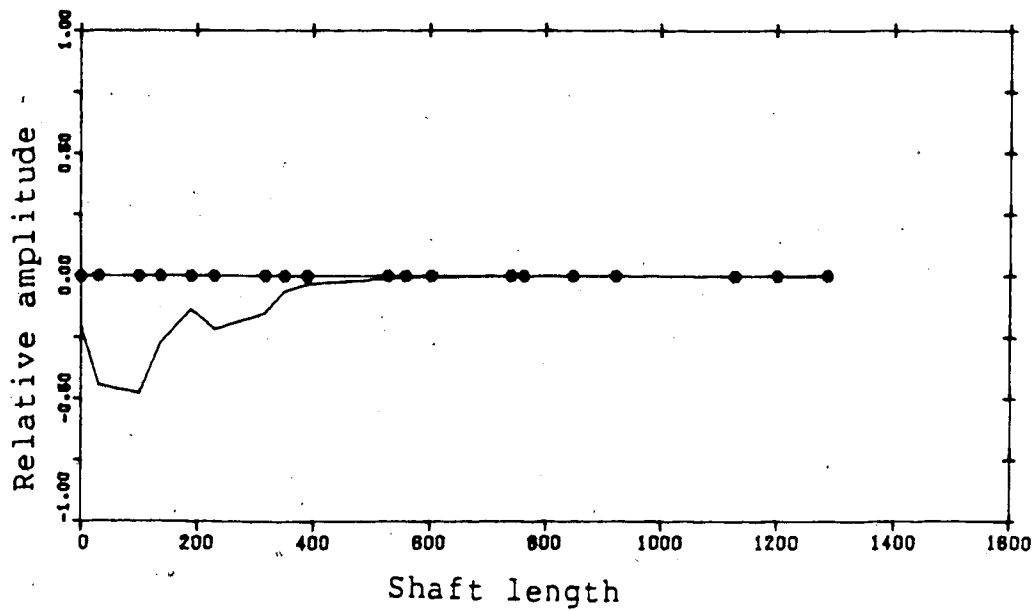Figure 8.8 4th Cr. 2078rpm: Hp-Ip mode
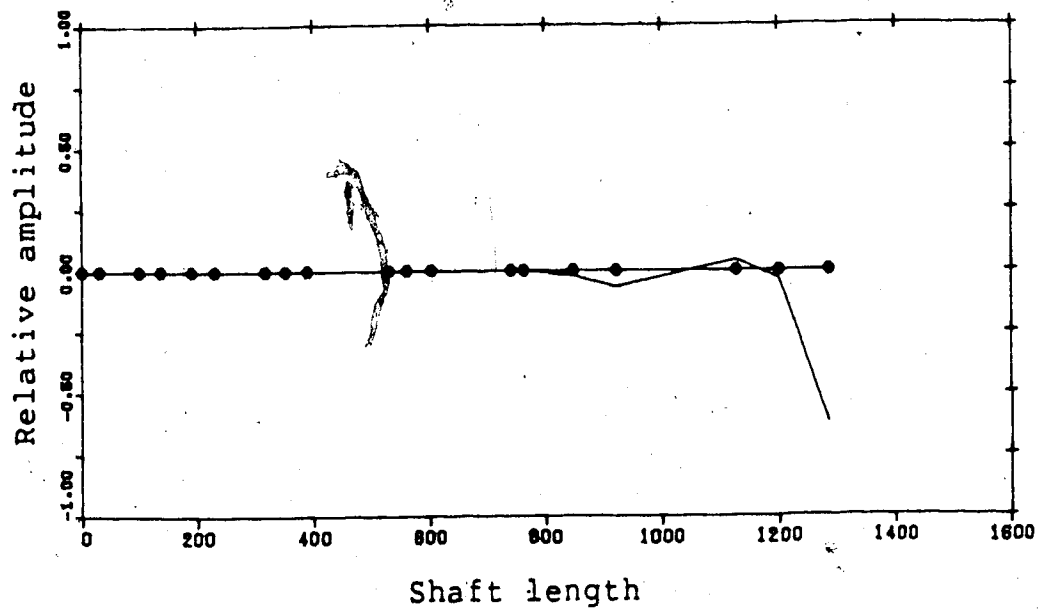
Figure 8.9 5th Cr. 2177 rpm: Hp-Ip mode

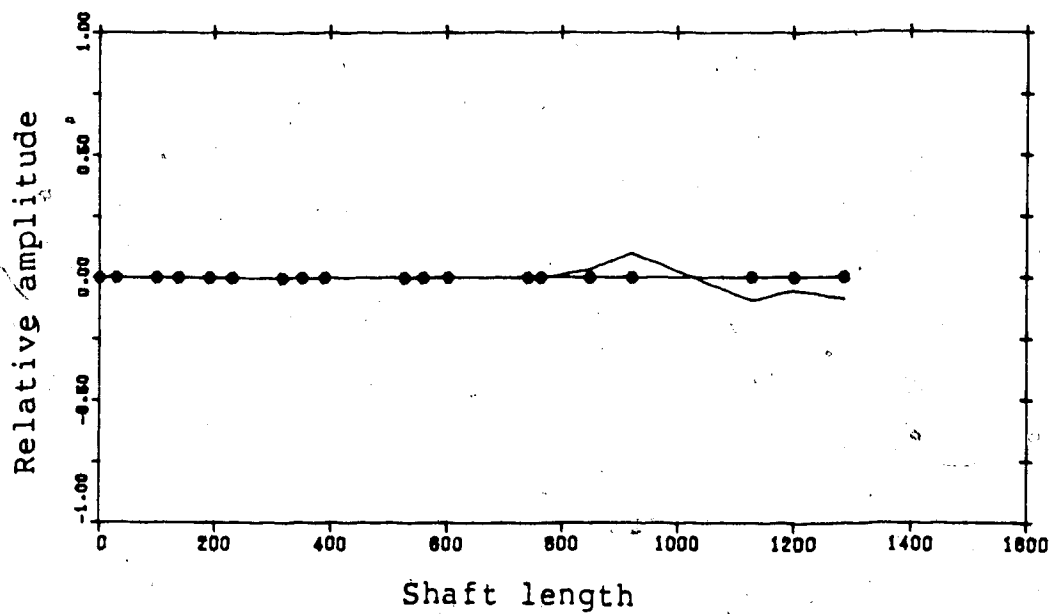Figure 8.10 6th Cr. 2651rpm: Collector mode
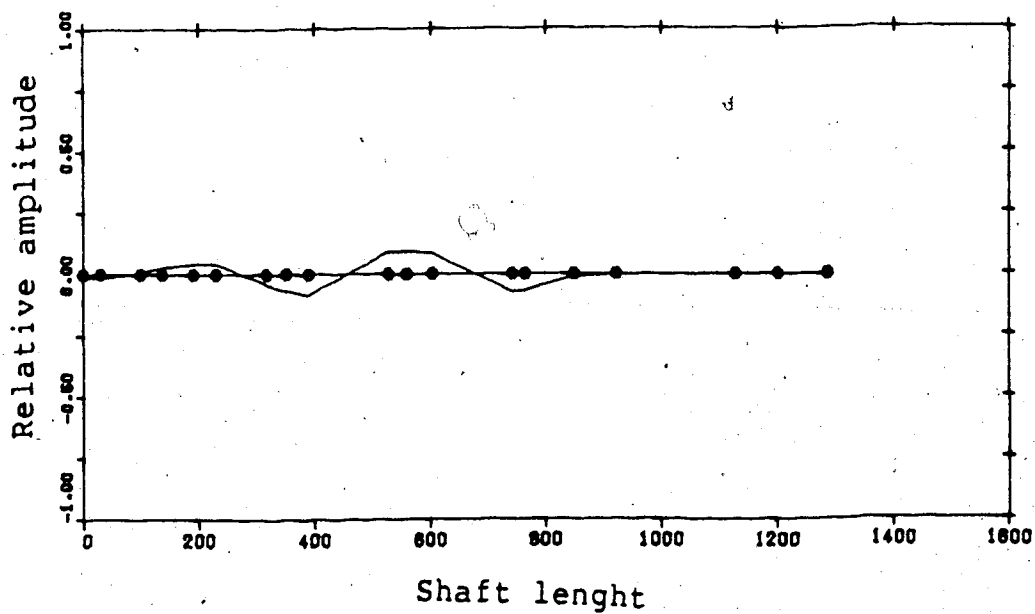
Figure 8.11 7th Cr. 3312rpm: Generator mode

Figure 8.12 8th Cr. 4539rpm: Combined mode
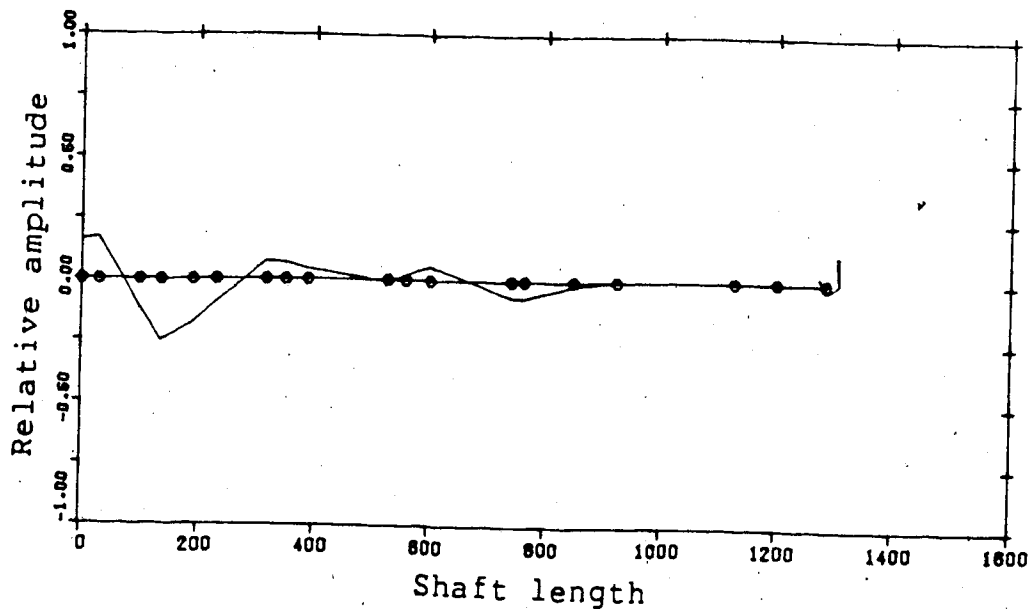
Figure 8.13 9th Cr. 5185rpm: Combined mode
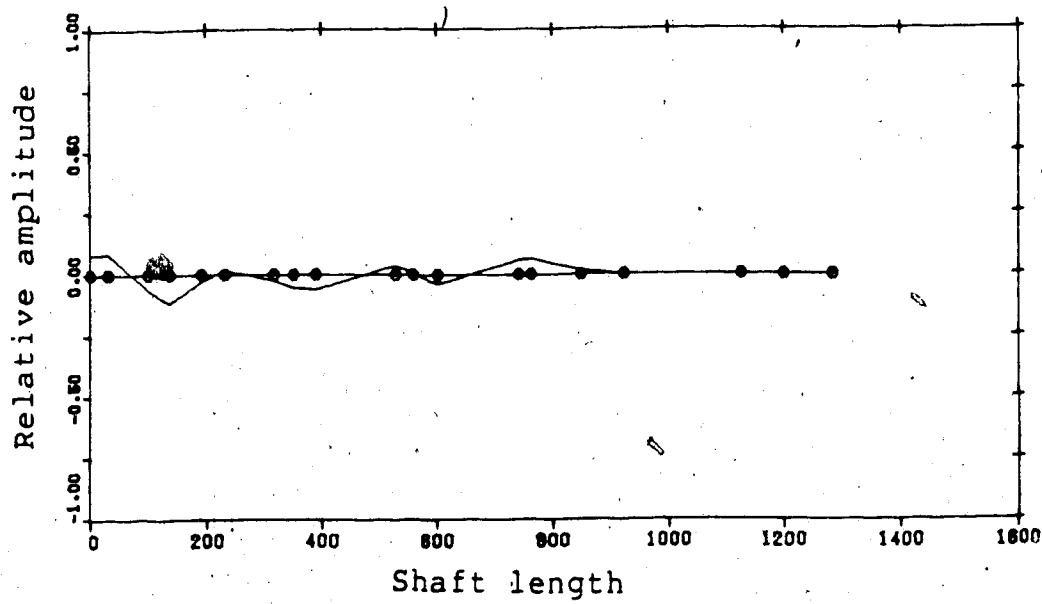
Figure 8.14 10th Cr. 5504rpm: Combined mode

full system results are available? In the present study the reason is to compare the two methods of reduction. A more valid reason is when the eigenvalues at different speeds have to be found, as in a stability study. Then, the less costly reduced system can be augmented with the changes occurring in the dynamic coefficients, and critical speeds at different running speeds can be found.

At the lower criticals all the turbo-generator spans are not activated. Critical speeds can belong to just one or a few neighbouring spans. The 6th critical excites only the collector shaft; 2nd and 3rd just the Lp-Ip spans; 4th and 5th excite the Hp-Ip. Some spans are totally unexcited in certain modes; the generator span does not participate in any of the 2nd, 3rd, 4th, 5th, 8th, 9th and 10th modes. This fact is to be borne in mind while using dynamic reduction for balancing and balance plane selection. For a single span rotor, the whole rotor (except for the node points) deflects at each critical speed. Whereas, a multi-span rotor with a span stiffer than the others, will not allow the stiff member to deform in the lower modes. If an unbalance exists in the stiff span, the response is now non-zero in the span and the lower modes will fail to form the deformed shape, on superposition.

Effectiveness of dynamic reduction of a single span can be described by the number of modes considered. For a multispan rotor the number of modes for each span have to be mentioned. The first ten modes of the turbo-generator has

only two generator modes.

Synchronous response is studied by placing an unbalance $mr = .01$ lb.sec^2 at node 16 corresponding to the generator. As mentioned before, the dynamic coefficients change with the running speed. Average values of dynamic coefficients, occuring at 3600 rpm, are used at all speeds to reduce the computation time. For more accurate determination of the response, dynamic coefficients at each of the running speeds have to be evaluated and used.

A dynamically reduced matrix of size 19 is used for the response study. It is to be mentioned here that response studies using this matrix will not match exactly with the results using the full matrix, as the eigenvalues did. This is because of the truncation error introduced due to the use of a few modes. Error is also induced if the reduction of a damped system is obtained using undamped modes. Yet, these errors are found to be negligible. Guyan reduction using static modes might do quite well for low speed response.

The response study with the unbalance in the generator, is shown in Figures 8.15 to 8.17 for three ranges of running speeds: at low running speeds, below the operating speed and finally at the operating speed and above. The abscissa denotes the shaft length in inches and the ordinate gives the absolute amplitude on a log scale. The locations of the balance planes, of the turbine rotors, available for trim balancing are indicated by the lines B1 to B6. The trim balancing planes of the generator are not shown, assuming
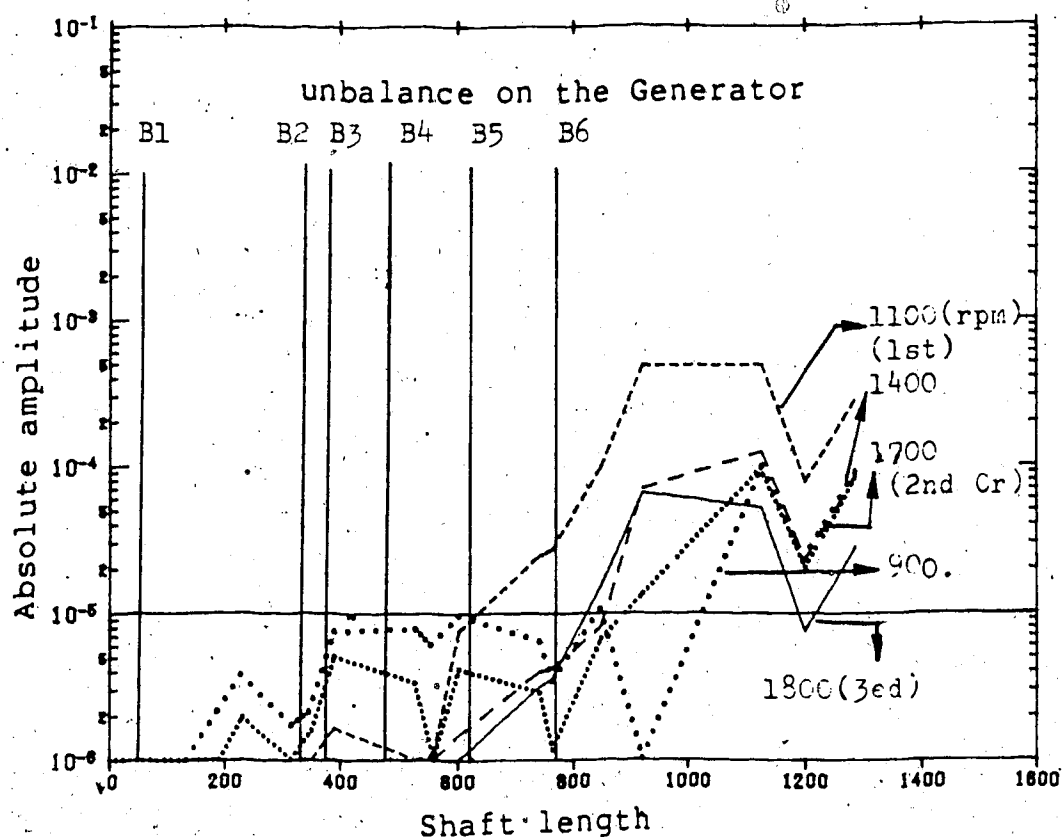
Figure 8.15 Response at low speeds
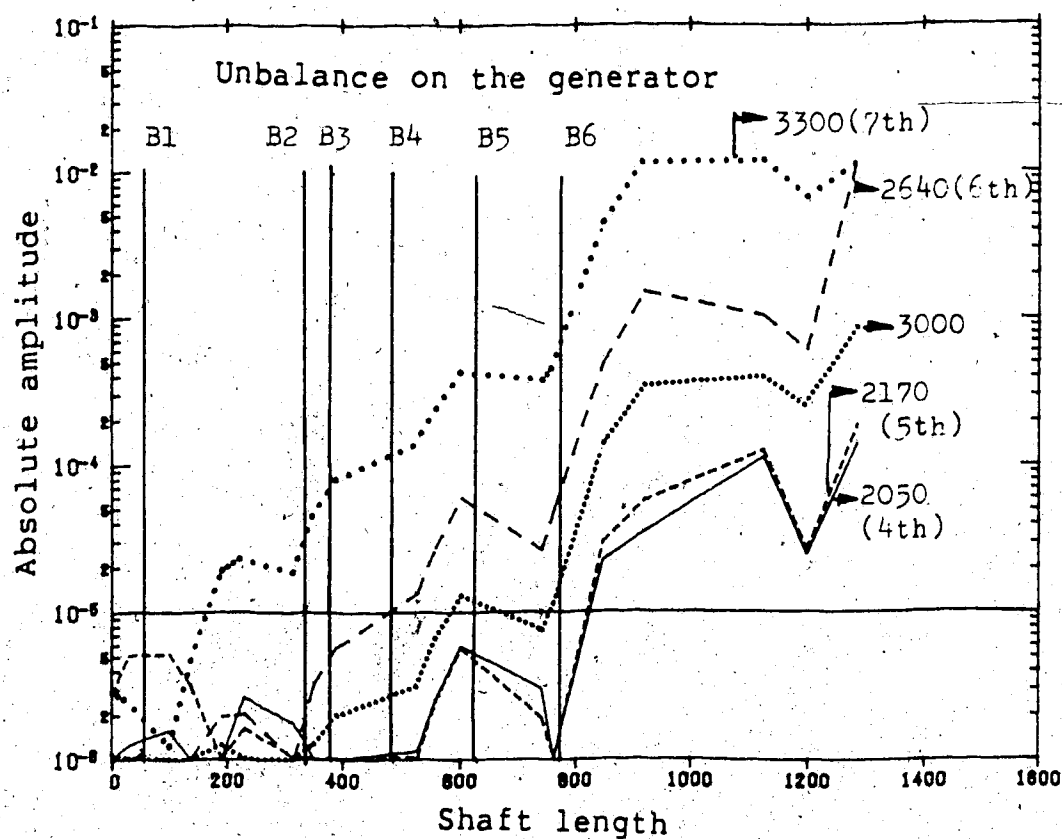
Figure 8.16 Response below operating speed
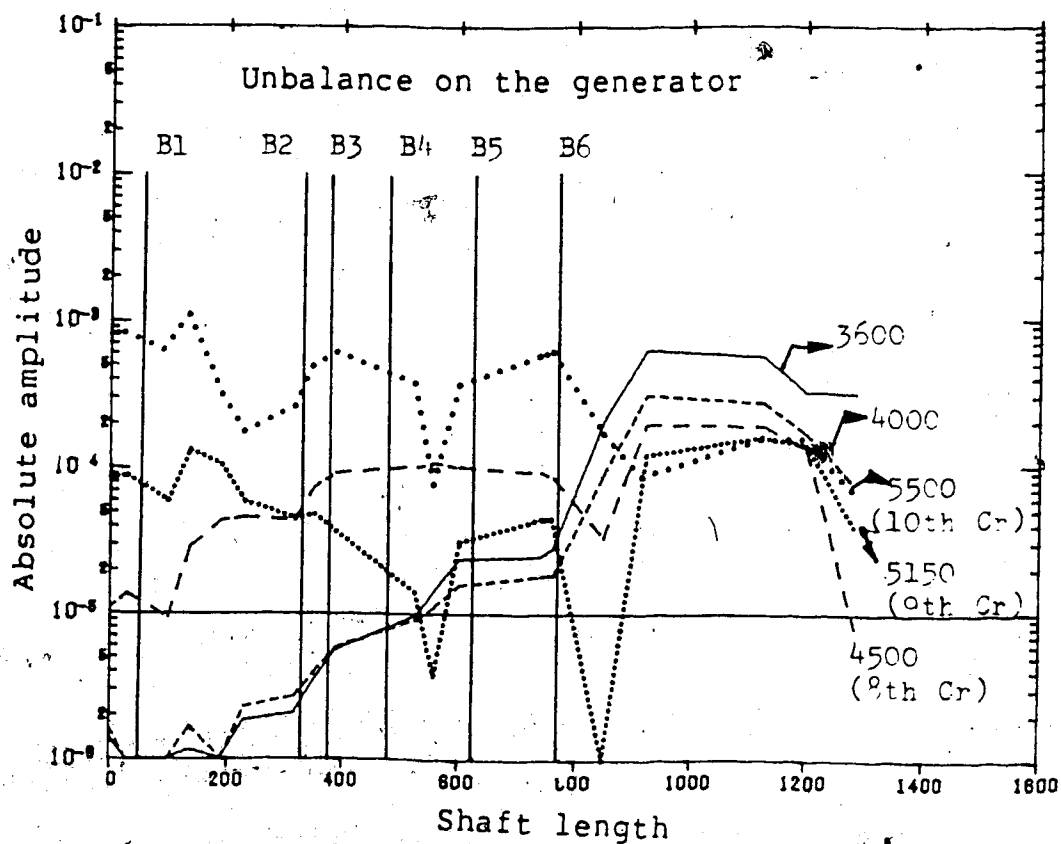
Figure 8.17 Response at and above operating speed
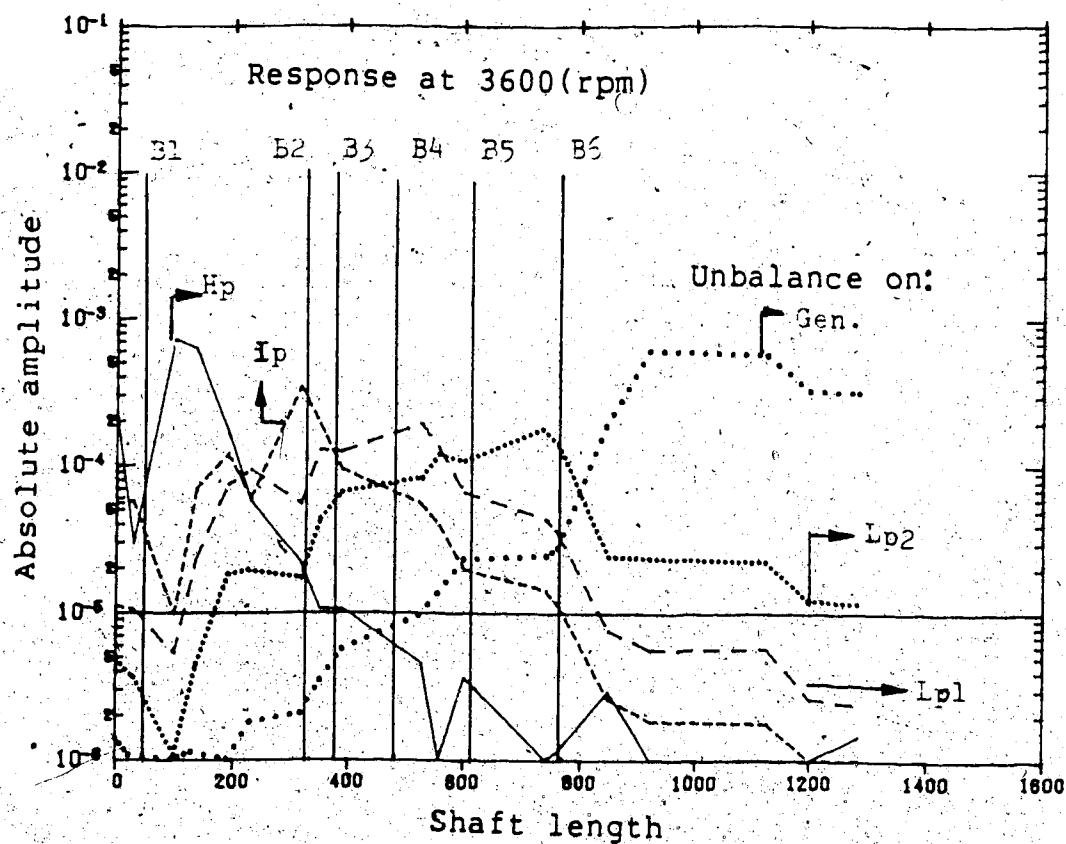
Figure 8.18 Unbalance in different spans

that these planes are already filled by previous balancing.

The deformed shape of the total length of the shaft is plotted for each running speed. The horizontal line at 10^{-5} inches is to indicate that amplitudes below are ineffective. This is not any absolute limit; compared to the largest amplitudes occuring(above .001") vibration below 10^{-5} is negligible. Naturally, this limit changes with the magnitude of the unbalance acting.

The response is not monotonically increasing with speed as the mode shapes close to the running speed dominate. The generator response below the operating speed of 3600 rpm (at 2600 and 3300 rpm) is higher than when the running speed is above the operating speed(at 4000 and 5500 rpm). This is because the generator is unexcited in the higher modes 8 to 10.

The effect of the generator unbalance on the other spans is also dependent on the mode shapes. Thus, below the running speed the critical speeds belong to the generator, Lp1 and Lp2, with the Hp and Ip in the ineffective zone.

Note that at 3000rpm, though a higher speed, amplitude is less than when the shaft is running at 2640, a critical speed.

The response on a span due to an unbalance on a different span (similar to flexibility/influence coefficient) is a measure of the coupling existing between the spans. This information is useful to determine the effectiveness of the balancing planes: if the spans are

totally uncoupled an unbalance on one cannot be corrected using balance planes on another.

In the modal balancing method, the first step is to run the shaft near the first critical speed (say at 1100 rpm) and the generator unbalance is corrected by placing weights in the available balancing planes. It can be readily seen from the response at that speed, Figure 8.15, that the balance planes B1 to B4 are ineffective. For the total balancing of the generator many balance planes (15 to 25, shown in Figure 8.1) are available. Whereas trim balancing is done using a limited number of planes, out of which only a few are effective (B5 and B6 for the present case).

The first few modes of the span with the unbalance are to be considered for modal balancing and not the first few system modes. Thus, the imbalance in the generator rotor is corrected at the 1st mode of the generator span (at 1138 rpm, incidentally also the 1st system mode) and next at the 2nd generator mode(at 3312 rpm, the 7th system mode) and not at the system 2nd critical(1716 rpm, an Ip-Hp mode). The effect of the non-generator modes and the combined modes, especially those near the running speed, transfer imbalance to the other spans, causing them to respond. These spans are considered next for balancing.

In the influence coefficient method balancing is done at the operating speed, 3600 rpm in this case. From the response curve, Figure 8.17, it is seen that, again, planes B1 to B4 are ineffective to correct the imbalance in the

generator.

To have a better understanding of the shaft behavior at the running speed and to find the effectiveness of the turbine trim balance planes to correct imbalances in their own spans, the rotor is run at the operating speed of 3600 rpm with an imbalance of $mr=.01$ lb sec^2 in each of the spans, Hp, Ip, Lp1, Lp2 and the generator; one at a time and the corresponding response is plotted in Figure 8.17.

It is seen in Figure 8.18 that the balance planes are very effective for imbalances occuring in their own planes. The position of the peaks will vary with the location and type of imbalance.

Only for the case of the spans with large imbalance or with the balance planes filled by previous balancing, as in the generator, is help from the neighbouring span balance planes taken.

8.6 Conclusions

The accurate finite element, the method of including disks inside the element, fluid film bearings and dynamic reduction have been applied to an actual turbo-generator unit. The results match closely with those observed in-situ; reported by Craggs, Ellyin and Pelot[91].

Dynamic reduction is more accurate than the classic Guyan reduction, especially for eigenvalue study. The reduced matrix of size 19 for the turbo-rotor considered, for the micro-computer which can be used for

analyzing large rotors in industry.

For a turbo-generator unit with rigid spans and rigid span couplings, a weight in a plane can correct imbalance in any other plane on the shaft. On the other hand for a flexible shaft with flexible span couplings, the correction planes have to be close to the planes of unbalance.

The intricate relation of the critical speeds, mode shapes, unbalance and span coupling is discussed using the response curves. Thus, optimum balance planes can be designed, for a given balancing method.

List of references.

1. Rayleigh., Theory of sound., MacMillan Co, London,
   293-294, 1887

2. Timoshenko,S.P., On the correction for the shear of the
   differential equation for transverse vibration of
   prismatic bars, London Phil Mag(6), Vol 41, 744-746,
   1921.

2. Timoshenko,S.P., On the transverse vibrations of bars of
   uniform cross-section, Phil Mag. S. 6, Vol 43, 125-131,
   1922.

4. Anderson,R.A., Flexural vibrations in uniform beams
   according to Timoshenko theory, Trans. ASME, Vol 175,
   504-510, 1953.

5. Dolph,D.L., On the Timoshenko beam vibrations, Qtrly.
   Appl. Mech., Vol.12, 175-187, 1954.

6. Trail-Nash,P.W., Collar,A.R., The effects of shear
   flexibility and rotatory inertia on the bending
   vibrations of beams, Qtrly.J.Mech.Appl.Math., 6,
   186-222, 1953.

7. Huang,T.C., The effect of rotatory inertia and shear
   deformation on the vibrations of beams treated by the
   approximate methods of Ritz and Galerkin, Proc. of the
   third U.S National Congress of Appl. Mech, ASME,

189-194, 1958.

8. Huang,T.C., The effect of rotatory inertia and shear deformation on the frequency and normal mode equations for uniform beams with simple end conditions, J.Appl. Mech., 28, 579-584, 1961.

9. Cowper,G.R., The shear coefficient in Timoshenko beam theory, J. Appl. Mech., Vol 33, Trans. ASME, series E, Vol 188, No 2, 335-340, 1966.

10. Prescott.J, Elastic waves and vibrations of thin rods, Phil. Mag., 33, 744, 1942.

11. Zienkiewicz,O.C., The finite element method, 3ed Edition, Mc Graw-Hill book Co, UK.

12. Huebner, K.H., The finite element method for engineers, John - Wiley and sons, N.Y..

13. Cook,R.D., Concepts and applications of finite element analysis, John-Wiley and Sons, 1974.

14. Archer,J.S., Consistent mass matrix for distributed mass systems, J.Struct. Div., Am. Soc. Civil Engrs., 89, 161-178, 1963.

15. Archer,J.S., Consistent matrix formulation for structural analysis using finite element techniques, AIAA. J, 3, 1910-1918, 1965.

16. Macalley, R.B., Rotary inertia correction for mass

matrix, General Electric Knolls atomic power lab.,
Schenectady, N.Y., Report DIG/SA, 63-73, 1963.

17. Davis,R., Henshell.R.D., Warburton.G.B., A Timoshenko
beam element , J. Sound. Vib., 22(4), 475-587, 1972.

18. Narayanaswami,R., Adelman.H.M., Inclusion of transverse
shear deformation in finite element displacement
formulation, AIAA. J., Vol. 12, 1613-1614, 1974.

19. Kapur, K. K., Vibrations of a Timoshenko beam using
finite element approach, J. Accoust. Soc. Am., Vol. 40,
5, 1058-1063, 1966.

20. Carnegie, W., Thomas,J., Dokumaci,E., An improved method
of matrix displacement analysis in vibration problems,
The Aero. Qrtly., 20, 321-332, 1969.

21. Nickell, R.E., Secor,G.A., Int. J. Num. Methods in Eng.,
5, 243-253, 1972.

22. Thomas,D.L., Wilson,J.M., Wilson,R.R., Timoshenko beam
finite element, J. Sound. Vib., 31(3), 315-330, 1973.

23. Thomas,J., Abbas,B.A.H., Finite element model for
dynamic analysis of a Timoshenko beam, J. Sound. Vib.,
41(3), 291-299, 1975.

24. Thomas,D.L., Comments on finite element model for
dynamic analysis of Timoshenko beam, J.Sound.Vib.,
46(2), 285-290, 1976.

25. Dawe,D.J.,A finite element for the vibration of Timoshenko beams, J.Sound.Vib, 60(1), 11-20, 1978.

26. Craggs,A., Hong,D.P., An accurate Timoshenko beam finite element , Dept. Mech. Eng., Univ. of Alta., 1980

27. Akella,S., Craggs,A., An accurate Timoshenko beam finite element, Dept. Mech. Eng., Univ. of Alta, 1982.

28. Lindberg,G.M., Vibration of nonuniform beams, The Aero. Qrtly., 387-395, 1963.

29. Carnegie,W., Thomas.J., Natural frequencies of long tapered cantilevers, The Aero Qrtly, Vol18, 309-320, Nov. 1967.

30. Thomas,J., Dokumaci,E., Improved finite elements for vibration analysis of tapered beams, The Aero. Qrtly, 39-46, Feb 1973.

31. To,C.W.S., Higher order tapered beam finite elements for vibration analysis, J. Sound. Vib., 63(1), 33-50, 1979.

32. To,C.W.S., a linearly tapered beam finite element incorporating shear deformation and rotatory inertia for vibration analysis, J. Sound. Vib., 475-484, March 1981.

33. Abbas, B.A.H., Thomas,J., The second spectrum of Timoshenko beams, J. Sound. Vib., 51(1), 123-137, 1977.

34. Bhashyam,G.R., Prathap,G., The second frequency spectrum of Timoshenko beams, J. Sound Vib., 76(3), 407-420,

1981.

35. Downs,B., Transverse vibrations of a uniform simply
    supported Timoshenko beam without transverse
    displacement, J. Apll. Mech., 43, 671-673, 1976.

36. Stephens,N.G., The Second frequency spectrum of
    Timoshenko beams, J. Sound. Vib., 84, 319-326, 1982.

37. Levinson,M., Cooke,D.W., On the two frequency spectra of
    Timoshenko beams, J. Sound. Vib., 84, 319-326, 1982.

38. Prathap,G., The two frequency spectra of Timoshenko
    beams - a reassessment, J. sound Vib., 90(3), 443-446,
    1983.

39. Pestel,E.C., Leckie,F.A., Matrix methods in elasto
    mechanics , Mc Graw-Hill Co, 1963.

40. Rankine,W.J., On the centrifugal force of rotating
    shafts, Engineer, Lond., Vol. 27, p249, 1869.

41. Jeffcott,H.H., The lateral vibration of loaded shafts in
    the neighbourhood of a whirling speed: The effect of
    want of balance, Phil. Mag., Ser. 6, Vol. 37, p304,
    1919.

42. Kimball,A.L., Internal friction theory of shaft
    whirling, General Electric Review, Vol. 27, p244, 1924.

43. Bishop,R.E.D., The Vibration of rotating shafts, J.
    Mech. Eng. Sci., Vol. 1, p50, 1959.

44. Bishop,R.E.D, Gladwell,G.M.L., The vibration and balancing of an unbalanced flexible rotor, J. Mech. Eng. Sci, Vol 1, p66, 1959.

45. Gladwell,G.M.L., Bishop,R.E.D., The vibration of rotating shafts supported in flexible bearings, J. Mech. Eng. Sci., Vol. 1, No. 3, p195-206, 1959.

46. Bishop,R.E.D., Gladwell,G.M.L., Michaelson,S., The matrix analysis of vibration, University press, Cambridge, 1965.

47. Lowey,R.G., Piarulli,V.J., Dynamics of rotaing shafts, The shock and vibration information centre, United States dept. of defence, publication SVM-4, 124p.

48. Eshleman,R.L., Eubanks,R.A., On the critical speeds of flexible rotors, J. Appl. Mech., Trans. ASME., Vol. 15, 369-375, 1968.

49. Myklestad,N.O., A new method of calculating natural modes of uncoupled bending vibrations of airplane wings and other types of beams, J. Aero. Sci., 11(2), p153, 1944.

50. Prohl, M. A., A general method for calculating critical speeds of flexible rotors, J. Appl. Mech., Vol 12, Trans. ASME., Vol. 67, 142-148, 1945.

51. Lund,J.W., Orcutt,F.K., Calculations and experiments on the unbalance response of a flexible rotor, J. Engg.

Ind.) Trans. ASME., Series B, Vol. 89, No. 4, 785-796, Nov. 1967.

52. Gasch,R., Vibrations of large turbo-rotors in fluid film bearings on an elastic foundation, J. Sound. Vib., Vol. 47, 53-73, 1976.

53. Ruhl,R.L., Dynamics of distributed parameter turbo-rotor system: Transfer matrix techniques, Ph. D. Thesis, Cornell Univ., Ithaca, N.Y., Jan. 1970.

54. Nelson,H.O., A finite rotating shaft element using Timoshenko beam theory, J. Mech. Design, Trans. ASME., Vol. 102, 793-803, 1980.

55. Rouch, K.E., Finite element analysis of rotor bearing system with matrix reduction, Ph. D. Thesis, Marquette Univ., 1977.

56. Goldstein,H., Classical Mechanics, 2nd Edition, Addison-Wesley publishing Co, London.

57. Lund,J.W., Rotor bearing dynamics design technology, computer program manual for rotor response and stability, Mech. Tech. Inc. Tech. Report, AFAPL-TR-65-45, Air force systems command, Wright Patterson Airforce Base, Ohio, May 1965.

58. Den Hartog,J.P., Mechanical vibrations, Mc Graw-Hill book Co, N.Y..

59. Green,R.B.,Gyroscopic effects on the critical speeds of
    flexible rotors, J. Appl. Mech., 369-376, 1948.

60. Eshelman,R.L., Eubanks,R.A., On the critical speeds of a
    continuous shaft-disk system, J. Eng. Ind., Trans.
    ASME., p645, 1967.

61. Craggs,A., Akella,S., Dynamics of rotor systems using
    finite elements, Seventh M/C. Dyn. Seminar, NRCC, 1982.

62. Craggs,A., Akella,S., Rotating shaft with continuous
    disks, Proc. of the ninth CAN-CAM, p137, 1983.

63. Dubois,G.B., Ocvirk,F.W., Short bearing approximation
    for full journal bearings, NACA, Report 1157, 1953.

64. Holmes,R., The vibration of a rigid shaft on short
    sleeve bearings, J. Mech. Eng. Sci., Vol 2, No. 4,
    337-341, 1960.

65. Kim,P.Y., Lowe,I.R.G., A comparative study of fluid film
    bearing coefficients, LTR-Eng-109, NRCC Lab. Report,
    1981.

66. Adams,M.L., Padovan,J., Insights into linearized rotor
    dynamics, J. Sound. Vib., 76(1), 129-142, 1981.

67. Smith, D.M., Journal bearings in turbomachinary, Chapman
    and Hall Ltd, London, 1969.

68. Hahn,E.J., The excitability of flexible rotors in short
    sleeve bearings, J. of Lub. Tech. Trans. ASME., 105-115,

Jan. 1975.

69. Lund,J.W., Spring and damping coefficients for the tilted pad journal bearings, ASLE. Trans. 7, 342-352, 1964.

70. Holmes,R., Non linear performance of turbine bearings, J. Mech. Eng. Sci., Vol. 12, No. 6, 377-380, 1970.

71. Newkirk,B.L., Taylor,H.D., Shaft whipping due to oil action in bearing, General Electric Review, 28, 559-568, 1924.

72. Lund,J.W., Stability and damped critical speeds of a flexible rotor in fluid film bearings, J. Eng. Ind. Trans. ASME, 509-517, May 1974.

73. Lund,J.W., Rotor bearing dynamics design Technology, part vii: The three lobe bearing and floating ring bearing, Report No. AFAPL - TR 65-45, Part vii, Wright Patterson Air Force Base, Ohio, Feb. 1968.

74. Lund,J.W., Tonnesoen,J., Analysis and experiments on multi- plane balancing of a flexible rotor, J. Eng. Ind., Trans. ASME., p233, Feb. 1972.

75. Bishop, R.E.D., Parkinson,A.G., On the isolation of modes in the balancing of flexible shafts, Proc. of the Inst. Mech. Engrs., Lon. Vol. 177, p407, 1963.

76. Bishop,R.E.D., Parkinson,A.G., On the use of balancing

machines for flexible rotors, J. Eng. for Ind., p561, May 1972.

77. Federn,K., Multiplane balancing of elastic rotors-Fundamental theories and practical application, General Electrical Tech. Info. series, No. 58GL121.

78. Kellenberger,W., Should a flexible rotor be balanced in N or (N+2) planes?, J. Eng. for Ind., Trans ASME., p548, Aug. 1972.

79. Goodman,T.P., A least squares method for computing balance corrections, J. Eng. for Ind. Trans. ASME., p273, Aug. 1964.

80. Parkinson,A.G., Darlow,M.S., Smalley,A.J., A theoretical introduction to the development of a unified approach to flexible rotor balancing, J. Sound. Vib., 68, 489-506, 1980.

81. Tessarzik,J.M., Badgley,R.H., Anderson,W.J., Flexible rotor balancing by exact point-speed influence coefficient method, J. Eng. Ind. Trans. ASME., p148, 1972

82. Shiraki, K., Kanki,H., New field balancing method of tandem connected multispan flexible rotor system, Dynamics of rotors, IUATM symposium, Lyngby, Denmark, p494, 1974.

83. Gnielka,P., Modal balancing of flexible rotors without

test runs: An experimental investigation, J. Sound. Vib., 90(2), 157-172, 1983.

84. Ellyin,F., Dynamic behaviour and design of turbo-generator support, Seventh m/c. Dyn. seminar, NRCC, 1982.

85. Kirk,R.G., Choudhruy,P.D.E., On the effect of support flexibility on the stability of rotors, IUTAM Symposium, LYNGBY, Denmark, 1974.

86. Morton,P.G., On the dynamics of large turbo-generator rotors, Proc. Inst. Mech. Engrs., Vol. 180 pt1, No. 12, p295-329, 1965.

87. Ramsden.J.N., A matrix for the solution of mixed rotating and nonrotating vibration systems, Int. J. Num. Methods in Eng., Vol. 1, 225-245, 1969.

88. Lindley,A.L.G., Bishop,R.E.D., Some research on the balancing of large flexible rotors, Proc. Inst. Mech. Engrs., Lon., 177(30), p811, 1963.

89. Last,B.P., The balancing of flexible turbine and generator rotors, Proc. Inst. Mech. Engrs., Vol. 180 pt1, 1209-1222, 1965.

90. Victor,F., Ellyin.F., Acceleration of unbalanced rotor through the resonance of supporting structure, J. of Appl. Mech., vol.48, Trans. ASME., 419-424, June 1981.

91. Craggs,A., Ellyin,F., Pelot,R., A computational model to aid the balancing of turbo-generator sets, Eighth M/C. Dyn. Seminar, NRCC, 1984.

Appropriate boundary conditions for a non-uniform beam

Assuming a steady state harmonic motion with a frequency ω, the transient functional reduces to a spatial function. For a non-uniform beam of length L it is given as:

$$J = \frac{1}{2} \int_0^L EI \, (\phi')^2 \, dx + \frac{1}{2} \int_0^L GKA \, \{(W')^2 - 2W'\phi + \phi^2\} \, dx$$

$$- \frac{\omega^2}{2} \int_0^L \rho A W^2 \, dx - \frac{\omega^2}{2} \int_0^L \rho I \phi^2 \, dx$$

Where the relation of shear slope $\psi = \phi - W'$, is used to eliminate ψ. For the case of a non-uniform beam, the cross-sectional area, A(x), and the moment of inertia, I(x), are included inside the integrals. Material constants ρ, E and G are assumed to be constant. Shape factor, K, is also assumed to be constant though, strictly speaking, it changes with the cross-sectional variations.

To get the appropriate boundary conditions variation is considered of the displacement variable, W, given as: $\delta W = \epsilon \eta_1(x)$ and of the rotational slope, ϕ, given as: $\delta \phi = \epsilon \eta_2(x)$. Variation of the functional is given by:

$$\delta J = \int_0^\ell [EI(x) \frac{d\phi}{dx} \eta_2' + GKA(x) (\frac{dw}{dx} - \phi)(\eta_1' - \eta_2)$$
$$- \rho\omega^2 (A(x) W \eta_1(x) - I(x) \phi \eta_2(x))]dx = 0 \qquad (A1)$$

Integration, by parts, the 1st and 2nd terms of the equation (A1) gives:

$$EI(x) \frac{d\phi}{dx} \eta_2]_0^\ell - \int_0^\ell \frac{d}{dx} (EI(x) \frac{d\phi}{dx}) \eta_2 dx \qquad (A2)$$

$$GKA(x) (\frac{dw}{dx} - \phi)\eta_1]_0^\ell - \int_0^\ell \frac{d}{dx} GKA(x) (\frac{dw}{dx} - \phi) \eta_1 dx \qquad (A3)$$

Equations of motion are obtained by substituting equations (A2) and (A3) in (A1) and using the theorem and assumptions of calculus of variations.

The appropriate boundary conditions for a non-uniform Timoshenko beam can be obtained from equations (A2) and (A3) at a boundary x=B where B=0 or 1.

The natural (force) boundary conditions are:

moment $EI(B)\phi'(B)$;

shear force $GKA(B)\psi(B)$.

The kinematic (forced, displacement) boundary conditions are:

1. rotation $\phi(B)$;

2. displacement $W(B)$.

Only one boundary condition from each of 1 and 2 conditions can be taken to obtain admissible boundary conditions. Other combinations will not make the functional stationary.

The following rigid boundary conditions can be obtained at the boundary x=B:

1. a free end by prescribing zero for

    a.   moment, $I(B)\phi'(B)$,

    b.   and shear force, $GKA(B)\psi(B)$;

2. a hinged end by prescribing zero for

    a.   moment, $I(B)\phi'(B)$,

    b.   and displacement, $W(B)$;

3. a fixed end by prescribing zero for

    a.   displacement, $W(B)$,

    b.   and rotation, $\phi(B)$.

Formulation of TM624 element

TM624 implies a Timoshenko beam element with the displacement variable represented by a polynomial of 6 constants and the shear variable by a polynomial of 2 constants. The last digit, 4, indicates the number of points used in Gaussian integration.

The functional for a steady state harmonic motion can be obtained in terms of W and ψ instead of W and ϕ:

$$J = \frac{\omega^2}{2} \left\{ \int_0^\ell \rho A W^2 \, dx + \int_0^\ell \rho I\left((W')^2 + 2W'\psi + \psi^2\right) dx \right\}$$

$$- \frac{1}{2} \left\{ \int_0^\ell EI\left((W'')^2 + 2 W'' \psi' + (\psi')^2\right) dx + \int_0^\ell G K A \psi^2 \, dx \right\}$$

To get the approximate functional we assume polynomials for the variables:

$$W = a_0 + a_1 x + a_2 x^2 + a_3 x^3 + a_4 x^4 + a_5 x^5$$

$$\psi = b_0 + b_1 x$$

The linear shear variable is exact for a constant shear strain, and for a linear variation as in a beam with a uniformly distributed load. For C_1 continuity a linear function is the minimum order required to represent the shear variable so that the first derivative term in the functional is represented. Similarly, a quadratic polynomial for the displacement variable is necessary to allow the second derivative to be non-zero.

The rotational slope is given by $W' + \psi$, and the bending moment is $EI(W'' + \psi')$. The vectors of polynomial constants $\{ a \}$ and nodal variables $\{ W_e \}$ are:

$$\lfloor \alpha \rfloor = \lfloor a_0 \ a_1 \ a_2 \ a_3 \ a_4 \ a_5 \ b_0 \ b_1 \rfloor$$

$$\lfloor w_e \rfloor = \lfloor w_i \ w_i' \ w_i'' \ \psi_i \ w_{i+1} \ w_{i+1}' \ w_{i+1}'' \ \psi_{i+1} \rfloor$$

where W, W', W''' and ψ are the variables at nodes i and i+1. Let:

$$
\begin{array}{ll}
\lfloor X0 \rfloor & \lfloor 1 \quad x \quad x^2 \quad x^3 \quad x^4 \quad x^5 \quad 0 \quad 0 \rfloor \\[2mm]
\lfloor X1 \rfloor & \lfloor 0 \quad 1 \quad 2x \quad 3x^2 \quad 4x^3 \quad 5x^4 \quad 0 \quad 0 \rfloor \\[2mm]
\lfloor X2 \rfloor & \lfloor 0 \quad 0 \quad 2 \quad 6x \quad 12x^2 \quad 20x^3 \quad 0 \quad 0 \rfloor \\[2mm]
\lfloor Y0 \rfloor & \lfloor 0 \quad 0 \quad 0 \quad 0 \quad 0 \quad 0 \quad 1 \quad x \rfloor
\end{array}
$$

Therefore we can write:

$$W(x) = X0 \ \{ a \},$$

$$W'(x) = X1 \ \{ a \},$$

$$W''(x) = X2 \ \{ a \},$$

$$\psi(x) = Y0 \ \{ a \},$$

$$\text{and } \{ w_e \} = [\ C \ ] \ \{ a \}.$$

where,

$$[C] = \begin{bmatrix} 1 & 0 & 0 & 0 & 0 & 0 & 0 & 0 \\ 0 & 1 & 0 & 0 & 0 & 0 & 0 & 0 \\ 0 & 0 & 2 & 0 & 0 & 0 & 0 & 0 \\ 0 & 0 & 0 & 0 & 0 & 0 & 1 & 0 \\ 1 & \ell & \ell^2 & \ell^3 & \ell^4 & \ell^5 & 0 & 0 \\ 0 & 1 & 2\ell & 3\ell^2 & 4\ell^3 & 5\ell^4 & 0 & 0 \\ 0 & 0 & 2 & 6\ell & 12\ell^2 & 20\ell^3 & 0 & 0 \\ 0 & 0 & 0 & 0 & 0 & 0 & 1 & \ell \end{bmatrix}$$

Hence

$$\{ a \} = [C^{-1}] \{ w_e \}$$

Term by term the functional can be approximated by the integrals:

$$M1 = \{w_e\}^T \{ \int_0^\ell \rho \, A[C^{-1}]^T \lfloor xo \rfloor^T \lfloor xo \rfloor [C^{-1}] \, dx \} \{w_e\}$$

$$M2 = \{w_e\}^T \{ \int_0^\ell \rho \, I[C^{-1}]^T \lfloor x1 \rfloor^T \lfloor x1 \rfloor [C^{-1}] \, dx \} \{w_e\}$$

$$M3 = \{w_e\}^T \{ \int_0^\ell \rho \, I[C^{-1}]^T \lfloor x1 \rfloor \lfloor yo \rfloor [C^{-1}] \, dx \} \{w_e\}$$

$$M4 = \{w_e\}^T \{ \int_0^\ell \rho \, I[C^{-1}]^T \lfloor yo \rfloor \lfloor x1 \rfloor [C^{-1}] \, dx \} \{w_e\}$$

$$M5 = \{w_e\}^T \{ \int_0^\ell \rho \, I[C^{-1}]^T \lfloor yo \rfloor^T \lfloor yo \rfloor [C^{-1}] \, dx \} \{w_e\}$$

$$K1 = -\{W_e\}^T \{ \int_0^\ell EI[C^{-1}]^T \lfloor x2 \rfloor^T \lfloor x2 \rfloor [C^{-1}] \, dx \} \{W_e\}$$

$$K2 = \{W_e\}^T \{ \int_0^\ell EI[C^{-1}]^T \lfloor x2 \rfloor^T \lfloor y1 \rfloor [C^{-1}] \, dx \} \{W_e\}$$

$$K3 = \{W_e\}^T \{ \int_0^\ell EI[C^{-1}]^T \lfloor y1 \rfloor^T \lfloor x2 \rfloor [C^{-1}] \, dx \} \{W_e\}$$

$$K4 = \{W_e\}^T \{ \int_0^\ell EI[C^{-1}]^T \lfloor y1 \rfloor^T \lfloor y1 \rfloor [C^{-1}] \, dx \} \{W_e\}$$

$$K5 = \{W_e\}^T \{ \int_0^\ell GKA[C^{-1}]^T \lfloor yo \rfloor^T \lfloor yo \rfloor [C^{-1}] \, dx \} \{W_e\}$$

the matrices are all 8x8 in size, with the advantage that they can be directly added to one another. Computational saving can be achieved by partioning the matrices corresponding to the displacement variables and their derivatives and those corresponding to the shear variable. Addition of the component matrices is obtained by an assembly routine in this case.

Let

$$M11 = [\, M1 + M2 + M3 + M4 + M5 \,]$$

$$K11 = [\, K1 + K2 + K3 + K4 + K5 \,]$$

where

$$M11 = \{ W_e \}' \, [\, M \,] \, \{ W_e \}$$

$$K11 = \{ W_e \}' \, [\, K \,] \, \{ W_e \}$$

Using the rules of matrix differentiation, we obtain the homogeneous equations of motion as:

$$\{ [K] - \omega^2 [M] \} \{ W_e \} = 0$$

Now, to be able to prescribe all rigid boundary conditions, we need to change the nodal variables to an appropriate set, W, ϕ, Aψ and Iϕ', as described in Chapter 2. A linear transformation is used to obtain this change.

Formulation of the element TM544

This is also a Timoshenko type element with the displacement variable represented by a polynomial with 5 constants, and the rotational slope by a polynomial with 4 constants, with a 4 point Gaussian quadrature is used for integration. The extra constant (since we have 9 polynomial constants with 8 nodal degrees of freedom per element), is obtained by imposing the costraint $\psi''' = 0$. This constraint implies that the piecewise representation of shear within the element is a quadratic function. If the true distribution is of a higher order then more elements are required for a closer approximation.

The displacement and rotational slope polynomials are:

$$W = a_0 + a_1 x + a_2 x^2 + a_3 x^3 + a_4 x^4$$
$$\phi = b_0 + b_1 x + b_2 x^2 + b_3 x^3$$

From the assumed condition, $\psi''' = 0$, we get $W'''' = \phi'''$ and $a_4 = b_3/4$. Defining the vectors of polynomial constants

and the nodal variables as:

$$\lfloor x \rfloor = \lfloor a_0' \; a_1 \; a_2 \; a_3 \; b_0 \; b_1 \; b_2 \; b_3 \rfloor$$

$$\lfloor W_e \rfloor = \lfloor W_1 \; W_1' \; W_2 \; W_2' \; \phi_1 \; \phi_1' \; \phi_2 \; \phi_2' \rfloor$$

The nodal variables selected are either the variables whose variation is assumed or their derivatives. Let:

$$\lfloor X_0 \rfloor = \lfloor 1 \; x \; x^2 \; x^3 \; 0 \; 0 \; 0 \; x^4/4 \rfloor$$

$$\lfloor X_1 \rfloor = \lfloor 0 \; 1 \; 2x \; 3x^2 \; 0 \; 0 \; 0 \; x^3 \rfloor$$

$$\lfloor y_0 \rfloor = \lfloor 0 \; 0 \; 0 \; 0 \; 1 \; x \; x^2 \; x^3 \rfloor$$

$$\lfloor y_1 \rfloor = \lfloor 0 \; 0 \; 0 \; 0 \; 0 \; 1 \; 2x \; 3x^2 \rfloor$$

A transformation can be obtained from the polynomial coefficients to the nodal variables:

$$\{ W_e \} = [C] \{ a \}$$

Hence

$$\{ a \} = [C^{-1}] \{ W_e \}$$

Where

$$[C] = \begin{bmatrix} 1 & 0 & 0 & 0 & 0 & 0 & 0 & 0 \\ 0 & 1 & 0 & 0 & 0 & 0 & 0 & 0 \\ 1 & \ell & \ell^2 & \ell^3 & 0 & 0 & 0 & \ell^4/4 \\ 0 & 1 & 2\ell & 3\ell^2 & 0 & 0 & 0 & \ell^3 \\ 0 & 0 & 0 & 0 & 1 & 0 & 0 & 0 \\ 0 & 0 & 0 & 0 & 0 & 1 & 0 & 0 \\ 0 & 0 & 0 & 0 & 1 & \ell & \ell^2 & \ell^3 \\ 0 & 0 & 0 & 0 & 0 & 1 & 2\ell & 3\ell^2 \end{bmatrix}$$

and

$$[C^{-1}] = \begin{bmatrix} 1 & 0 & 0 & 0 & 0 & 0 & 0 & 0 \\ 0 & 1 & 0 & 0 & 0 & 0 & 0 & 0 \\ -3/\ell^2 & -2/\ell & 3/\ell^2 & -1/\ell & 1/2\ell & 1/4 & -1/2\ell & 1/4 \\ 2/\ell^3 & 1/\ell^2 & -2/\ell^3 & 1/\ell^2 & -1/\ell^2 & -1/2\ell & 1/\ell^2 & -1/2\ell \\ 0 & 0 & 0 & 0 & 1 & 0 & 0 & 0 \\ 0 & 0 & 0 & 0 & 0 & 1 & 0 & 0 \\ 0 & 0 & 0 & 0 & -3/\ell^2 & -2/\ell & 3/\ell^2 & -1/\ell \\ 0 & 0 & 0 & 0 & 2/\ell^3 & 1/\ell^2 & -2/\ell^3 & 1/\ell^2 \end{bmatrix}$$

[C^{-1}] is given for this element, as it is selected for further study. If elements with varying cross-sections are used the corresponding [C] matrix will change with the element length 1. The internal variables can now be expressed in terms of the nodal variables { W_e} as:

$$W = \lfloor x_0 \rfloor \, [C^{-1}] \, \{W_e\}$$

$$W' = \lfloor X_1 \rfloor \, [C^{-1}] \, \{W_e\}$$

$$\phi = \lfloor Y_0 \rfloor \, [C^{-1}] \, \{W_e\}$$

$$\phi' = \lfloor Y_1 \rfloor \, [C^{-1}] \, \{W_e\}$$

The approximate functional J can now be written as:

$$J = \frac{1}{2} \{W_e\}^T \, [KA] \, \{W_e\} + \frac{1}{2} \{W_e\}^T [KB] \, \{W_e\} - \frac{1}{2} \{W_e\}^T [KC] \, \{W_e\}$$

$$+ \frac{1}{2} \{W_e\}^T \, [KD] \, \{W_e\} - \frac{1}{2} \{W_e\}^T \, [KE] \, \{W_e\} - \frac{\omega^2}{2} \{W_e\}^T \, [MA] \, \{W_e\}$$

$$- \frac{\omega^2}{2} \{W_e\}^T \, [IA] \, \{W_e\}$$

The component stiffness and mass matrices are given as:

$$[KA] = \int_0^L EI \, [C^{-1}]^T \, \lfloor Y_1 \rfloor^T \, \lfloor Y_1 \rfloor \, [C^{-1}] \, dx$$

$$[KB] = \int_0^L GKA \, [C^{-1}]^T \, \lfloor X_1 \rfloor^T \, \lfloor X_1 \rfloor \, [C^{-1}] \, dx$$

$$[KC] = \int_0^L GKA \, [C^{-1}]^T \, \lfloor X_1 \rfloor^T \, \lfloor Y_0 \rfloor \, [C^{-1}] \, dx$$

$$[KD] = \int_0^L GKA \, [C^{-1}]^T \, \lfloor Y_0 \rfloor^T \, \lfloor Y_0 \rfloor \, [C^{-1}] \, dx$$

$$[KE] = \int_0^L GKA \, [C^{-1}]^T \, \lfloor Y_0 \rfloor^T \, \lfloor X_1 \rfloor \, [C^{-1}] \, dx$$

$$[MA] = \int_0^L \rho A \, [C^{-1}]^T \, \lfloor X_0 \rfloor^T \, \lfloor X_0 \rfloor \, [C^{-1}] \, dx$$

$$[IA] = \int_0^L \rho I \, [C^{-1}]^T \, \lfloor Y_0 \rfloor^T \, \lfloor Y_0 \rfloor \, [C^{-1}] \, dx$$

Integration is carried out by the four point Gaussian quadrature scheme. These four points vary with the element length l. Formulating with the non-dimensional parameter $\epsilon = x/l$ will enable the use of the element matrices for tapered elements. All these elements are of the same size, 8x8, allowing direct addition. The component matrices can be identified: [MA] is the translatory inertia matrix; [IA] is the rotatory inertia matrix, [KA] is the stiffness matrix due to bending; [KB], [KC], [KD] and [KE] are the stiffness matrices due to shear.

The approximate homogeneous equations of motion are obtained by the first variation of J with respect to $\{ W_e \}$ which is given as:

$$\frac{\partial J}{\partial \{W_e\}} = 0$$

$$\therefore \left[[KA] + [KB] - [KC] - [KE] + [KD] \right] - \omega^2 \left[[MA] + [IA] \right] = \{0\}$$

$$\text{or } [K*] - \omega^2 [M*] = \{0\}$$

Where [K*] and [M*] are the stiffness and mass matrices of the Timoshenko beam element, with respect to the nodal variables W, W', ϕ and ϕ. To obtain these matrices in terms of the chosen variables (refer to Chapter 2), W, ϕ, Aψ and Iϕ', a linear relation is expressed between these two sets:

$$
\begin{Bmatrix} w_i \\ w_i' \\ w_{i+1} \\ w_{i+1}' \\ \phi_i \\ \phi_i' \\ \phi_{i+1} \\ \phi_{i+1}' \end{Bmatrix}
=
\begin{bmatrix}
1 & 0 & 0 & 0 & 0 & 0 & 0 & 0 \\
0 & 1 & -1/A_i & 0 & 0 & 0 & 0 & 0 \\
0 & 0 & 0 & 0 & 1 & 0 & 0 & 0 \\
0 & 0 & 0 & 0 & 0 & 1 & -1/A_{i+1} & 0 \\
0 & 1 & 0 & 0 & 0 & 0 & 0 & 0 \\
0 & 0 & 0 & 1/I_i & 0 & 0 & 0 & 0 \\
0 & 0 & 0 & 0 & 0 & 1 & 0 & 0 \\
0 & 0 & 0 & 0 & 0 & 0 & 0 & 1/I_{i+1}
\end{bmatrix}
\begin{Bmatrix} w_i \\ \phi_i \\ A_i\psi_i \\ I_i\phi_i' \\ w_{i+1} \\ \phi_{i+1} \\ A_{i+1}\psi_{i+1} \\ I_{i+1}\phi_{i+1}' \end{Bmatrix}
$$

As before linear transformation is used for obtaining the matrices with respect to the new set of variables.

Formulation of TM654

This, again, is a Timoshenko element with a polynomial of 6 coefficients for the displacement variable and a polynomial with 5 coefficients for the rotational slope and uses a 4 point Gaussian integration scheme. This higher order element is obtained using the same constraint as in TM624, $\psi'' = 0$. The displacement and rotational slope polynomials are given as:

$$W = a_0 + a_1 x + a_2 x^2 + a_3 x^3 + a_4 x^4 + a_5 x^5$$

$$\phi = b_0 + b_1 x + b_2 x^2 + b_3 x^3 + b_4 x^4$$

Using the constraint condition we get, $W''' = \phi''$.
Differentiating W and ϕ and using the constraint condition
we get:

$$6a_3 + 24a_4 x + 60a_5 x^2 = 2b_2 + 6b_3 x + 12b_4 x^2$$

For constant coefficients; the two polynomials are
equal if the coefficients of each power of x are equal. For
this case we get:

$$6a_3 = 2b_2$$
$$24a_4 = 6b_3$$
$$60a_5 = 12b_4$$

We define the vectors:

$$\lfloor xo \rfloor = \lfloor 1 \ x \ x^2 \ 0 \ 0 \ \frac{x^3}{3} \ \frac{x^4}{4} \ \frac{x^5}{5} \rfloor$$

$$\lfloor x1 \rfloor = \lfloor 0 \ 1 \ 2x \ 0 \ 0 \ x^2 \ x^3 \ x^4 \rfloor$$

$$\lfloor Y0 \rfloor = \lfloor 0 \ 0 \ 0 \ 1 \ x \ x^2 \ x^3 \ x^4 \rfloor$$

$$\lfloor Y1 \rfloor = \lfloor 0 \ 0 \ 0 \ 0 \ 1 \ 2x \ 3x^2 \ 4x^3 \rfloor$$

$$\lfloor \alpha \rfloor = \lfloor a_0 \ a_1 \ a_2 \ b_0 \ b_1 \ b_2 \ b_3 \ b_4 \rfloor$$

$$\lfloor we \rfloor = \lfloor w_i \ w_i' \ w_{i+1} \ w_{i+1}' \ \phi_i \ \phi_i' \ \phi_{i+1} \ \phi_{i+1}' \rfloor$$

the relation of the nodal variables and the polynomial coefficients is given by:

$$\{ W_e \} = [C] \{ a \}$$

Where

$$[C] = \begin{bmatrix} 1 & 0 & 0 & 0 & 0 & 0 & 0 & 0 \\ 0 & 1 & 0 & 0 & 0 & 0 & 0 & 0 \\ 1 & \ell & \ell^2 & 0 & 0 & \ell^3/3 & \ell^4/4 & \ell^5/5 \\ 0 & 1 & 2\ell & 0 & 0 & \ell^2 & \ell^3 & \ell^4 \\ 0 & 0 & 0 & 1 & 0 & 0 & 0 & 0 \\ 0 & 0 & 0 & 0 & 1 & 0 & 0 & 0 \\ 0 & 0 & 0 & 1 & \ell & \ell^2 & \ell^3 & \ell^4 \\ 0 & 0 & 0 & 0 & 1 & 2\ell & 3\ell^2 & 4\ell^3 \end{bmatrix}$$

The rest of the procedure is the same as in the formulation of TM544 and uses the same transformation matrix to obtain the mass and stiffness matrices to the required variables.

Formulation of an element using trigonometric functions

Functions other than algebraic polynomials can be used for the variables. Fourier has shown that any periodic function can be represented by a series of harmonic functions. Let us assume the displacement and the rotational slopes as:

$$W = a_0 + a_1 \sin \frac{\pi x}{\ell} + a_2 \cos \frac{\pi x}{\ell} + a_3 \sin \frac{2\pi x}{\ell}$$
$$+ a_4 \cos \frac{2\pi x}{\ell} + a_5 \sin \frac{3\pi x}{\ell} + a_6 \cos \frac{3\pi x}{\ell}$$

$$\phi = b_0 + b_1 \sin \frac{\pi x}{\ell} + b_2 \cos \frac{\pi x}{\ell} + b_3 \sin \frac{2\pi x}{\ell}$$
$$+ b_4 \cos \frac{2\pi x}{\ell} + b_5 \sin \frac{2\pi x}{\ell} + b_6 \cos \frac{3\pi x}{\ell}$$

Using the constraint condition $\psi''' = 0$, we get the relation $W'''' = \phi'''$. The coefficients of like harmonic functions can be equated since each is orthogonally independent. We then obtain,

$$\begin{Bmatrix} a_1 \\ a_2 \\ a_3 \\ a_4 \\ a_5 \\ a_6 \end{Bmatrix} = \frac{-\ell}{\pi} \begin{Bmatrix} -b_2 \\ b_1 \\ -b_4/2 \\ b_3/2 \\ -b_6/3 \\ b_5/3 \end{Bmatrix}$$

The vectors of polynomial constants and nodal variables are:

$$\lfloor \alpha \rfloor = \lfloor a_0 \quad b_0 \quad b_1 \quad b_2 \quad b_3 \quad b_4 \quad b_5 \quad b_6 \rfloor$$

$$\lfloor w_e \rfloor = \lfloor w_1 \quad w_1' \quad w_2 \quad w_2' \quad \phi_1 \quad \phi_1' \quad \phi_2 \quad \phi_2' \rfloor$$

Variables at interior points are given as:

$$W(x) = \lfloor X0 \rfloor \{a\}$$

$$\phi(x) = \lfloor Y0 \rfloor \{a\}$$

$$W'(x) = \lfloor X1 \rfloor \{a\}$$

$$\phi'(x) = \lfloor Y1 \rfloor \{a\}$$

Where

$$\lfloor Y0 \rfloor = \lfloor 0 \quad 1 \quad \sin\frac{\pi x}{\ell} \quad \cos\frac{\pi x}{\ell} \quad \sin\frac{2\pi x}{\ell} \quad \cos\frac{2\pi x}{\ell} \quad \sin\frac{3\pi x}{\ell} \quad \cos\frac{3\pi x}{\ell} \rfloor$$

$$\lfloor Y1 \rfloor = \lfloor 1 \quad 0 \quad \frac{\ell}{\pi}\cos\frac{\pi x}{\ell} \quad \frac{-\ell}{\pi}\sin\frac{\pi x}{\ell} \quad \frac{\ell}{2\pi}\cos\frac{2\pi x}{\ell} \quad \frac{-\ell}{2\pi}\sin\frac{2\pi x}{\ell}$$
$$\frac{\ell}{3\pi}\cos\frac{3\pi x}{\ell} \quad \frac{-\ell}{3\pi}\sin\frac{3\pi x}{\ell} \rfloor$$

$$\lfloor X1 \rfloor = \lfloor 0 \quad 0 \quad \sin\frac{\pi x}{\ell} \quad \cos\frac{\pi x}{\ell} \quad \sin\frac{2\pi x}{\ell} \quad \cos\frac{2\pi x}{\ell} \quad \sin\frac{3\pi x}{\ell} \quad \cos\frac{3\pi x}{\ell} \rfloor$$

The relation between the nodal variables and the coefficints of the functions is :

$$
\begin{bmatrix} w_1 \\ w_1' \\ w_2 \\ w_2' \\ \phi_1 \\ \phi_1' \\ \phi_2 \\ \phi_2' \end{bmatrix} =
\begin{bmatrix}
1 & 0 & -\frac{\ell}{\pi} & 0 & \frac{-\ell}{2\pi} & 0 & \frac{-\ell}{3\pi} & 0 \\
0 & 0 & 0 & 1 & 0 & 1 & 0 & 1 \\
1 & 0 & \frac{\ell}{\pi} & 0 & \frac{-\ell}{2\pi} & 0 & \frac{\ell}{3\pi} & 0 \\
0 & 0 & 0 & -1 & 0 & 1 & 0 & -1 \\
0 & 1 & 0 & 1 & 0 & 1 & 0 & 1 \\
0 & 0 & \frac{\pi}{\ell} & 0 & \frac{2\pi}{\ell} & 0 & \frac{3\pi}{\ell} & 0 \\
0 & 1 & 0 & -1 & 0 & 1 & 0 & -1 \\
0 & 0 & \frac{-\pi}{\ell} & 0 & \frac{2\pi}{\ell} & 0 & \frac{-3\pi}{\ell} & 0
\end{bmatrix}
\begin{bmatrix} a_0 \\ b_0 \\ b_1 \\ b_2 \\ b_3 \\ b_4 \\ b_5 \\ b_6 \end{bmatrix}
$$

Again the mass and stiffness matrices can be transformed as before. This element is not tested.

Static response with Timoshenko beam

The elementary strength of materials approach, using the Euler beam theory or the pure bending theory gives tables for deflection, total slope, shear force and bending moment starting from the differential equation $M = EIW''$, obtained from the pure bending theory, along with the prescribed end conditions.

For deep beams the shear deformation also accounts for the loading. The resulting static response is described by the following equations:

Bending moment : $M = -EI\phi'$.

Shear force : $V = GKA\psi$.

Deformation : $W' = \phi - \psi$.

For a distributed loading of a rate q per unit length, the uncoupled equations in W and ϕ are:

$$EI\,\phi''' = q$$

$$EI\,W^{IV} = q - \frac{EI}{GKA}\,q''$$

The differential equations of static equilibrium along with the boundary conditions and continuity conditions are solved to obtain the deflection, slope, bending moment and

shear force.

The method is illustrated for a simply supported beam with a concentrated load at some arbitrary distance 'a' from one end. Results with other boundary conditions and loadings are also presented.

For, x between 0 and a , we get:

$$\frac{Pb}{\ell} x = -EI \; \phi'$$

$$\phi = \frac{-Pbx^2}{2EI\ell} + C_1$$

$$\frac{Pb}{\ell} = GKA(w' - \phi)$$

$$\therefore w = \frac{Pbx}{GKA\ell} - \frac{Pbx^3}{6EI\ell} + C_1 x + C_3$$

For, x between a and 1, we get:

$$\frac{Pbx}{\ell} - P(x-a) = -EI\frac{d\phi}{dx}$$

$$\phi = \frac{-Pbx^2}{2EI\ell} + \frac{Px^2}{2EI} - \frac{Pax}{EI} + C_2$$

$$\frac{-Pa}{\ell} = GKA(w' - \phi)$$

$$w = \frac{-Pax}{GKA\ell} - \frac{Pbx^3}{6EI\ell} + \frac{Px^3}{6EI} - \frac{Pax^2}{2EI} + C_2 x + C_4$$

The constants are solved using the conditions: W=0 at x=0 and x=1; and W and ϕ are continuous at x =a. Substituting the constants, we get the beam parameters which

are given for the case when x is between o and a:

$$w = \frac{Pbx}{GKA\ell} - \frac{Pbx^3}{6EI\ell} - \frac{Pa^2}{2EI} x + \frac{Pa}{3EI\ell} (\ell^2 + \frac{a^2}{2}) x$$

$$\phi = \frac{-Pbx^2}{2EI\ell} - \frac{Pa^2}{2EI} + \frac{Pa}{3EI\ell} (\ell^2 + \frac{a^2}{2})$$

$$GKA\psi = \frac{Pb}{\ell}$$

$$EI\phi' = \frac{-Pbx}{\ell}$$

when x is between a and 1 the parameters are:

$$w = \frac{-Pax}{GKA\ell} - \frac{Pbx^3}{6EI\ell} + \frac{Px^3}{6EI} - \frac{Pax^2}{2EI}$$
$$+ \frac{Pa}{3EI\ell} (\ell^2 + \frac{a^2}{2}) x + \frac{Pa}{GKA} - \frac{Pa^3}{6EI}$$

$$\phi = \frac{-Pbx^2}{2EI\ell} + \frac{Px^2}{2EI} - \frac{Pax}{EI} + \frac{Pa}{3EI\ell} (\ell^2 + \frac{a^2}{2})$$

$$GKA\psi = \frac{-Pa}{\ell}$$

$$EI\phi' = \frac{-Pbx}{\ell} + P(x-a)$$

2.Simply supported with a concentrated load P at the centre

This is a special case of the previous example with a = 1/2; but is solved independently to check.

For x between 0 and 1/2:

$$W = \frac{Px}{2GKA} - \frac{Px^3}{12EI} + \frac{PL^3}{16EI} \, x$$

$$\phi = \frac{-Px^2}{4EI} + \frac{PL^2}{16EI}$$

$$A\Psi = P/2GK$$

$$I\phi' = -Px/2E$$

Due to symmetry only one half of the beam results are shown.

3. Clamped- Clamped with concentrated load P at the centre

For x between 0 and 1/2:

$$W = Px/2GK + PLx^2/16EI - Px^3/12EI$$

$$\phi = PLx/8EI - Px^2/4EI$$

$$A\Psi = P/2GKA$$

$$I\phi' = PL/8E - Px/2E$$

Again due to symmetry only one half of the beam is considered.

4. Clamped- Free beam with a concentrated load P at the free end

For x between 0 and 1:

$$W = Px/GKA - Px^3/6EI + PLx^2/2EI$$

$$\phi = -Px^2/2EI + PLx/EI$$

$$A\Psi = P/GK$$

$$I\phi' = (PL - Px)/E$$

5. Uniformly loaded simply-supported beam

Let q_0 be the load per unit length.

For x between 0 and 1/2, we get the beam parameters as:

$$w = \frac{q_0}{2GKA}\left[\frac{\ell^2}{4} - x^2\right] + \frac{q_0}{EI}\left[\frac{x^4}{24} - \frac{\ell^2 x^2}{16} + \frac{5\ell^4}{384}\right]$$

$$\phi = \frac{1}{EI}\left(\frac{q_0 x^3}{6} - \frac{q_0 \ell^2 x}{8}\right)$$

$$GKA\psi = -q_0 x$$

$$EI\phi' = \frac{q_0 x^2}{2} - \frac{q_0 \ell^2}{8}$$

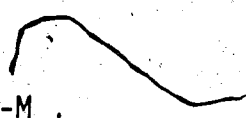Again, symmetry makes description of half the beam complete.

6. Cantilever beam with end moment

For x between 0 and 1, the beam parameters are:

$$W = -\frac{M}{EI}\frac{x^2}{2} \quad , \qquad GKA\psi = 0 \quad ,$$

$$EI\frac{d\phi}{dx} = -M \quad .$$

$$\phi = -\frac{Mx}{EI} \quad ,$$

A few of the commonly occuring basic cases have been shown.

Ritz method for uniform and tapered, simply supported
Timoshenko shaft

Assuming a harmonic motion of frequency, ω, for the
displacement, W, and rotational slope, ϕ, the kinetic and
potential energy terms give the frequency equation:

$$\omega^2 = \frac{\int_0^L EI(\phi')^2 dx + \int_0^L GKA\left(\phi - \frac{dw}{dx}\right)^2 dx}{\int_0^L \rho A W^2 dx + (1 - 2h) \int_0^L \rho I \phi^2 dx} \tag{C1}$$

Where h is the spin to whirl velocity ratio to accomodate
different shaft whirling rates. The displacement and
rotational slope are given as functions of the shaft length:

$$w(x) = \sum_{i=1}^{N} Ci \ f_i(x) \tag{C2}$$

$$\phi(x) = \sum_{i=1}^{M} di \ g_i(x).$$

Where each of the functions f_i and g_i are chosen to
satisfy the specified boundary conditions. The assumed
functions, not being exact, constrain the system raising its

critical speeds. Ritz method selects the function coefficients to minimize the frequency, by equating to zero the partial derivatives of ω^2 with respect to all the constants ci and di . Equating these derivatives to zero gives linear equations in the desired coefficients and the characteristic equation. Denoting the numerator of equation (C1) by Nr and the denominator by Dn, we can write $\omega^2 Dn = Nr$. Also, we obtain:

$$D_n \left[\frac{\partial}{\partial C1} \int_0^L \{GKA(w')^2 - 2\phi w' \, GKA - \omega^2 \rho A w^2\}dx \right] = 0$$

$$D_n \left[\frac{\partial}{\partial di} \int_0^L \{EI(\phi')^2 + GKA \phi^2 - 2 \, GKA \, \phi \, w' - \omega^2 \rho I(1-2h)\phi^2\}dx \right] = 0$$

If the appropriate variable functions, equation (C2) which satisfy the boundary conditions are known then equation (C3) can be solved for the corresponding critical speeds.

H-H uniform shaft; trigonometric functions

The variables expressed as the trigonometric series:

$$W = \sum_{i=1}^N Ci \, \sin \frac{i\pi x}{L}$$

$$\text{and } \phi = \sum_{i=1}^N di \, \cos \frac{i\pi x}{L}$$

satisfy the hinged boundary conditions at x=0 and L. Taking one term for each variable we get:

$$w = C_1 \sin \frac{\pi x}{L} \text{ and } \phi = d_1 \cos \frac{\pi x}{L}$$

Substituting in equation (C3) and simplifying we get a set of linear algebraic equations in c_1 and d_1. Non-trivial solutions in W and ϕ are obtained by equating the determinants of the coefficients to zero.

$$\begin{vmatrix} (GKA \dfrac{\pi^2}{L} - \omega^2 \rho A L & -\pi GKA \\ -\pi GKA & \dfrac{EI\pi^2}{L} + GKAL - (1 - 2h) \omega^2 \rho I L \end{vmatrix} = 0$$

The characteristic equation is:

$$\pi^4 - p^4 \left[(1 - 2h)\pi^2 \left(\frac{k}{L} \right)^2 + \frac{E\pi^2}{GK} \left(\frac{k}{L} \right)^2 + 1 \right]$$

$$+ p^8 \frac{E}{GK} \left(\frac{k}{L} \right)^4 = 0$$

where $\dfrac{\rho L^4 \omega^2}{E k^2}$ is replaced by p^4. When k/L is zero, the Euler beam solution, $p = \pi$, is obtained.

H-H linearly tapered element; algebraic functions

We will use the Linearly tapered element defined by
Lindberg. For an element of length L, with the two end nodes
at i and i+1. This element is also described in Chapter 2.
The area at any point x is $A(x) = K_1 hd$
Cross-sectional moment of inertia $I(x) = K_2 hd^3$
The linearly varying dimensions h and d of the shaft are
given as:

$$h(x) = h_i \{ 1-(1-H)x/L \}$$

$$d(x) = d_i \{ 1-(1-D)x/L \}$$

Where

$$H = h_{i+1}/h_i = a$$

$$D = d_{i+1}/d_i = \beta$$

The variation of the area and the moment of inertia is given
by:

$$A(x) = A_i \{1 + a_1 \frac{x}{L} + a_2 \frac{x^2}{L}\}$$

$$I(x) = I_i \{1 + b_1 \frac{x}{L} + b_2 \frac{x^2}{L^2} + b_3 \frac{x^3}{L^3} + b_4 \frac{x^4}{L^4}\}$$

Where

$$a_1 = (1-H)+(1-D)$$

$$a_2 = (1-H)(1-D)$$

$$b_1 = -\{ 3(1-D) + (1-H) \}$$

$$b_2 = 3(1-D)^2 + 3(1-D)(1-H)$$

$$b_3 = -\{ (1-D)^3 + 3(1-D)^2(1-H) \}$$

$$b_4 = (1-D)^3(1-H)$$

Trigonometric functions are inconvenient for tapered shafts as orthogonality is not applicable; algebraic functions are more useful. Let:

$$w = C_1 x(\ell - x)$$

$$\phi = d_1 \left(\frac{x^3}{3} - \frac{\ell x^2}{2} + \frac{\ell^3}{12} \right)$$

The hinged boundary conditions; $W=0$ and $I\phi' =0$, are satisfied at the two ends $x=0$ and $x=1$. The integrals are calculated as:

$$\int_0^L A(x) \, (w')^2 dx = C_1^2 \, A_0 \, L^3 \, K7$$

$$\int_0^L A(x) \, W^2 dx = C_1^2 \, A_0 \, L^5 \, K8$$

$$\int_0^L A(x) \, \phi(x) \, w' dx = A_0 \, L^5 \, d_1 \, C_1 \, K3$$

$$\int_0^L A(x) \, \phi^2 dx = d_1^2 \, A_0 \, L^7 \, K4$$

$$\int_0^L I(x) \cdot \phi^2 \, dx = d_1^2 \, I_0 \, L^7 \, K5$$

$$\int_0^L I(x)(\phi')^2 \, dx = I_0 \, L^5 \, d_1^2 \, K6$$

Where A_0 and I_0 are the area and moment of inertia at the root corresponding to the ith node at x=0; and the constants are:

$$K7 = .333333 + a_1(.166667) + a_2(.133333)$$

$$K8 = .033333 + a_1(.016667) + a_2(.009523)$$

$$K3 = .033333 + a_1(.016667) + a_2(.013095)$$

$$K4 = .003373 + a_1(.016865) + a_2(.001300)$$

$$K5 = .003373 + b_1(.016865) + b_2(.001300) + b_3(.001108)$$
$$+ b_4(.000974)$$

$$K6 = .013333 + b_1(.016667) + b_2(.009524) + b_3(.005952)$$
$$+ b_4(.003968)$$

Substituting these values in the Ritz's equation and differentiating the characteristic equation is obtained, which in the determinant form is:

$$\begin{vmatrix} GKA_0 \, K7 \, L^3 - \omega^2 \rho A_0 \, K8L^5 & - GKA_0 \, K3 \, L^5 \\ - GKA_0 \, K3 \, L^5 & GKA_0 \, K4L^7 + EI_0 L^5 K6 \\ & - \omega^2 \rho I_0 h^* \, K5 \, L^7 \end{vmatrix} = 0$$

Substituting $\dfrac{I_0}{A_0} = k_0{}^2$, $\omega^2 = \dfrac{E\,k_0{}^2 p^4}{\rho L^4}$ and rearranging will give:

$$h^* E^2 \left(\frac{k_0}{L} \right)^6 K8 \ K5 \ p^8 - p^4 \left\{ E \left(\frac{k_0}{L} \right)^2 K8 \ GKK4 \right.$$

$$+ E^2 \left(\frac{k_0}{L} \right)^4 K8 \ K6 + h^* \ GK \ K7 \ E \ K5 \left(\frac{k_0}{L} \right)^4 \left. \right\}$$

$$+ \left\{ G^2 \ K^2 \ K7 \ K4 + E \left(\frac{k_0}{L} \right)^2 K6 \ GKK7 - (GKK3)^2 \right\} = 0$$

The solution p is the non-dimensional frequency of the tapered beam considered.